In Vitro Measurement of Fluid Pressurebehind the Acetabular Cup

Sydney, Sarah

Award date:
2013

Awarding institution:
University of Bath

Acknowledgements

I would like to thank my supervisors, Professor Tony Miles and Dr Irene Turner, for their patience, support and guidance; Richard Weston and Samantha Wright, for their assistance in constructing and testing the rig; Mr John Timperley and the team at the PEOC Exeter; Elizabeth McGivern, Tom Baker and their colleagues at Stryker; my support crew from Team Bath Street (Auguste, Fran, Keri and especially Johan); and my parents for their love and support.

Abstract

Periacetabular osteolysis is a significant complication following total hip replacement surgery. It is believed to be caused by wear debris and high fluid pressures within the joint capsule. To investigate the mechanisms by which high fluid pressures are generated in total hip replacement, a physical model of the hip joint was constructed, the Acetabular Pressure Transmission Rig (APTR).

An aluminium chamber held the bone analogue, a polyurethane hemisphere with a 52mm acetabular cavity, and the prosthetic components, a 28mm femoral head and various uncemented cups, were inserted without press-fit to simulate cup loosening. A synovial fluid analogue was introduced into the chamber through an elevated reservoir. Rigid transmission tubes conducted fluid pressures from the cup-cavity interface to external transducers. The APTR was loaded under various conditions and the pressures produced by the loading regimes were analysed.

Pressures over 35kPa, previously shown by other groups to cause osteolysis, were measured within the APTR, reaching a maximum of 131.3kPa measured at the pole of the cup. Changes in load application led to pressure changes within the APTR, with higher loading frequency and magnitude leading to higher median pressure amplitudes. The presence of different component features, such as screw holes in the metal shell, was also shown to affect periacetabular pressures. Tests with a fibrous rim interposed between the prosthetic cup and the test cavity showed an 88% reduction in periacetabular pressures, as the increased rim interference between cup and cavity prevented fluid ingress behind the cup. A larger initial separation between the loading head and the acetabular cup caused a significant increase in measured pressures, with a 0.15mm increase in head-cup separation producing a 53% increase in pressures measured at the pole of the cup. Pressure differentials between different transducer sites indicated the ability for fluid flow behind the cup, which can be related *in vivo* to the movement of particulate debris to periacetabular bone.

The APTR was able to measure clinically significant pressures and to analyse the effects of modifying component and loading characteristics with currently available prosthetic components. This makes the rig useful in a clinical context, as it has been shown to be capable of testing a broad range of component types under a wide range of conditions. Its use will ensure new prostheses and fixation modes can be designed in such a way as to eliminate the damaging fluid pressures currently observed in artificial hip joint replacements.

List of Symbols and Abbreviations

Abbreviation	Description
Δ	Delta – change in value
ρ	Rho – density
APTR	Acetabular Pressure Transmission Rig
BW	Body weight
CFD	Computational fluid dynamics
CHP	Cyclic hydrostatic pressure
COC	Ceramic-on-ceramic
CoCr	Cobalt-chromium
CT	Computed tomography
ED	External diameter
FE	Finite element (analysis)
g	Gravity
GPa	Gigapascals
Hz	Hertz
ID	Internal diameter
IL	Interleukin (eg IL-1, IL-6)
kPa	Kilopascals
kN	Kilonewtons
LF	Load factor
M-CSF	Macrophage colony-stimulating factor
MD	Macrophage-derived
MOP	Metal-on-polyethylene

MOM	Metal-on-metal
MPa	Megapascals
n	Number of tests / repetitions
OA	Osteoarthritis
OPG	Osteoprotegerin
PE	Polyethylene
PGE	Prostaglandin E
PIV	Particle Image Velocimetry
PMMA	Polymethyl methacrylate
PU	Polyurethane
PVC	Polyvinyl chloride
RANK	Receptor activator of nuclear factor kappa-B
RANKL	Receptor activator of nuclear factor kappa-B ligand
THA	Total hip arthroplasty
TNF	Tumour necrosis factor
UHMWPE	Ultra-high molecular weight polyethylene

Table of Contents

Index of Figures

Index of tables

1. Introduction

This thesis presents the development and testing of a rig to measure fluid pressures behind the acetabular cup in an *in vitro* model of the replaced hip joint.

During 2011 over 71,600 primary total hip arthroplasty (THA) procedures were performed in the UK (NJR, 2012). This procedure is most commonly undertaken to treat osteoarthritis (CJRR, 2012, AOA, 2012, NJR, 2012, Garellick et al., 2010). While THA is an extremely successful surgical procedure, around 11% of THA procedures each year are revision procedures, where one or both components are removed and replaced, mostly due to loosening of the components within the joint (aseptic loosening). This loosening is often caused by osteolysis, the active resorption of bone tissue behind the implant.

Osteolysis is a multi-factorial problem, and its characteristics are continually being explored, however it is commonly accepted that the presence of wear debris from prosthetic components and high fluid pressures in the joint contribute to the development of osteolysis. The aim of this project was to construct a test rig that will enable the *in vitro* study of factors influencing osteolysis around acetabular cups, specifically the generation of high fluid pressures.

To design this rig, it was necessary to review the published literature to understand the causes and progression of osteolysis. Results of this literature review are presented, to introduce hip anatomy, osteoarthritis and the THA procedure, and to provide background information for the understanding of osteolysis in the replaced hip joint.

Using this information, design requirements for a physical model of the hip joint were identified. This thesis outlines these design requirements, and the steps taken to incorporate these features into the rig design. The test rig, named the Acetabular Pressure Transmission Rig (APTR) was constructed and tests were carried out to assess the magnitudes of fluid pressures under different rig conditions. This thesis details the results and the clinical implications of these tests.

2. Literature Review

2.1 Hip anatomy

The hip joint comprises the head of the femur and the acetabulum of the pelvis (Figure 1), and is one of the main load-bearing joints in the body. The articulation of the ball-shaped femoral head inside the deep, concave acetabulum gives the joint intrinsic stability, while still allowing the wide range of motion required in everyday activities. The joint is surrounded by a fibrous joint capsule and large, strong muscles.

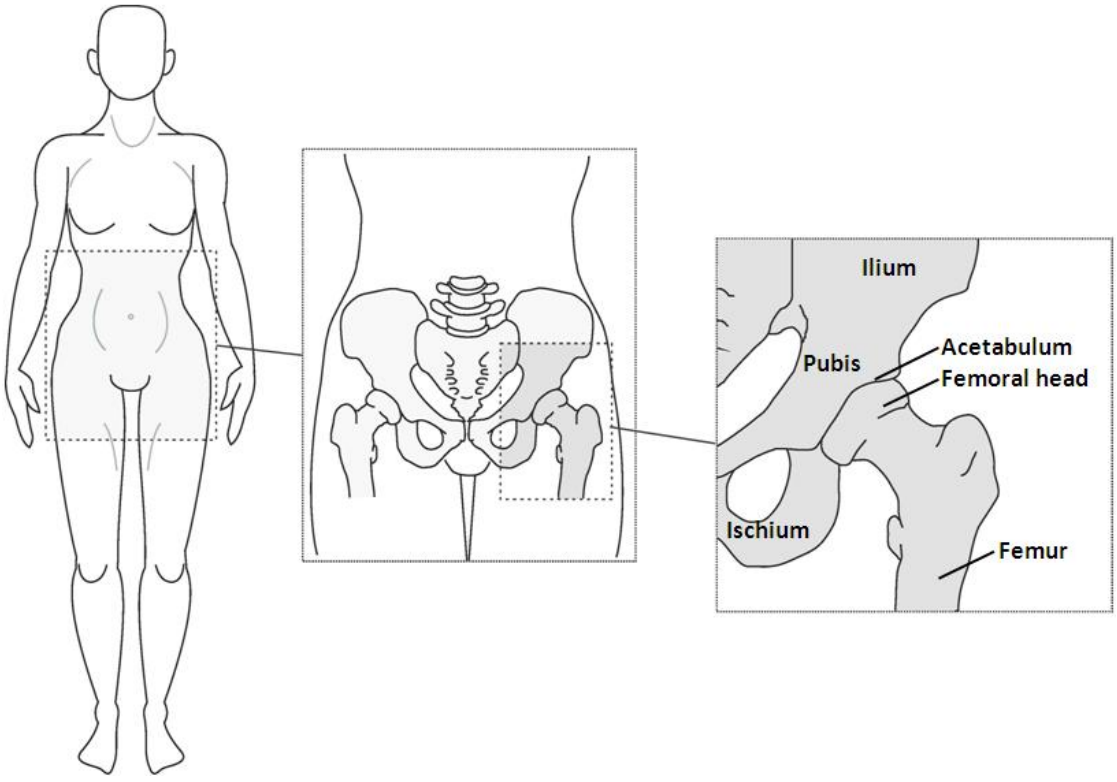

Figure 1: Anterior view showing structures of the hip joint within the body. Author's own image.

Femur

The femur (shown in Figure 2a) is the longest bone in the body. The length of the femur facilitates the biomechanical requirements of gait, and its high strength is necessary to transmit muscular and weight-bearing force. The femoral head (indicated in Figure 2b) forms two-thirds of a sphere and articulates inside the acetabulum. The angle between the femoral neck and shaft (shown in Figure 2c) is approximately 125°. Hips with neck-shaft angles higher than this value are classified as coxa valga; neck-shaft angles lower than 125° are classified as

coxa vara. The offset, or distance between the centre of the femoral head and a line bisecting the long axis of the femur (Figure 2c), may also vary, independent of the neck-shaft angle.

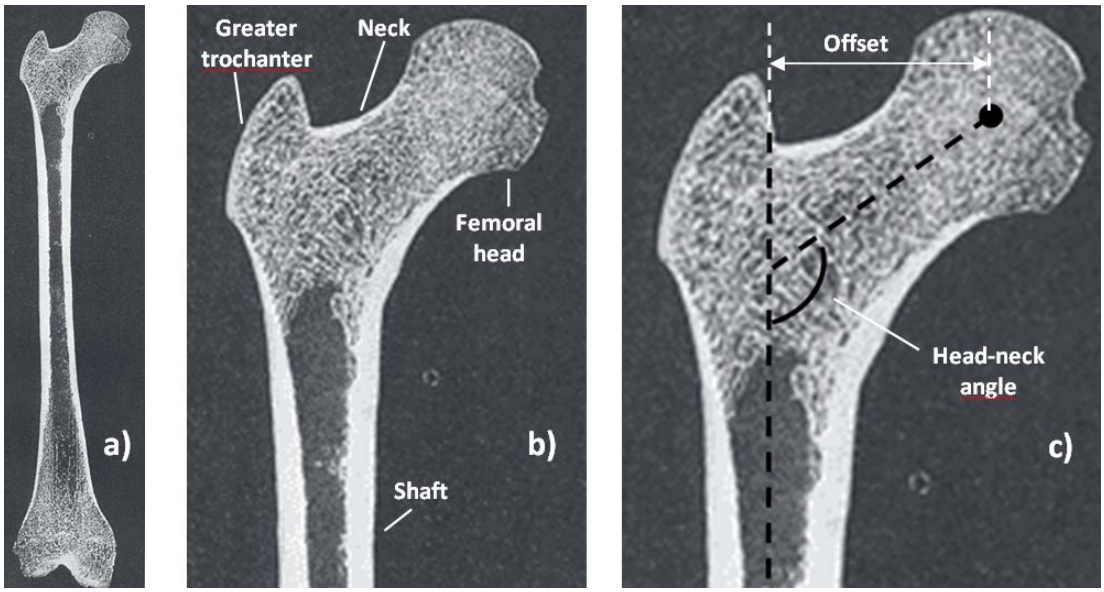

Figure 2: Images showing features of femoral bone. a) Femur bone. b) Proximal femur, showing bony landmarks. c) Proximal femur, showing offset and head-neck angle (as defined by Charles et al. (2004)). All images modified from Gray (1918).

Acetabulum

The pelvis is made up of three bones fused together – the ilium, ischium and pubis (Figure 3). These bones unite in the acetabulum, a concave structure that articulates with the femoral head. The orientation of the acetabular opening is called acetabular version. The normal acetabulum is anteverted, orientated approximately 15º anteriorly. Anterior and posterior columns of bone surround the acetabulum (Figure 3) and provide strength to transmit stresses from the trunk to the lower limbs.

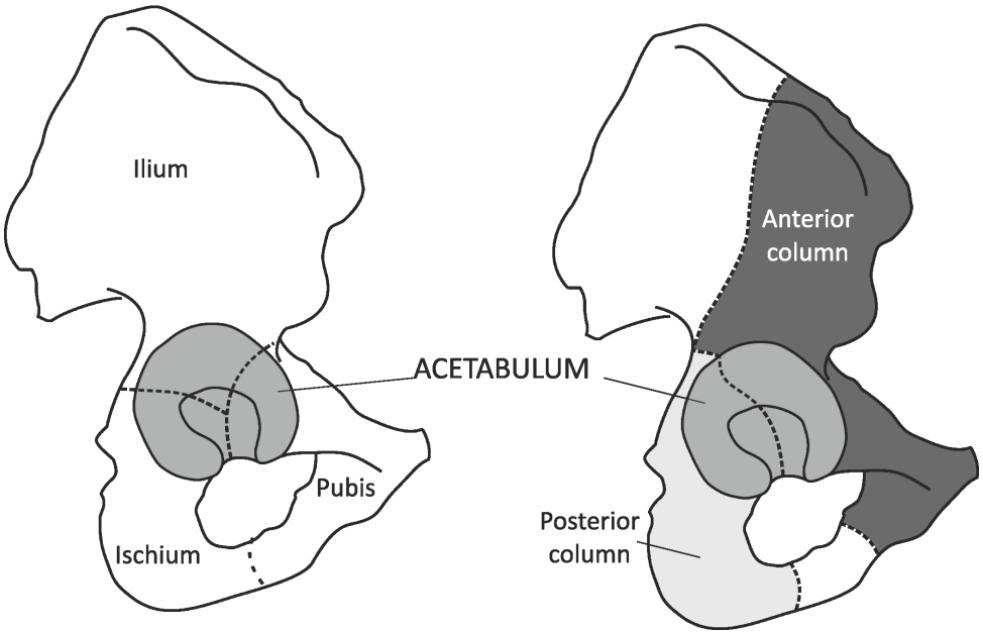

Figure 3: Sketch of pelvis showing lateral view of a) pelvic bones and b) anterior and posterior columns of pelvis. Author's own image, based on illustration from Gray (1918), and information from Nordin and Frankel (2001).

2.1.1 Soft tissue structures

Hip stability is augmented by the soft tissue structures of the joint - the joint capsule, capsular ligaments, glenoid labrum and hip joint musculature.

Joint capsule

The hip joint capsule is a strong, dense connective tissue structure that forms a supportive sheath around the articulating surfaces. One side is attached to the periphery of the acetabulum and the other side extends to cover the neck of the femur (Figure 4).

It is made up of two sets of fibres, longitudinal and circular, and the arrangement of these fibres gives the hip joint directional strength and contributes to the stability of the joint. The longitudinal fibres are greatest in amount at the upper and anterior capsule, where the greatest amount of resistance is required, and they are reinforced by accessory ligaments (iliofemoral, pubocapsular and ischiocapsular ligaments, as shown in Figure 4). Circular fibres are mostly found at the lower posterior part of the capsule, and form a collar around the neck of femur.

.

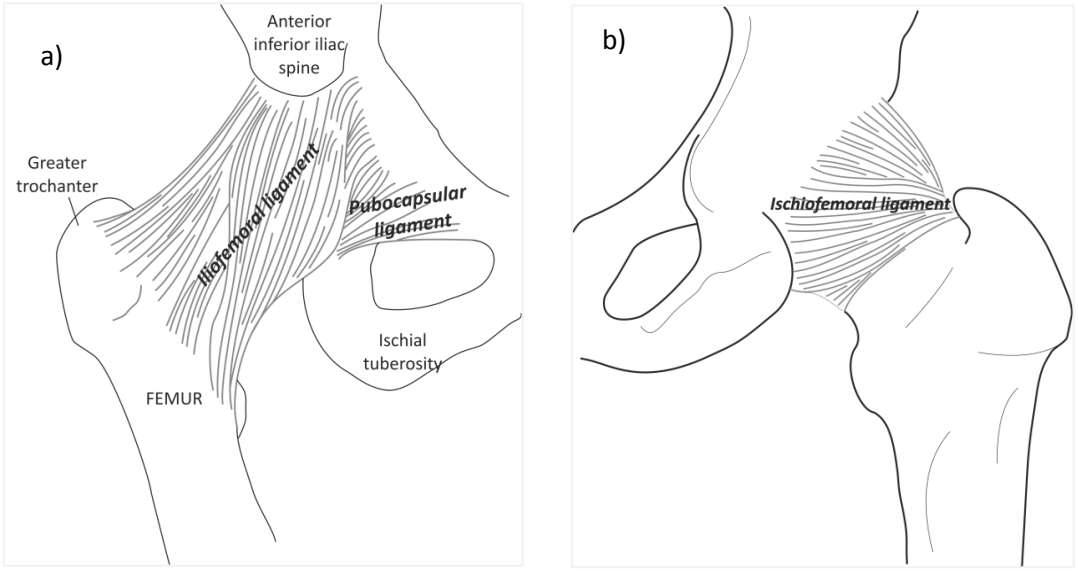

Figure 4: Right hip joint, showing joint capsule and capsular ligaments. a) Anterior view; b) posterior view. Author's own images, based on illustrations from Gray (1918).

The joint capsule also protects the joint, and encloses the space to allow synovial fluid lubrication. A soft-tissue layer called the synovial membrane lines the interior surface of the capsule. It has two layers – the subintima (outer layer) and intima (inner layer). Fibroblasts in the intimal layer manufacture hyaluronan and lubricin, the major components of synovial fluid. Intimal macrophages phagocytose (engulf and digest) cellular debris and pathogens from the synovial fluid.

Labrum

The glenoid labrum (shown in Figure 5) is a fibrocartilage rim on the margin of the acetabulum; deepening the joint cavity, increasing the coverage of the femoral head and increasing the joint's resistance to dislocation or subluxation. The labrum also acts as a seal preventing joint fluid from flowing in and out of the joint space.

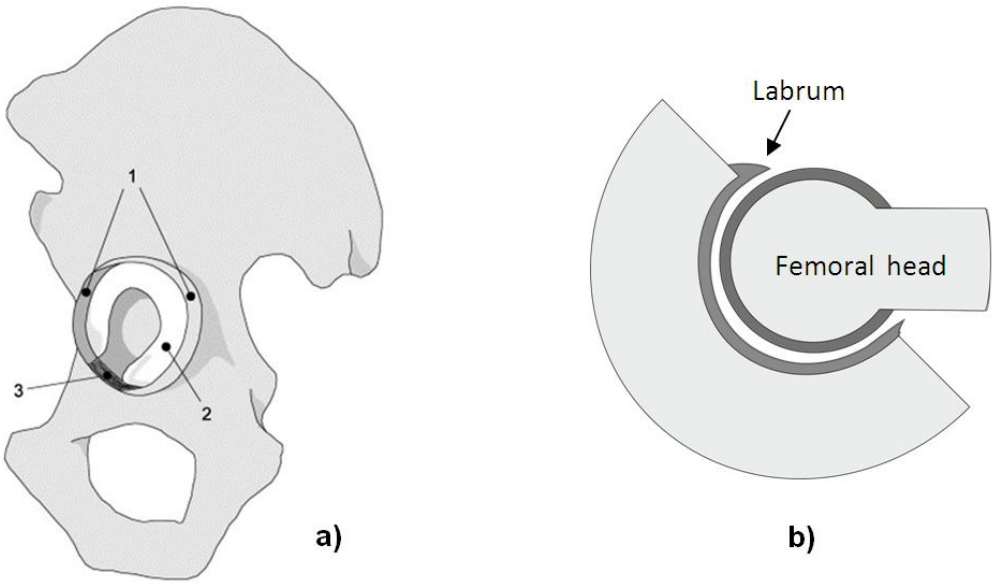

Figure 5: Image showing the function of the labrum. a) lateral view of pelvis, with the glenoid labrum (1), attached to the articular cartilage (2) and forming a complete rim with (3) the transverse acetabular ligament (image from Ferguson et al. (2000), with permission); and b) a sketch of the femoral head within the socket, indicating the position of the labrum around the femoral head.

Hip joint musculature

There are 17 muscles that control motion of the hip. These can be divided into groups based on function – extensors, flexors, abductors, adductors, external rotators and internal rotators. These groups of muscle contract at various times during the gait cycle and this contraction causes relative femoral movement as well as compressive forces of the head on the acetabulum. Some of the major muscles, and their actions, are described in Figure 6. The anterior view (a) shows the hip flexors (green), adductors (yellow), abductors (red), and external rotators (blue). The posterior views (b and c) show gluteal muscles, including abductor (red), extensor (purple), adductors (yellow), and external rotators (blue).

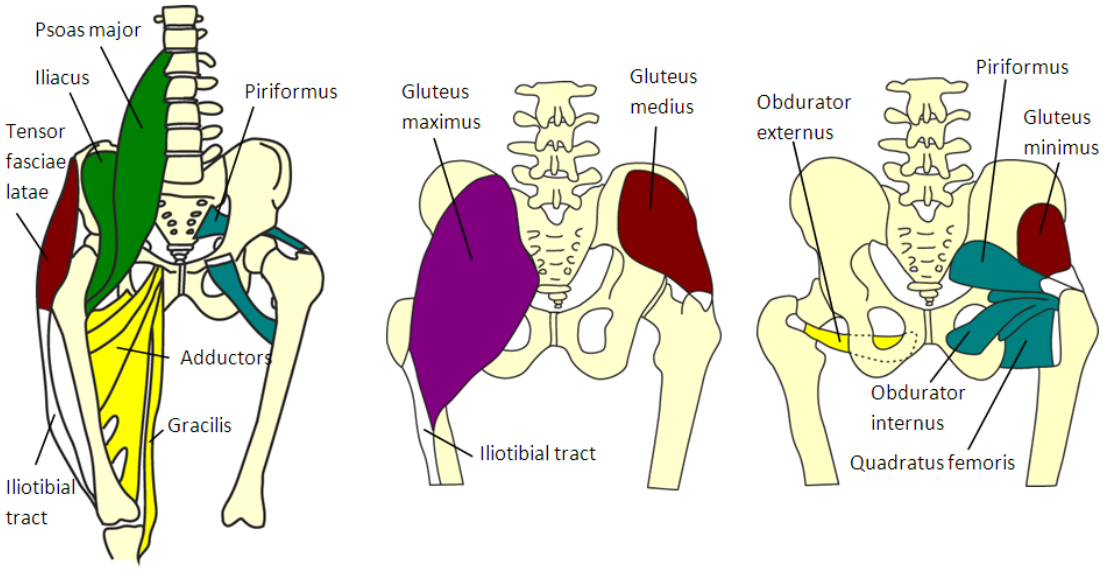

Figure 6: Diagrams showing the major muscles of the hip. Images modified by the author, from Wikipedia (2006) (public domain source).

Articular cartilage

Articulating surfaces of the femur and acetabulum are covered by a layer of articular cartilage (Figure 7). The articular cartilage surface of the acetabulum forms a curved half-moon surface that supports the load track of the femur during gait. This cartilage provides a low-friction, wear-resistant surface that facilitates load transfer and motion between articulating surfaces.

a) b)

Figure 7: Sketch showing articular cartilage (in grey) of the articulating surfaces; a) cartilage of the acetabulum, surrounding the acetabular fossa and b) cartilage covering the femoral head. Author's own images, modified from Gray (1918).

Healthy articular cartilage is formed from a hydrated extracellular matrix that is synthesised and maintained by a small population of chondrocytes. The matrix is made up of mostly collagen fibres and proteoglycans. The collagen forms a fibrous network, providing the structural framework of the matrix. Cartilage is permeable and saturated with interstitial fluid

(water). This fluid is concentrated near the articular surface and allows nutrient and waste transfer between chondrocytes and synovial fluid. When loaded in compression, up to 70% of the water may be exuded by the cartilage. This composition means that cartilage has viscoelastic, anisotropic and non-linear mechanical properties under load.

Collagen fibrils have high tensile strength, and are oriented parallel to the surface of the cartilage in the superficial zone, making the structure resistant to wear caused by the articulation of bearing surfaces. However cartilage is avascular and, once damaged, has limited capability for repair.

Synovial fluid

Synovial fluid is a viscous, non-Newtonian fluid that occupies the free space within the joint capsule. It is egg-like in consistency, and contains hyaluronan and lubricin as well as proteinases and collagenases. Synovial fluid is thixotropic, which means its viscosity decreases as the shear rate increases. This allows it to maintain lubrication while allowing joint motion during high levels of activity. As well as decreasing friction between the articulating cartilage surfaces, synovial fluid provides nutrients to joint tissues and acts as a shock absorber.

2.1.2 Joint Loading

The pelvis forms a rigid frame allowing the weight of the trunk and upper body to be transferred to the lower limbs. Load is transferred from the articulating surface of the acetabulum to the femoral head, through the femoral neck and metaphysis and then to the shaft of the femur. Load is supported by the microstructure of the bones – trabeculae in the pelvis and femur are oriented in a lattice that is strong in the direction of load. During gait, the head of the femur moves in the acetabulum, so the direction of the resultant force on the acetabulum also moves, as shown in Figure 8.

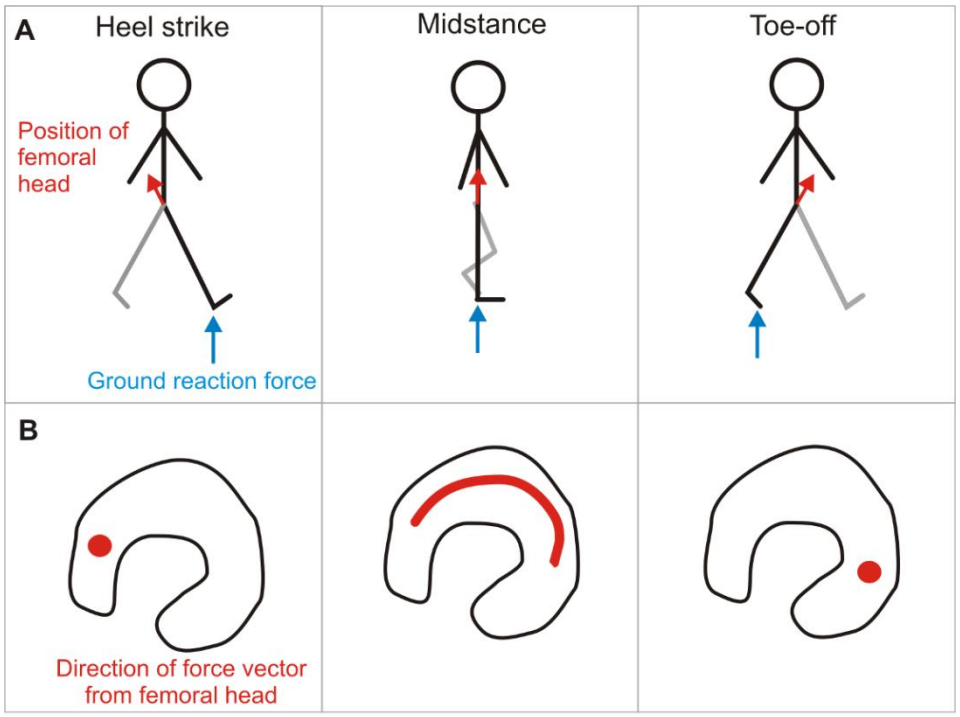

Figure 8: Schematic showing the position and direction of force acting on the lunate surface of the acetabulum at different points in the gait cycle. Author's own image.

This resultant force on the acetabulum is made up of the ground reaction force, transmitted through the bones of the leg, and muscle forces, as the action of muscle contraction during movement pulls the head of femur into the acetabulum.

2.2 Osteoarthritis

Osteoarthritis (OA) is a degenerative joint disease that affects articulating joints. The hip joint is a common site of osteoarthritis; according to a study from the United States, one in four people can expect develop symptomatic OA by the age of 85 (Murphy et al., 2010).

The exact causes and progression of OA are unclear but it is accepted that a variety of factors, including developmental, metabolic, and biomechanical factors, may initiate processes leading to a loss of articular cartilage in the joint. Identified risk factors for the development of osteoarthritis include a family history of OA, obesity, joint injury, and repetitive heavy joint loading (2007).

Osteoarthritis causes a softening, fibrillation, ulceration and loss of articular cartilage. It is also associated with sclerosis (increase in density) of subchondral bone and the growth of

osteophytes (bone spurs). Healthy articular cartilage increases the load-bearing surface area of the joint (thus reducing stress on underlying bone). When this surface degenerates, the growth of osteophytes occurs in response to the resulting higher bone loading, as the body attempts to increase the surface area and thus reduce peak loads on the bone. The synovial membrane and the joint capsule become thicker and the amount of synovial fluid can increase.

Clinical symptoms of OA may include joint pain, inflammation, tenderness, stiffness, and limitation of joint movement. If a patient's condition is not improved by medication, walking aids or other non-invasive techniques, a total hip arthroplasty (THA), commonly known as a hip replacement, may be performed.

2.3 Total hip arthroplasty

In 2011 there were 71, 672 primary hip replacement procedures recorded in the England and Wales National Joint Registry (NJR, 2012). In this procedure the articulating surfaces of the hip joint are replaced by new, highly polished bearing surfaces – the acetabular cup and femoral head (Figure 9).

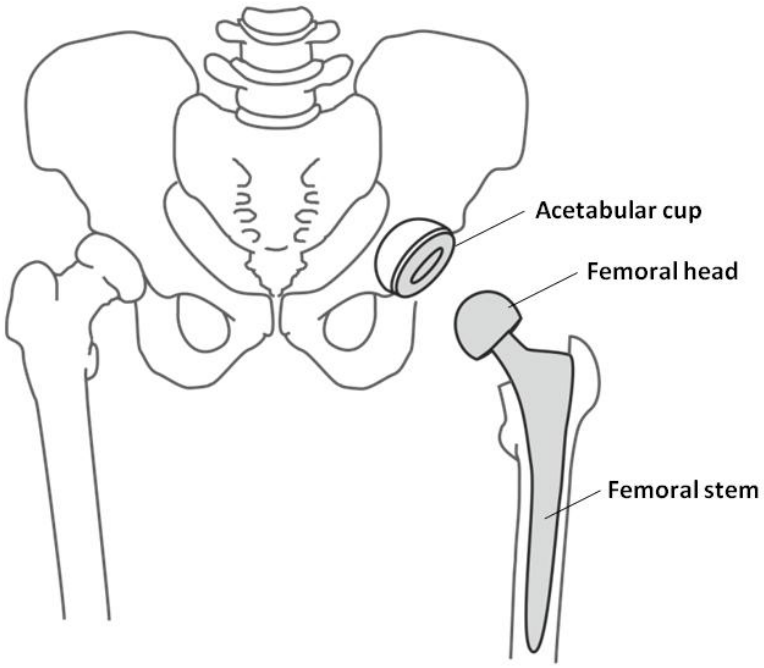

Figure 9: Image showing acetabular cup and femoral head position after total hip replacement. Author's own image.

The femoral head is supported by a stem that restores the offset of the femoral neck, and extends into the medullary canal of the proximal femur. The acetabular component replaces the damaged bearing surface of the acetabulum and restores acetabular alignment (version). An x-ray of a replaced right hip, with an arthritic hip on the contralateral side, is shown in Figure 10. In the performance of THA surgery, the hip joint is exposed by cutting or displacing surrounding muscles and dividing the joint capsule. The femoral head is dislocated and supporting ligaments are cut. The head is removed at the level of the greater trochanter, and the femoral canal is prepared for insertion of the femoral stem. The acetabular cavity is reamed, removing the remaining cartilage and creating a clean bone surface. The acetabular cup is then implanted, followed by the insertion of the femoral stem.

Figure 10: Radiograph showing the replaced right hip of a 61-year-old woman. The left hip shows radiological signs of osteoarthritis (joint space loss and progression of cystic changes). Image from Ritter et al. (1996), with permission.

Replaced bearing surfaces

Acetabular cups can be made of a single piece of ultra-high molecular weight polyethylene (UHMWPE), or modular cups with metal backing and an insert of PE, ceramic or metal. Femoral heads may be ceramic or metal, fixed to a metal stem. The different bearing combinations are outlined in Table 1.

Table 1: Bearing combinations used in THA(indicated by ● mark)

Cup material	Head material	
Cemented cups	Metal (CoCr)	Ceramic (Alumina)
Polyethylene (UHMWPE)	●	●
Uncemented cups		
Metal	●	
Metal backing, ceramic liner		●
Metal backing, PE liner	●	●

The current most common type of bearing combination used in THA in the UK is metal-on-polyethylene (MOP) - 64.4% of all primary procedures in the UK use this combination (2012), as shown in Figure 11. Over the last eight years there has been a significant reduction of metal-on-metal (MOM) articulation (due to adverse reactions and high revision rates) but a significant increase in the use of the ceramic-on-ceramic (COC) bearing (from less than 2,000 in 2003 to nearly 17,000 in 2011). Hip resurfacing has declined from 4,350 cases in 2009 to just 1,801 cases in 2011.

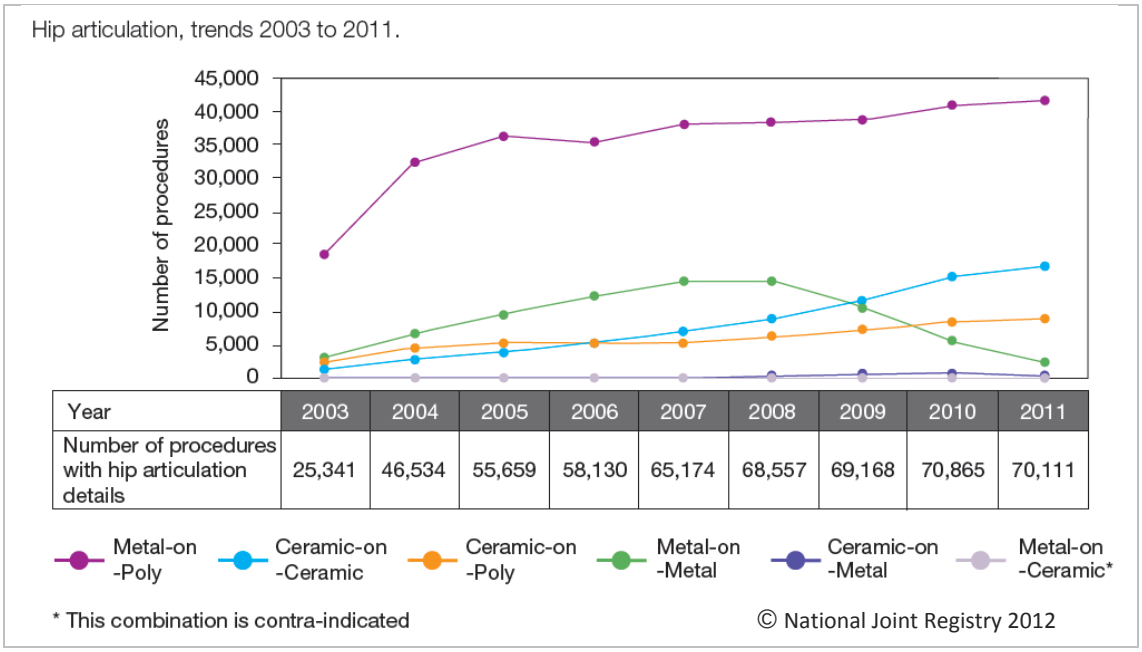

Figure 11: Bearing surface trends in the UK, 2003-2011. Image from the National Joint Registry, NJR (2012), with permission.

Components for use in THA may be cemented (fixed into the body with polymethylmethacrylate (PMMA) bone cement), or uncemented (with mechanical or biological fixation). This will be discussed further in subsequent paragraphs.

Component fixation

In total hip arthroplasty, components are secured in the body either with bone cement (cemented fixation) or with mechanical fixation such as screws or the ingrowth of bone (uncemented fixation). A combination of cemented and cementless components (hybrid fixation) is also used. Resurfacing prostheses are also used, where the bearing surfaces are replaced but more bone is conserved due to smaller implant dimensions. The proportion of cemented and cementless implants has plateaued in the UK over the last 2 years, after a decrease in cemented and increase in cementless operations from 2005-2009 (as shown in Figure 12). Hybrid fixation has shown a slight increase, and resurfacing and large head MOM implants have decreased. The following paragraphs introduce these fixation methods (illustrated in Figure 13) in more detail.

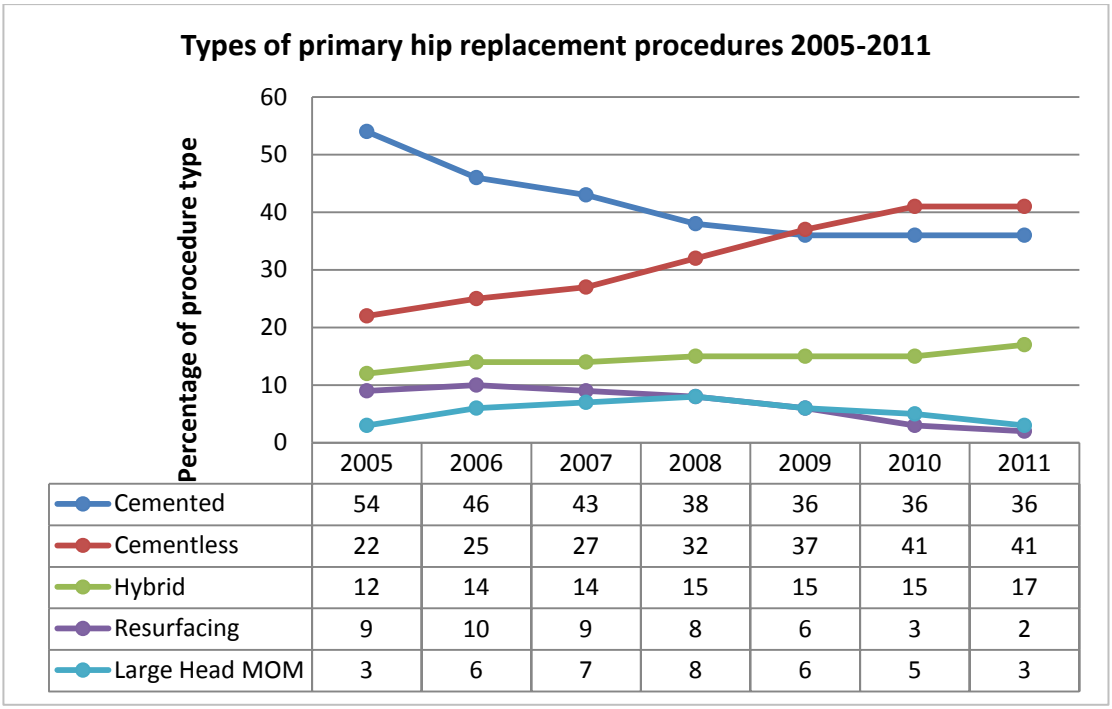

	2005	2006	2007	2008	2009	2010	2011
Cemented	54	46	43	38	36	36	36
Cementless	22	25	27	32	37	41	41
Hybrid	12	14	14	15	15	15	17
Resurfacing	9	10	9	8	6	3	2
Large Head MOM	3	6	7	8	6	5	3

Figure 12: Trends in primary hip replacements 2005-2011. Data obtained from the UK National Joint Registry (NJR, 2012)

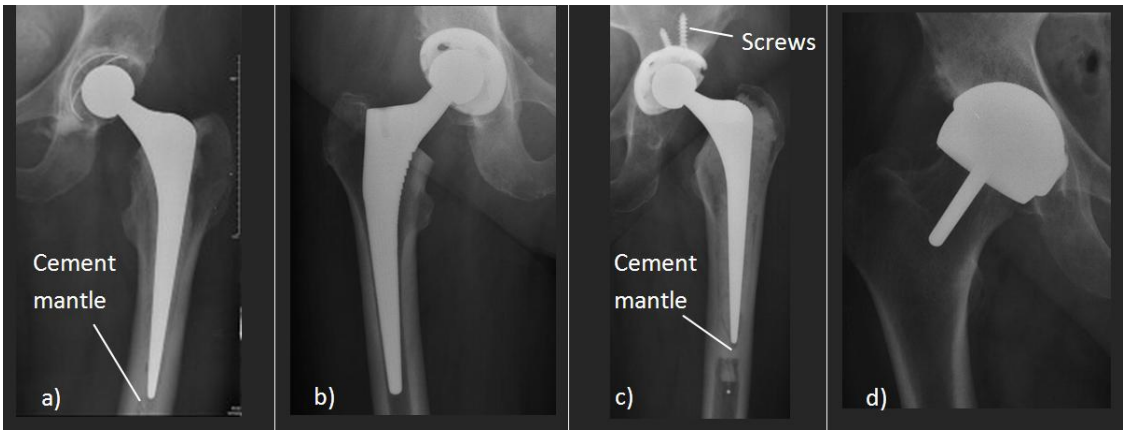

Figure 13: Anteroposterior radiographs showing different fixation methods: a) cemented Exeter hip b) uncemented Corail stem; c) hybrid fixation with cemented stem and uncemented cup (with screws); and d) hip resurfacing. Images from Pluot et al. (2009), with permission.

Cemented fixation

In cemented fixation, PMMA bone cement is used to fix components to the supporting bone structures. Cement is placed in the prepared cavity before component insertion and pressurised for maximum fixation strength. Cement fixation is achieved through macrolocking (cement extending into drilled holes) and microlocking (interdigitation of cement into cancellous bone), shown in Figure 14.

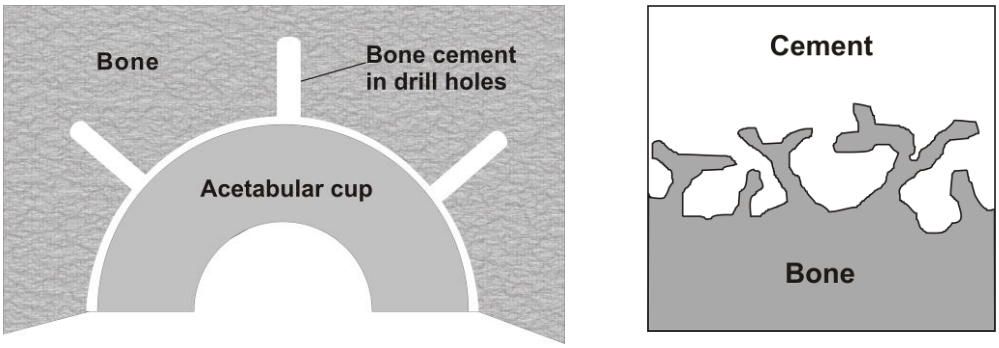

a) b)

Figure 14: Cement macrolocking and microlocking. a) Schematic showing cemented cup with drill holes for extra fixation. b) Schematic showing interdigitation of cement into interstices of bone.

A robust cement mantle is critical to the successful fixation of a cemented cup. The amount of interdigitation of the cement with bone affects the strength of the cement-bone interface (Mann et al., 1999, Flivik, 2005). Good initial cemented fixation is dependent on technical factors – the surgical preparation of the bone bed, the effective preparation, pressurisation

and penetration of cement (Papagelopolous and Morrey, 2003) and the correct selection and positioning of acetabular implants.

Uncemented fixation

Most uncemented acetabular cup systems consist of a metal shell coupled with a polyethylene (PE) or ceramic liner (NJR, 2012). Secure uncemented fixation relies initially on the press-fit principle (Macdonald et al., 1999), or the presence of screws or other mechanical coupling, and then on the progression of bone ingrowth into the implant.

Press-fit cups have a flattened hemispherical shape, and are 1-2mm larger than the size of the acetabular cavity, to use the pre-load between load and bone for initial implant stability (illustrated in Figure 15). Press-fit requires good quality acetabular bone (Morscher, 1992), as this implant shape causes high compressive force at the cup periphery (although not at the dome of the acetabulum).

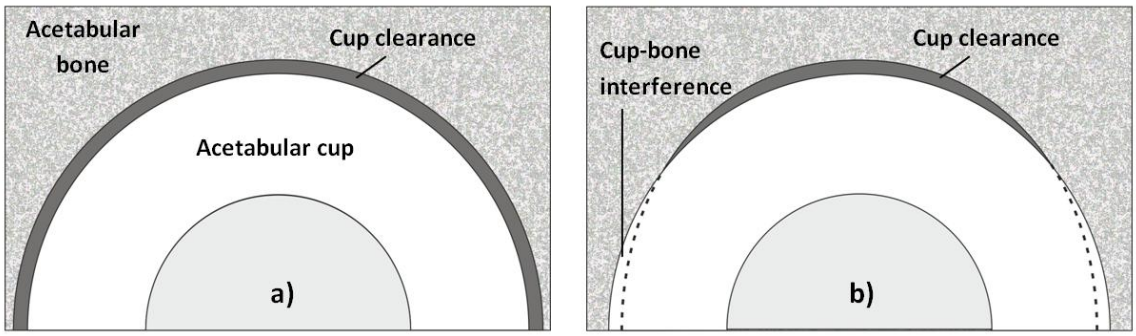

Figure 15: Image showing (a) cup fit without press-fit dimensions and (b) press-fit cup with implant wider than acetabular cavity.

The initial stability provided by press-fit or screws allows bone ingrowth to occur at the surface of the implant. For bony ingrowth to occur, there must be adequate contact between the component and bone (Harris et al., 1976) and adequate mechanical stability (Kienapfel et al., 1999). Uncemented components have a porous-coated surface (shown in Figure 16a) that allows the ingrowth and interconnection of bone tissue. In well-functioning uncemented acetabular cups, bone ingrowth into the porous coating has been shown to occupy an average of 32% of the surface (Engh et al., 1993).

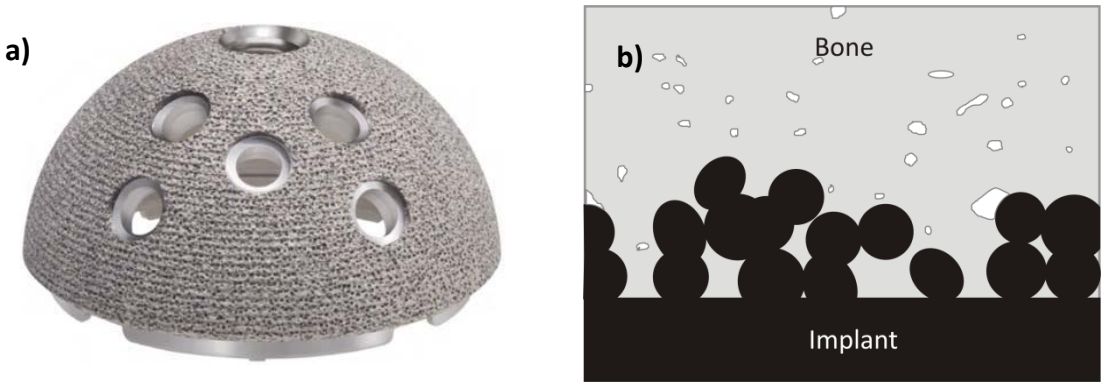

Figure 16: Images showing porous-coated implant and interactions with bone. a) Stryker Tritanium acetabular shell, with a titanium porous coating for bone ingrowth; b) illustration of bone ingrowth into porous-coated femoral stem (based on a high-magnification image of a transverse histological section at the level of the lesser trochanter, three years after operation. (Engh et al., 1987).

Bone remodelling

Long-term uncemented fixation depends on the ingrowth of bone into the porous surface of the implant. This ingrowth occurs through the process of bone remodelling – the process by which bone tissue is removed and replaced. This remodelling is facilitated by osteoclasts, bone cells which remove bone tissue, and osteoblasts, cells which build bone matrix and induce mineralisation of this matrix. The activity of these cells is mediated by chemical signals, and the process of remodelling occurs in several stages – activation, bone resorption, reversal and bone formation. These stages are illustrated in Figure 17.

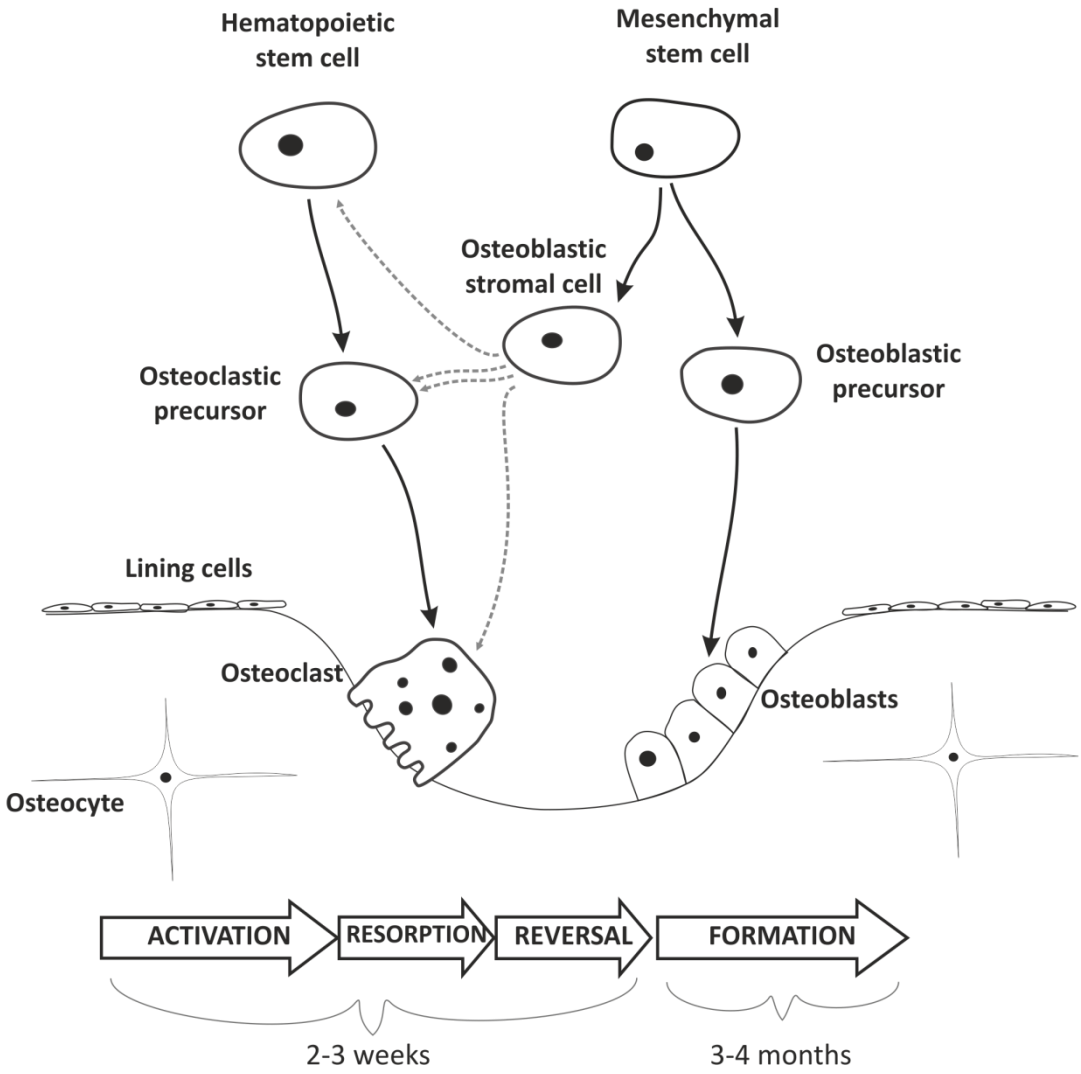

Figure 17: Image showing cells involved in bone remodelling. Image author's own, based on an illustration from Carmona (2004).

The activation phase involves cells from the osteoblast lineage acting on hematopoietic cells to cause them to differentiate into osteoclasts, which, when activated, can fasten onto the bone, and seal off an area to be resorbed. The activated osteoclast forms a ruffled border, which secretes hydrogen ions to dissolve the mineral phase of the bone, and packets of enzymes to break down the matrix. After resorption, a brief reversal phase occurs, in which a thin layer of protein forms on the resorbed surface, to help form a strong bond between the old bone and the newly-formed bone. Following this, in the formation phase, the osteoblasts begin to lay down new bone, by producing the collagen that forms the bone matrix, as well as the calcium- and phosphate-rich mineral phase. Some osteoblasts are buried in the matrix and form osteocytes, which form part of the network that allows bone to respond to mechanical load. Other osteoblasts remain as thin lining cells on the surface of the bone. Bone formation

occurs over a much longer time period (3-4 months) than the preceding phases (activation, resorption and reversal occur over 2-3 weeks).

If the action of osteoclasts and osteoblasts is not balanced, either too much bone is produced, or not enough bone is replaced, causing a net bone loss. The osteoclast activation leading to this bone loss is caused by chemical signals, described in further detail in section 2.6.

Hybrid implants

Hip arthroplasty procedures with a cemented stem and cementless acetabular cup are termed hybrid implants. Reverse-hybrid implants (with a cementless stem and cemented cup) have also been used but are much less common (15% of hybrid implants, compared to 85% standard hybrid in 2011 (NJR, 2012)).

Resurfacing

Hip resurfacing was developed to preserve more of the remaining bone of the femur and acetabulum, to allow provision for future surgeries, especially for younger patients. Resurfacing prosthesis use MOM bearings and hybrid fixation, and the short femoral component and thin acetabular surface require minimum bone to be removed (Schmalzried, 2007). However local adverse tissue reactions and high failure rates have been reported with this technique and a reduction in the use of these implants has been observed since 2009 (NJR, 2012).

Selection of fixation type

The average age of THA patients in the UK was 67.2 years in 2011 (NJR, 2012). Despite the trend observed in other countries that hip replacement patients are getting younger ((Garellick et al., 2010)), the UK joint registry data describe a very consistent age range of THA patients over the last eight years (NJR, 2012). Different fixation methods and different types of hip replacements are recommended for different patient demographics ((NJR, 2012)) Although recent joint registry data and meta-analyses have suggested no difference in outcome between cemented and cementless implants in young people (Hailer et al., 2010, Morshed et al., 2007), uncemented prostheses are more commonly implanted in younger patients, while older patients more commonly receive cemented prostheses. The graphs in Figure 18, using data from the UK's National Joint Registry, show the percentage of each procedure type for males and females in different age groups.

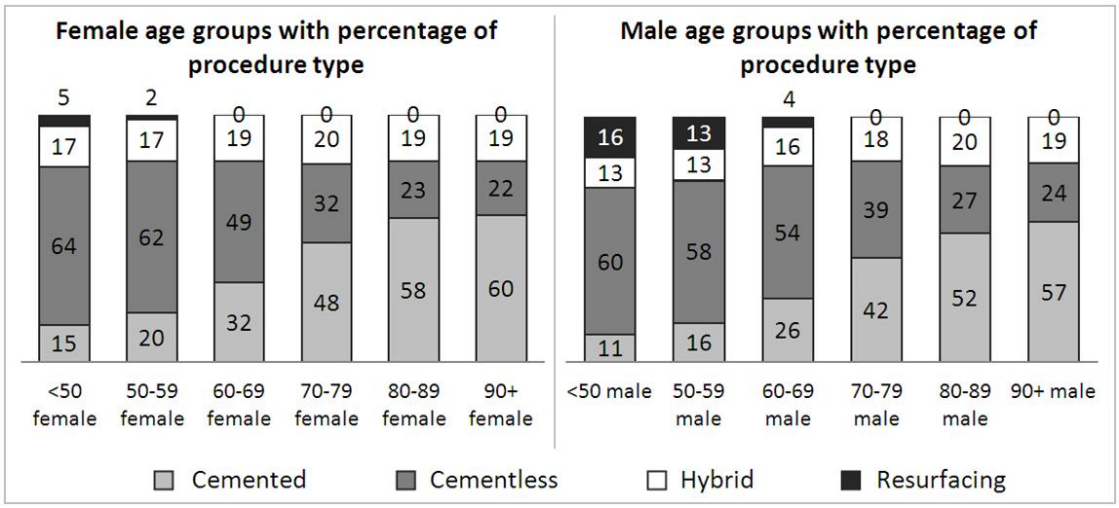

Figure 18: UK Joint Registry data on implant types by age group. Graph produced using data from the UK National Joint Registry data (NJR, 2012).

2.4 Failure of THA

Despite improvements in component design and operative technique over the years, revision surgery (where one or both components are removed and replaced) still made up 11% of hip replacement procedures in the UK in 2011 (NJR, 2012), and similar figures are seen in other countries' hip registers (10-12% in Sweden, 12.5% in Australia, 10.8% in Canada, 13% in New Zealand) (AOA, 2012, Garellick et al., 2010, NZOA, 2012, CJRR, 2012). Revision surgery is performed to treat infection, joint pain and implant loosening. A total of 8,639 hip revisions were reported in the UK in 2011. In single-stage revisions, both cup and stem were removed in 45% of cases, the acetabular component in 30% and the femoral stem in 15% of cases. Survivorship studies agree that the acetabular component is twice more likely to require revision than the femoral component (Clohisy and Harris, 1999, Schulte et al., 1993, Ritter et al., 1990, Mulroy and Harris, 1996, Williams et al., 2002).

Apart from the detrimental effects for the patient, the requirement for revision surgery places a higher burden on healthcare providers (NHS hospitals performed 84% of all hip revision procedures in 2011 (NJR, 2012)). Revision rates have been predicted to double by the year 2026 (Kurtz et al., 2007).

For many years, the most common cause of acetabular revision has been aseptic loosening (Schulte et al., 1993, Mullins et al., 2007, Hamadouche et al., 2002, Mulroy and Harris, 1996, Stauffer, 1982, Harris and Penenberg, 1987, AOA, 2012, Garellick et al., 2010, CJRR, 2012, NJR, 2012), the loosening of prosthetic components in the absence of infection.

2.5 Aseptic loosening

Aseptic loosening (loosening in the absence of infection) is the biggest cause of failure in THA worldwide and the acetabular component is more likely to fail than the femoral component. Survivorship studies agree that the acetabular component is twice as likely to require revision compared to the femoral component (Clohisy and Harris, 1999, Schulte et al., 1993, Mulroy and Harris, 1996, Ritter et al., 1990, Williams et al., 2002). Using roentgenographs, a loose acetabular cup can be identified by cup migration, cement fracture or radiolucency around the cup (Schmalzried et al., 1992b).

This aseptic loosening can be caused by poor initial fixation, or a subsequent adverse change in component fixation. This loss of fixation can be caused by the active resorption or dissolution of bone tissue, termed osteolysis.

To reduce the incidence of acetabular cup loosening, and subsequent THA failure, it is important to understand the conditions under which osteolysis occurs. The following sections will explore the current knowledge of the origins and progression of osteolysis following total hip arthroplasty.

2.6 Osteolysis

Osteolysis refers to an abnormal resorption or dissolution of bone tissue and has emerged as the dominant postoperative problem in total hip arthroplasty (Harris, 1995). Osteolysis is often asymptomatic and may not present with symptoms until significant bone loss and cup loosening have occurred (Baker et al., 2009). Once known as 'cement disease', osteolysis has been proven to occur in both cemented and uncemented components, with different presentations, as described in subsequent paragraphs.

Presentation and detection of acetabular osteolysis

Osteolysis is a progressive condition, generally appearing in the hip joint 5-10 years after surgery (Harris, 2001, Garcia-Cimbrelo and Munuera, 1992, Willert et al., 1990). Symptoms can include groin pain and decreased range of motion in the hip joint, as well as acetabular fracture. However osteolysis is often asymptomatic and so the visualisation of the hip joint is valuable in the detection of the condition. Following total hip arthroplasty, the patient is required to return for follow-up exams to monitor the condition of the joint. In the UK, these

exams are routinely performed 6-12 weeks post-surgery, 12 months after surgery, and subsequently every five years. During these exams radiographs are taken to assess component position and fixation.

Radiological signs of osteolysis include a well-defined border between the implant and the bone, or the presence of a bone defect that can be clearly outlined (as shown in Figure 19). (Engh et al., 2002) Although follow-up radiographs are the standard practice for follow-up exams, several groups have shown radiographs can underestimate the extent of osteolysis, and that 3D computed tomography is a more effective assessment tool (Robertson et al., 1998, Zimlich and Fehring, 2000, Walde et al., 2005).

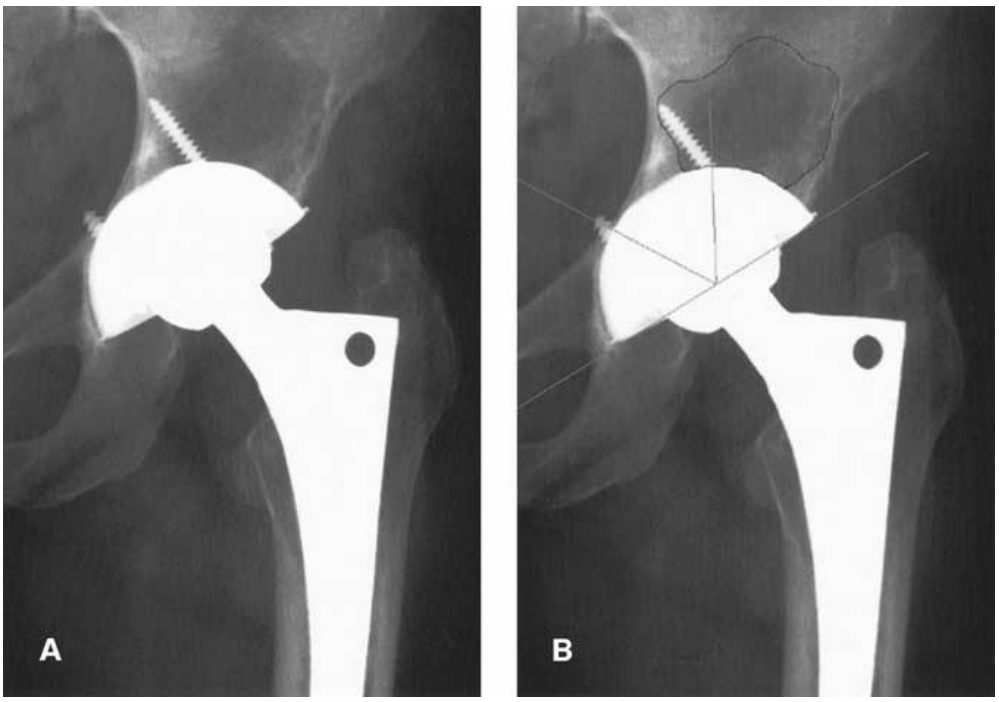

Figure 19: A) Anteroposterior radiograph of a hip believed to have osteolysis; B) A radiograph of the same patient, with the osteolytic lesion outlined by a surgeon. Image from Engh et al. (2002), with permission.

Osteolysis and cemented fixation

In cemented sockets osteolysis generally presents as linear resorption between the cement and the bone, beginning at the periphery and progressing towards the dome of the cup, as shown in Figure 20.

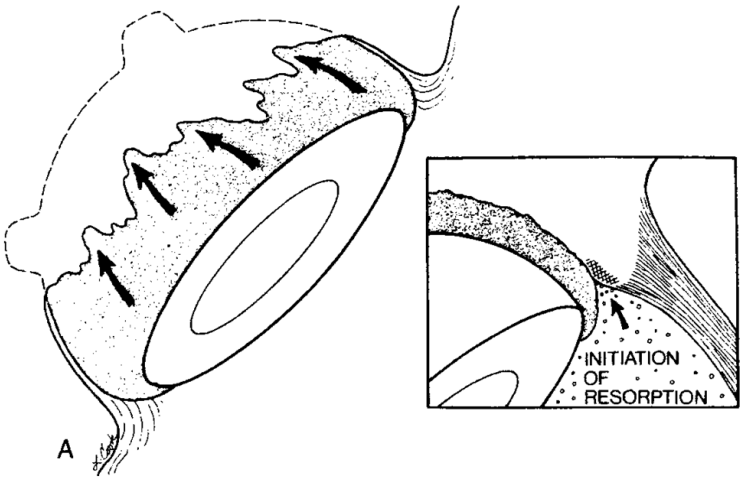

Figure 20: Schematic showing progression of linear osteolysis. Image from Schmalzried et al. (1992b), with kind permission from Springer Science+Business Media B.V..

Osteolysis and uncemented fixation

Osteolysis in cementless cups generally develops in the form of expansile ballooning lesions (Maloney et al., 1999) which may be present in apparently well-fixed implants (see Figure 21). Although this focal osteolysis may be asymptomatic and the implant may remain stable, the progression of pelvic lesions can lead to acetabular fracture. In a radiographic assessment of twenty-three hips with pelvic osteolysis, the average size of lesions behind acetabular cup was around 2.4 x 1.9 cm; the largest single lesion was 7 x 5 cm (Schmalzried et al., 1998).

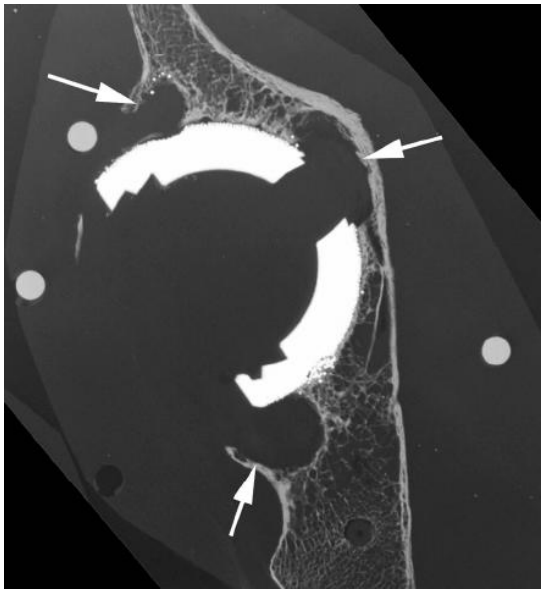

Figure 21: a) slab radiograph of a sectioned cadaver specimen, showing areas of expansile osteolysis (indicated with arrows). Image from Leung et al. (2005), with permission.

Two groups using the same acetabular reference system have used computed tomography (CT) to assess periacetabular osteolysis in cementless cups at autopsy (Leung et al., 2005, Kitamura et al., 2005) and at clinical follow-up (Egawa et al., 2009a). These results differ (shown in Table 2), especially in the lesion size and the occurrence of lesions at the centre of the cup, but they agree that the majority of lesions occur in the superior-inferior axis.

Table 2: Position of lesions from two different CT studies. Image of the hip from Kitamura et al. (2005); superimposed data from Egawa and Kitamura.

Study	(Kitamura et al., 2005)	(Egawa et al., 2009a)
Results	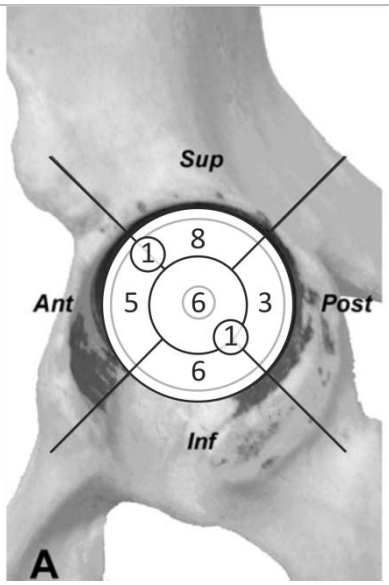	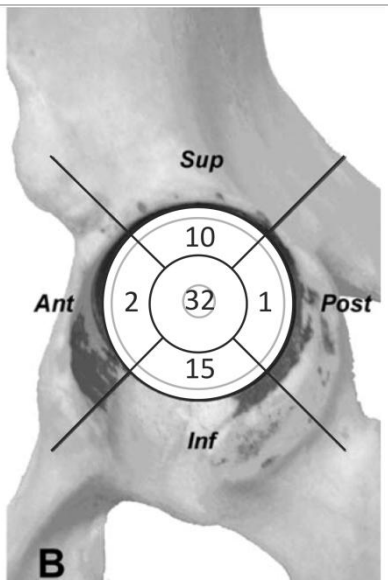
Number of hips	44	34
Average lesion size	5.6 ± 11.4 cm^3 (range, 0.3-54.6 cm^3)	24.5 ± 18.9 cm^3 (range, 1.1-73.3 cm^3)

Cell activity leading to osteolysis

Osteolysis is caused by the action of osteoclasts resorbing bone at a rate greater than that of the new bone production by osteoblasts. This imbalance in the bone remodelling process is caused by the increased activation of osteoclasts, as described in section 2.3, Figure 17.

Figure 22 shows the effects of hormones and local factors on osteoclast activation. The osteoblastic stromal cell produces several proteins that regulate osteoclast formation, including *macrophage colony stimulating factor* (m-CSF), which acts on its receptor (c-fms) to increase the number of precursor cells available to form osteoclasts. The osteoblastic cells also produce the protein called *receptor activator of nuclear factor kappa B ligand* (RANKL),

which can bind to a receptor (RANK) on the osteoclast precursor cells, stimulating osteoclast differentiation and proliferation. These osteoblastic cells also produce osteoprotegerin (OPG), a protein that can bind to RANKL, blocking its interaction with RANK and therefore blocking the formation of osteoclasts. When stimulated by hormones and local factors (shown on the left), the osteoblastic cell increases production of RANKL and decreases production of OPG, causing an increase in osteoclast activation and causing a net imbalance between bone resorption and production. The ways in which osteoclasts can be activated in the hip joint after THA, outside of the normal remodelling process, will be discussed in the following sections.

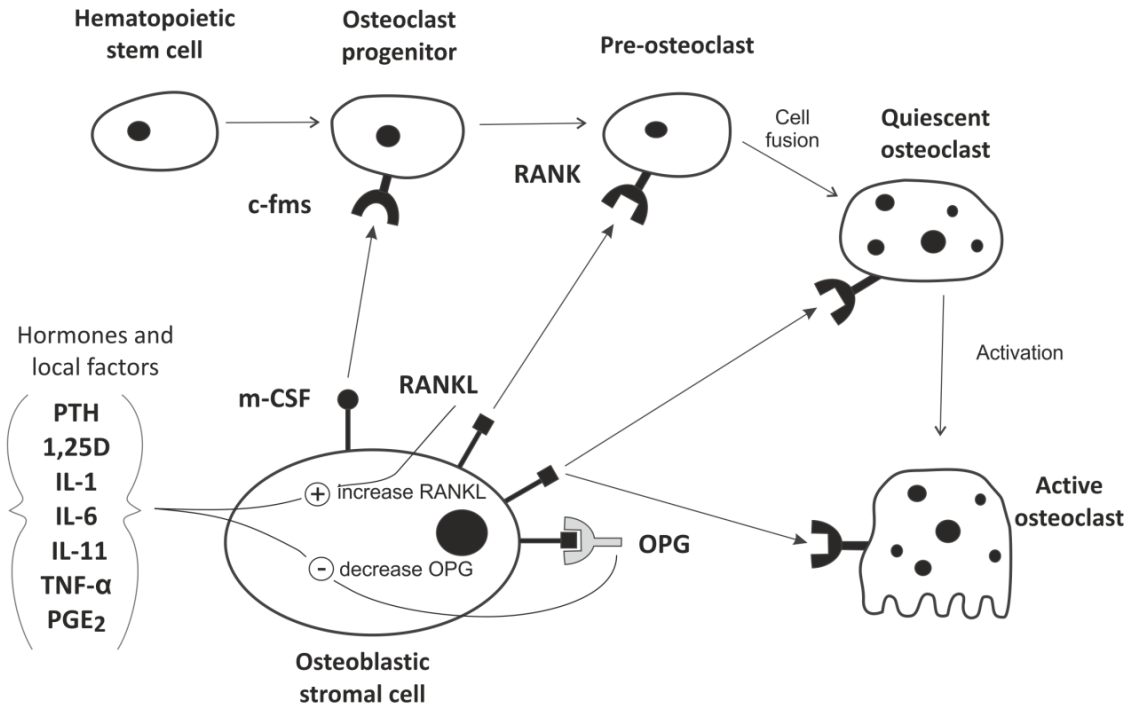

Figure 22: The activation of osteoclasts by the presence of RANKL. Image author's own, based on an illustration from Carmona (2004).

It is necessary to understand the processes in which these factors are produced, and the mechanisms by which loosening and osteolysis can occur. This knowledge will allow osteolysis-reducing component design modifications and operative changes to be identified, improving the outcomes for both the patient and the healthcare system. There are two central theories for the causes of osteolysis: wear debris and fluid pressure.

2.7 Wear debris

The production of wear debris and the body's response to the presence of wear particles have been extensively researched (Howie et al., 1988, Murray and Rushton, 1990, Horowitz et al., 1993, Landgraeber et al., 2008, Garcia-Cimbrelo and Munuera, 1992, MacQuarrie et al., 2004, Koseki et al., 2005) to determine the mechanisms of this bone loss and possible ways to prevent this.

The presence of wear debris can cause implant failure by initiating an inflammatory response in the joint. The immune response is dependent on particle characteristics– shape, size, particle material composition, surface properties and amount of wear (Ingham and Fisher, 2000, Koseki et al., 2005) (Kubo et al., 1999). This response involves the mononuclear phagocyte system, which acts to detect, engulf and dissolve foreign material, in a process called phagocytosis. Macrophages arise from bone-marrow-derived monocytes in the blood, and are activated when foreign bodies are detected. This activation involves the macrophage enlarging, to engulf and destroy the foreign material. Macrophages release a range of chemical signals during this process, including cytokines and mediators involved in the activation of osteoclasts, such as IL-1, IL-3, IL-6, TNF-α, and PGE_2 (Ingham and Fisher, 2000). As shown in Figure 22, these factors stimulate osteoclast differentiation and activation, leading to an imbalance in the bone remodelling process and a net bone loss. This debris-induced bone loss can compromise the fixation of the implant, and leading to loosening and failure (Amstutz et al., 1992).

Production of debris particles

A relative sliding motion between the prosthetic head and cup under cyclic load can cause the erosion of material from one or both surfaces. When undergoing relative motion under stance load, the presence of surface asperities may cause microscopic adhesions between cup and femoral head, which can become plastically deformed and welded together. The continued surface motion causes this weld to break and wear particles are produced. These wear particles can remain between articulating surfaces, as abrasive particles which can continue to remove material from the prosthetic surfaces under dynamic load. Other particles such as debris from surgical instruments and bone particles have also been observed, which could contribute to further wear as third-body particles between bearing surfaces.

Clinical studies of debris and osteolysis

Clinical studies of debris and osteolysis have shown that the presence of wear particles in the replaced hip joint is linked to the presentation of osteolysis. Acetabular osteolysis has been investigated in a study of specimens retrieved from 32 THA patients with areas of periprosthetic bone loss (23 from reoperations and eight from autopsy) (Schmalzried et al., 1992a). In all subjects, intracellular wear debris was found in macrophages which were present at the osteolytic region, with the number of macrophages in a direct relationship with the degree of bone resorption. A similar study of 18 THA patients during revision surgery found a significantly higher concentration of PE wear particles in osteolytic areas (Kobayashi et al., 1997).

Animal models of debris and osteolysis

Animal models have shown that the introduction of particles to joints *in vivo* can cause bone resorption. The presence of PE particles in a rat knee has been shown to cause a chronic immune response, including periprosthetic bone loss, in weight-bearing tests (Allen et al., 1996) and non-weight bearing studies (Howie et al., 1988). In a rabbit model, other wear particles (cobalt-chromium alloy, stainless steel alloy, alumina and titanium alloy, as well as UHMWPE) have been introduced to the knee joint (Kubo et al., 1999), causing different degrees of macrophage activity. UHMWPE, cobalt-chromium and stainless steel induced more severe tissue reactions than titanium and alumina ceramics. The effects of these particles on animal joints was found to be dependent on the stability of the implant. In a rat model, the presence of PE particles did not affect the interface fixation of a stable osseointegrated implant in the rabbit knee, and in a canine model, PE particles were found in greater amounts around Ti prostheses compared with the HA-coated implants (which had a higher percentage of bone ingrowth after 12 months). These studies indicate the need for access to periprosthetic space for the immune system to react to the presence of particles (this will be discussed in further paragraphs).

Cell culture models of debris and osteolysis

In-vitro biological studies have investigated the reaction of cells to the presence of wear particles. Mouse macrophages have been cultured in the presence of various debris particles (high density PE, PMMA), and results showed that the presence of debris causes macrophages to express PGE_2. (Murray and Rushton, 1990) and can increase osteoclastic differentiation and activity (Anderson et al., 2001) Similarly, culture of human bone-marrow macrophages with retrieved prosthesis-derived wear particles showed that particles induce macrophages to increase TNF production, which stimulates differentiation of cells to the osteoclast phenotype

(Merkel et al., 1999). These cell culture models show that the presence of wear debris causes macrophages to produce hormones and local factors that induce osteoclast differentiation and proliferation, adding to the theory that wear debris causes osteolysis.

Wear rate and osteolysis

Many studies have investigated the role of debris particles and the rate of wear in osteolytic THA failure. The effects of wear rate on osteolysis appear to be affected by the bearing surface material. Schmalzried and colleagues observed a direct relationship between volumetric wear and decreased implant fixation stability; from a review of the literature they suggest a hip bearing wear rate of 0.1 mm/y as a wear threshold for polyethylene (Schmalzried et al., 1992b). However a study of osteolysis in the hips of 28 patients with ceramic-on-ceramic bearings, using radiographs and CT scans, showed no correlation between wear volume and osteolysis volume (Hernigou et al., 2009). Clinical studies using radiographs to assess osteolysis have found high wear rates correlate with the development of osteolysis; however similar studies using CT methods of assessment have produced conflicting results (Egawa et al., 2009b).

Wear has been reported in many radiologically- and clinically-stable hips – if wear was the only cause, more of these worn hips would show some degree of loosening. Manley et al (2002) performed a clinical study on 322 patients at 10 years follow-up, which showed no correlation between wear rate and revision rate for loosening and no correlation between wear rate and revision rate for osteolysis. The cup type with the highest loosening rate (HA-coated press-fit component) did not have notable wear compared to the other groups. In a randomised study of THA patients with cross-linked and non-cross-linked PE cups (Leung et al., 2007), the wear rate in patients with osteolysis was well below the threshold of 0.1mm (0.03 ±0.05mm/year).

Although there is compelling evidence that the presence of wear debris particles can stimulate osteolysis, there is evidence to suggest this is not the only factor to cause this bone loss.

Loosening as a cause of wear

Some groups argue that loosening could be the cause, rather than the result, of these wear processes. For example, a loose component can potentially generate more particulate debris, as relative motion can cause a higher rate of abrasive wear of bone and implant surfaces (Bischoff et al., 1994). Debris particles may arrive at the prosthesis-bone interface secondary

to implant loosening, caused by early loss of fixation (Mjoberg, 1994, Aspenberg and Herbertsson, 1996).

Micromotion

Micromotion can be described as a recoverable movement of the implant relative to the surrounding bone. This micromotion can be caused by poor initial fixation, or a modulus mismatch between the stiff prosthetic components and the more flexible acetabular bone. The degree of micromotion varies according to the fixation method and location of measurement (Won et al., 1995). If the micromotion has a high enough amplitude it can impair bone growth (Perren, 2002, Goodman, 1994), further contributing to the loss of bone around loose prostheses.

Bone deformation during loading may allow micromotion at the bone-implant interface to occur (Massin et al., 1996). The deformation of an implanted cup due to loading may also facilitate micromotion. Joint subluxation and relocation with impact can cause micromotion between the acetabular cup and the PE liner in modular components (Amirouche et al., 2008).

Micromotion indicates an interface gap and therefore a channel of access to periacetabular bone; this will be explained in further paragraphs. In addition, a canine model of micromotion has shown that implant micromotion dramatically increases the inflammatory response in the joint (Jones et al., 2001). As well as activating macrophages, micromotion may increase production of particulate debris due to increased relative movement between implant surfaces.

This micromotion may also allow fluid and particle access to periprosthetic spaces. Fibrous membranes are most commonly present at the periphery of acetabular implants (Schmalzried et al., 1992b), possibly developing as a reaction to this micromotion. The physical presence of this membrane may then contribute to further implant micromotion.

The introduction of particles into various *in vivo* animal models has failed to reproduce the bone-loss effect (Aspenberg and Herbertsson, 1996, Van der Vis et al., 1998b). The contribution of wear particles to osteolysis and implant failure cannot be ignored; however other factors must also be investigated. Another theory of implant loosening is that waves of fluid pressure within the joint can initiate damage to the retroacetabular bone. Intracapsular

fluid pressure, and its potential role in osteolysis and aseptic loosening, has been investigated using various clinical and laboratory methods, described in the next section.

2.8 Fluid pressure and osteolysis

Several studies have put forward the theory that increased fluid pressure in the joint space can cause, or contribute to, osteolysis (Van der Vis et al., 1999, Van der Vis et al., 1998b, Skoglund and Aspenberg, 2003a, Skripitz and Aspenberg, Aspenberg and van der Vis, 1998, Evans et al., 2006b, van der Vis et al., 1998a). This increase in fluid pressure may be caused by joint effusion, or the movement of a loose component within the joint capsule. High fluid pressures in the joint may prevent adequate blood perfusion and cause osteocyte death, leading to pressure-induced necrosis and resorption of bone (Skripitz and Aspenberg, 2000, Aspenberg and van der Vis, 1998). High cyclic fluid pressure can also increase the synthesis of the signalling molecule 1,25D s, which stimulates osteoclast formation and activity (Evans et al., 2006b). These effects can lead to osteolytic bone loss in the replaced joint.

2.9 Pressure generation- fluid movement in joint capsule

Intracapsular pressure in the healthy joint should not be increased in the usual range of motion (Wingstrand et al., 1990). Joint effusion (an increase in intra-articular fluid volume) often accompanies joint disease, causing a higher intracapsular pressure. Along with joint effusion, this intracapsular pressure is affected by capsular compliance, joint position and muscle action (Levick, 1983). Intracapsular pressures measured in different joint positions are shown in Table 3.

Table 3: Intracapsular pressures measured in different joint positions

Ref	Study Participants	Conditions (with mean pressures)			
		45° of hip flexion	*Extension*	*Extension + inward rotation*	*Extension + outward rotation*
(Robertsson et al., 1997)	Patients before revision of THA (n = 18, mean age 77 [66-90])	**1.60 kPa** (0 – 3.7kPa)	**3.47 kPa** (0 – 8 kPa)	**21.20 kPa** (3.2–37.2 kPa)	**4.00 kPa** (0.4–8.9 kPa)
(Tarasevicius et al., 2007)	Patients with OA, before THA (in lateral decubitus position after release of short rotators) (n = 31, age n/a)	**0.29 kPa** (± 1.3kPa)	**2.11 kPa** (± 4.4kPa)	**1.83 kPa** (± 3.5kPa)	**1.61 kPa** (± 3.2kPa)
(Robertsson et al., 1995)	Patients with coxarthritis, before surgery (n = 18, mean age 70 [46-83])	**2.83 kPa** (± 1.9kPa)	**6.58kPa** (± 5.3kPa)	**14.06 kPa** (± 10.1kPa)	**5.43 kPa** (± 4.3kPa)

The highest joint pressures are observed in climbing stairs and by sitting down or rising from a chair; pressures up to 103kPa have been measured during these actions (Hendrix et al., 1983).

In a healthy joint, increased intra-articular pressures may reduce over time due to a gradual distension of the joint capsule. However as osteoarthritis develops, capsular elasticity decreases (Lloyd-Roberts, 1953), preventing the increase of volume and decrease in pressure. This reduced capsular compliance, combined with the joint swelling causes a decrease in the range of motion that can be achieved without increasing joint pressures (Tarasevicius et al., 2007).

In 17 patients with THA, joint pressures between 20 and 69kPa (mean 27.5kPa) have been measured during walking. One study compared the pressures in 18 hips before revision for aseptic loosening, with 34 unrevised, clinically and radiographically stable hips, and found that intracapsular pressures were significantly higher in loose hips (Robertsson et al., 1997).

Some researchers believe that fluid flow, not fluid pressure, drives the osteolytic process (Johansson et al., 2009, Fahlgren et al., 2010). Computational fluid dynamics (CFD) studies modelling the hip joint have shown that during joint subluxation, an area of low pressure is created by the increase in gap volume between the head and the cup (Lundberg et al., 2007, Holzer et al., 2012). This area of low pressure causes fluid flow into the bearing surface, as demonstrated by particle-image velocimetry (PIV) studies (Lundberg et al., 2007) CFD analysis shows that a similar effect may occur during joint flexion (Holzer et al., 2012). Separation of the head and cup of up to 2.8mm (average 1.2mm) has been measured during gait motions under fluoroscopy (Lombardi et al., 2000); this separation may also trigger fluid flow.

Similarly, the movement of a loose cup may cause fluid flow at the implant-bone interface. Preoperative pressure measurements have shown that hips with loose components generally had higher intracapsular pressures than hips with well-fixed implants (Robertsson et al., 1997). A modular liner, able to move relative to the shell in a modular cup, has also been shown to cause significant pressure waves (over 600kPa) *in vitro* (Walter et al., 2005), by two different pumping actions (see Figure 23). In diaphragm pumping, a space exists between the non-congruent liner and the metallic shell containing joint fluid and wear debris. When the hip is loaded, the polyethylene liner deforms, the volume of the space is reduced, and the fluid and wear debris are forced through the apical hole to the retroacetabular bone. In the piston pumping case, a loose locking mechanism allows the liner to come part-way out of the metallic shell. When the hip is loaded, the liner is pushed back into the shell, pumping fluid and wear debris through the apical hole.

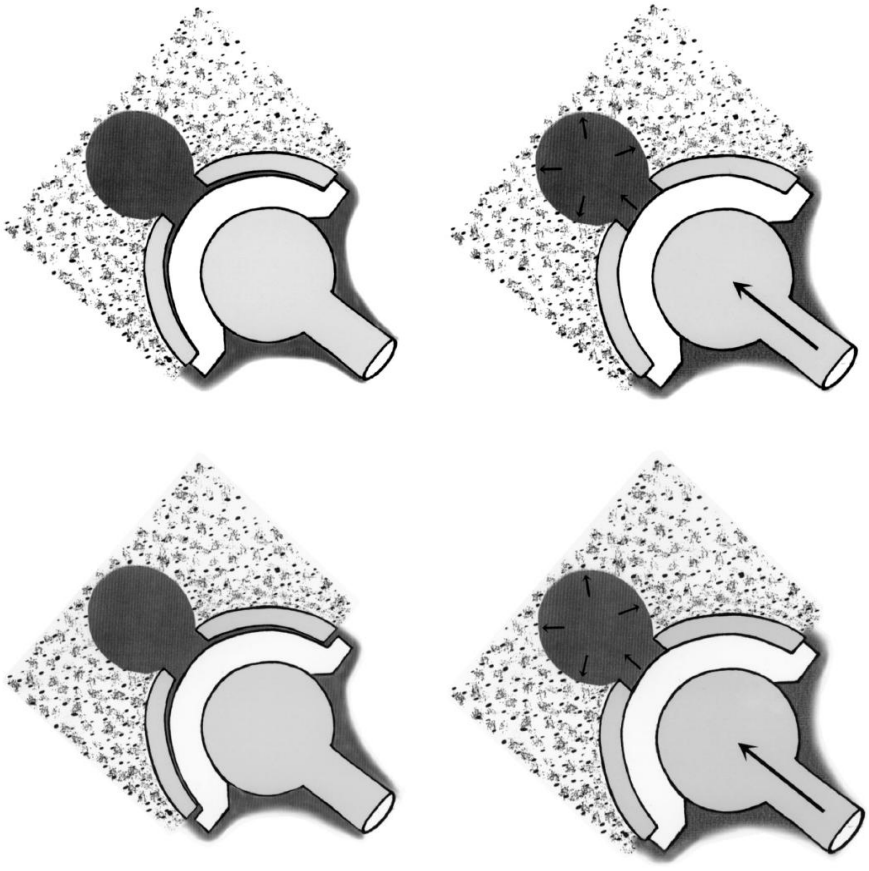

(a)

(b)

Figure 23: (a) Diaphragm pumping. (b) Piston pumping. Image from Walter et al. (2005), with permission.

In a healthy hip, the acetabular bone is protected from pressure fluctuations by the cartilage that completely lines the articulating surface of the joint. Healthy cartilage has a low hydraulic conductivity and covers all the articulating surfaces of the joint. This protects subchondral bone from the flow of pressurised synovial fluid. In the replaced hip the cartilage is absent and a robust connection between the implant and the body must protect the periacetabular bone.

2.10 Access to periacetabular bone

Local pressure gradients will lead to fluid flow in the joint space. However, contact with periprosthetic bone is required for fluid pressure & flow to cause damaging bone resorption (Manley et al., 2002). In several studies, osteolysis is only observed where the fluid is in contact with the bone (Szuszczewicz et al., 1997, Stamenkov et al., 2010, van der Vis et al., 1998a).

The entire area that is accessible to joint fluid and debris can be termed the 'effective joint space' (Schmalzried et al., 1992a). If the interface between the implant and the surrounding bone is not sealed, fluid and debris may move into this space, coming into contact with the periprosthetic bone and causing osteolysis and aseptic loosening. If there are screw holes, loose screws, or a backside gap, and fluid has access to these via a loose liner or insufficient cup fixation, the effective joint space is enlarged to include periprosthetic areas. Deformation of the cup under load, or deformation of the acetabular bone (Ling et al., 2010), may allow the passage of fluid between cup and bone.

As previously described, cemented implants generally loosen at the cement-bone interface, and it is this interface that, if loose, increases the effective joint space to include periacetabular areas. During routine subtraction arthrography, high intracapsular pressures have been shown to force contrast medium into bone-cement interfaces that may not have been otherwise observed (Hendrix et al., 1983).

In a clinical study of 65 uncemented hips, bone ingrowth has been observed radiographically to be slower around the acetabular cup component than around the femoral stem (Emans et al., 2009), meaning there is a longer period of access to periprosthetic space in the cup component. In well-functioning uncemented acetabular cups, bone ingrowth into the porous coating has been shown to occupy an average of 32% of the surface (Engh et al., 1993). There is evidence that a hydroxyapatite coating can induce circumferential bone ingrowth, forming a protective barrier against debris migration (Emans et al., 2009). In an *in vitro* study, the porosity of the bone has been shown to affect the ability of particles to migrate into periprosthetic bone spaces (Libouban et al., 2009), suggesting that bone characteristics can also affect the size of the effective joint space.

One study (Kitamura et al., 2005) of retroacetabular osteolysis in uncemented cups showed that in 67% of the osteolytic lesions , a clear communication pathway could be identified (see Figure 24). Thirty-one lesions showed clear communication pathways: around the rim, through a central hole, associated with a screw or screw-hole, or through multiple pathways. Lesions with a clear communication pathway were larger than lesions without a clear pathway. Lesions with multiple communication pathways or communication through a dome hole were larger than those with communication through a screw-hole or around the rim.

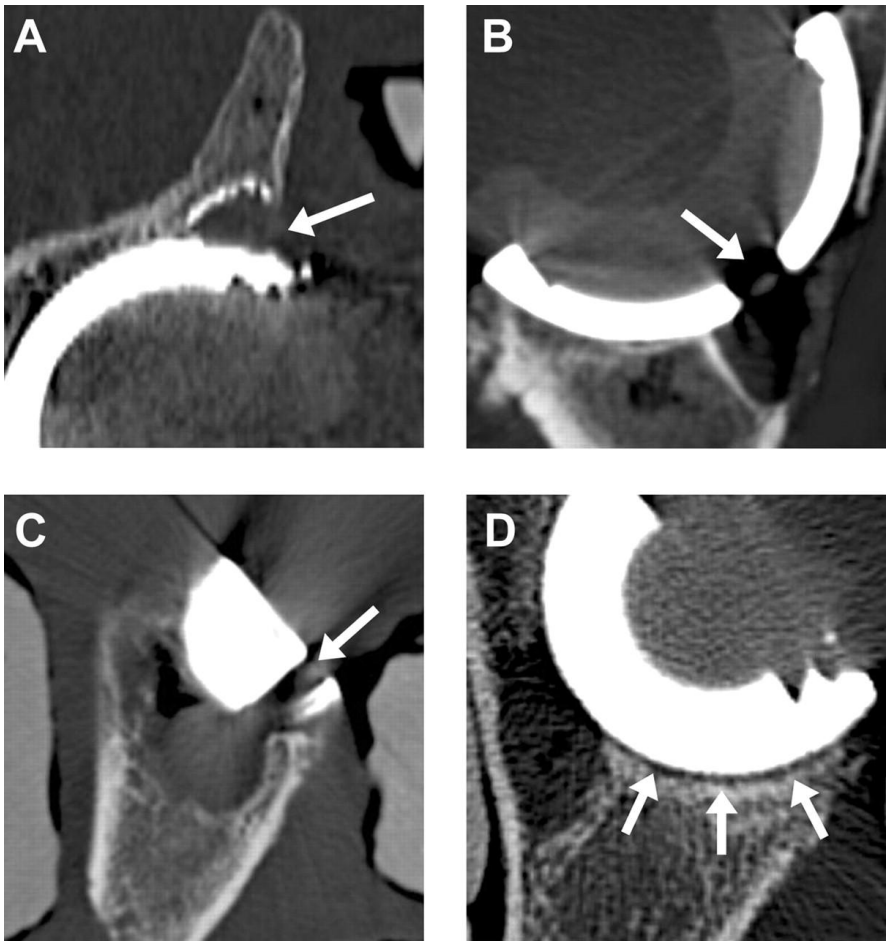

Figure 24: Examples (from CT scans,) of different communication pathways between osteolytic lesions and the joint space. Communication is possible around the rim (A), through a central hole (B), around a screw-hole (C) and through a gap between bone and implant surface (D). Image from Kitamura et al. (2005), with permission.

A thin fibrous membrane can form between the implant and the bone, early in the life of the implant (Jones et al., 2001), in both cemented (Schmalzried et al., 1992b) and uncemented implants (Engh et al., 1993). This may occur initially as a response to surgical trauma, or progress over time due to mechanical or biological factors (Spector et al., 1990). There is discussion about whether this membrane acts as a barrier to wear debris and fluid pressure, or whether it facilitates the pumping of fluid to periprosthetic spaces. In rabbits this fibrous tissue, in conjunction with a press-fit implant, has been shown to form a barrier that closes the interface against polyethylene particles (Frokjær et al., 1999). However, cyclic compression of such a membrane has been shown to induce osteolysis in the underlying bone, in rabbit (Van der Vis et al., 1999) and rat (Skripitz and Aspenberg, 2000) models. Once there is access to bone adjacent to the implant, subsequent resorption of periprosthetic bone could lead to greater access and further scope for damage, as illustrated in Figure 25.

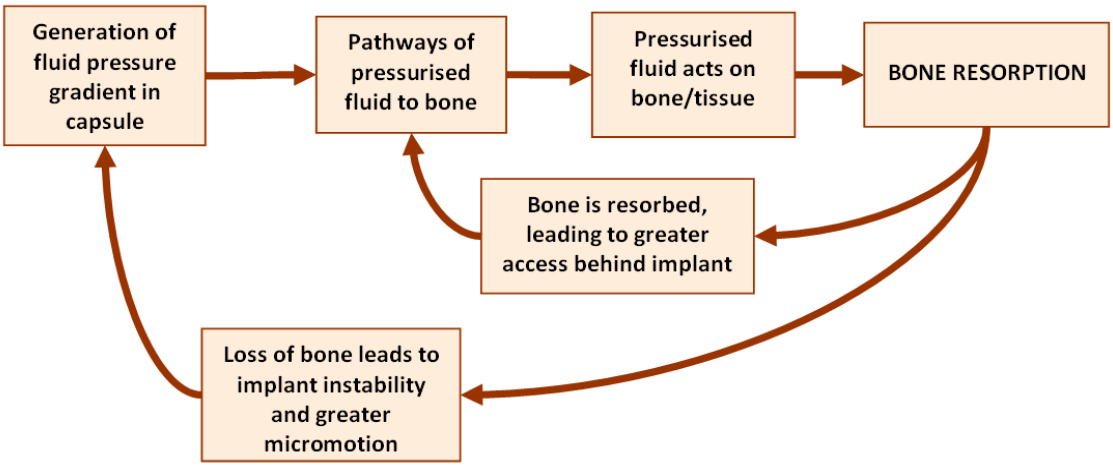

Figure 25: Flow chart showing cycle of access, fluid pressure generation and bone resorption

2.11 Effects of pressure on bone

The effects of fluid pressure on bone have been investigated in cell culture studies and animal models. Generally, cell culture models have involved the application of air pressure to monocyte-derived macrophages in cell culture plates in an incubator, and the subsequent analysis of cytokine expression. Most animal models have been performed by Aspenberg and colleagues, using the pressure application rig shown in Figure 26 (Skripitz and Aspenberg, 2000, Skoglund and Aspenberg, 2003b).

Cell culture models of fluid pressure

Cyclic pressures applied to macrophage cell cultures have shown that exposure to pressure waves at different amplitudes (up to 138kPa) for one hour stimulates the production of bone-resorbing cytokines by macrophages (Evans et al., 2006b, Evans et al., 2006a, McEvoy et al., 2002, Sampathkumar et al., 2003, Ferrier et al., 2000). Cyclic and static pressure were applied to monocyte-derived (MD) macrophages in a standard cell culture plate, sealed inside a Perspex vessel and placed within an incubator (Ferrier et al., 2000). This vessel was pressurised from a cylinder of air under the different regimes of cyclic hydrostatic pressure (CHP) described in Table 4.

Table 4: Results of investigations into effects of cyclic fluid pressure

Study	Test details	Test factors	Significant results
(Ferrier et al., 2000)	138kPa CHP applied to MD macrophages for one hour, at 0.05Hz or 0.5Hz.	IL-1β IL-6 TNF-α	Both frequencies were found to increase expression of IL-6 and TNF-α; only the higher frequency regime increased expression of IL-1β.
(McEvoy et al., 2002)	CHP of 138kPa, 69kPa, 34.5kPa and 17.3kPa applied to MD macrophages for 1h, and tests at 17.3kPa were performed with or without contact with UHMWPE particles	IL-1β IL-6 TNF-α	All four pressure levels resulted in increased secretion of IL-1β, IL-6 and TNF-α. This effect was greatest at 34.5kPa. Testing with pressure and PE particles had a synergistic effect on production of these cytokines.
(Sampathkumar et al., 2003)	CHP of 34.5kPa applied to monocyte culture for 1h, with or without contact with UHMWPE particles	M-CSF PGE_2	Secretion of M-CSF and PGE_2 was increased in cultures exposed to CHP. Particles and pressure together had a synergistic effect on the expression of M-CSF and PGE_2.
(Evans et al., 2006b)	34.5 kPa CHP applied to MD macrophages for 1h at a cycle of 2sec on, 2sec off.	$1,25D_3$	Cyclic pressure increased synthesis of $1,25D_3$ by macrophages.

This work has shown that cyclic hydrostatic pressure, applied to human peripheral blood macrophages, stimulated the activity of pro-resorptive factors and chemokines. It also postulates that the synergistic effect between particles and pressure in THA could accelerate osteolysis and implant loosening.

Animal models of fluid pressure

Animal models have investigated the effects of induced hydrostatic pressure on bone. Cyclic pressures of up to 600kPa have been applied to rat tibiae *in vivo* through a soft tissue membrane, causing osteoclastic bone resorption in pressurised areas (Skoglund and Aspenberg, 2003a, Skripitz and Aspenberg, 2000). This was performed by implanting a titanium plate into a rat tibia, with a removable centre plug, which could be replaced with a pressure piston for the application of cyclic pressure (Figure 26). This figure shows how a) the titanium plate is implanted into the rat tibia, and new bone grows up to the surface of the central plug; b) after 4 weeks, the central plug can be replaced with a hollow plug (arrow); c) a

pressure piston replaces the hollow plug and is surrounded by a plastic lining to prevent fluid escape, and fibrous tissue can grow in the gap between the piston and the bone; and d) the piston is forced down, compressing the fibrous tissue to create fluid pressure in the new bone. A similar rat model found that short loading spikes (93kPa, for 0.3sec, 20 cycles twice a day for 2 weeks) cause bone resorption. This resulted in the theory that fluid flow, not just fluid pressure, contributes to osteolysis (Fahlgren et al., 2010).

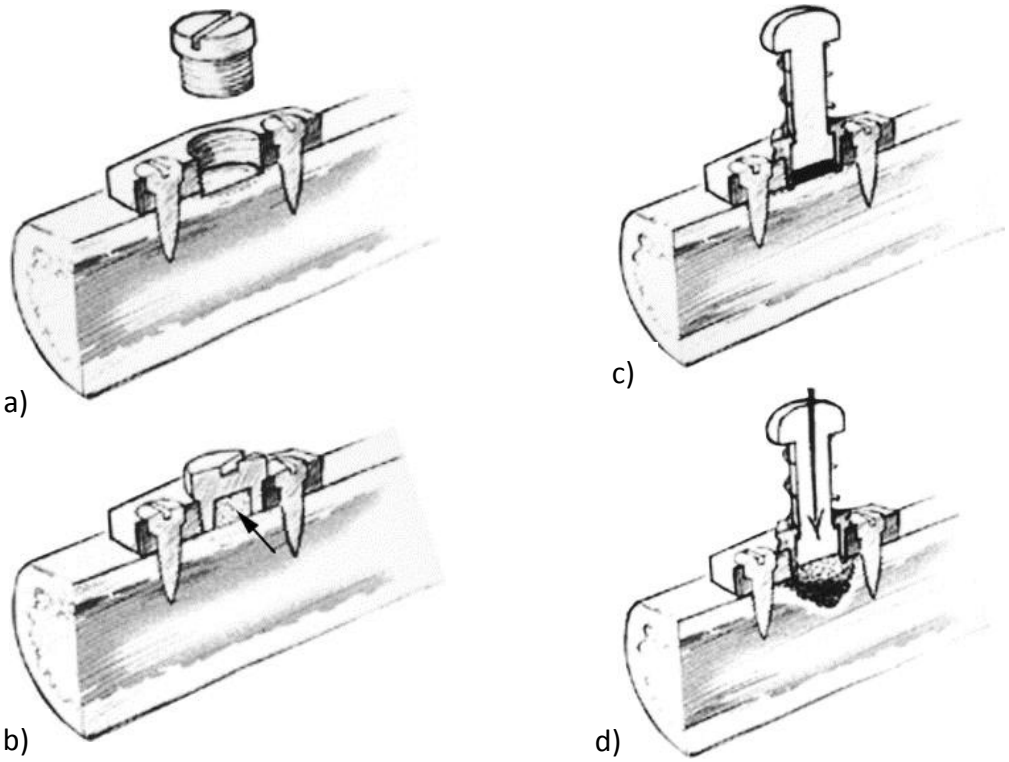

Figure 26: Sketch of rig used to apply cyclic pressure to rat tibiae. Image from Skoglund and Aspenberg (2003b), with permission.

Although it is debated whether the presence of particles and pressure together have a synergistic effect on osteolysis and bone resorption (McEvoy et al., 2002, Sampathkumar et al., 2003, Skoglund and Aspenberg, 2003a), there is consensus among researchers that both contribute to bone loss. A representation of the process by which debris and pressure cause osteolysis is shown in Figure 27. These two factors stimulate the macrophage to produce hormones and local factors such as PGE2 and IL-6, which have been shown previously (Figure 22) to cause osteoblasts to increase the production of RANKL and decrease OPG, thus stimulating osteoclast proliferation and differentiation.

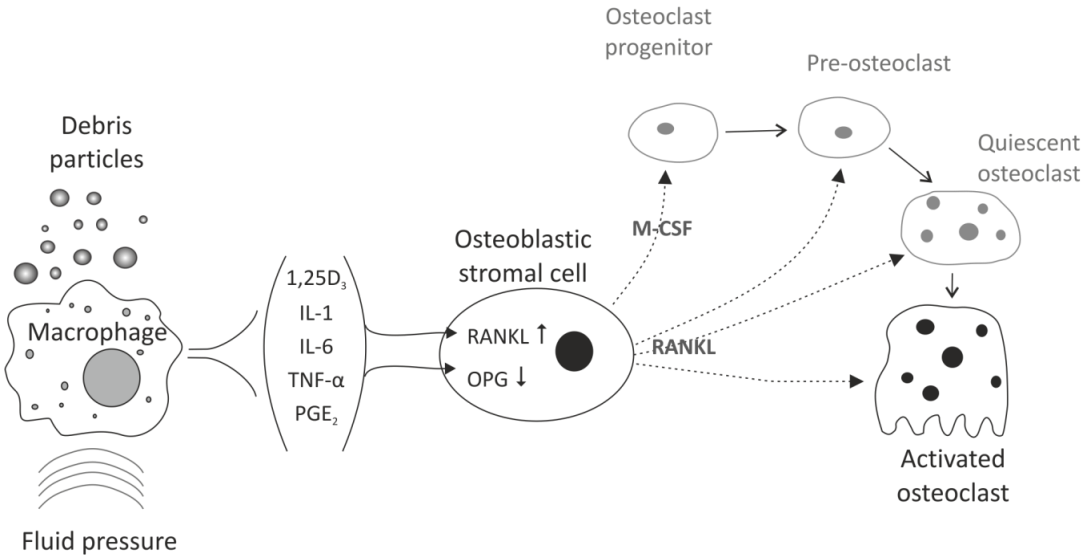

Figure 27: Process of activating osteoclasts from the presence of debris particles and fluid pressure. Author's own image.

Constant fluid pressure can also produce resorption in animal models. A constant pressure of 20 kPa, applied to rabbit tibiae for 2 weeks through a fluid-filled titanium chamber, produced bone resorption in all pressure specimens (Van der Vis et al., 1998b). In some there was evidence of osteocyte cell death, as the lacunae surrounding the area of pressure were generally empty. High continuous fluid pressures may also disrupt the local circulation in the hip joint (Jayson, 1970, Kiaer, 1994). High induced intra-articular pressures (26.6kPa for 10 hours or more) in canine hips has been shown to cause avascular necrosis (bone death due to lack of blood supply) (Soto-Hall et al., 1964), however these high levels of constant pressure are unlikely to occur in the THA patient.

The fibrous membrane in the replaced joint has been shown to cause osteolysis when compressed, as described in section 2.10. However the study by Fahlgren et al (2012), showed that osteoclast differentiation and bone loss can be caused by fluid pressure and flow, even in the absence of the fibrous membrane.

2.12 Effect of component features on fluid movement

The effects of component features on the presentation of osteolysis have been explored in *in vivo* studies. Osteolytic lesions *in vivo* have been observed to correspond with holes in the acetabular shell (Walter et al., 2004, Stamenkov et al., 2010). A rise in pressure in these lesions, without a corresponding change in the hip joint pressure, indicates there is a

mechanism for pressure generation either due to a 'pumping action' of the acetabular component, or due to deformation of the bone surrounding the lesion, changing the volume and therefore the pressure in the lesion (Walter et al., 2004). Components with multiple holes were more likely to have osteolytic lesions adjacent to the holes, while components with a single hole had mostly peripheral (rim) lesions (Stamenkov et al., 2010). However, incidence data on pelvic osteolysis in 513 hips (Schmalzried et al., 1999) showed no direct correlation between the presence of screws or screw holes in the acetabular component and the incidence of osteolysis in the pelvis.

The effects of changing component features have also been measured using *in vitro* models. Khalily and colleagues (1998) performed a test to investigate fluid ingress through modular acetabular components. Tests with a loading chamber showed that different component features, such as a peripheral seal, can affect the access of fluid and debris to the periacetabular bone. Similarly, Walter *et al* showed that a non-congruent liner in a modular cup can act as a pressure pump (2005).

Knowledge of the effects of component features on fluid movement and pressure is necessary when designing new components. These contradictory findings suggest further work is needed to understand the influence of these effects.

2.13 Measurement of pressures on bone

As summarised in Table 3, joint fluid pressure has been measured in arthritic patients (Robertsson et al., 1995), before total hip arthroplasty (Hendrix et al., 1983, Tarasevicius et al., 2007) and before revision surgery (Robertsson et al., 1997). Pressures have also been measured in osteolytic lesions, as well as in the hip joint capsule, in patients with pelvic osteolysis (Walter et al., 2004). This is an invasive procedure which involves the insertion of a needle into the hip joint space.

To investigate pressure magnitudes without needing a human subject, attempts have been made to create mechanical models that allow pressures to be measured *in vitro*. Bartlett *et al* (2008) tested a model of a cemented femoral stem, to determine whether a 'femoral stem pump' exists – whether the movement of a de-bonded stem within the cement mantle can cause clinically relevant pressures. This model comprised a chamber in which a loose half-sized stem was seated in a thick cement mantle. Axial load (between 1.3kN and 0.2kN) and

torque could be applied to the stem, and fluid pressures were measured using external pressure transducers at the sites of predicted highest flow rates. A filler tank applied a constant pressure head to the rig, and a water jacket kept the cement close to body temperature. A schematic of the rig is illustrated in Figure 28.

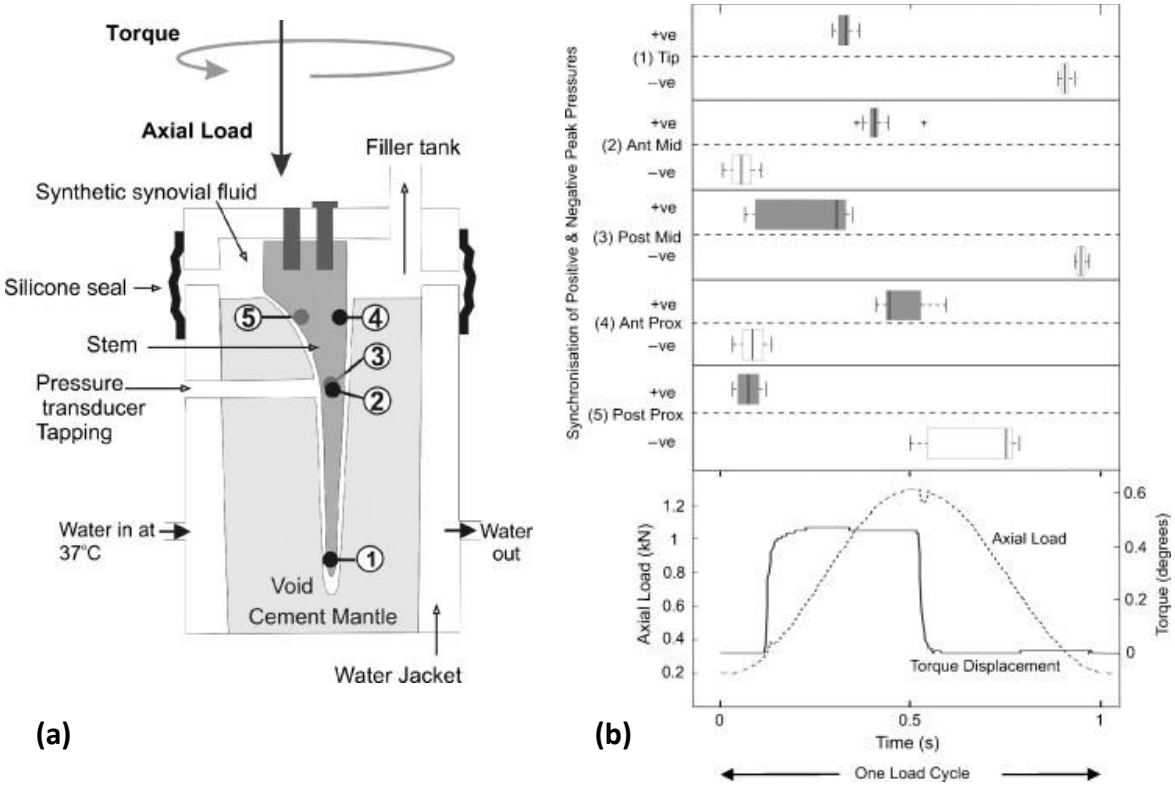

Figure 28: Showing details from the 'femoral stem pump' study, including (a) Schematic of the rig, showing the transducer tapping sites (numbered), and (b) boxplots showing the position in the load cycle of peak positive pressures (in grey) and peak negative pressures (in white) recorded at the five pressure tapping sites. Images from Bartlett et al. (2008), with permission.

The model showed that the stem can act as a pressure pump, with pressures up to 17kPa measured. Although not the 35kPa described by McEvoy and colleagues (2002) as having the greatest effect on osteolysis, the model used a half-sized stem and it can be speculated that higher pressures would be measured with a full-sized stem. This work was useful in investigating pressure generation with a loose cemented stem. Since acetabular cups have a higher incidence of loosening and osteolysis than stems, it would be appropriate to investigate mechanisms for pressure generation with a prosthetic cup.

This has been explored by Walter *et al* (2005), this time investigating relative movement between the liner and shell in a modular acetabular cup. The group used an aluminium fluid chamber, as shown in Figure 29a.

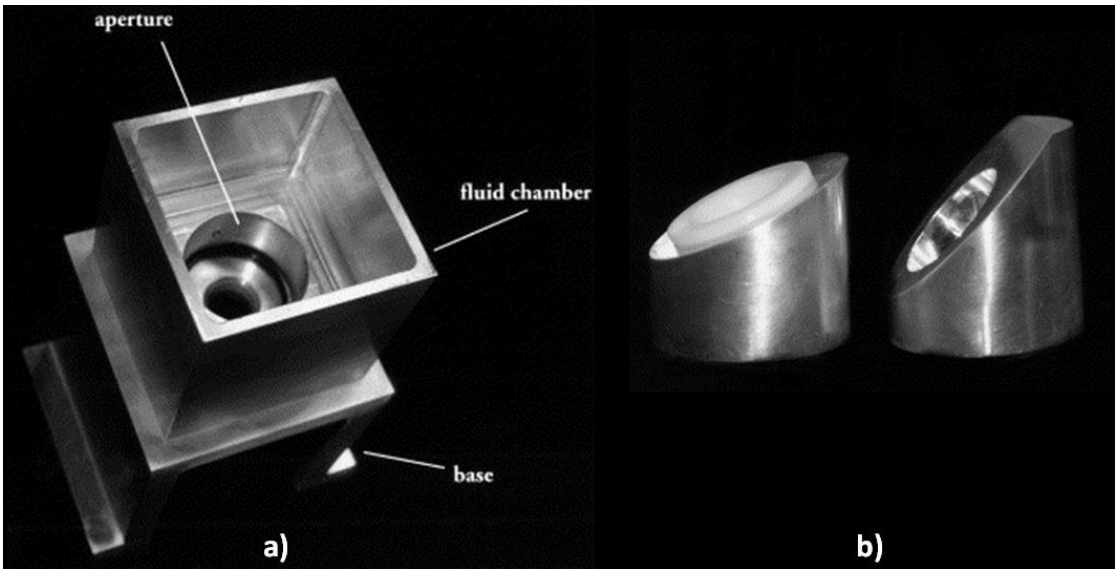

Figure 29: Image of rig used in 'pistoning liner' study, showing (a) aluminium test chamber and (b) inserts representing the components with loose liners, at two different test angles (23°, shown with liner, and 46°, shown without liner). Image from Walter et al. (2005), with permission.

Aluminium inserts with holes and PE liners (Figure 29b) were loaded with axial compressive load through a 28mm femoral head. Bovine serum was used as the joint fluid. An artificial pressure gradient was applied by attaching a vacuum pump to the lower chamber. A transducer was threaded into the bottom of the aluminium cup so that there was a 1mm space between the transducer and the liner. Load angles of 23° (the angle of the load on acetabular component during walking) and 46° (the angle of load when rising from a chair) were tested. Pistoning motion of the liner produced pressures eight times higher than without pistoning, and pressures over 600kPa were measured.

These two studies represent the two most significant *in vitro* mechanical studies into fluid pressures and flow in total hip replacement. However they are both limited by the inability to include actual prosthetic components and to include the more complex components of the replaced hip joint (including the fibrous membrane and the periprosthetic bone). It is therefore essential to be able to test periprosthetic fluid pressures in a more sophisticated *in vitro* model.

2.14 Summary of findings from literature

The literature indicates that osteolysis can be caused by wear debris, fluid pressure, or a combination of the two. The inference that fluid pressure stimulates the osteolytic process is a more recent theory and so fewer studies have been performed in this area. Current models investigating fluid pressure and flow in THA fall into two categories – living-cell models (animal or cell models) and *in vitro* tests.

Extensive cell culture studies have shown that cyclic hydraulic pressures of 35kPa or more can cause cell changes and the activation of osteoclasts. In animal models, resorption has been produced by cyclic or constant pressures. These living-cell models have produced compelling evidence of the deleterious effect of fluid pressure on bone.

In vitro mechanical tests have explored the ways in which fluid pressures may be generated with loose implants. Pressures of over 600kPa have been measured. However, these are all very simplified representations of the replaced hip joint and may not adequately represent *in vivo* conditions. Building on this knowledge, a more sophisticated *in vitro* model is needed to investigate the magnitudes of fluid pressures produced under different conditions. This thesis will describe the process of designing and testing such a rig.

2.15 Project aims and hypotheses

The literature has shown that fluid pressures over 35kPa can cause resorption stimulating cytokines to be produced and for osteocyte damage to occur. It is valuable to determine experimentally whether clinically significant pressures can be generated behind a loose acetabular cup. If a pressure differential occurs in the hip chamber, joint fluid (and the debris it carries) can be forced to flow behind a loose cup *in vivo*, which has been stated as a cause of periprosthetic osteolysis.

The aim of this study is to design and construct a test rig approximating the human acetabulum (including component fixation, acetabular bone, synovial fluid and joint loading) which can be used to measure periacetabular pressures. The rig will be used to test whether clinically-significant pressures may be generated under different conditions (different loading and component features). The following chapter will detail how the rig was designed and constructed.

3. Design Requirements

3.1 Introduction

To achieve the aims of the project, a physical model of the hip joint was constructed, referred to as the Acetabular Pressure Transmission Rig (APTR). This model, representing important aspects of the *in vivo* conditions and important structural elements of a replaced hip joint, would facilitate the performance of repeatable tests and the measurement of pressures. Prosthetic components were to be loaded in the presence of a synovial fluid analogue in order to investigate the fluid pressure characteristics behind the acetabular cup and in the joint capsule.

3.2 Design requirements

It was important that the APTR model approximated, as closely as possible, the *in vivo* conditions in the replaced hip joint. From the description of hip anatomy in the previous chapter, the important elements required in a physical model were determined. These elements, and their predicted effect on pressure (based on information from the previous chapter), are outlined in Figure 30.

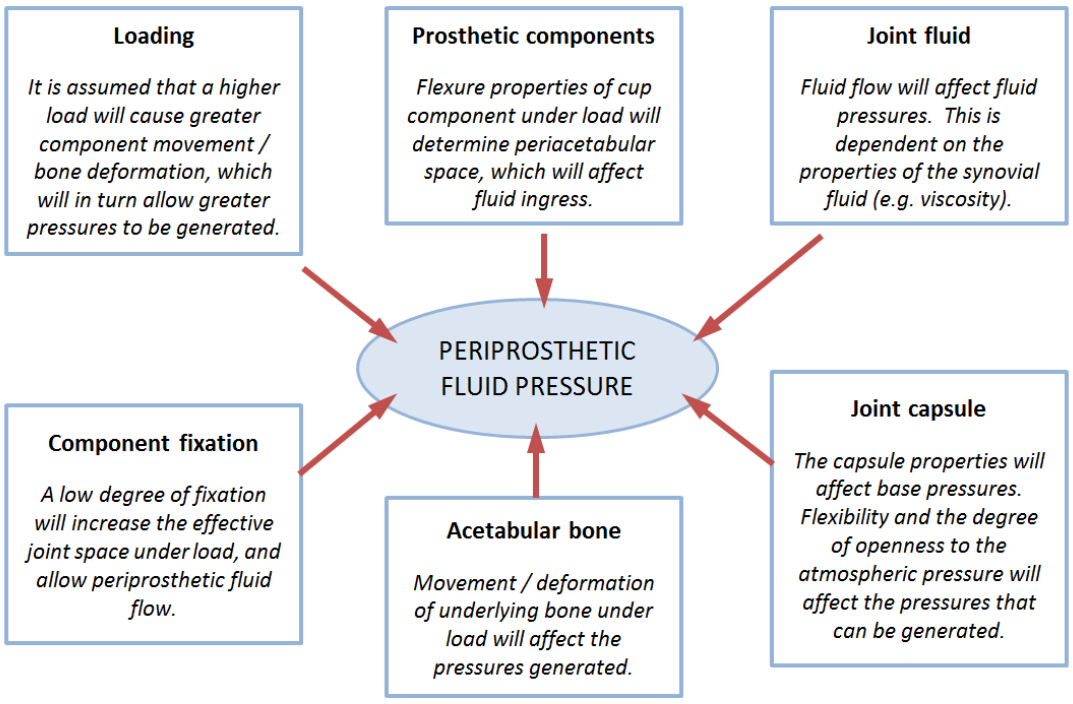

Figure 30: Diagram showing main factors affecting *in vivo* fluid pressures in the replaced hip capsule

The methods by which other researchers have represented these elements using *in vitro* studies were examined, along with results from APTR pilot studies in these areas (Appendix 1 and 2). This information informed the design decisions to be made about how to approximate these elements in an *in vitro* mechanical test rig.

3.3 Representative loading

A primary requirement was that the rig could be loaded in a repeatable, measureable and clinically relevant way. This necessitated measurements taken from *in vivo* and *in vitro* studies of joint loading.

Joint loading characteristics

The hip joint undergoes a complex loading pattern during everyday activities. The acetabulum transfers load to the femoral head at different angles and magnitudes depending on the movement, as shown in Figure 31.

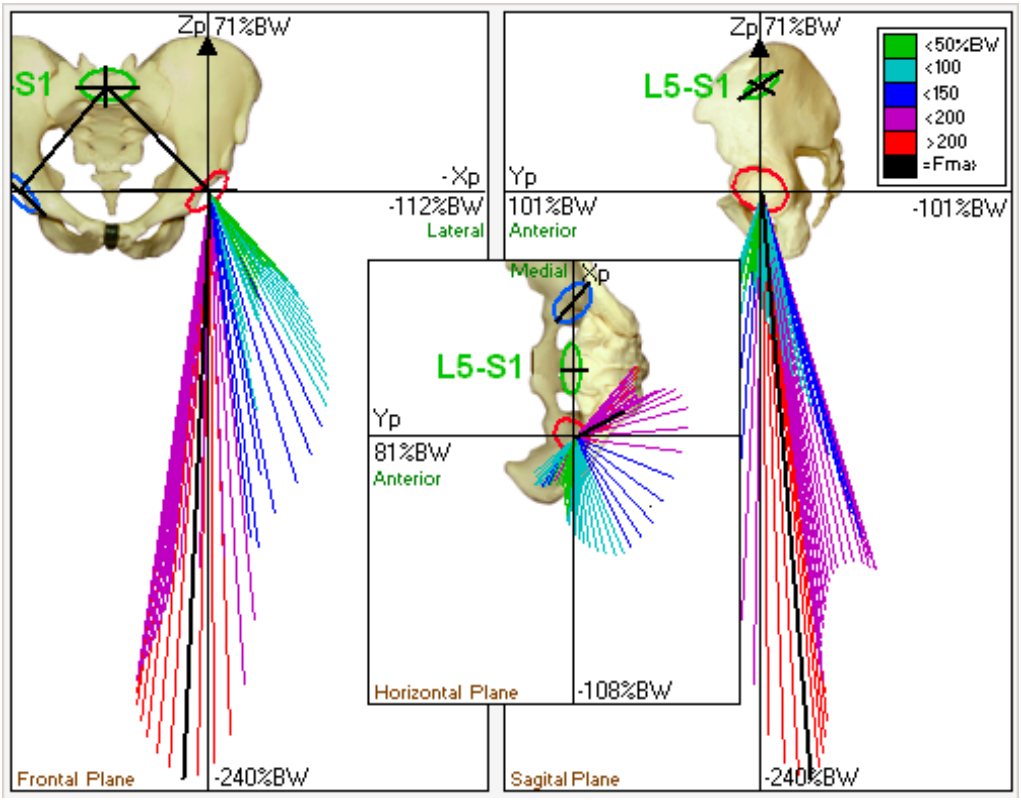

Figure 31: Image from HIP98 program, showing vectors of hip contact forces relative to the pelvis. The colours display the magnitude of load, relative to body weight (%BW). Image from Bergmann et al. (2001), with permission.

Microseparation, a separation of the head and cup components, can occur *in vivo* (as shown in Figure 32). During the surgical procedure of THA many supporting soft tissue structures, particularly the joint capsule, are cut or disrupted. Post-operatively, separation of the head from the cup is resisted only by the remaining soft-tissue structures and the interacting geometries of head and cup. The reduced soft-tissue support can lead to head-cup microseparation during gait and causes an increased risk of microseparation or dislocation of the joint (Johnston et al., 2000, Komistek et al., 2000). Lombardi et al (2000) showed that head-cup microseparation of up to 2.8mm can be measured *in vivo*. Dennis *et al* (2001) measured at an average of 3.3mm of separation in 10 subjects with unconstrained THA, with a range of between 1mm and 5mm.

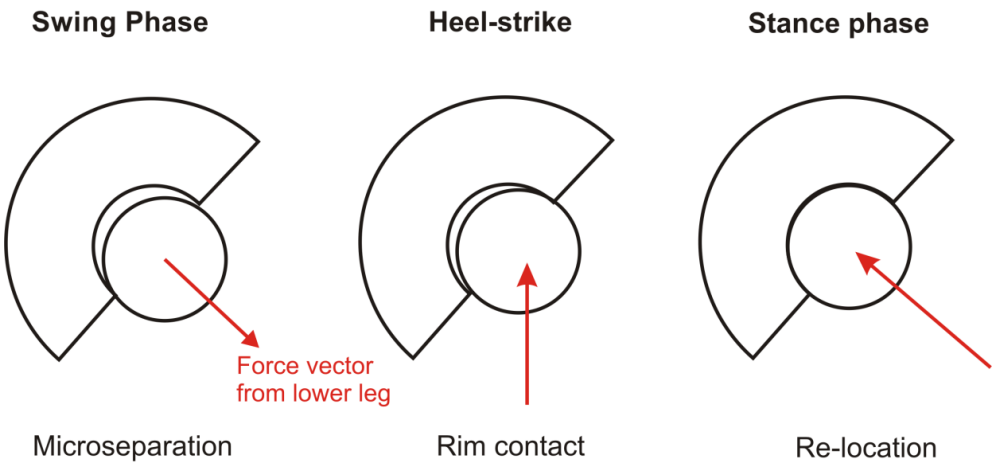

Figure 32: Diagram showing head-cup microseparation

Loading magnitude

According to the British Standard for hip joint simulators (BS 7251-7:1990, Section 3.3), the maximum applied peak load (representing the load in early stance) should be at least 1.5kN.

In tests in a hip simulator, the loading regime has typically been based on a patient weight of 125kg (Tong et al., 2008, Wang et al., 2009) in order to accelerate the time to failure. However, since the average patient weight in survivorship studies was usually found to be around 70kg (Mulroy and Harris, 1990, Garcia-Cimbrelo and Munuera, 1992, Mulroy and Harris, 1996, Tompkins et al., 1997, Clohisy and Harris, 1999, Williams et al., 2002), the loads selected for the APTR study were based on this patient weight.

Using an instrumented hip prosthesis, Stansfield *et al* showed that prosthetic components undergo loads of between 2.5 and 3 x BW during gait (2003). The minimum loads were just above zero, around 0.25 x BW (assumed to be due to muscle forces acting on the hip). Similarly, using instrumented prostheses in four patients, Bergmann and colleagues measured average maximum loads of 2.38 x BW during walking at 4km/h, with higher loads in stair climbing, and stumbling actions (1993, 2001).

Loads used in the APTR study were based on the assumption of a body weight of 70kg. Loads between 0.25 and 2.5 x BW are in the range of 170N – 1700N for this body weight level. This is similar to the loads applied in pressure testing by Walter *et al* (sinusoidal compressive loads cycling between 50N and 2000N), where components were tested in a rig to measure pressures in an osteolytic lesion behind a modular cup. In the APTR unit, loads were applied in a similar range. In initial testing a compressive load of between 0.01kN and 1.0kN was applied to the components.

Along with a load representative of part of the gait cycle, a 'relocation from microseparation' situation was also investigated. This was achieved by commencing the cyclic load test with the head and cup separated by up to 1mm. This simulated component re-engagement following a microseparation condition. To make sealing and loading easier the components were loaded in an inverse configuration, (see Figure 33), with the femoral head loading vertically into an acetabular block. This arrangement has been used in hip loading tests by other groups (Tong et al., 2008, Won et al., 1995, Walter et al., 2005).

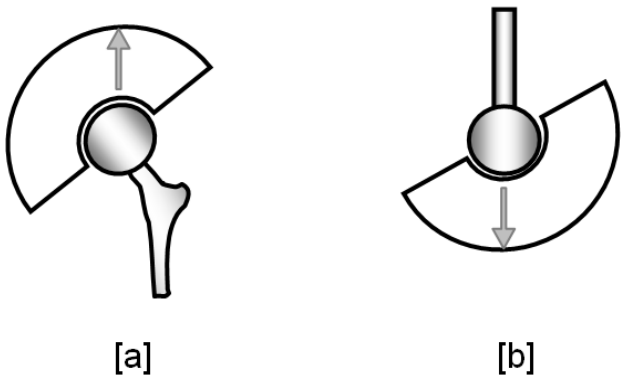

Figure 33: Schematic showing [a] the configuration of loading in the replaced hip, and [b] the configuration of loading in the APTR.

Loading frequency

The British Standard also states that the frequency of loading should be between 0.5Hz and 1Hz. The generally accepted walking frequency is 1Hz and this was used for the majority of tests with the APTR unit.

Loading angle

Ideally tests would be performed using a hip joint simulator, which can simulate all angles of the gait cycle. However, with the loading apparatus available, only axial loading could be applied. The loading angle was changed by altering the configuration of the acetabular block. This approach has also been used in the study by Walter et al (2005), where the components were tested at 23° and 46°, based on the two main angles of loading during walking and rising from a chair respectively.

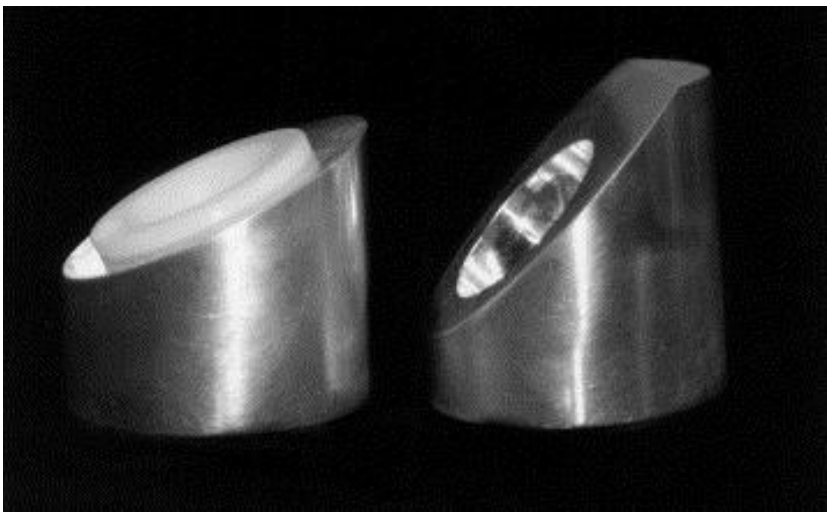

Figure 34: Image showing rig components used in the piston pumping study. Aluminium test blocks with load angles of 23° and 46° are pictured. Image from Walter et al (2005), with permission.

The APTR was designed to be loaded at different angles, initially at 0° (axially loaded) and 30° (see Figure 35). Different loading angles required alternative rig capsule seals to be designed (see Section 3.5)

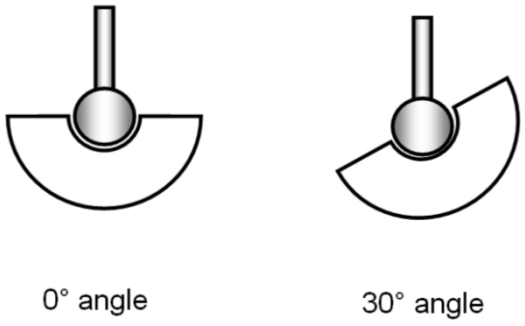

Figure 35: Loading angles used in the APTR unit

Loading regime selection

In summary, the loading regime initially selected for testing was a compressive load rig with a sinusoidal wave form between 0.01kN and 1kN, at a frequency of 1Hz for 50 cycles. Loads could be applied to the acetabular cup axially and at an angle of 30°, and a re-location condition could also be tested on the first cycle of loading.

3.4 Synovial fluid and analogues

A synovial fluid analogue for use in this rig needed to be a nonconductive fluid, with shear and viscosity values representative of synovial fluid *in vivo*.

Synovial fluid properties

Synovial fluid is an incompressible, non-Newtonian fluid. It is a dialysate of blood plasma, with the addition of hyaluronan and lubricin. This composition gives synovial fluid its thixotropic properties (Hlavacek, 2001). As a thixotropic fluid, synovial fluid exhibits shear thinning behaviour – at rest it is viscous but under shear stress (i.e. during joint motion) it becomes less viscous and more able to flow within the joint. In osteoarthritis, the amount of synovial fluid can increase and the fluid exhibits reduced hyaluronic acid content, reducing the viscosity of the fluid (Fam et al., 2007).

Synovial fluid analogues

There are several commonly-used substances that replace synovial fluid when *in vitro* testing is undertaken. The properties of these different fluids, as well as properties of healthy and arthritic synovial fluid, can be found in Table 5. Viscosity values are temperature-dependent and so temperatures have been specified where necessary.

The British Standard for hip joint simulators (BS 7251-7:1990, Annex B) (1990) recommends a lubricant based on bovine serum, kept at body temperature (37° C) during testing. This bovine serum is derived from bovine blood plasma and has been used in many *in vitro* hip joint studies. The use of bovine serum would have required higher levels of component sterilisation and biological controls, measures that were not considered necessary for the development of the experimental test rig for this study. A non-biological synovial fluid analogue was therefore required.

Phosphate-buffered saline (PBS) has been widely used to represent synovial fluid *in vitro*. In a study in 2005, Kurtz *et al* used PBS at room temp (22°C) to test peak fluid pressures at screw holes in a generalised joint-replacement model, with a PE liner and a metal backing with screw hole (Kurtz et al., 2005). Similarly, normal saline has been used in a rig that measured fluid permeability *in vitro* around femoral stems with different surface finishes (Crawford et al., 1999), as well as the effects of the acetabular labral seal on fluid flow and permeability (Ferguson et al., 2003).

Table 5 suggests that the viscous flow properties of PBS are unlike those of synovial fluid, making it not ideal for use in pressure studies, where viscosity will affect fluid movement in the rig. Furthermore, saline is a conductive fluid, making it incompatible with the transducers chosen for the APTR (see section 3.9).

Vegetable oil has also been used in pressure studies. Bartlett *et al* used it in their femoral piston pumping pressure study (Bartlett et al., 2008), and in subsequent tests on the effects of stem surface properties on pressures (2009a, 2009b). Although it is a Newtonian fluid, unlike synovial fluid, the viscosity of vegetable oil at 20°C is comparable with that of synovial fluid in OA at 25°C (Table 5).

Table 5: Properties of synovial fluid compared with different analogues used in the literature

Fluid (At 20° unless otherwise specified)	**Density** (g/cm^3)	**Kinematic viscosity** (mPa s)	**Refs**
Healthy synovial fluid	1.01 (from specific gravity, ref water)	366-1406	(Fam et al., 2007, Ropes et al., 1939, Ropes et al., 1940)
Synovial fluid in OA		Lower than healthy synovial fluid 31-36 (at 25°)	(Fam et al., 2007)
Blood	1.06	300 – 400	(Thiriet, 2008)
Bovine serum	0.996	690	(Singh et al., 2005)
Water	1.00	0.89-1.002	(Lide, 1991)
Vegetable oil	0.91	65 – 163	(Bartlett et al., 2008, Noureddini et al., 1992, Lide, 1991)
Phosphate-buffered saline / normal saline (0.5mol/kg)	Similar to water	1.024	(Kestin et al., 1981)

Synovial fluid analogue selection

Vegetable oil was thus chosen as the synovial fluid analogue to be used in the rig. This fluid was chosen due to its availability, low cost, comparable viscosity, and the relative ease of rig maintenance (compared with using biological fluids). Vegetable oil is a nonconductive fluid that is compatible with the choice of transducers (see Section 3.9), and was ideal for the design and testing process of a new rig.

3.5 Joint capsule analogue

A joint capsule should enclose the components and the bone to seal the synovial fluid inside the test area. To replicate *in vivo* conditions in a joint capsule, the rig capsule needed to be a sealed but not completely closed system. The capsule/sealing mechanism needed to be able

to sustain a stable unloaded pressure on the rig fluid, similar to those measured in arthritic hips *in vivo*.

Joint capsule properties

The joint capsule surrounds the hip joint and contains the synovial fluid. In a healthy joint the capsule is flexible and the synovial fluid is able to perfuse into articular cartilage under higher pressures. In an arthritic hip the capsule loses elasticity and the resting joint pressure increases. The rig chamber should therefore be capable of maintaining this pressure.

Joint capsule design

In preliminary testing with a flexible sheath as joint seal it was found that such a membrane was too difficult to seal and could induce artificial pressure waves within the chamber (see Appendix 1). Following this, a rigid capsule and seal were designed for the rig chamber. Due to the inflexibility of the chamber seal, a different sealing component needed to be used for the different loading angles tested (see Section 3.3). The static pressure to simulate the joint space fluid pressure was applied by an oil reservoir held at a height 0.775m above the rig, creating a stable pressure head.

3.6 Appropriate bone analogue

Material to represent the acetabular bone was required to allow a repeatable manufacturing or machining process, have the appropriate mechanical properties and a highly consistent internal structure. The material needed to be capable of replicating a robust and reproducible bone-implant interface and allow bone defects to be introduced, specific to the type of implant and fixation used.

Acetabular bone mechanical properties

A bone analogue should have similar mechanical properties to pelvic bone. Values of Young's modulus and Poisson's ratio for different types of human bone are shown in Table 6.

Table 6: Mechanical properties of bone

Bone type	E (GPa)	Poisson's ratio	Ref
Cortical Bone	10-17	0.3	(Nordin and Frankel, 2001, Udofia et al., 2004, Bronzino, 2000)
Cancellous Bone	0.1 - 0.8	0.2	(Nordin and Frankel, 2001, Udofia et al., 2004, Bronzino, 2000)

The deformation of pelvic bone under load may have an effect on the contact between the implant and the bone and thus affect the ability of pressurised fluid to access periacetabular bone (illustrated in Figure 36). An acetabular analogue should be able to represent this deformation.

As highlighted in section 2.6, osteolysis can take the form of expansile lesions extending into the bone, especially in uncemented components. It is desirable to be able to represent these in the bone analogue in the APTR unit.

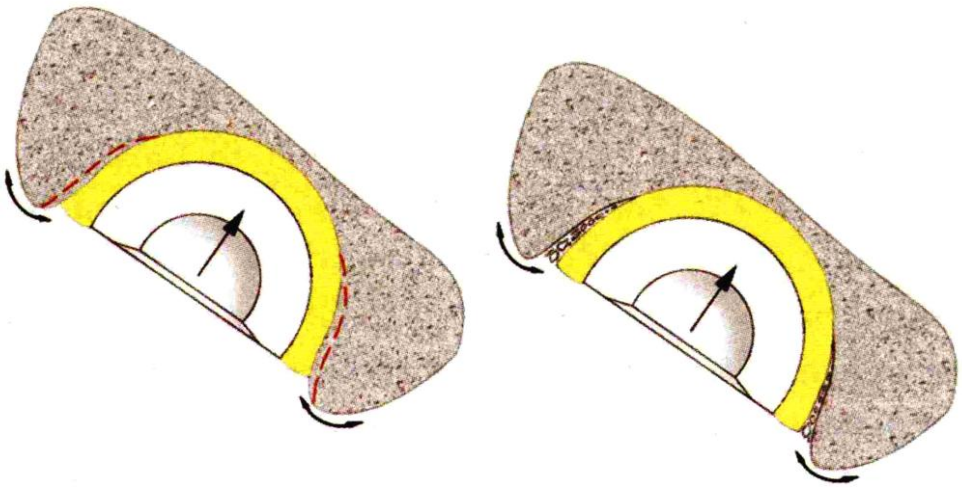

Figure 36: Image showing the deformation of acetabular bone under load and its possible effect on the effective joint space. Image from Ling et al. (2010), reproduced with kind permission of Exeter Hip Publishing.

Bone analogues

Adult cadaver pelves have been used to represent bone in previous studies – unembalmed, stripped of soft tissues (Won et al., 1995) and positioned upside down in the loading apparatus. The use of cadaver bone were not considered for use in the APTR due to the restricted availability, short usable life of samples, and a high inter-specimen variability between samples.

One group investigating fluid pumping around acetabular cups with apical screw holes used rigid aluminium blocks to simulate the bone (Walter et al., 2005). Pressure results from this study are questionable, as finite element (FE) studies (Sara et al., Pedersen et al., 1982) have shown that the deformation properties of the bone material can significantly affect component stresses and contact pressures, which may have an effect on fluid pressures.

Many groups have used more deformable bone analogues in mechanical testing, such as the commercially available Sawbones polyurethane (PU) foam (Sawbones Europe AB, Malmö, Sweden). Sawbones foam cubes of different densities (0.2 g/cm^3 and 0.5 g/cm^3) have been used in several studies (Adler et al., 1992, Baleani et al., 2001).

Synthetic PU foam has been shown to be a reliable and appropriate substitute for trabecular bone for mechanical studies (Szivek et al., 1995). Foam models have also been used to assess cup stability in many studies (Adler et al., 1992, Jamieson et al., Baleani et al., 2001, Macdonald et al., 1999, Kaneko, 2000). Although repeatable and widely-used, these foam models can only represent a single-phase material. Other materials used as bone analogues include fat-filled carbon foam (Bitsch et al., 2008), polyurethane resin blocks (Olory et al., 2004) and glass-fibre reinforced epoxide tubes (Macdonald et al., 1999).

Several groups have attempted to model the composite structure of pelvic bone in their *in vitro* studies. One group created an epoxy model, with an outer layer of epoxy resin, and a core of epoxy foam (Jacob et al., 1976). These two layers were connected rigidly so shear forces could be transmitted without slip. Another group (Jamieson et al., 2010) added external reinforcing structures, to simulate the columns of the ilium, ischium and pubis. Mechanical properties of composites from these studies are shown in Table 7. Although desirable to include in the APTR model, these composite properties would be difficult to produce repeatably.

Table 7: Mechanical properties of composite materials used for *in vitro* studies

Acetabular model	Cancellous bone	Cortical bone
Cadaver bone (Jamieson et al., 2010, Jacob et al., 1976)	Density = 0.1 – 1.4 g/cm^3 E = 785 MPa	Tensile strength = 166 – 198 MPa E = 11.8 GPa
Polyurethane (Jamieson et al.)	Density = 0.16 g/cm^3	Tensile strength = 200 MPa
Epoxy (Jacob et al., 1976)	Epoxy foam E = 373 MPa	Epoxy resin E = 4119 MPa (Jacob et al., 1976)

Due to the complex structure of the pelvis, its mechanical properties and response to load are difficult to model. It is widely accepted that flexion of the pelvic bone occurs but the magnitude of this movement has not been quantified.

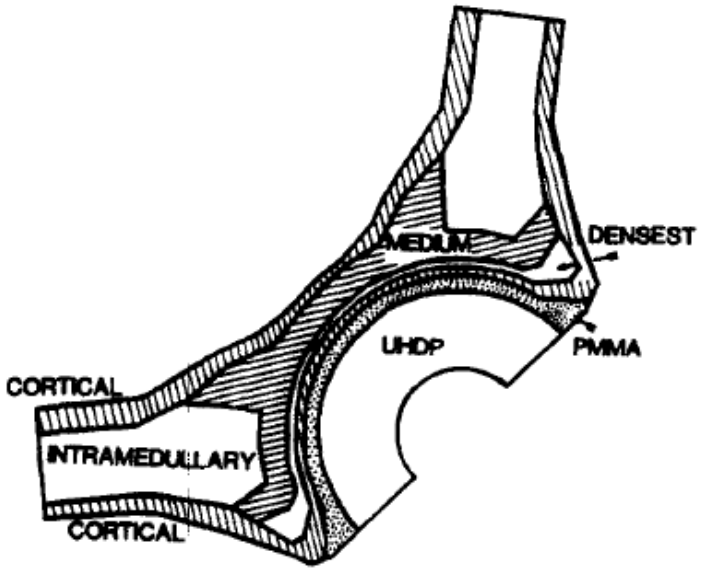

Figure 37: A mid-frontal plane section, one of the asymmetric FE models used to assess stress distribution. Image from Pederson (1982), with permission.

A simple axisymmetric model (Figure 37) has been used to assess stress distribution in THA (Pedersen et al., 1982). The authors believed that due to the almost-hemispherical shape of the acetabular component, cement, subchondral bone and underlying trabecular bone, this area could be represented by a simple axisymmetric model, to gain some general insight into the behaviour of the periprosthetic area.

Working with this hypothesis, in the APTR model a simplified hemispherical pelvic bone analogue was desired for testing with the APTR model. To assess how the deformation of the periacetabular structure affects fluid pressures, a hemispherical bone analogue was designed. It was hypothesised that variation to the thickness of the hemisphere will vary the amount of deformation.

The APTR unit should also be capable of representing bone defects such as focal osteolysis regions in testing. These defects have been represented using *in vitro* bone analogues, either machined by hand using an osteotome and burr (Adler et al., 1992), or more precisely using a custom milling fixture (Jamieson et al., 2010). However to ensure repeatability in the APTR model, it was desirable for these defects to be precision-machined along with the bulk analogue.

Bone analogue selection

Preliminary testing was performed using Sawbones 30pcf closed-cell foam (Appendix 1). In order to have more control over the shape properties of the bone analogue, a mouldable material was investigated.

An epoxy foam hemisphere was moulded for use as a bone substitute (Appendix 2). This material has been used successfully in other studies (Jacob et al., 1976) but it was found to be difficult to obtain reproducible hemisphere samples for the APTR. Thus, an alternative bone analogue was sought and several different candidate materials were tested, as detailed in Appendix 3.

M650 model board (SikaBlock M650, John Burn & Co. Ltd, Birmingham, UK) was chosen for testing due to its similarity to Sawbones 30pcf, and similarity to bone properties. To assess the influence of deformation of the periacetabular structure on fluid pressures, a hemispherical bone analogue was used. Variation of the thickness of the hemisphere would vary the amount of deformation (see Figure 38). The highly controlled machining process was also capable of introducing reproducible defects into the material, to simulate osteolytic lesions. The process of machining these hemispheres can be found in Appendix 4.

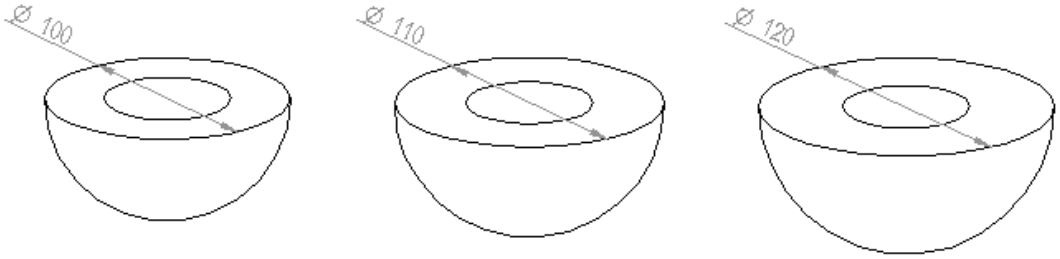

Figure 38: SolidEdge drawing of different hemisphere sizes produced for testing

3.7 Prosthetic components

To improve the clinical relevance of the rig testing, common prosthetic components were used. Metal-on-polyethylene is the most common bearing surface combination in primary THA in the UK (64.4%) (NJR, 2012) and Canada (78%) (CJRR, 2012). A 28mm femoral head is the most common head size (44%) (NJR, 2012, CJRR, 2012) and metallic femoral heads are the most commonly used. Of the cemented cups, the Stryker Contemporary cup (Stryker, Mahwah) is the most commonly implanted (NJR, 2012). Trident hemispherical cups (Stryker, Mahwah) are the second-most commonly used uncemented cups (20%), behind the Pinnacle cup from De Puy (AOA, 2012).

For initial APTR tests a 52mm Osteolock shell with cluster screw holes (Howmedica) with a hooded PE liner (modified to be loose within the shell) was loaded with a 28mm femoral head. To investigate the hypothesis that the presence of screw holes in the acetabular shell affects fluid pressures behind uncemented cups, Trident cups with and without screw holes were also tested with the same 28mm femoral head (see Figure 39).

Figure 39: Images of prosthetic components used in the APTR study. a) Osteolock acetabular cup (hooded liner not shown); b) Trident cup with X3 Polyethylene insert; c) 28mm femoral head used in all tests.

3.8 Clinically-relevant implant fixation

The conditions at the interface between the bone and the implant needed to be considered, as the component fixation has a large effect on pressure generation.

Loosening of a component can be assessed radiographically, by the observation and measurement of a radiolucent line between the implant and the bone. The definitions developed by DeLee and Charnley (1976) to classify cup loosening are still commonly referred to, with the location and extent of lucencies around the cup measured in three specific zones. A continuous radiolucent line that is present in all these radiographic zones and at least 2mm wide is a sign of acetabular loosening. Progressive cup migration on serial radiographs can also be used as a determinant of cup loosening (Schmalzried et al., 1992b, Garcia-Cimbrelo and Munuera, 1992).

In pilot studies with the preliminary APTR design, (see Appendix 2), a clear difference could be observed between different cup designs, with the cup with lower interference (smaller space between implant and bone analogue) producing higher pressure results than the cup with larger periprosthetic space. This implied that the component fixation, or the way in which the cup interacted with the bone analogue, would be a major factor in the pressures measured by the APTR model.

The implantation and fixation techniques needed to be repeatable and clinically relevant (to model 'good' fixation and poor initial fixation). In total hip replacement surgery, the cup component is placed into position and impacted using several sharp blows of a small mallet. This impaction should be simulated in the APTR test setup.

A fibrous membrane analogue was chosen to form part of the fixation modelling as it could affect the mechanical behaviour of the loaded joint (Weinans et al., 1990). Ideally the membrane should have the ability to absorb and exude fluid and have comparable mechanical properties. The shape and positioning of this membrane in the model was also important.

Implant fixation modelling

As discussed in the previous chapter, there are two main fixation options for prosthetic cups – cemented or uncemented fixation. These two fixation methods have previously been simulated in *in vitro* pressure studies. Cemented fixation was represented by Bartlett et al

using a de-bonded femoral stem moving within a thick cement mantle. (2008, 2009a, 2009b) Uncemented fixation was simulated by Walter et al (2005), using aluminium blocks to represent the well-fixed acetabular shell and custom-machined PE liners attached to simulate a loose liner and a non-congruent liner. The strength of simple models such as these is repeatability of results but to test with real prosthetic components the APTR unit must simulate the cup-bone fixation conditions.

Fibrous membrane

As previously described, a thin layer of fibrous material can form between the implant and the bone, in areas where there is a space between the implant material and bone, in both cemented and uncemented implants.

The fibrous membrane is often referred to as the synovial-like membrane due to its histological and biochemical similarity to the joint synovial membrane. Fibrous tissue has a layered, mat-like structure with collagen fibres running parallel to the interface surface. It has low resistance to tension and shear, with a low elastic modulus (Van der Vis et al., 1999, Hori and Lewis, 1982, Ling, 1986). With or without cement, the fibrous membrane is the most compliant structure in the replaced joint (Hori and Lewis, 1982). It is believed to have a non-linear stress-strain curve, becoming stiffer at increasing loads (Goldring et al.). Fibrous tissue exudes fluid under compressive load and is able to reimbibe fluid after load is removed (Hori and Lewis, 1982).

The physical properties of the membrane may vary widely – from a thin layer, a few cell layers thick, surrounding a stable implant, to a 2-3mm thick, fibrous membrane that continues to grow and widen around a loosened prosthesis. If the membrane thickness exceeds 0.5mm, it can significantly decrease the stability of the implant and increase micromotion between implant and bone (Schmalzried et al., 1992b).

Due to these mechanical properties, the presence of a thick fibrous tissue membrane is likely to affect fluid movement and pressure within the joint capsule following THA. An *in vitro* representation of implant fixation needs to incorporate an appropriate analogue for the fibrous membrane.

Fibrous membrane analogue

In previous studies by Waide and colleagues, the mechanical effect of a fibrous membrane has been approximated by a layer of silicone elastomer (RTV 184 with 5% silicone oil) (2004a) applied to the bone with the use of a spacer and vacuum system (2004b). A soy-based wax barrier (EcoSoyaTM CB-135, Maryville, TN) has also been used to simulate a femoral cement-bone interface (Cherukuri et al., 2010). This wax barrier increased the interface micro-motion *in vitro*, generating values similar to those obtained from cadaver specimens. When a simple latex membrane was used in a similar way in APTR pilot studies, pressures behind the completely loose cup were higher with a membrane than without (Appendix 1), and produced higher displacement values, representative of interface micro-motion.

These flexible, impermeable membranes approximate the mechanical behaviour of the fibrous membrane under load but not the fluid interactions that may occur. As part of the current study, a permeable fibrous membrane analogue material was sought for use in the rig.

In a study by a colleague (Wright et al., 2012), permeability, reabsorption and compression tests (detailed in Appendix 5) were performed on various candidate materials, including silicone rubber and a woven cloth material. The properties of two of these materials are shown in Table 8 and compared with the properties of the *in vivo* fibrous membrane as found by Hori and Lewis (1982).

Table 8: Properties of fibrous membrane material and analogues

Material	Composition details	Permeable?	% Reabsorption	Elastic modulus (MPa)
Fibrous membrane (Hori and Lewis, 1982)	Collagen fibres in parallel sheets, layered in 'matlike' structure.	Yes	n/a	1.98
Vileda all-purpose cloth	55% Viscose, 10% cotton, 20% polypropylene, 15% polyester	Yes	65.6	1.33
Silicone rubber	High tear, two-part moulding rubber, addition cure	No	0	2.81

Although both silicone rubber and the all-purpose cloth had similar elastic moduli to the *in vivo* membrane material, the silicone was not permeable and thus deemed inappropriate for use. The all-purpose cleaning cloth was made of fibrous strands woven together into a 1mm-thick,

compressible, oil-permeable membrane. A structural comparison of this material with the fibrous tissue from the study by Hori & Lewis (Hori and Lewis, 1982) is shown in Figure 40.

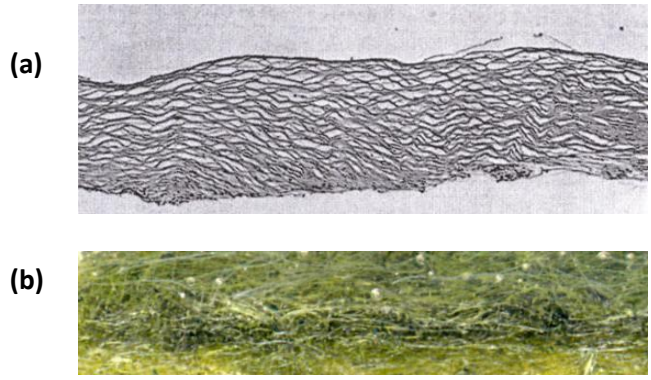

Figure 40: Image showing a) cross-section of fibrous tissue and b) cross-section of Vileda cloth selected to represent fibrous tissue (Wright et al., 2012).

Similarities between the cross-sections of the two materials can be seen, with layers of wavy fibres running perpendicular to the material surfaces. Due to its structure, and its properties of fluid interaction and elastic modulus, the Vileda all-purpose cloth was chosen for use as a fibrous membrane analogue.

Head-cup adhesion

From laboratory experience (see Appendix 1 and 2), and from studies by other groups (Clarke et al., 2003), it is known that a thin film of the lubricating fluid between the head and cup can cause the bearing to 'stick together' – for the cup to adhere to the loading head. The implication for testing with the APTR unit is that the cup and loading head will essentially move as one unit.

The thin film has cohesive force (sticking the fluid to itself) and adhesive force (sticking the fluid to the solid surface). For the head to move in the y-direction, relative to the cup, these adhesion forces must be overcome. At the dome of the cup there are pure adhesion forces resisting motion; at the periphery of the cup it is the shear force within the fluid (cohesion force), or viscosity, resisting this motion. With a well-fixed cup (Figure 41a), the friction between the cup and bone is greater than the cohesion force created by the viscosity of the fluid, and the head is able to disengage from the cup. With poor fixation between cup and bone (Figure 41b), the friction force between the cup and bone is less than the cohesion force within the fluid, and the head and cup will move together as a single unit.

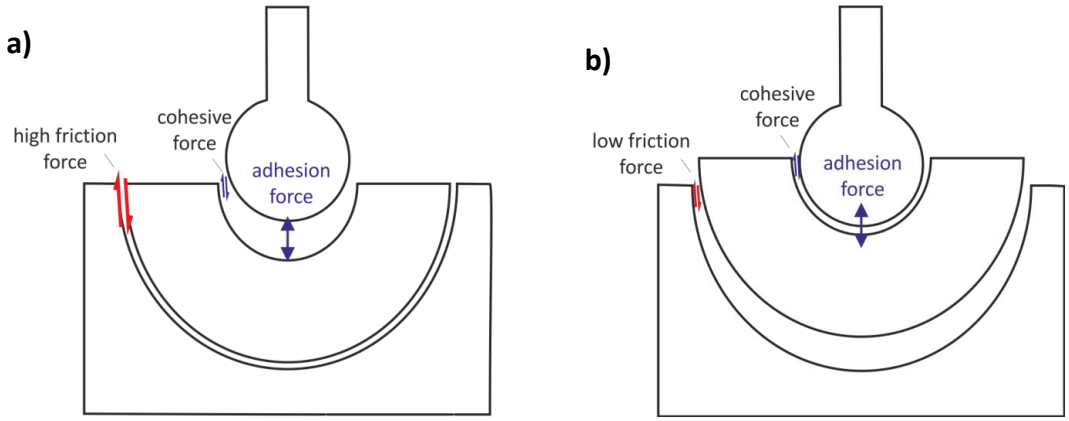

Figure 41: Image showing forces and head-cup behaviour, related to head-cup adhesion effect.

This affects fixation modelling – if the cup is completely loose, the adhesion force between the head and the cup will overcome the fixation force and the cup will disengage completely from the bone analogue as the head is raised. It is important to take this behaviour into account when analysing results from the APTR model.

Implant fixation selection

It was decided that the most repeatable fixation mode to represent in the rig would be a completely loose cup, with an insufficient press-fit interference, modelled by matching the cup diameter with the cavity instead of over-sizing the cup (see Figure 42).

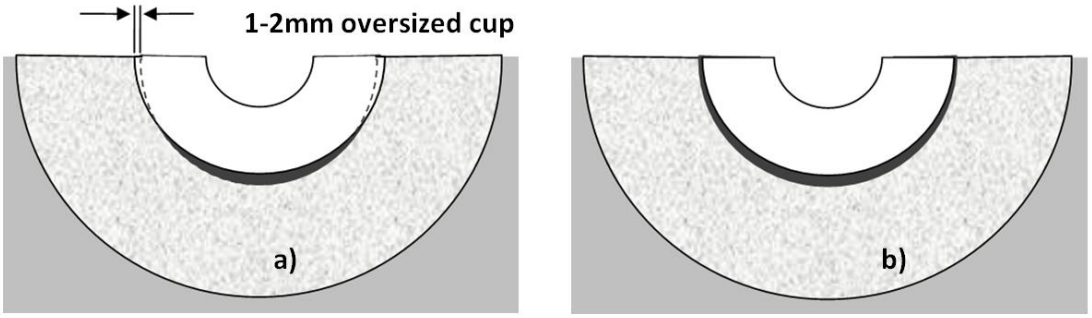

Figure 42: Image of a) good press-fit cup fixation, and b) cup fixation used in APTR setup

To approximate the effect of impaction of the cup by the surgeon *in vivo*, in the APTR testing the cup was positioned in the test hemisphere by hand, and checked for alignment with a spirit level, before undergoing a pre-load of 1kN for 20 cycles at 1Hz.

The effects of a fibrous membrane between cup and bone were modelled using a 10mm wide, 1mm thick circumferential band of the membrane analogue material described in the earlier

paragraph, around the periphery of the cup, as shown in Figure 43. Due to the low degree of clearance between the cup and the cavity, this membrane is compressed to less than 0.5mm under load.

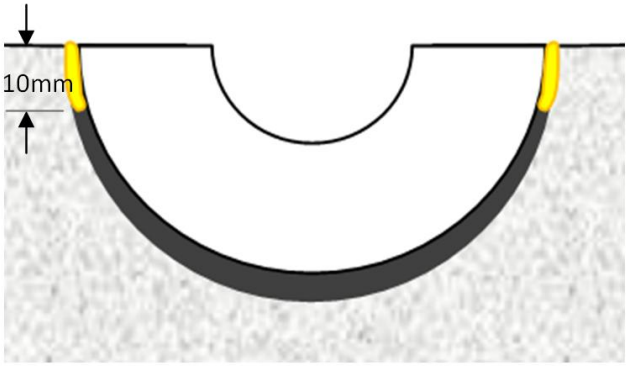

Figure 43: Image showing fibrous membrane position behind cup

3.9 Appropriate pressure measurement system

Predicted pressure range

Intra-articular pressure should be distinguished from contact pressure – this is pressure within the synovial joint cavity, not the contact pressure between opposing joint surfaces. Several studies have measured pressures associated with the hip joint *in vivo* (Walter et al., 2004, Wingstrand et al., 1990, Soto-Hall et al., 1964, Tarasevicius et al., 2007). Resting pressures in the hip joint capsule have been measured from 0 kPa to 37kPa, depending on the joint orientation, and pressures up to 103 kPa were recorded during sitting or rising from a chair (Hendrix et al., 1983).

Pressures generated by poorly-fixed femoral components and loose liners have also been explored by *in vitro* mechanical models (Ferguson et al., 2003, Walter et al., 2005, Khalily et al., 1998, Bartlett et al., 2008), with pressures up to 684 kPa recorded (Walter et al., 2005). Preliminary tests with an early APTR model iteration produced pressures of up to 200kPa (Appendix 1 and 2), although these were amplified by a latex membrane. Sub-atmospheric pressures were also observed in preliminary tests.

Based on these results, the possible pressures were expected to be between 100kPa and 200kPa, with negative pressures also possible. The transducer to be used in the APTR must be able to measure pressures over this range.

Transducer selection

Transducers must be able to measure the predicted range of pressures, including negative pressures. Although previous *in vitro* models have measured up to 684kPa, and initial pilot studies measured 200kPa, further pilot studies indicated that maximum pressures expected in the APTR unit would be around 100kPa. The introduction of sensors should not significantly disrupt other elements of the rig. To minimise the impact on the host material, the smallest possible transducer that could measure pressures over 100kPa was used. Transducers chosen for the final rig were Kulite XT-190 miniature pressure transducers (Kulite Sensors Ltd, Basingstoke, UK), rated to a maximum pressure of 170kPa.

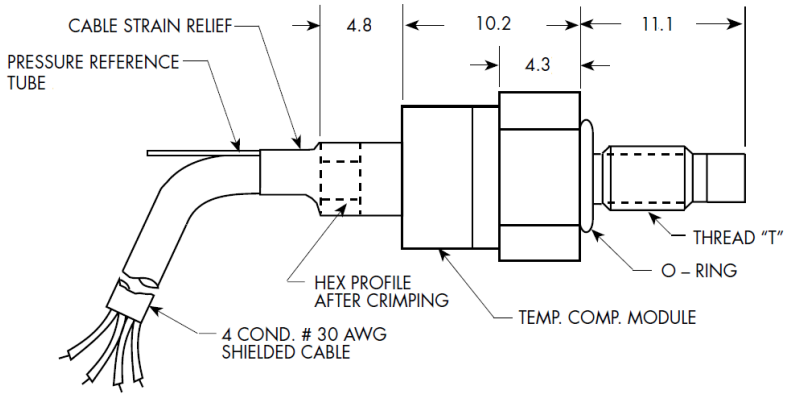

Figure 44: Schematic of Kulite XT-190 transducer (dimensions in mm). Image from Kulite Sensors Ltd, with permission.

Despite the small size of these transducers, a relatively large clearance was required for placement at the bone-implant interface. To minimise transducer impact on the host material, and for ease of assembly, it was determined that these transducers would be placed at a distance from the implant-bone interface. This will be explained in the next section.

Pressure transmission

Fluid pressures cannot be measured directly at the interface. The disruption of the bone analogue structure is illustrated in Figure 45 a). For this reason, pressure transmission tubes were used to transmit pressures from the cup-bone interface to the transducers (Figure 45 b).

Transmission channels have been successfully used in a study by Bartlett *et al* (2008), to measure pressures at the stem-cement interface.

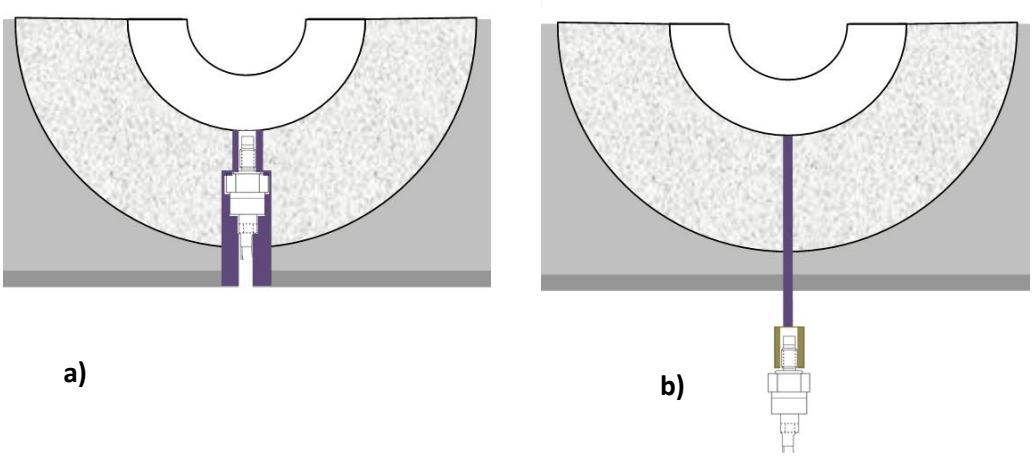

Figure 45: Comparison of required clearance with and without a transmission channel. a) clearance required for transducer at interface (surface clearance radius up to 16 mm, clearance volume 13 773 mm^3), and b) clearance required for transmission channel (clearance radius 1.75 mm, clearance volume 904 mm^3).

To measure pressures within the rig, pressure transducers needed to be in direct communication with the area of interest, in this case the implant-bone interface. Preliminary studies have shown that transmission holes drilled into the host material can deform under load (Appendix 1). Flexible tubing was introduced to reduce this deformation (Appendix 2), but the relative motion between the test hemisphere and the rig chamber still produced artefacts in the pressure signal. These results prompted the use of rigid transmission tubing for the final rig.

The transmission tubes between the measurement face and the pressure transducer needed to accurately transfer pressures to the transducer. These tubes were required to be as short as possible, with a sufficient diameter to minimise frictional losses, and be of equal lengths if comparisons were to be made between pressures measured on different transducers.

Base pressure

In the replaced hip, a positive pressure is present in the capsular fluid, while the periacetabular bone remains at neutral pressure (Hendrix et al., 1983, Robertsson et al., 1997). This pressure difference has been simulated by the application of a negative periprosthetic pressure in the Walter rig (2005), and in the Bartlett study by an elevated filler tank (2008). In the APTR

model, a positive base pressure was imposed on the rig with the application of a pressure head – a tube of fluid that applied a constant pressure to the rig (see Figure 46).

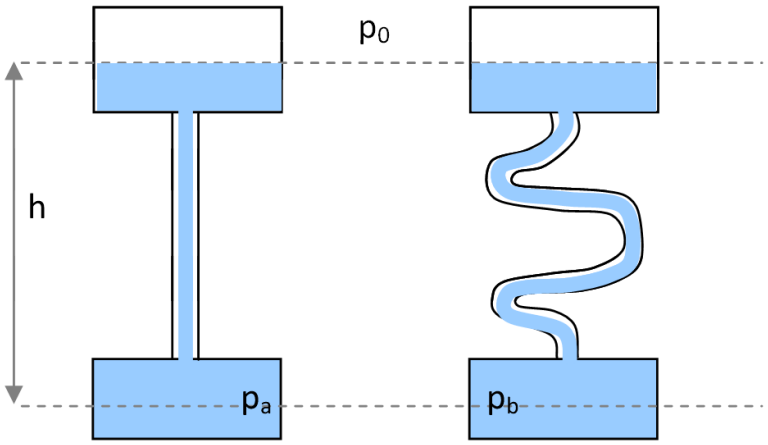

$$p_a = p_b = p_0 + \rho gh$$

Figure 46: diagram showing pressures generated by a height of fluid

This fluid-filled tube was attached to an oil reservoir, to ensure that pressure fluctuations within the rig would not significantly affect the height of the fluid. Resting joint pressures *in vivo* have been measured between 0 and 37 kPa (see Table 3), so the oil reservoir was positioned to apply a base pressure to the rig that falls within this range. Increasing the height of the reservoir would increase the base pressure applied to the rig, allowing the effects of joint effusion to be explored.

Positioning of pressure channels

In order to investigate the fluid pressure characteristics behind the cup, three transducers were placed in communication with the cup-cavity interface, at the positions shown in Figure 47.

As previously described in section 2.6, a high incidence of osteolytic lesions have been observed in the superior zone of the cup, as well as in the central area. (Leung et al., 2005, Kitamura et al., 2005). Transducers were placed in the test hemisphere to measure pressures within these zones. The pole transducer was placed in the central zone of the cup, in line with the direction of loading when loaded axially. Similarly, the angled transducer was placed in the superior zone, in line with the axis of loading when the APTR was tested at a 30° angle.

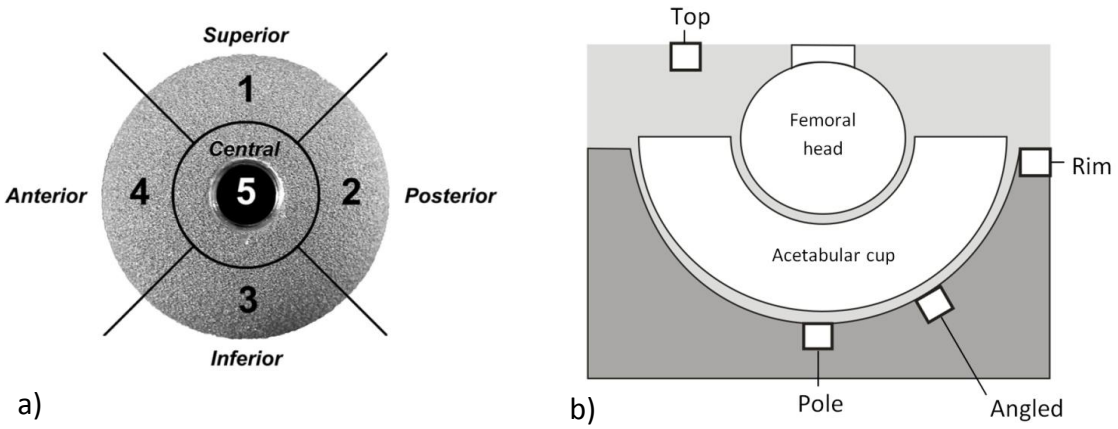

Figure 47: Schematic showing regions of interest for pressure channel positioning, including a) the different zones of the cup, as defined by Kitamura and colleagues (Image from Kitamura (2005) with permission); and b) the positions of pressure measurement within the chamber.

The rim contact area between cup and bone has previously been identified as a potential pathway for fluid ingress (Kitamura et al., 2005), so a third transducer was placed at the rim of the cup, with its centre point 5mm from the surface of the test hemisphere, to measure the magnitude of pressures at the rim. The top transducer was placed in communication with the chamber fluid, in order to assess whether pressure fluctuations were occurring within the bulk fluid.

3.10 Summary of design decisions

- Rig loading – 1kN 1Hz cyclic sinusoidal load at two load angles (axial and 30°), with a single-cycle micro-motion simulation.
- Synovial fluid analogue – vegetable oil was chosen due to its comparable viscosity properties and its compatibility with the rig design.
- Joint capsule – a rigid chamber was used, with a pressure head applied through an elevated pressure reservoir.
- Bone analogue – M650 model board, with similar properties to Sawbones 30pcf foam, was machined into a hemisphere with a central acetabular cavity, for use as the bone analogue.
- Prosthetic components –an Osteolock acetabular cup with a loose hooded PE liner and a Stryker Trident cup with and without screw holes in the metal shell were obtained, to be loaded through a 28mm metal femoral head.

- Component fixation – a completely loose fixation situation was simulated, with the option of a fibrous membrane between implant and bone analogue material.
- Pressure measurement - transducers were Kulite XT-190 pressure transducers, measuring interface pressure through rigid transmission tubes.

3.11 Chapter Discussion & Conclusions

The aims of this chapter were to identify the design requirements for the rig, and to use these requirements, as well as results from preliminary studies, to make design decisions with respect to the rig. The main design requirements were identified as the pressure measurement system, the loading applied to the rig, the synovial fluid analogue used, the joint capsule design, the analogue material simulating pelvic bone, the prosthetic components and the fixation of these components in the bone analogue. This chapter outlined how the critical design decisions for the rig were made, using information from pilot studies and from the wider literature, to ensure these important elements were represented in the APTR model. The next chapter explains the construction and preliminary testing of this rig.

4. APTR Design and Development

The design decisions made in Chapter 3 were incorporated into the design of the APTR model. This chapter details its construction and preliminary testing.

4.1 Chapter Aims

The aims of this chapter are to describe the construction and development of the APTR model, to outline preliminary testing and the changes based on this testing, to present the results of further testing (to determine whether clinically significant pressure results can be obtained) and to discuss the implications and relevance of these test results for the APTR model.

4.2 Rig Description

The APTR rig comprised three main components – the rig chamber, the rig cover plate and the oil reservoir, as shown in Figure 48. These components were mounted in the Dartek for loading and attached to a data recording system. The construction and assembly of the rig components is presented below.

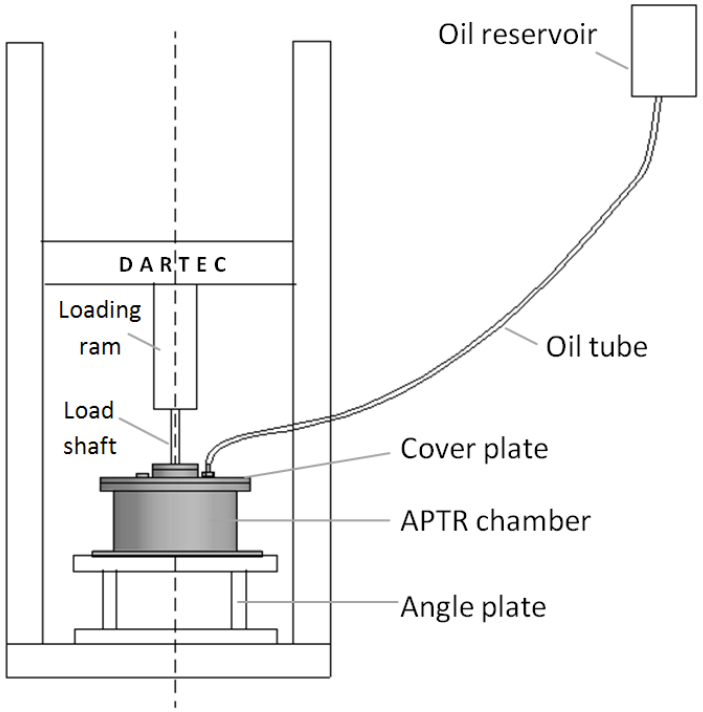

Figure 48: Schematic of rig showing rig chamber, rig cover plate and oil reservoir seated in Dartek

Rig chamber

The rig chamber (shown in Figure 49) comprised an aluminium cylinder attached to a 6mm aluminium base plate. The base plate was attached via screw holes to an angle plate that could be set to any angle between 0° and 90°. An aluminium rim was bonded to the top of the cylinder to provide space for the sealing O-ring (NBR O-ring, Brammer UK) and sealing screws. The custom-machined test hemisphere (M650 model board, John Burn, Birmingham UK, see Appendix 4) was seated in the centre of the rig chamber using Woods metal (Bend Alloy 70°C, Lowden Metals, Halesowen, UK), and centred using a custom introducer tool.

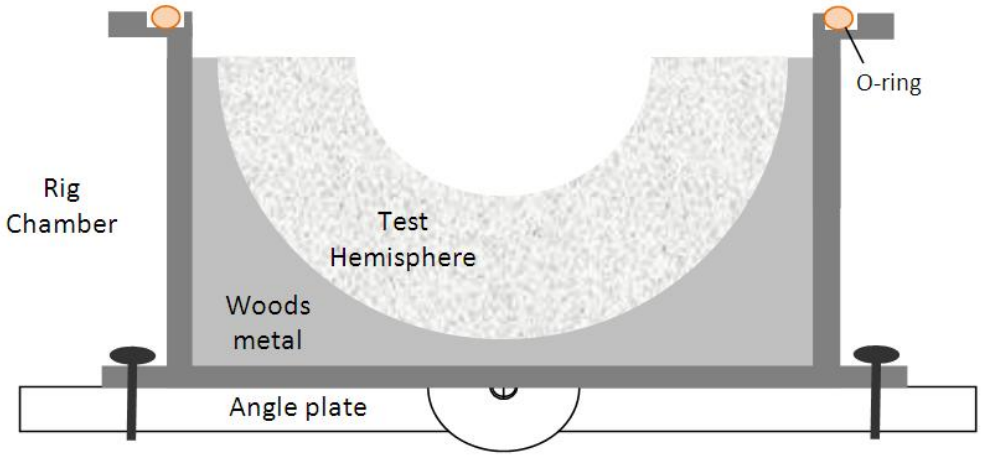

Figure 49: Schematic of rig chamber

Pressure transmission channels were drilled into the rig, through the chamber wall, the Woods metal and the test hemisphere, at three positions as shown in Figure 51. Tungum pressure transmission tubes with female AGS pipe nuts were sealed into the transmission channels with silicone sealant (Dow Corning 794F Neutral Silicone). Acetabular prosthetic components were then fitted inside the hemisphere cavity. For initial testing this was a 52mm ED Osteolock prosthetic cup with a loose hooded liner. An inner sealing ring (12mm neoprene cord, Seals Direct UK) was placed around the hemisphere to restrict the volume of fluid and to provide further sealing within the chamber (shown in Figure 50).

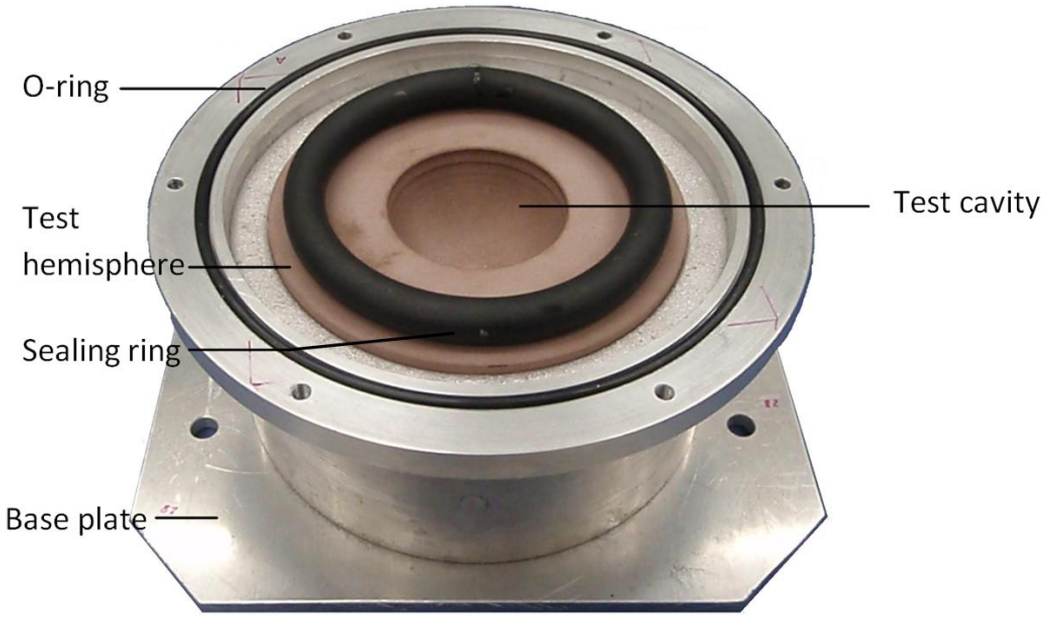

Figure 50: Image showing rig components (without transmission holes or tubes)

Four pressure transducers (XT190 Miniature Pressure Transducer, Kulite, New Jersey) were attached to the APTR rig. One was screwed in to the rig cover plate, and three were attached to the transmission tubes via customised pressure fittings (as shown in Figure 51).

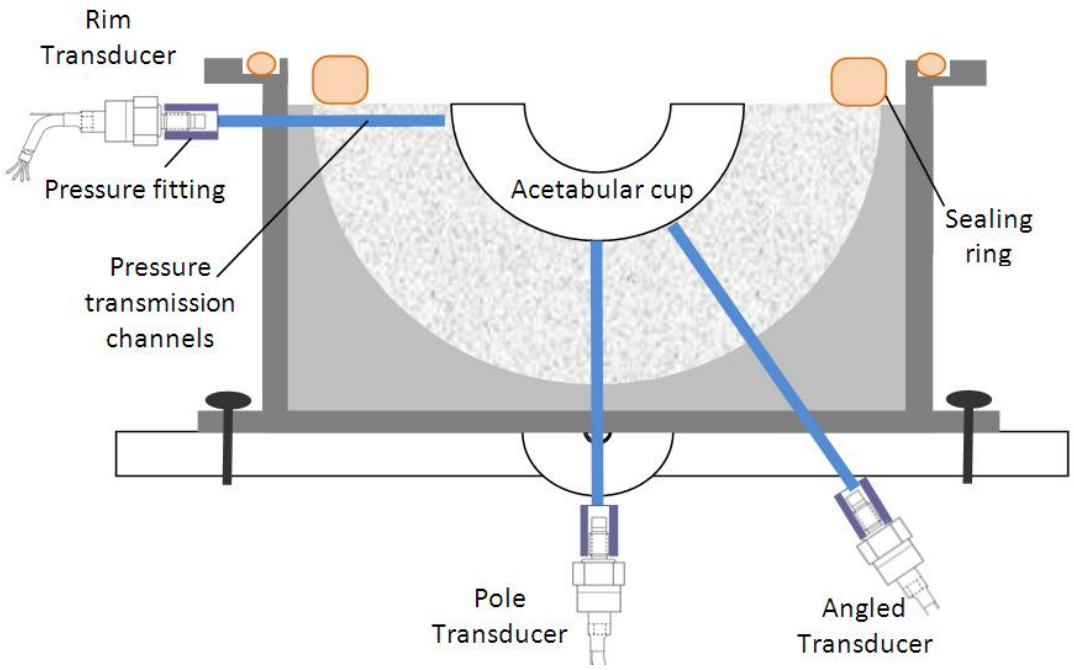

Figure 51: Schematic of rig chamber with components fitted

Rig cover plate

The two-part rig cover plate consisted of a plate and a seal (see Figure 52). The plate was machined from a 6mm aluminium plate, with a 45mm hole in the centre. A transducer attachment part and a tube attachment for joining the oil reservoir to the rig chamber were also attached to this plate. A detachable aluminium seal held a silicone sealing sheath in place, which allowed the load shaft to move axially to load the components while constraining the oil in the chamber (Figure 52).

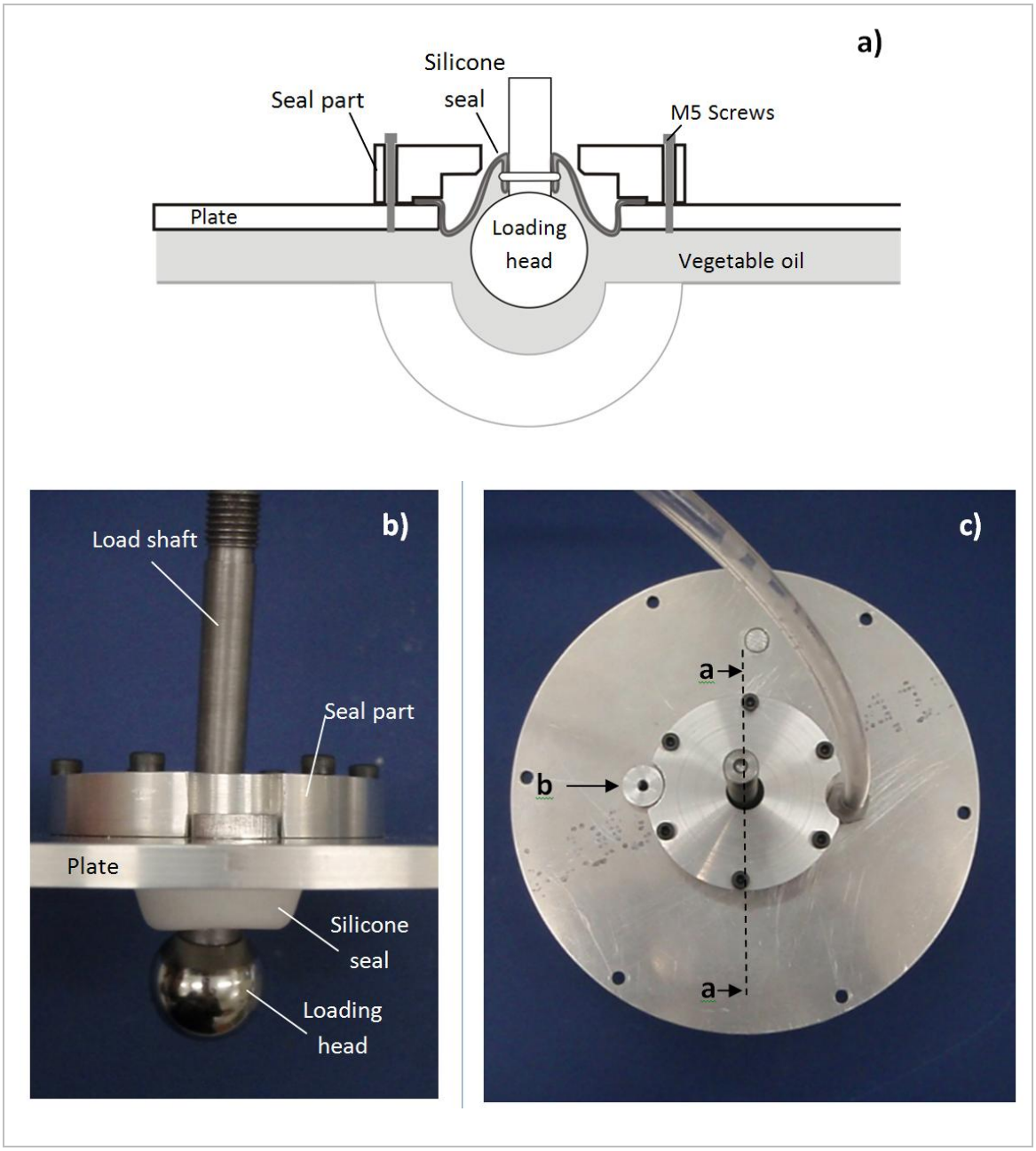

Figure 52: Details of rig top seal and interactions with loading head: a) illustration showing cutaway view of the sealing of the head in the rig (oil tube and transducer are hidden); b) side view of the top plate and c) top view of the part, including the direction of the view in b), and the cutting plane for the illustration in a).

Oil reservoir

A modified wound drainage device (Redon wound drainage system 600, Medinorm, Germany) was used as an oil reservoir, as shown in Figure 53 [a]. This reservoir was supported on a retort stand to provide a static head of 775mm, and connected to the rig cover plate using a clear 9mm PVC tube (see Figure 53 [b].

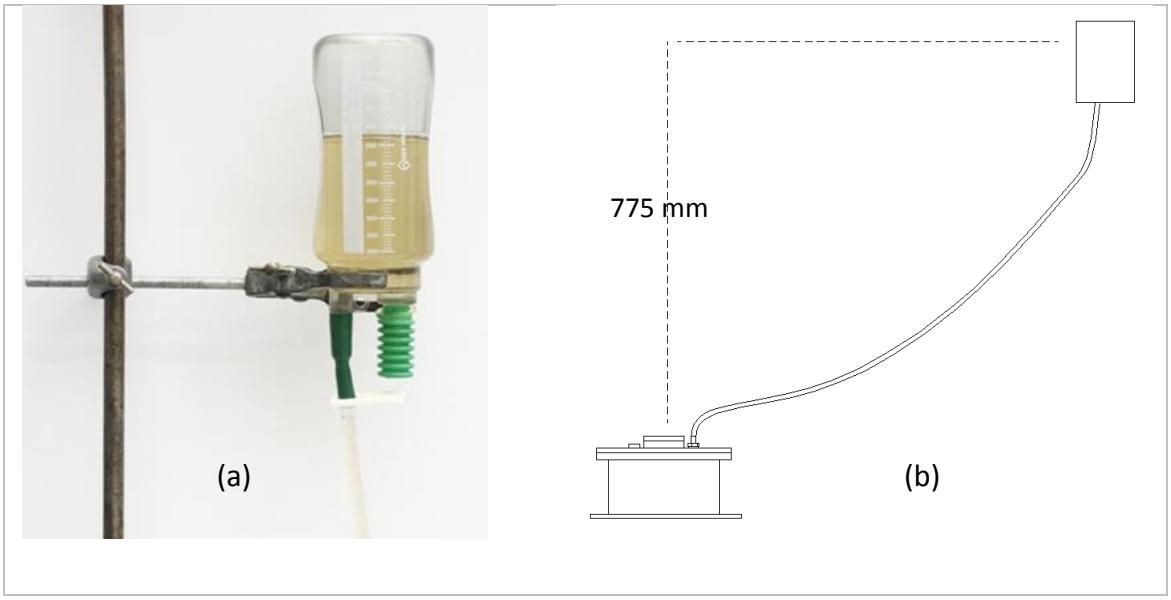

Figure 53: [a] image of modified wound drainage device used as oil reservoir; [b] Schematic showing reservoir position above rig top

4.3 Instrumentation

The preliminary instrumentation of the APTR is outlined in Figure 54. The Dartek was controlled by the Workshop 96 program (Workshop 96 Toolkit, V2.18, Zwick Testing Machines Ltd, UK), which was programmed for the chosen loading regime. Movement of the loading head was executed in load control. The load-displacement outputs during testing were recorded on the PC that programmed the controller.

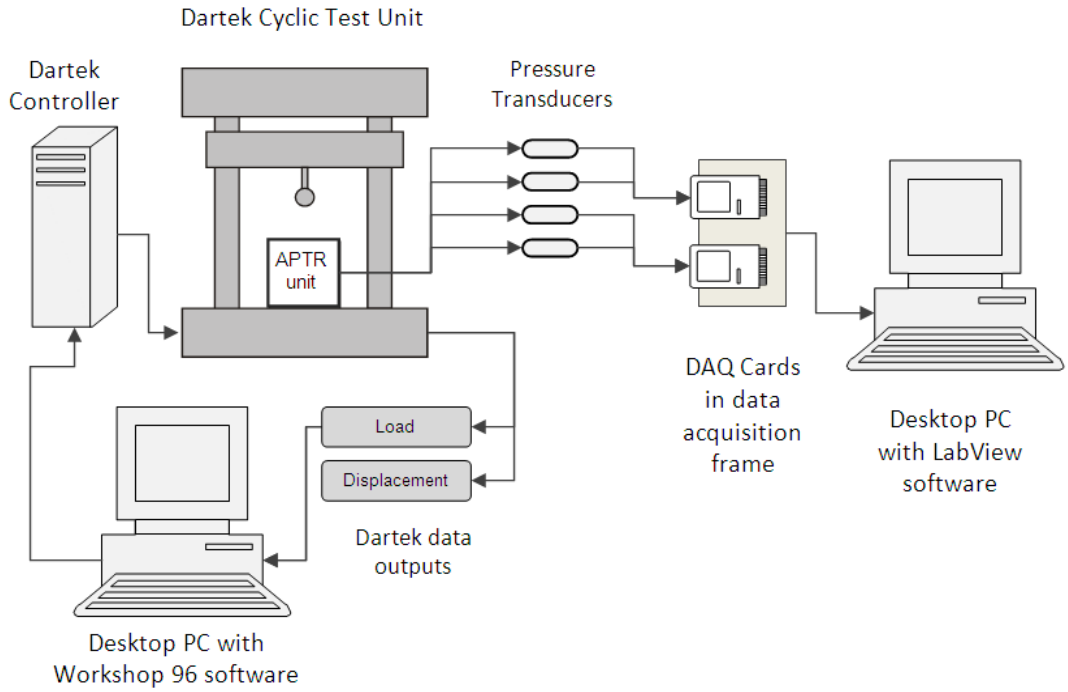

Figure 54: Schematic describing the components and connections in instrumentation of the APTR rig

Transducers connected to a data processing frame with two data acquisition (DAQ) cards were used to measure the pressure at different points in the rig. Data were recorded by LabView software (LabView 7.1, National Instruments) on the PC connected to the data frame with a sampling rate of 20Hz. Pressure data were collected in volts and converted to kilopascals using calibration equations. Once the data were calibrated, the mean pressure amplitude between load cycle 40 and 45 was calculated for each test, by plotting the data in Excel, identifying cycles 40-45 and taking the amplitude over this period.

4.4 Calibration

Transducers were calibrated using a 20 bar calibration module (Druck DPI 610). For each channel, 10 calibration datasets were collected, with at least eight points in each dataset. During calibration, the applied pressures were increased and then decreased to ensure no hysteresis effects. Calibration curves were obtained from this data from each transducer. Results from this calibration test can be found in Table 9. Once these calibration equations were obtained, preliminary testing could be completed.

Table 9: Calibration equations for each transducer channel

Transducer	Calibration (kPa)	
	Conversion factor	Uncertainty (kPa / V)
Top	**P = 19.914 V**	2.55 x 10-3
Rim	**P = 19.867 V**	3.08 x 10-3
Angled	**P = 19.998 V**	3.51 x 10-3
Pole	**P = 19.763 V**	2.95 x 10-3

The uncertainty values, representing the residuals from the least squares fitting of the calibration curve, are extremely low, indicating the accuracy of the calibration values. Pressure measurements were obtained by multiplying the voltage outputs from the transducers by these conversion factors. Pressures are presented with respect to atmospheric pressures (gauge pressure measurement). The offsets of the calibration curves were therefore determined by assuming that pressures on the transducers were zero before they were connected to the rig.

4.5 Preliminary test results

Cup insertion

The Osteolock 52mm ED cup was modified so the locking liner was loose and free to move approximately 2mm axially with respect to the metal shell. The cup was inserted by hand, so that the top of the metal shell was continuous with the surface of the test hemisphere. The shell was inserted without any mechanical fixation and without a press-fit condition due to the external diameter being equal to the cavity diameter. This fixation condition was chosen to represent a completely loose cup, with no mechanical fixation of the cup within the cavity, as described in section 2.5.

Test Methods

Preliminary tests were performed, to assess the rig performance and determine the most appropriate method of data analysis. This preliminary testing was completed under several different conditions, using the Osteolock prosthetic cup, with a loose hooded liner. These were:

- Testing at different frequencies (0.25Hz, 0.5Hz, 1Hz, 1.5Hz).
- Testing with and without a fibrous membrane (see Figure 55).
- Testing with a screw hole in the metal shell of the prosthesis covering or not covering the opening of the angled pressure transmission tube (see Figure 56).

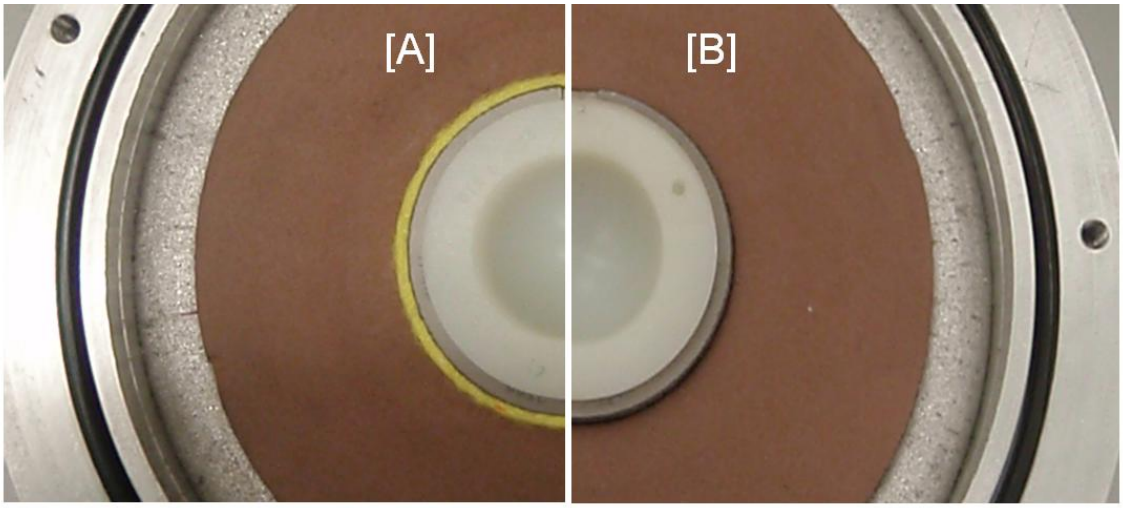

Figure 55: image showing prosthetic cup [A] with membrane and [B] without membrane

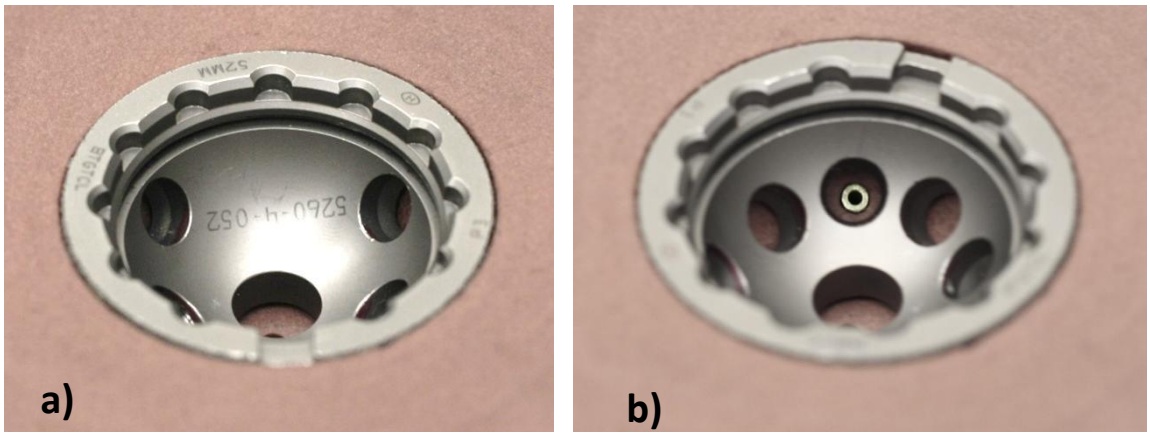

Figure 56: Image of the Osteolock cup without the PE liner, showing the screw hole in the metal shell (a) covering the angled pressure tube and (b) in communication with the tube opening.

A single test set involved setting up the rig, performing a series of tests and then dismantling and cleaning the rig (cleaning procedure is detailed in Appendix 6). Six test sets were performed, the first two investigating the effect of a periprosthetic membrane on pressure, and the following four to investigate the effects of frequency and the positioning of the screw holes on the measured pressures.

4.6 Results

Pressure readings from the transducers were calibrated using the values in Section 4.4. Sample calibrated data is shown in Figure 57, showing the type of data generated by the four pressure transducers at different points in the APTR.

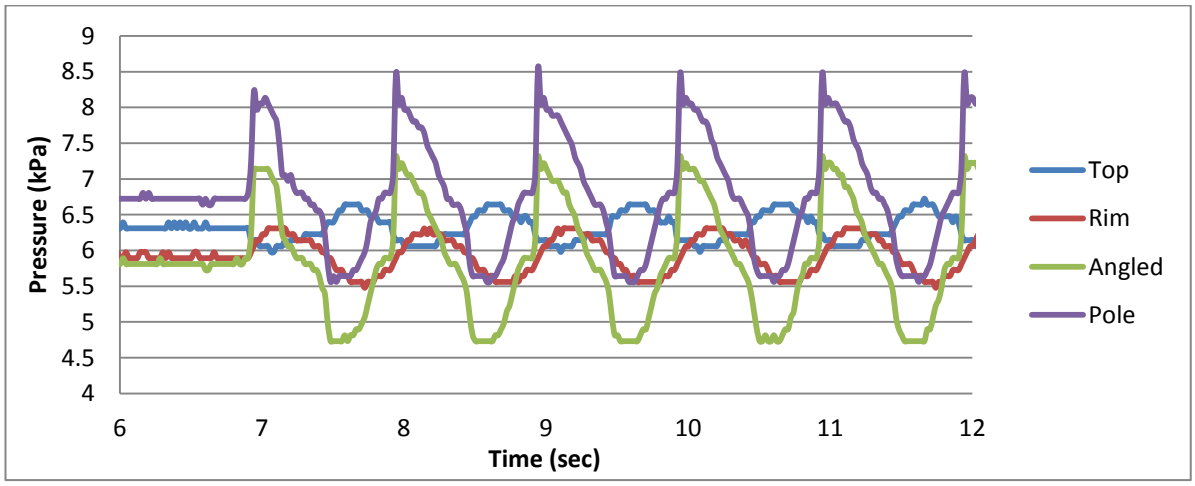

Figure 57: Example of calibrated data from a single preliminary test (first five load cycles shown)

Using Microsoft Excel, these data were analysed to find the pressure amplitude of each test. Analysing graphs of the signal data, it was apparent that some signals were irregular towards the start of the test, possibly due to bedding in of the implant in the cavity, or possibly trapped air bubbles behind the cup. To ensure the pressure amplitude values were representative of the test data and not affected by these signal regularities, a steady-state period of the test data was defined as the period between load cycles 40 and 50 (an example of signal amplitude is shown in Figure 58). Pressure amplitude was defined as the difference between the maximum and minimum pressure values during this period (Figure 58[A]). This value would give a measure of the pressure changes due to loading. The factors affecting pressures in the APTR unit were explored using these values, as outlined in the following paragraph.

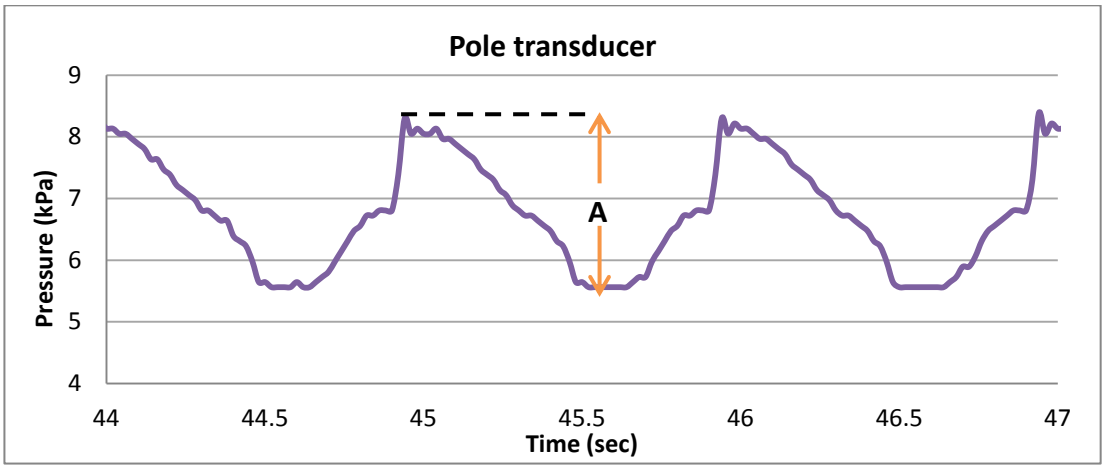

Figure 58: Image showing signal amplitude [A] at load cycle 45

Notes on boxplots

Boxplots in this thesis describe the significant features of the data, as described in Figure 59. In many boxplots, y-axis scales have been adjusted to highlight differences in the data.

Median: The line in the centre of the boxplot, the median line, indicates the central measurement in the sample.

IQR: The inter-quartile range describes the middle two quarters of the data, and the IQR box shows the boundaries of this range.

Whiskers: The top whisker marks the highest data point observed within 1.5 IQR lengths of the 3rd Quartile (top of the IQR box); the bottom whisker marks the lowest value within 1.5 IQR lengths of the 1st Quartile (bottom of the box).

Outliers: Data points that fall outside 1.5 x IQR from the limits of the IQR box are considered outliers and the values are indicated with circles.

Extreme outliers: data points that lie over 3 x IQR are considered extreme outliers and the values are indicated by flat lines.

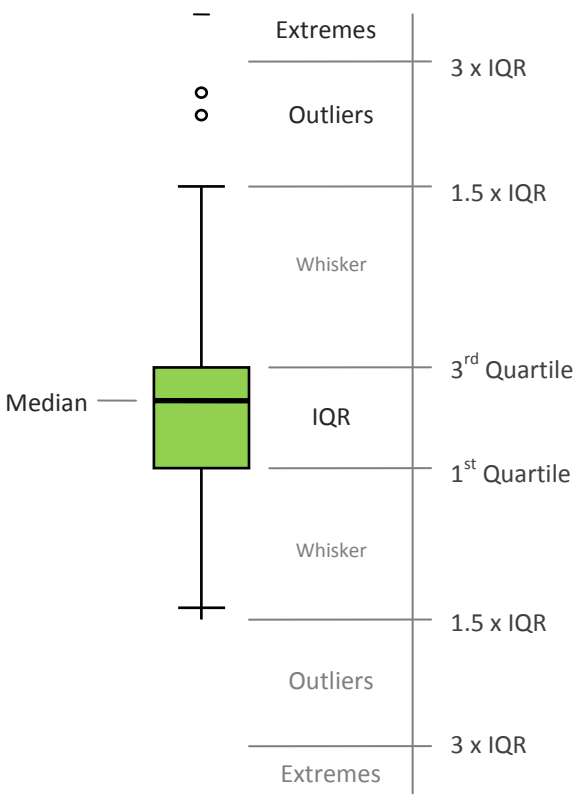

Figure 59: Explanation of boxplot data presentation

Observations from initial testing

General observations

A rig was constructed that could measure pressure behind a completely loose cup in a hip joint analogue. Different pressure amplitudes were measured on different transducers, with the highest pressures measured on the Angled and Pole transducers. The pressure amplitudes measured on the top transducer had a lower amplitude, as it was measuring pressure fluctuations in the bulk chamber fluid.

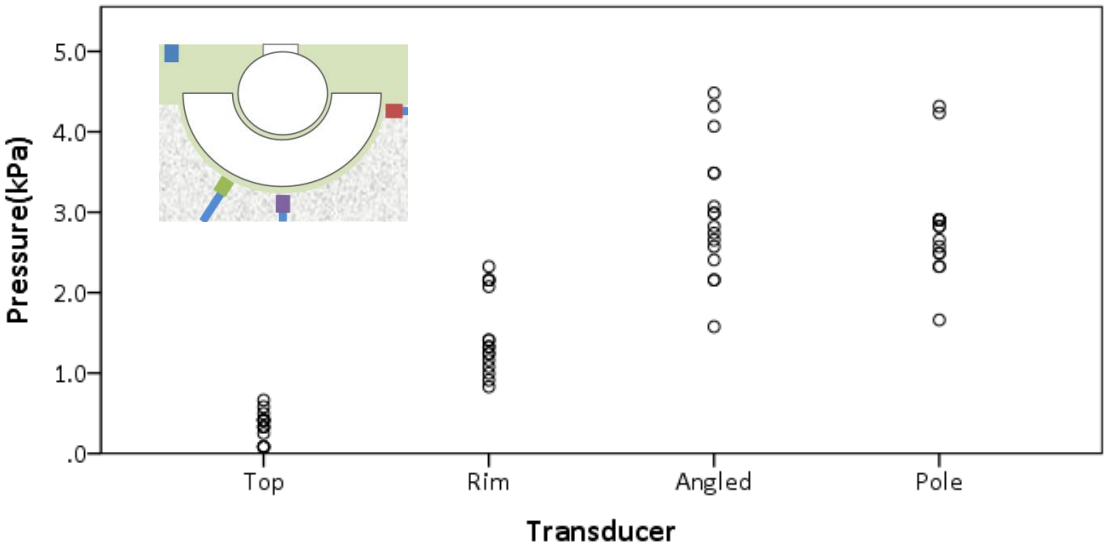

Figure 60: Graph showing the range of pressures measured on different transducers.

The pressure amplitudes measured during testing were very low, less than 5kPa, much lower than the values indicated from pilot testing (Appendix 1 and 2). This may have been due to leaks in the system, described in the next paragraph.

Observation of rig leakage

This rig was designed to test components at different angles and a flexible sheath was incorporated into the rig top seal to facilitate different loading configurations. However this sheath was prone to leaks and breakage and was therefore deemed unsuitable for continued use in the APTR model. A different approach was required for the next iteration of the rig. Leaks were also observed from the transmission channels; an improved sealing system was also required for further testing. Once these areas of improvement were identified, no further tests were performed with this configuration of the APTR; this accounts for the low number of tests in this section.

Effect of local features on transducer pressures

To investigate the effect of a component feature close to a transmission channel, a series of tests were completed with the angled transmission channel either communicating with a screw hole (Figure 56 b) or being covered by the shell (Figure 56 a). These tests were conducted without a membrane, at a frequency of 1Hz. At least six tests were performed under each condition (uncovered n=10, covered n=6), and results of these tests are summarised in Figure 61.

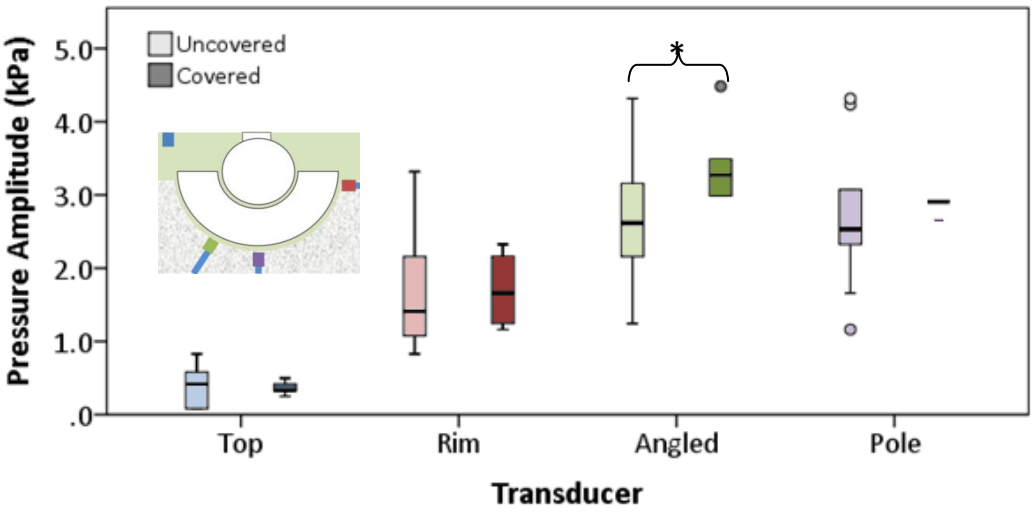

Figure 61: Boxplots comparing pressures measured with the angled transmission tube covered or in communication with the screw hole. Statistically significant differences are shown with a * ($p < 0.05$)

Mann-Whitney analysis was performed to determine if any transducer measured a significant difference. A pressure amplitude increase when the screw hole was covered was observed on the angled transducer (Mann-Whitney, $p = 0.031$). As the angled transducer was in communication with the screw hole it was expected to be the one most affected by this change in component geometry local to the transmission tube. Although the rim transducer appeared to record a higher median pressure with the transmission tube covered, this was not statistically significant at the 0.05 level. Top and pole transducers also measured no significant difference.

Tests were also performed with the APTR unit, with and without a fibrous membrane (Figure 93), to determine its effect on pressures measured by the APTR unit. Mann-Whitney U analysis was performed on the data to determine if this difference was significant. While the

other transducers showed no significant difference at the 0.05 level, the pressures on the rim transducer were significantly higher in the presence of a membrane ($p = 0.037$).

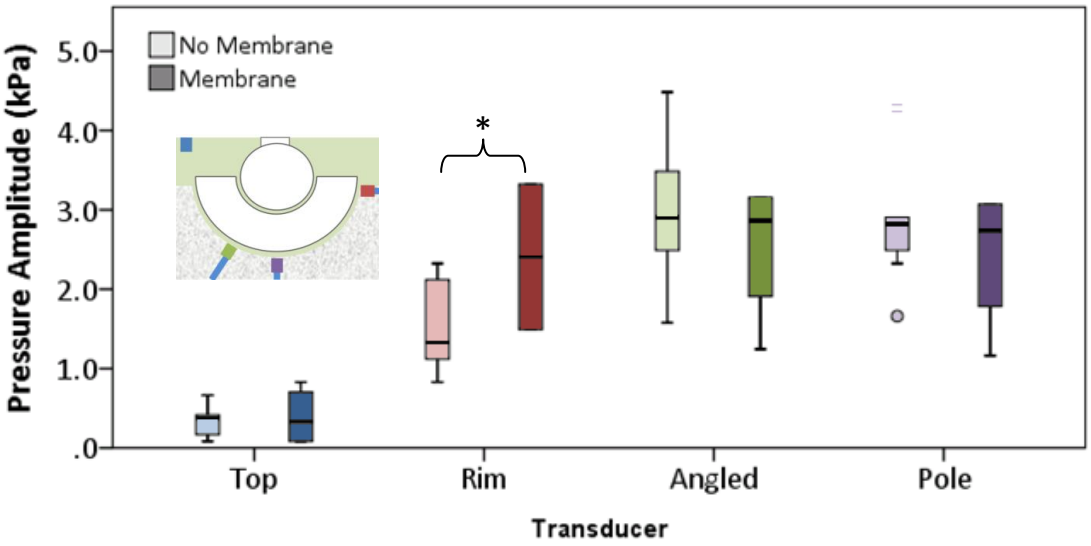

Figure 62: Effect of membrane on pressures in initial axial testing. Statistically significant differences are shown with a * ($p < 0.05$)

The top transducer, measuring pressure changes in the bulk chamber fluid, was not affected by the presence of a membrane, the change in frequency, or the position of the screw holes. These tests yielded evidence that changes to features adjacent to the transmission channels affected the pressures measured by the APTR unit.

Effect of changing frequency

Rig loading at 1kN at different frequencies showed a positive linear trend on the angled and pole transducers – increasing the frequency of loading increased the magnitude of pressures measured on these channels.

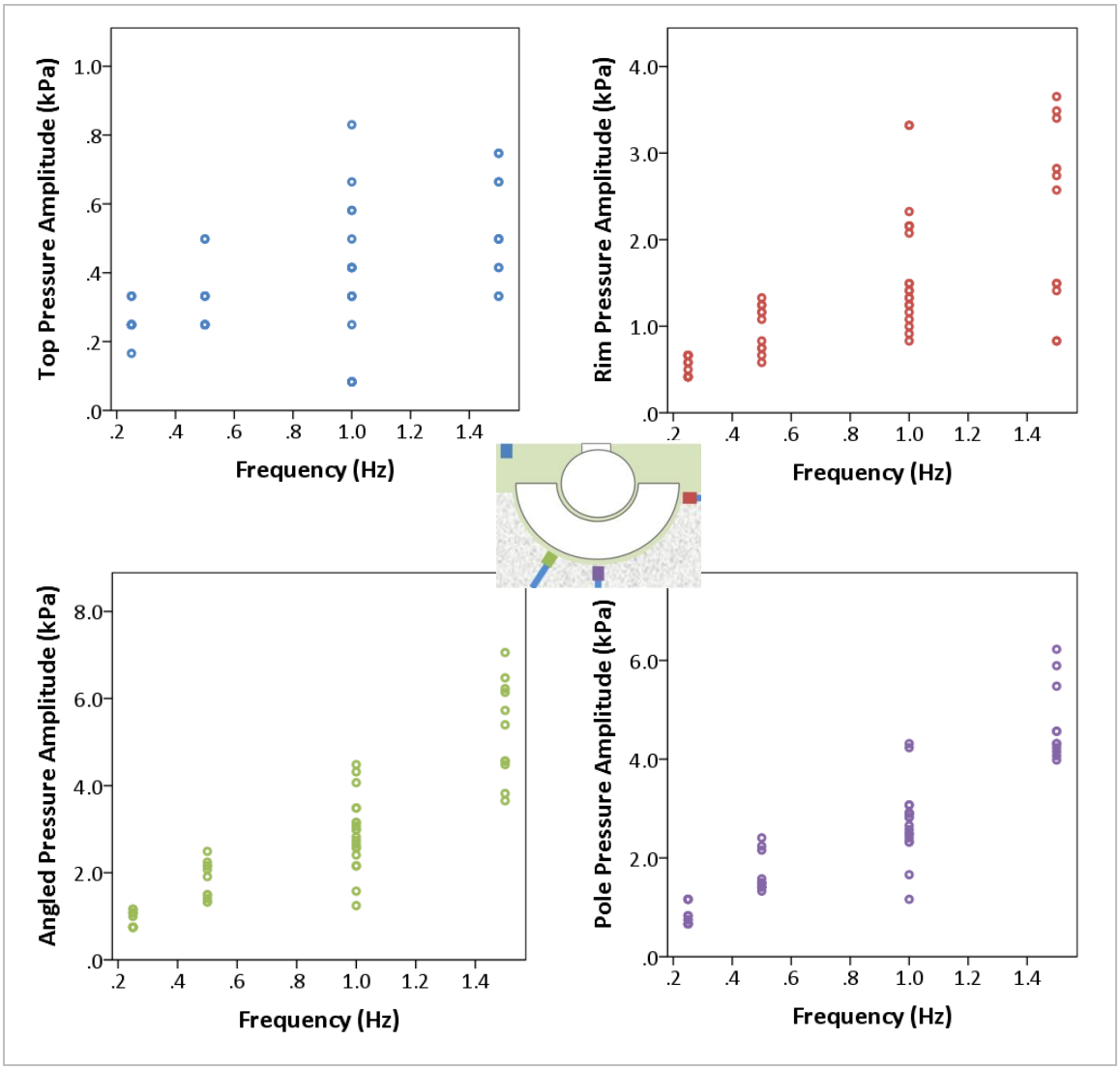

Figure 63: Graphs showing the relationship between frequency and pressure

The frequency of loading is a measure of the rate of movement of the loading head – a higher rate corresponds to higher pressure. It was hypothesised that this increased rate of movement caused higher instantaneous pressures behind the cup. If an incompressible fluid is unable to escape from a space, when the volume is decreased the pressure in the fluid increases. In the APTR, the viscosity of the oil reduces the speed at which it flows out of the periprosthetic space when the volume is decreased due to cup loading, causing pressure spikes to be measured on the transducers. When the cup is loaded at a higher frequency, this volume decrease is faster, and the pressures due to this decrease are higher.

Link between displacement and pressure

High initial pressures were observed in tests with an initial higher displacement of the loading head. At the beginning of the first test (without a membrane), a large 'spike' in pressure was measured on the first test cycle, as shown in Figure 64. It was hypothesised that this pressure spike is caused by the head coming into contact with the cup after a higher start position, effectively simulating a "re-engagement following microseparation" condition (as described in section 3.3 and shown in Figure 32).

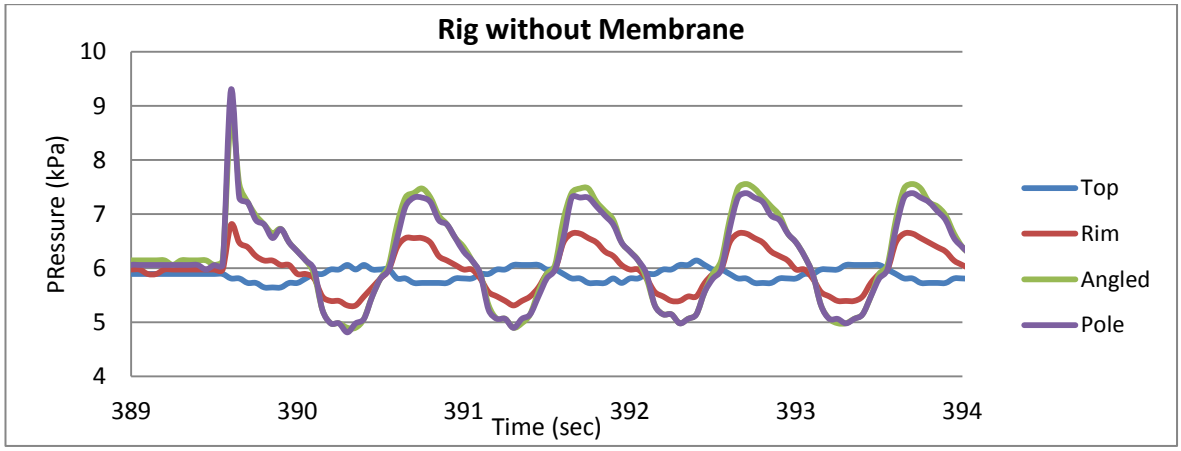

Figure 64: Graph showing the pressure spike on the first load cycle

This hypothesis was validated by examining the displacement data for the same test (shown in Figure 65). This showed a displacement 'jump' of over 0.34mm, almost 1.5 times as high as the displacement amplitude during the rest of the testing (displacement amplitude 0.24mm). This jump produced higher pressure amplitudes on all transducer channels, the pole channel in particular. To investigate the effects of displacement amplitude on pressure, the displacement data from the first cycle of testing were plotted against pressures measured on this first cycle. (Figure 66).

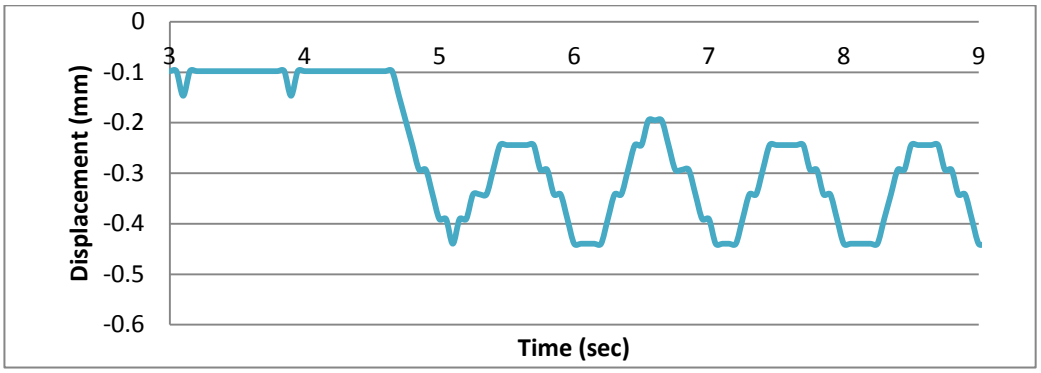

Figure 65: Graph showing the displacement output of the APTR loading head, without a membrane, at the start of a test

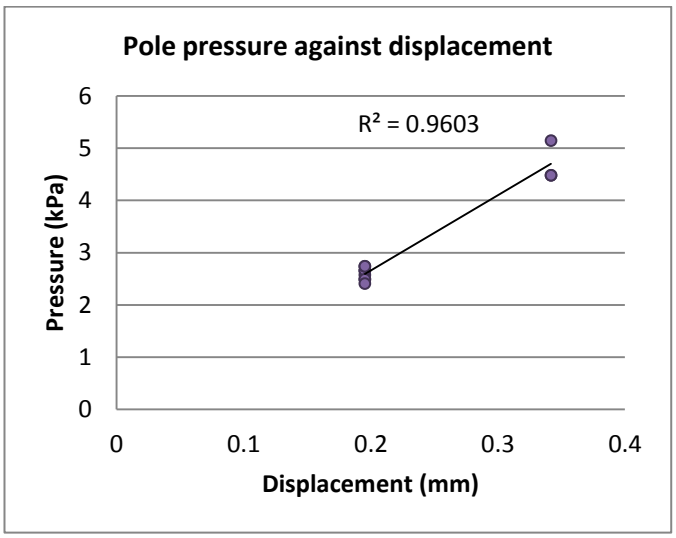

Figure 66: Plot of the relationship between pole pressure data and displacement data on the first cycle of loading, at 1Hz(n = 12). The line indicates the trend of the data, and the R^2 value indicates the 'goodness of fit' of the trendline (for perfect fit $R^2 = 1$)

Although the highest pressures were measured with the highest displacement, the initial pressure spike may be caused by the speed of head movement rather than the displacement value itself (as discussed in the previous section on loading frequency). Due to the low number of samples in this preliminary study, the nature of this relationship is still speculative and should be explored in greater detail in further tests.

The low resolution of the data curve in Figure 65 suggests an insufficient sampling rate on the displacement channel. This was identified as an area for improvement in the next iteration of the APTR model.

Phase analysis

An observation from Figure 64 was that the rig top transducer appeared to be out of phase by approximately π radians (half a cycle). So, shortly after the highest pressures were recorded on the transducers behind the cup, the pressures at the rig top transducer were lowest. To investigate this further, the synchronisation of load/displacement and pressure data was required (for the testing described in this section, these outputs were recorded separately).

Variability of data

To assess the variability of the data between tests and within tests, pressure amplitude data under the same test conditions (without a membrane, tested at 1Hz) were plotted. Data appear to be slightly variable within each data set and more variable between different sets (as shown in Figure 67), even under the same fixation and loading conditions. This inter-test variability is likely due to the fact that the rig was dismantled and cleaned between tests.

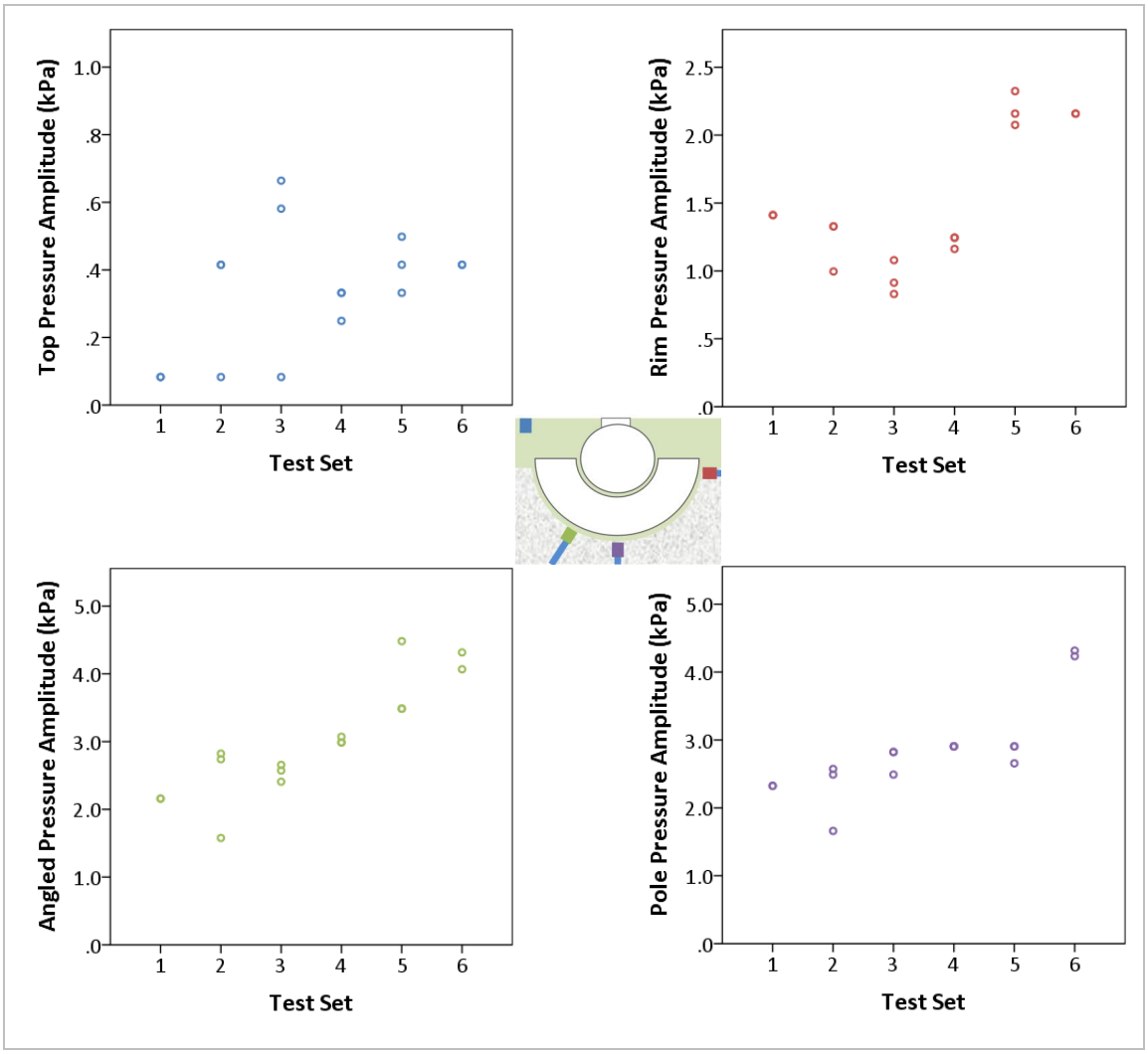

Figure 67: Pressure values for each transducer, from 1kN1Hz tests over the six different test sets.

Repeated tests showed a degree of inter-test variability. The rig leaked intermittently from the top seal and from the transmission tubes, which was observable as a disruption to the pressure signal. If the signal was affected by leakage in the data range from which pressure amplitude was calculated, the results would be skewed.

Several times when the rig was dismantled, the cup appeared to have moved obliquely inside the cavity under loading. It is possible that the head-cup adhesion effect (described in section 3.8) may have caused the cup to disengage from the cavity as the loading head moved up, and slip obliquely before re-engaging with the cavity under load. This change in cup position may have added to the variability of results between tests. For this reason a preloading condition was required for further testing.

Required improvements

From the tests described in this section, several modifications were identified to improve results of the next stage of testing. To investigate the phase characteristics of the signal, the load/displacement and pressure signals needed to be synchronised. A higher sampling rate was also identified as a requirement in future testing, to produce more accurate displacement data. The data analysis procedure, whereby each test was analysed manually in Excel, was time consuming and inefficient and needed to be automated before a large volume of tests would be completed at a higher sampling frequency. Sealing of the transmission tubes needed to be improved and an alternative top sealing approach was required to allow different angles of loading. To prevent slippage of the cup inside the cavity, the need for a pre-loading procedure to seat the cup properly was also identified. To make the loading more representative of *in vivo* gait, the rig should be loaded at different angles. Initially 30 degrees was chosen for as the angle for testing.

4.7 Summary of findings from axial testing

- Pressure amplitudes were lower than expected, possibly due to leaks in the system
- Higher displacement values appeared to cause higher pressures
- Tests indicated that features close to a transmission tube affected pressures
    - Rim transducer higher pressures with membrane
    - Screw holes in the shell caused lower pressures measured on the angled transducer when the transmission tube was in communication with a screw hole (vs smooth shell)
- Several improvements were identified as necessary before a large number of tests could be performed with the APTR.

4.8 Improvements to APTR

Based on initial axial testing, a number of improvements were made to the APTR model. These will be described in the following paragraphs.

Better top seal mechanism

A detachable aluminium top seal was machined, with a 14mm hole in the top of the part. This hole housed a copper tube with a heat-shrink sheath that allowed the loading head (attached

to a load shaft (Figure 68) to move up and down within the rig. One top seal was constructed for each angle tested, with the copper tubes angled accordingly. The improved top seal design allowed the rig to be used at an angle other than 0° (axial loading). For initial testing 30° was chosen as the new test angle (Figure 69), as described in section 3.3.

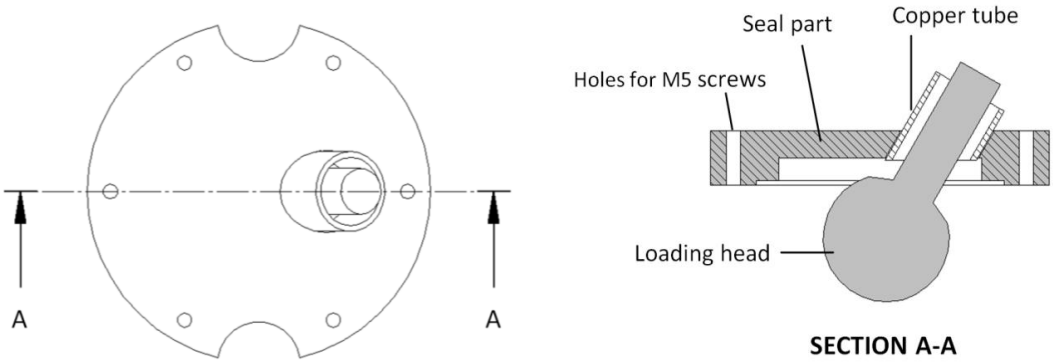

Figure 68: Schematic of improved top seal(heat-shrink sheath not shown)

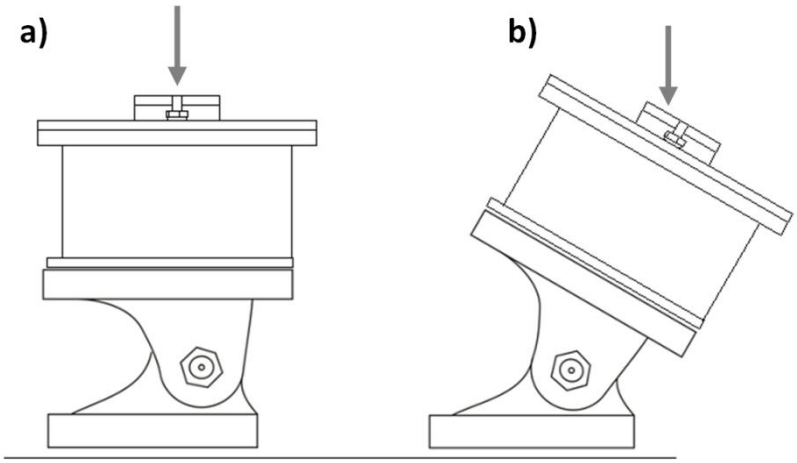

Figure 69: Schematic of APTR mounted on angle plate (side view), with arrows showing direction of loading at (a) 0° and (b) 30° (side view, transducers and oil tube hidden)

Improvement to transmission tube sealing

The holes drilled into the APTR chamber for the transmission tubes were widened (from 3.0mm to 3.5mm) so that a better film of silicone sealant could be applied around the transmission tube. This reduced leakage on these tubes.

Pre-seating routine

Before the introduction of oil into the APTR, a pre-seating routine was applied to the Osteolock acetabular cup, loading at a 30° angle for 20 cycles at 1kN, 1Hz. This was intended to replicate the effect of implant insertion by a surgeon, in which several strong blows with a mallet are applied to the acetabular cup during THA surgery.

Improvement of APTR instrumentation

Data from the Dartek and the transducers were synchronised by connecting the Dartec output leads to the data acquisition frame that was recording the pressure data. These data were recorded in one six-channel LabView program so that the load and pressure data could be compared. The new instrumentation setup is illustrated in Figure 70, with the previous connection setup shown in the faded area, and the new connections highlighted in bold. The data sampling frequency was increased from 20Hz to 50Hz, to improve the quality of the data acquired during testing.

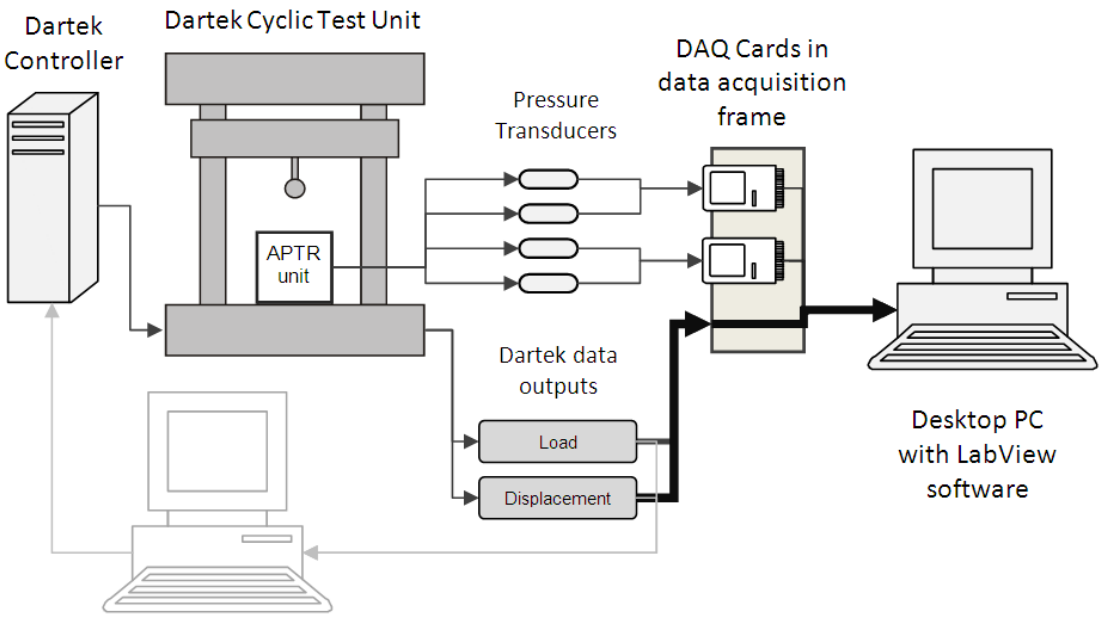

Figure 70: Schematic showing the components and improved data connections in the APTR instrumentation (previous connections in grey).

Development of Matlab routine

In order to streamline the data analysis process, especially once the sampling frequency (and hence number of data points) was increased; a Matlab routine was developed, in conjunction with a colleague, to extract the most relevant values from the data. This Matlab code can be found in Appendix 7.

4.9 Test methods for further testing

Two test groups were completed in this series, with 6-8 test sets performed with the Osteolock 52mm cup (with loose liner as in the preliminary testing) in each test group. Within each test set was a testing routine containing five individual test conditions. An outline of this test routine is shown in Figure 71.

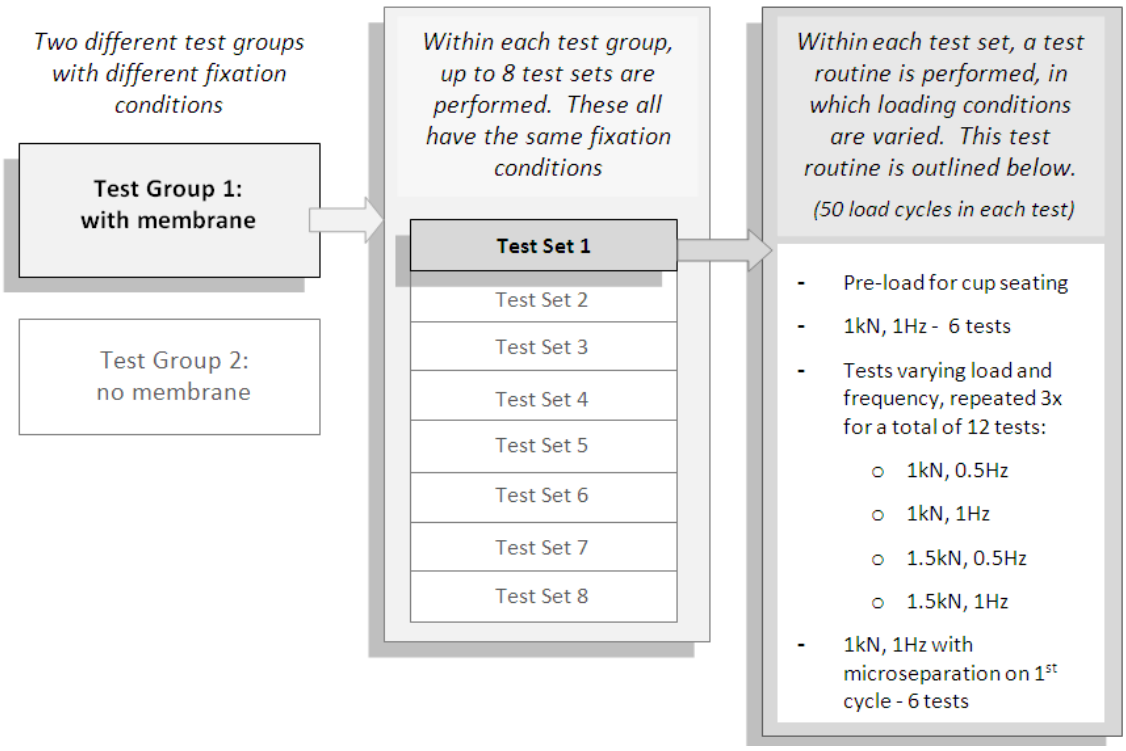

Figure 71: Summary of testing regime

The rig was tested to assess the effects of changing loading conditions, specifically the frequency and magnitude of the loads applied to the APTR. The presence of a fibrous membrane was also investigated by including a 10mm wide, 1mm thick band of the membrane analogue material around the rim of the cup. The results of these tests are presented in the next section.

4.10 Results from 30° angle testing

Initial results

As before, pressures were calculated from transducer outputs using calibration values. These data were further analysed by obtaining the important values using a Matlab program (Appendix 7). The start and end base pressures were the pressure values measured before and after loading. The first-cycle values were the maximum and minimum pressures measured in the first cycle of loading, and the first-cycle amplitude was the difference between the two. Similarly, the steady-state values were the maximum and minimum pressure and the amplitude at cycle 47, chosen as a point at the end of the test at which variation in test data is minimal (the steady-state period, as described in section 4.5). These values are shown in Figure 72 and Figure 73.

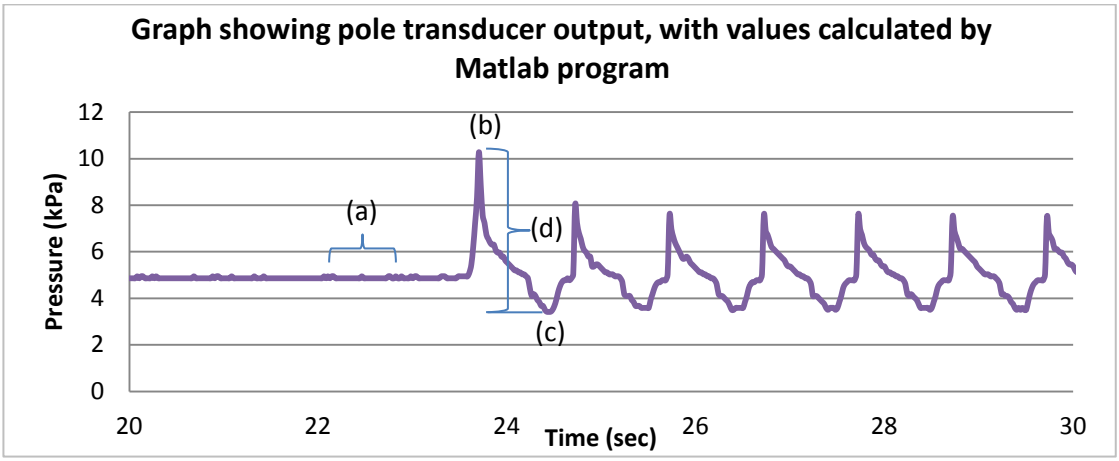

Figure 72: Graph 1 showing (a) start base pressure, (b) 1st cycle maximum, (c) 1st cycle minimum, and (d) 1st cycle pressure amplitude.

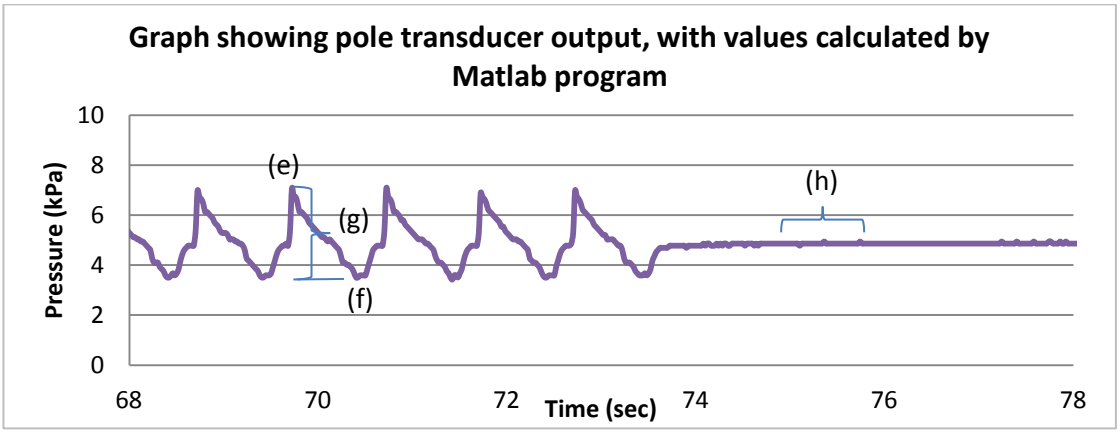

Figure 73: Graph 2 showing (e) steady-state maximum pressure, (f) steady-state minimum, (g) steady-state pressure amplitude and (h) end base pressure

To investigate the effects of the different loading and fixation conditions on pressures, the pressure amplitudes, maximum pressures, base pressures and the maximum and minimum pressures with respect to the base pressure were compared under the different conditions, using the SPSS statistical analysis programme (IBM SPSS Statistics Version 19, IBM Corporation, New York). Results of this analysis are presented in the next section.

Test Results

Effect of increasing sampling frequency

Increasing the sampling frequency in the LabView program from 20Hz to 50Hz produced no real improvement in the quality of displacement data, as can be seen from Figure 74. After investigation of the instrumentation this was found to be due to the low rate of displacement data measured by the Dartek while testing in load control.

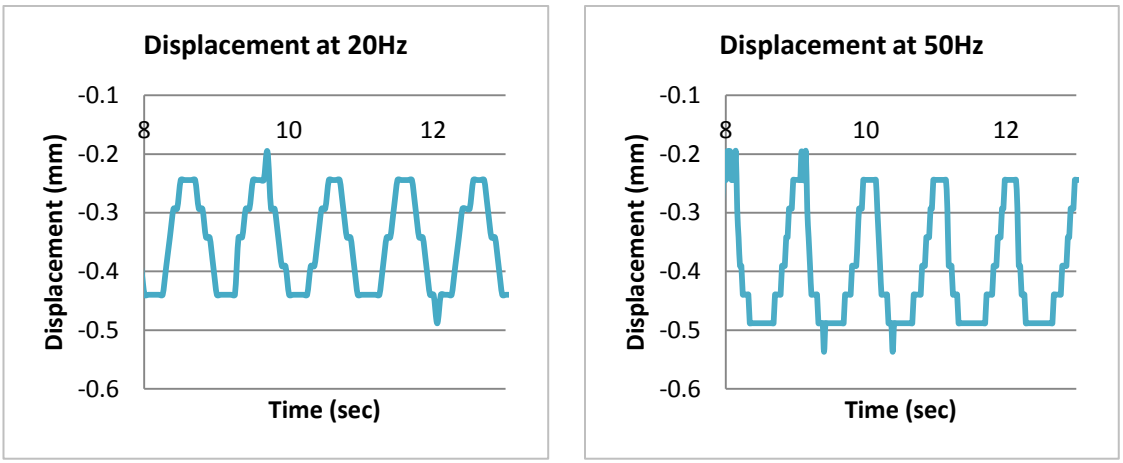

Figure 74: Comparison of 20Hz and 50Hz sampled data

Variability of results

Pressure amplitude data from each test were plotted on a graph to assess the spread of data and the variability of test data in this series, as shown in Figure 75.

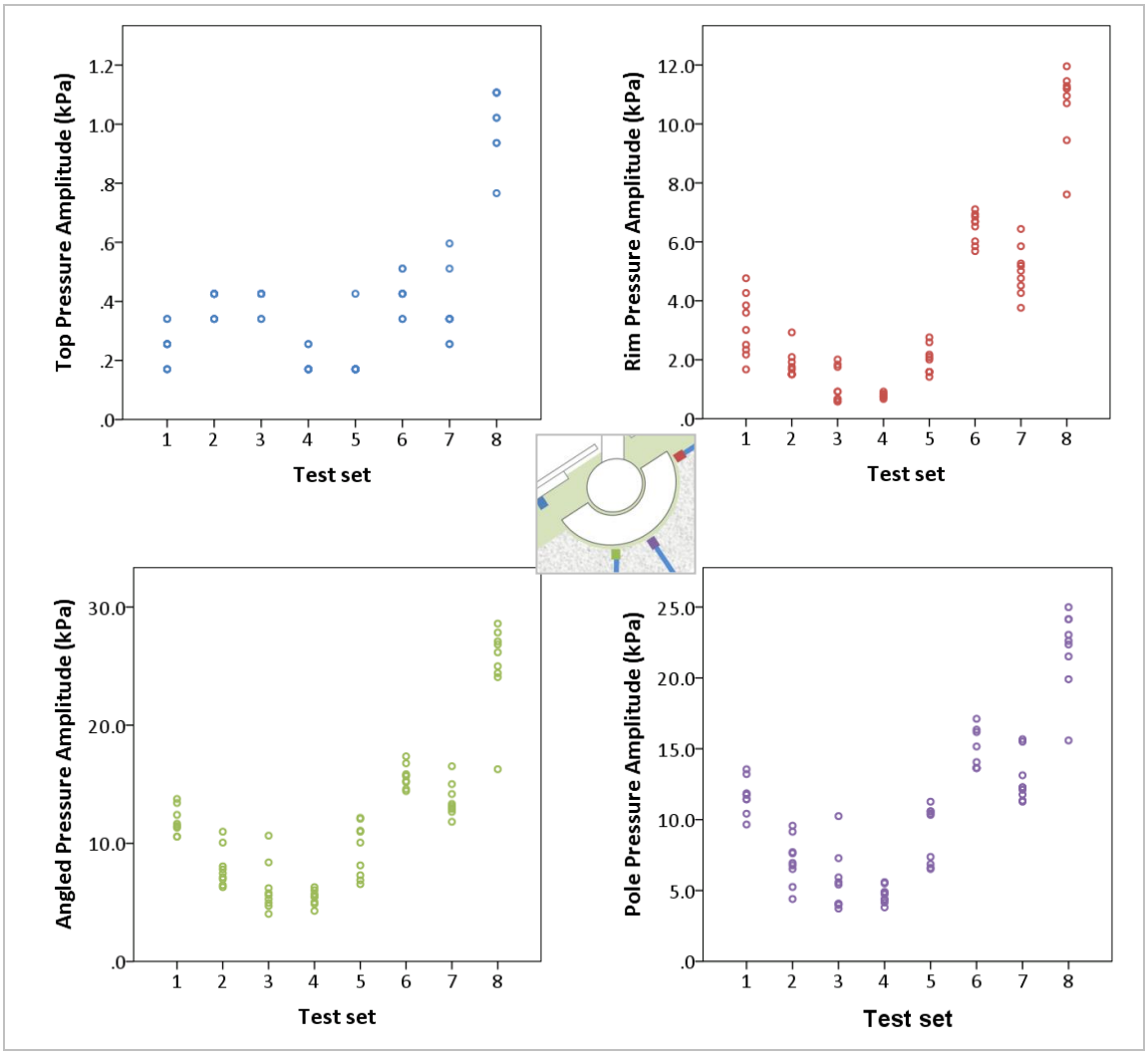

Figure 75: Graphs showing pressure amplitude data from different data sets. For each test set, n=9.

An assessment of the spread of data from testing showed that the pressure data from test 8 appeared to be significantly higher than the values from other tests. This increase in pressure in test 8 reflects the fact that there was an operator error when zero-ing the load channel of the Dartek during set-up, causing displacement amplitudes to be significantly higher in these tests (Figure 76). As previously described, higher displacement is linked to higher pressures. For this reason the data from Test 8 were excluded from further analysis.

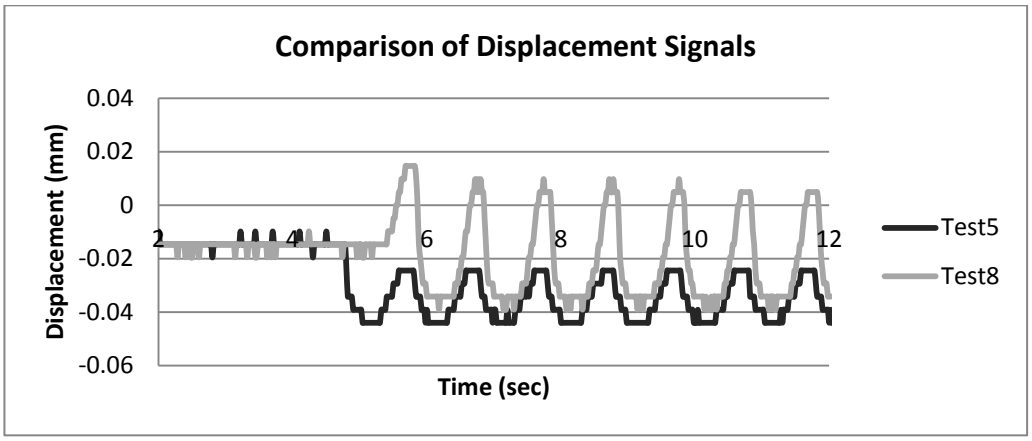

Figure 76: Comparison of sample displacement data from Test 5 and Test 8.

Variability in the initial axial testing was thought to be due to the leaking of the rig combined with cup slippage. Measures were taken to prevent this by improving the seal in the top of the chamber, improving the seal around the transmission tubes, and introducing a pre-seating routine before testing. To determine whether these effects improved variability in the tests at 30°, the data from axial and 30° tests were compared, as shown in Figure 77 .

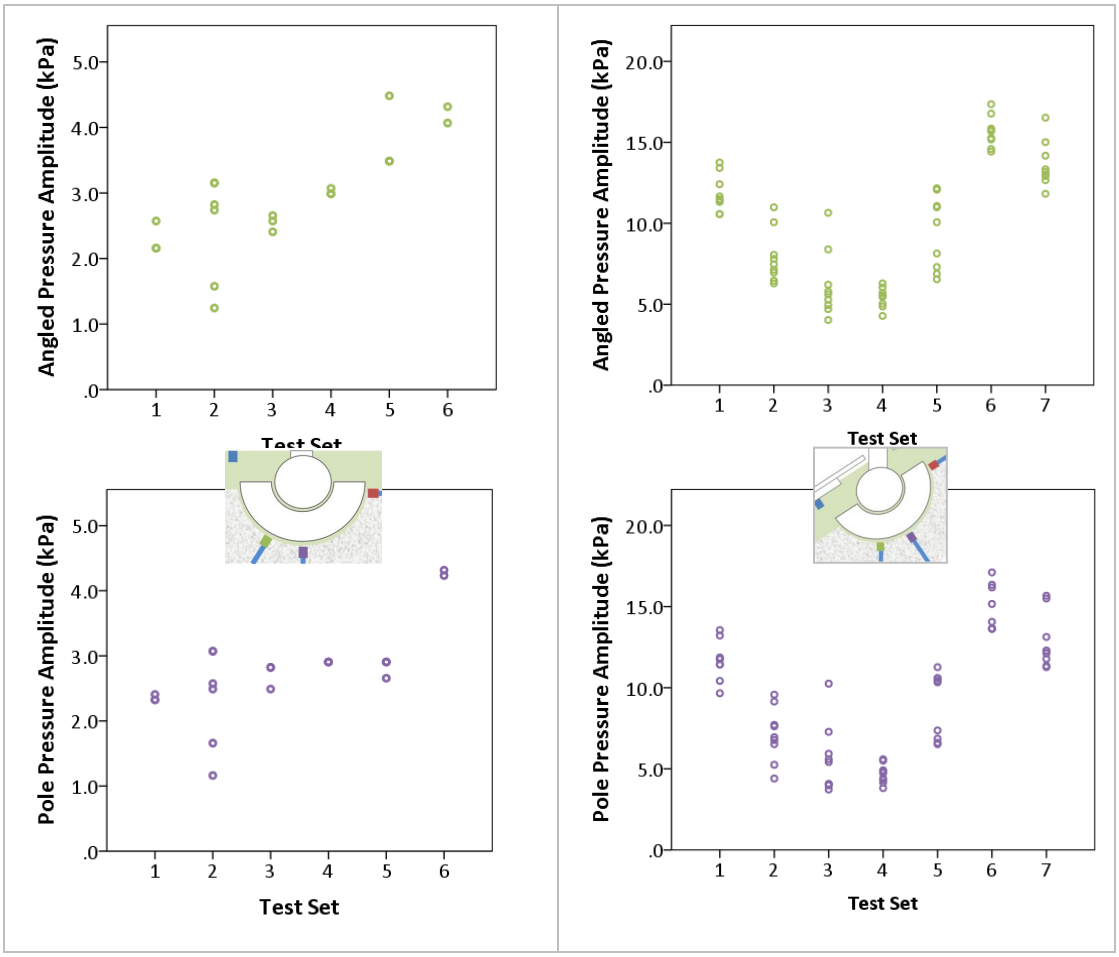

Figure 77: Comparison of data from axial and 30° testing. The scale of the pressure axis on the axial testing graphs is different from 30° tests to better visualise the data.

To further analyse the variability of data, the inter-quartile range (IQR) of the steady-state pressure amplitude results was assessed in Excel, to provide a measure of the variability of measurements in the axis of loading. A comparison of IQR from the pole transducer in axial testing, and the angled transducer in 30° testing, is shown in Table 10.

Table 10: Comparison of data variability between initial axial tests and angled tests.

Test conditions	Median (kPa)	IQR (kPa)	IQR as % of median
Pole transducer, axial testing	2.822	0.415	**14.71 %**
Angled transducer, 30° testing	10.567	6.877	**65.08 %**

The pressure amplitudes measured in the 30° tests were much higher than the pressures measured during axial testing. This may be a reflection of the improved sealing mechanisms leading to fewer leaks and thus higher pressures, and may also be influenced by the change in loading angle. While improvements to the rig's integrity may have increased the pressures, the variability of data measured at 30° is still very high. This may be due to slight errors in setting up the angled tests, as well as possible unpredictable cup movement due to the loose liner and loose cup fixation. Due to the precise geometry of the interaction between the rig chamber, the loading head and the prosthetic components when loading at 30°, any slight misalignment can significantly affect results. It was difficult to consistently set up the rig at this angle based on the current design. Also, when the rig was disassembled after testing, on some occasions it was observed that the prosthetic cup had slipped obliquely inside the test cavity. It is unknown whether this slippage occurred during testing or while the loading head was being moved up during disassembly, but this may also have influenced results. Further improvements to the rig are required to reduce inter-test variability.

Effect of change in angle

Tests were performed with the APTR loaded at an angle of 30, as shown in Figure 69 (b). Steady-state pressure amplitudes produced under the 1kN, 1Hz loading regime in these tests were compared with steady-state pressures from the previous test series (under the same loading conditions but loaded at 0° angle). Results of this comparison are shown in the four boxplots in Figure 78. Displacement values were also compared (Figure 79).

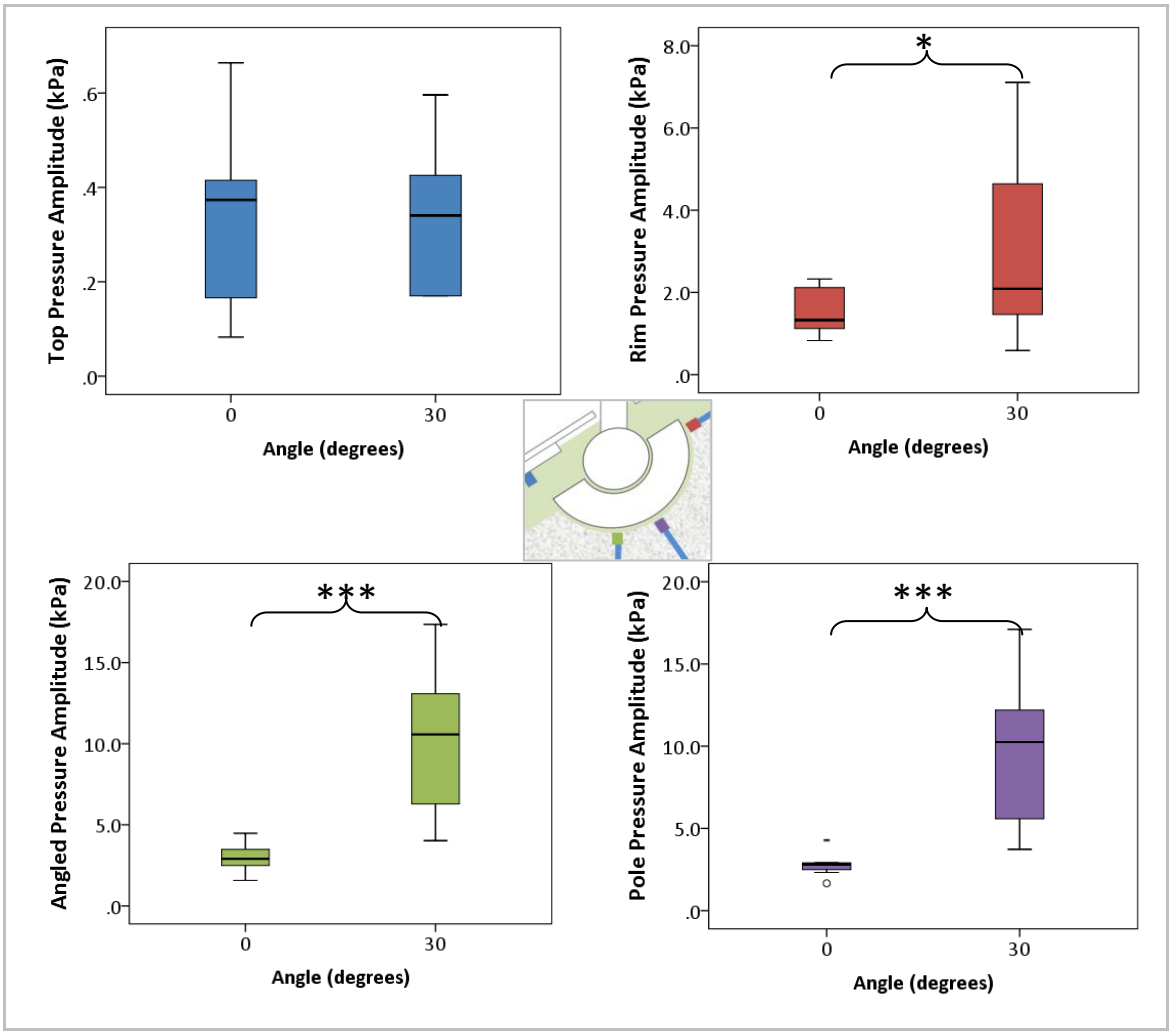

Figure 78: Boxplots of the pressure amplitudes from testing at angles of 0° (n=16) and 30° (n=63). A statistically significant difference is indicated by stars – [*]= p ≤ 0.05; [**] = p ≤ 0.01; [***] = p ≤ 0.001.

Higher pressures were produced behind the cup (on the rim, angled and pole transducers) when loaded at 30°, and Mann-Whitney 2-sample tests in SPSS showed that this difference was significant (Figure 78). No significant difference was found between the top transducer pressure amplitudes at different angles. A greater spread of pressure data was observed in the 30° tests. The displacement in the 30° tests (shown in Figure 79) was significantly higher than the displacement in axial tests (p = <0.05).

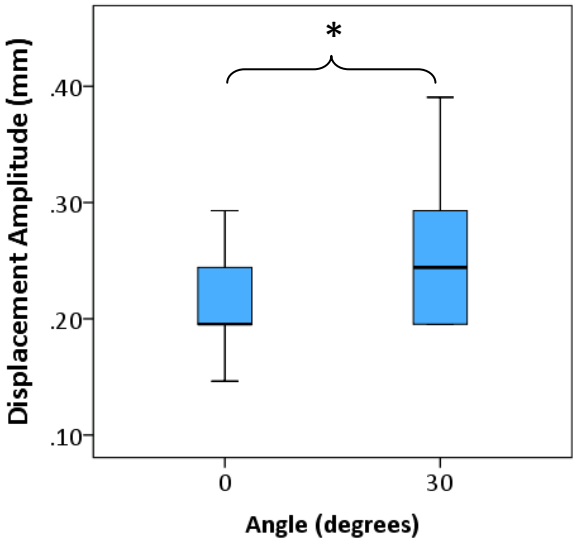

Figure 79: Boxplot showing displacement values from the tests at different angles. The 0° test data were obtained from the initial test series, while 30° test data was from the current test series. A statistically significant difference (p=0.05) is indicated by a star [*].

Base pressure analysis

To validate the pressures measured in this test series, the base pressures were compared with expected pressure values calculated from the pressure head formula. These expected values were calculated using the formula:

$$P = \rho g h$$

Where **ρ** is the density of the fluid (density of vegetable oil is 0.91 g/cm^3 (1991, Noureddini et al., 1992), **g** is gravity (g = 9.81ms^{-2}) and **h** is the height of fluid above the measurement point. Values for **h** for each transducer were found using the rig geometry outlined in Figure 80.

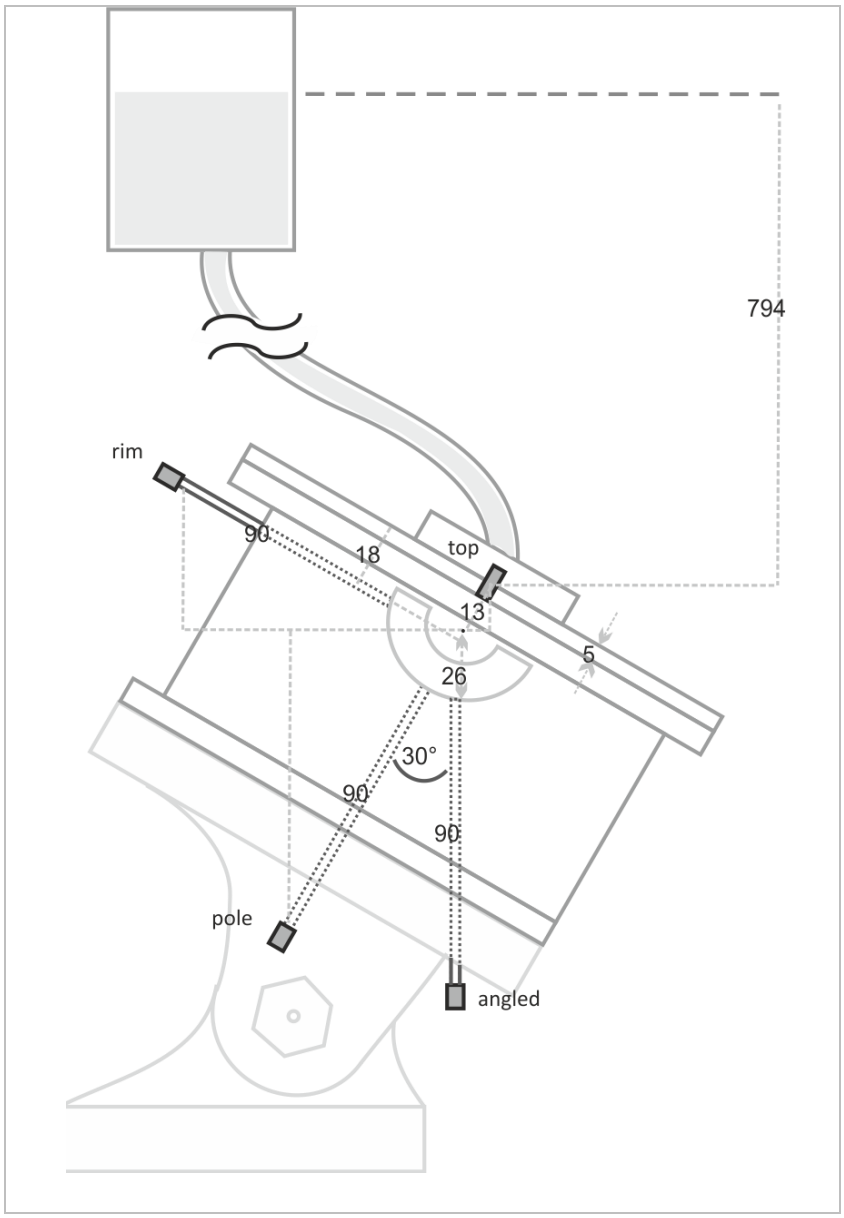

Figure 80: Image of rig geometry for base pressure calculations. All measurements in mm.

Base pressure values were measured from all tests, and compared with the calculated base pressures. This comparison is shown in Figure 81.

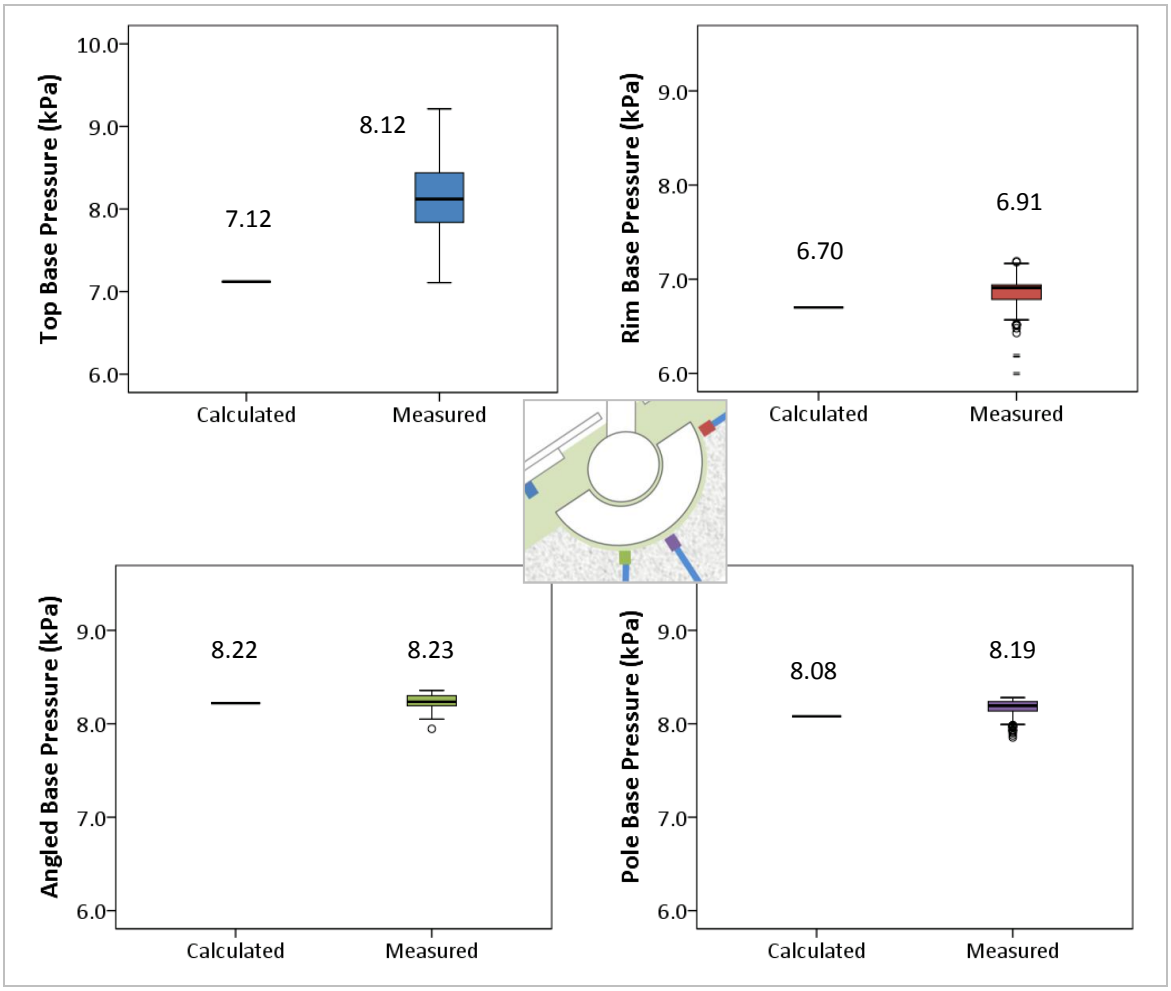

Figure 81: Base pressure calculated using the method outlined in Figure 80, compared with base pressures measured during testing (n=126). Calculated pressure values, as well as median measured base pressures, are displayed.

Figure 81 shows that the rim, angled and pole base pressures measured during testing closely match the pressures calculated in Figure 80. However, the top transducer appears to have a much greater variation than the other channels, with higher base pressures than were expected from the base pressure calculation.

This variation may have been due to air bubbles being trapped in the chamber during oil introduction, or due to the way the offset was calculated. When calculating pressure values, the initial pressures on all the transducers was assumed to be zero, as described in section 4.4. These initial pressures were measured before oil introduction, when the rim, angled and pole transducers were disconnected from the rig, but the top transducer was already connected to the top plate. It is possible that the initial pressure data on the top transducer was influenced by the sensor being plugged into the rig when the offset was calculated. This variation on the

top pressure transducer is an effect that must be taken into account when analysing results. This test confirms the accuracy of base pressures measured behind the cup.

Effects of load

Cyclic sinusoidal loads of 1kN and 1.5kN were applied to the APTR at a frequency of 1Hz, for 50 cycles. It was assumed that higher loads would lead to higher pressure amplitudes measured behind the cup. Boxplots of the results of these tests in the steady-state period are shown in Figure 82.

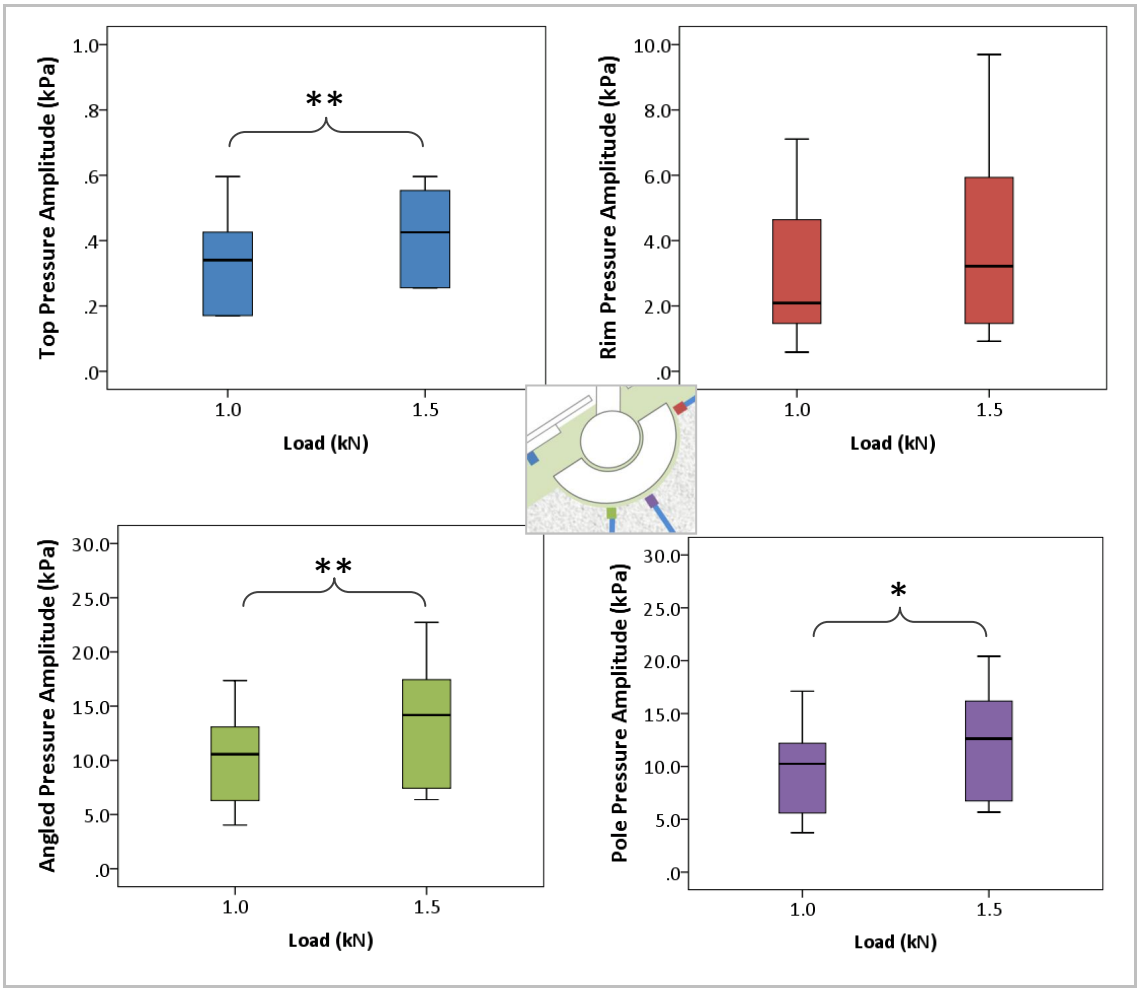

Figure 82: Boxplots showing the effects of changing load amplitude on the pressure amplitudes measured on each transducer at 1kN (n=63) and 1.5kN (n = 20). A statistically significant difference is indicated by stars – [*]= p ≤ 0.05; [**] = p ≤ 0.01; [***] = p ≤ 0.001.

As predicted, higher applied loads produced higher pressures behind the Osteolock cup. Mann-Whitney U analysis was used to compare median values for the two different loads, and the distributions in the two groups differed significantly (Mann–Whitney, $P < 0.05$ two-tailed). The median pressures were found to be significantly higher with the higher load of 1.5kN on

the top, angled and pole transducers. Although the median rim pressures were higher with a higher load (3.22 kPa compared to 2.09 kPa), this difference was not statistically significant (p=0.114). This testing showed that the APTR was sensitive to changes in load magnitude applied through the prosthetic head, and that the higher load produced conditions in the rig which generated higher pressures.

Comparing the displacement values for the different load amplitudes, it can be seen that there is a slight increase in displacement amplitude with a higher load (Figure 83). Mann-Whitney U analysis of the data showed that this increase was statistically significant at the 0.05 level (p=0.013). An increase in displacement amplitude indicates the loading head travelled further in the in the chamber to apply the higher load. It can be assumed that this displacement could have caused deformation of the prosthetic cup, the bone analogue, or both materials. This deformation would have changed the periacetabular geometry and led to altered fluid pressure and flow behind the cup under higher load.

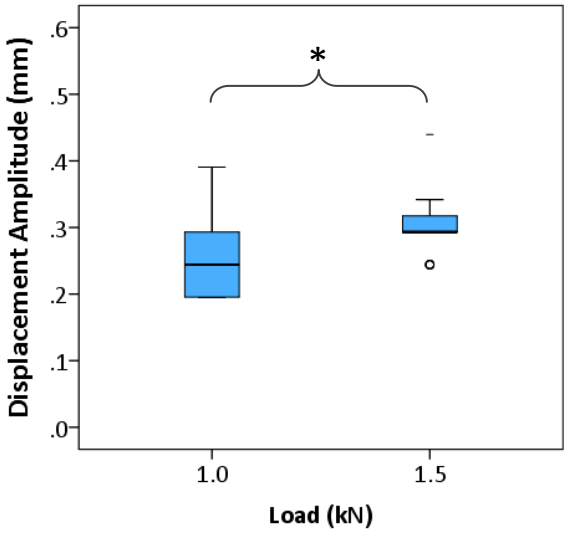

Figure 83: Boxplot showing displacement data from testing at 1kN (n=63) and 1.5kN (n = 20). A statistically significant difference (p=0.05) is indicated by a star [*].

These load tests were conducted under the test schedule shown in Figure 71, with initial tests at 1kN followed by a variation of higher loading magnitudes and lower frequencies. To determine whether the testing at 1.5kN had an effect on the subsequent pressures when tested at 1kN, the data from the tests 1-6 (1kN, 1Hz tests before higher loading) and tests 7-9 (1kN, 1Hz after tests with higher loading) were compared (Figure 84).

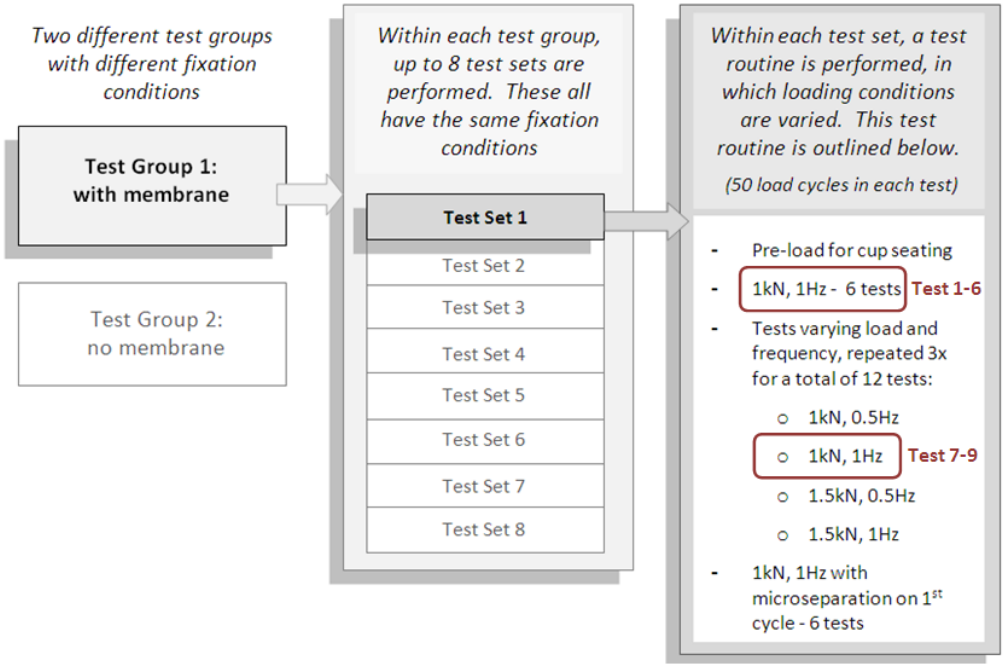

Figure 84: Test schedule showing position of Test 1-6 and Test 7-9, before and after higher loading

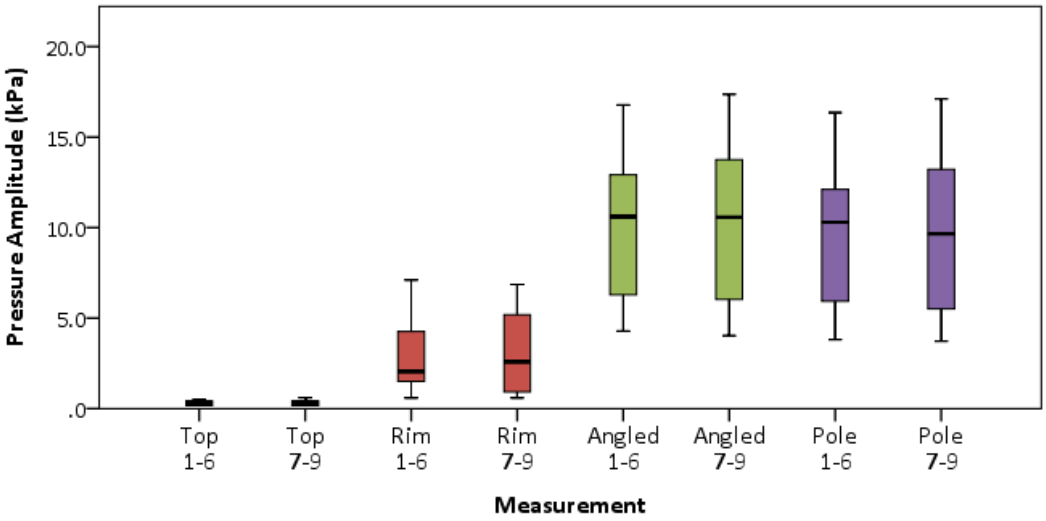

Figure 85: Boxplot showing difference in pressure amplitude from Test 1-6 (n=42) and Test 7-9 (n=21). No statistically significant differences were measured.

Mann-Whitney analysis was applied to determine whether there was a statistically significant difference between these data. The analysis showed that the application of a higher load did not affect pressures measured after the application of this load. This indicates that the higher displacement due to higher load (as shown in Figure 83) causes a recoverable degree of deformation in the test cavity.

Effects of frequency

Cyclic loads were applied to the APTR chamber at frequencies of 0.5Hz and 1Hz, for 50 cycles. Pressure amplitude values in the steady state period under these two conditions (under a 1kN load magnitude) were compared (see Figure 86).

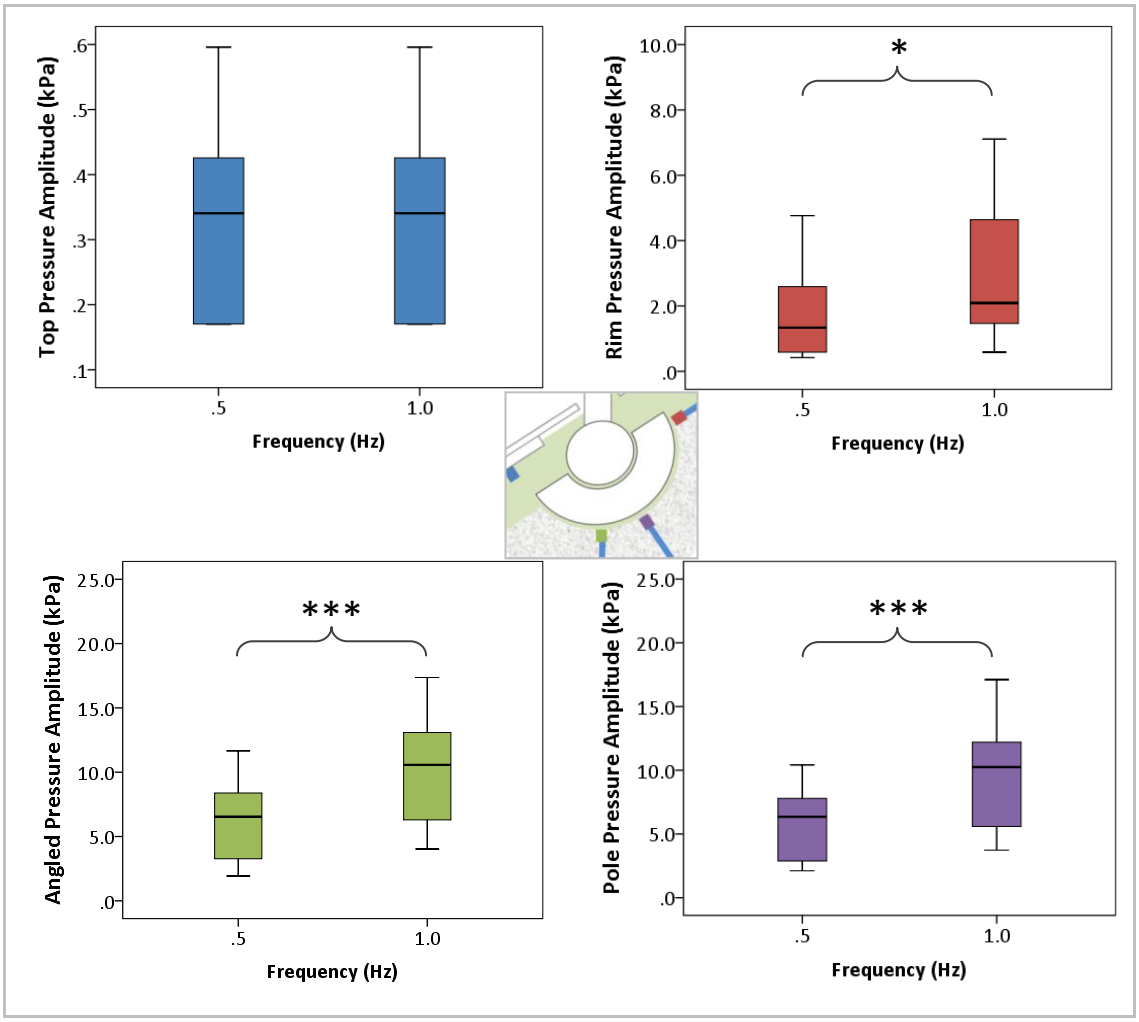

Figure 86: Boxplots showing the effects of changing load frequency. Pressure amplitudes measured on each transducer are shown (0.5Hz, n=21; 1Hz, n=63). A statistically significant difference is indicated by stars – [*]= p ≤ 0.05; [**] = p ≤ 0.01; [***] = p ≤ 0.001.

No significant difference was observed on the top transducers (p=0.594), while a positive difference was observed on rim, angled and pole transducers (p= 0.028, p<0.000 and p<0.000 respectively).

Statistical analysis using the Mann-Whitney U test showed that there was no significant difference in pressures measured by the top transducer with a change in frequency. A higher loading frequency caused significantly higher pressure amplitudes to be measured on transducers behind the cup. This implies that the frequency of movement of the loading head,

as well as the magnitude of force applied, has an effect on the generation of fluid pressure behind the cup. Higher loading frequency leads to higher pressure amplitudes.

Effects of "relocation from microseparation" condition

Six tests in each series were initiated with the loading head at a higher starting position, causing it to have a higher initial displacement amplitude (median value 0.59mm compared with 0.44mm), simulating a microseparation-relocation condition, as shown in Figure 87, which caused a pressure spike (Figure 88). These tests were all performed at 1kN and 1Hz, with and without a membrane. effect of a higher initial displacement was investigated by comparing the pressure amplitude in the first load cycle with the amplitude under steady-state conditions (load cycle 47), as shown in Figure 73. The results of these tests are shown in Figure 89 and Figure 90.

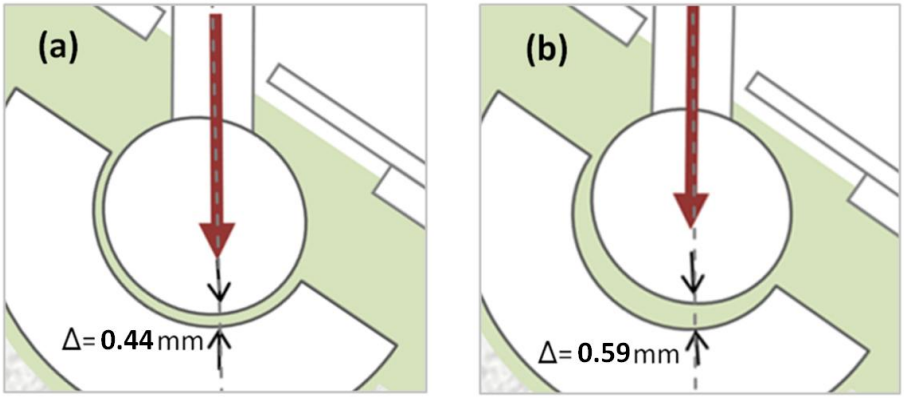

Figure 87: Schematic showing (a) regular head start position, compared with (b) relocation head start position

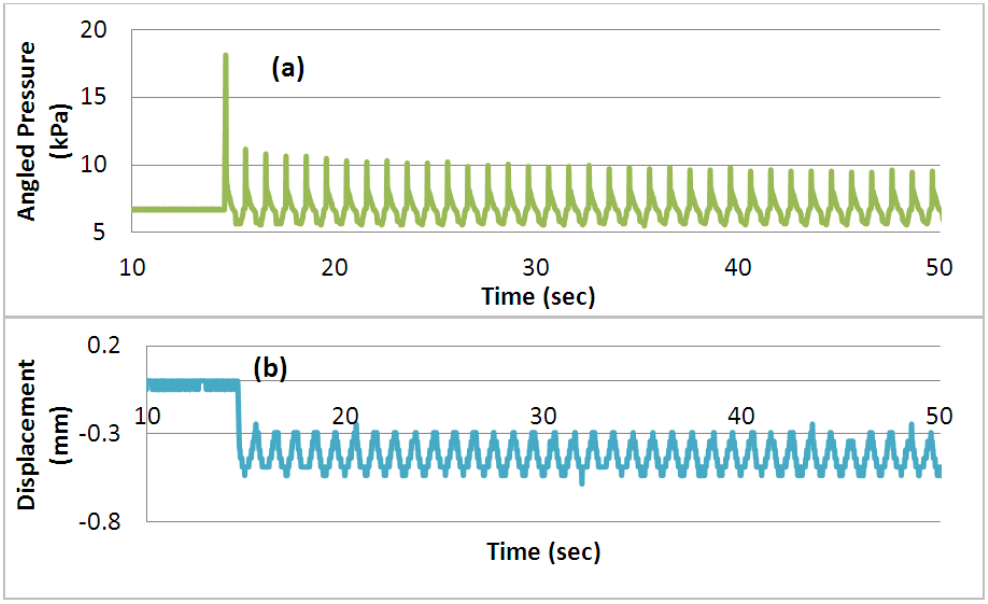

Figure 88: An example of relocation test data, with (a) data from Angled transducer and (b) Displacement data, demonstrating the first-cycle pressure spike and the higher initial displacement.

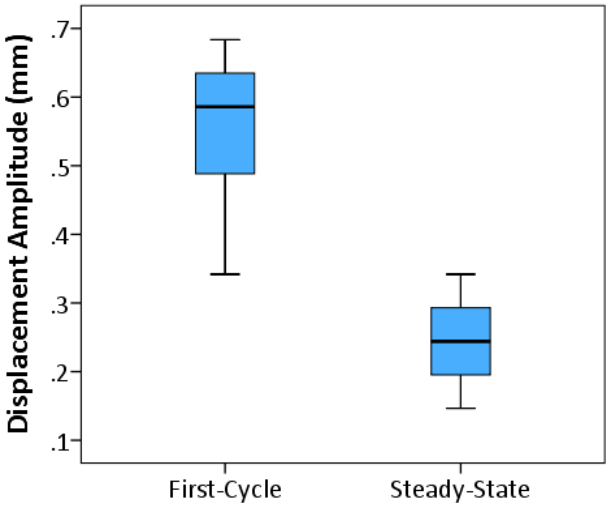

Figure 89: Boxplot showing displacement data from the first cycle and the steady-state period of tests with a higher initial displacement

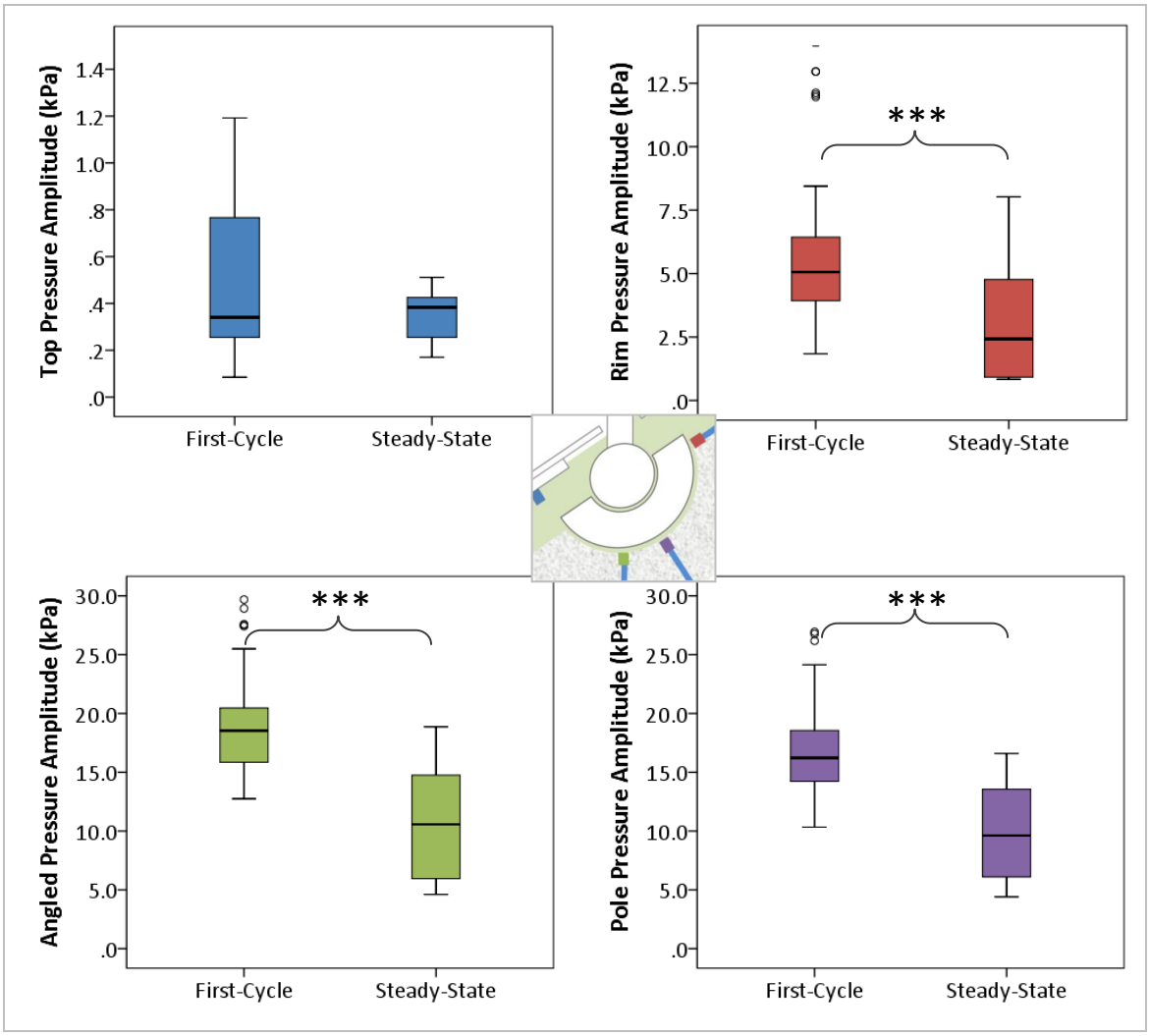

Figure 90: Boxplots showing pressure amplitudes under relocation loading conditions, comparing first-cycle pressures with steady-state pressure values (n = 44 in both groups). A statistically significant difference is indicated by stars – [*]= p ≤ 0.05; [**] = p ≤ 0.01; [***] = p ≤ 0.001.

Mann-Whitney analysis showed that the relocation condition caused a significant increase in pressure amplitudes behind the cup (p = <0.001 on rim, angled and pole transducers). Displacement values (Figure 89) were also significantly higher under the first-cycle relocation condition (p = <0.001) which could account for the increased pressures. As previously shown, displacement amplitude has a significant impact on measured pressures.

To determine whether there was a pressure spike on the tests performed under normal loading conditions, the first cycle and steady-state pressure values from test at 1kN and 1Hz were compared. Results are shown in Figure 91. Displacement values were shown to be significantly higher on the first cycle of these tests (Figure 92).

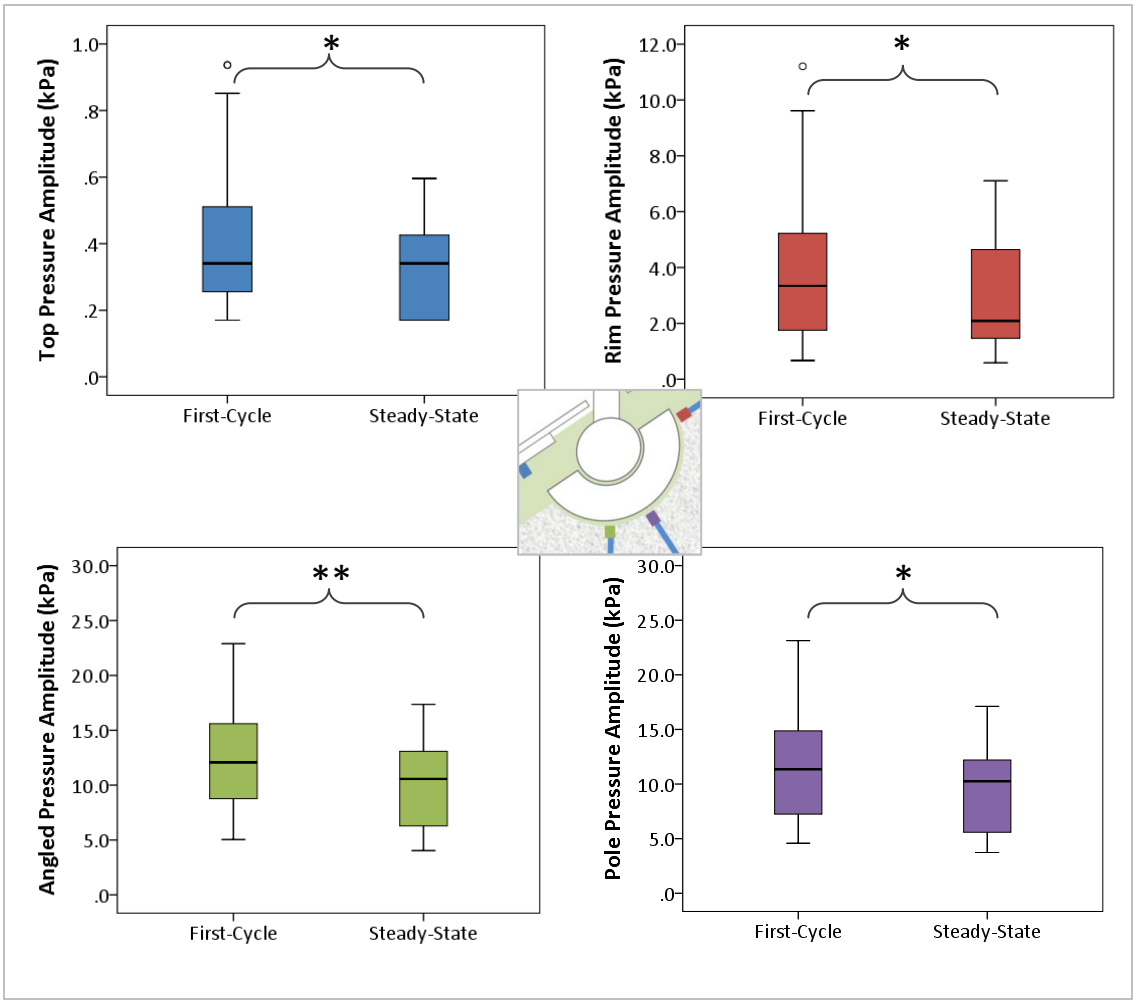

Figure 91: Boxplots showing pressure amplitudes under normal loading conditions, comparing first-cycle pressures with steady-state pressure values (n = 63 in both groups). A statistically significant difference is indicated by stars – [*]= p ≤ 0.05; [**] = p ≤ 0.01; [***] = p ≤ 0.001.

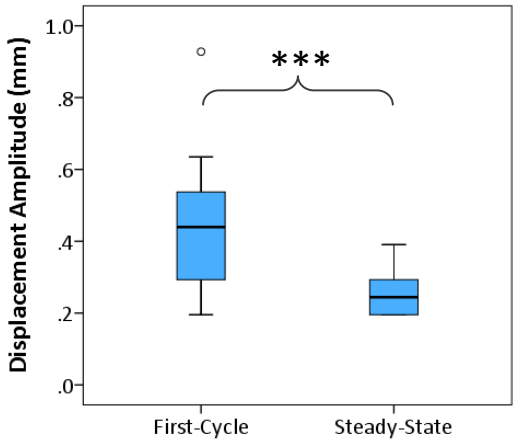

Figure 92: Boxplot showing displacement data from the first cycle and the steady-state period of tests under normal loading conditions.

This analysis showed that the 'relocation distance' (the separation of the head within the cup) had a significant effect on the pressures measured behind the cup, on the rim, angled and pole transducers, and this relocation occurs in all tests, not just those with a higher induced displacement. This increase in pressure appears to be linked to the higher displacement value measured in the first cycle of these tests.

Effects of membrane

The Osteolock cup was loaded at 1kN at 1Hz frequency, with and without a 10mm-wide rim of fibrous material between the implant and the test hemisphere (Figure 93), to determine its effect on pressures measured by the APTR unit.

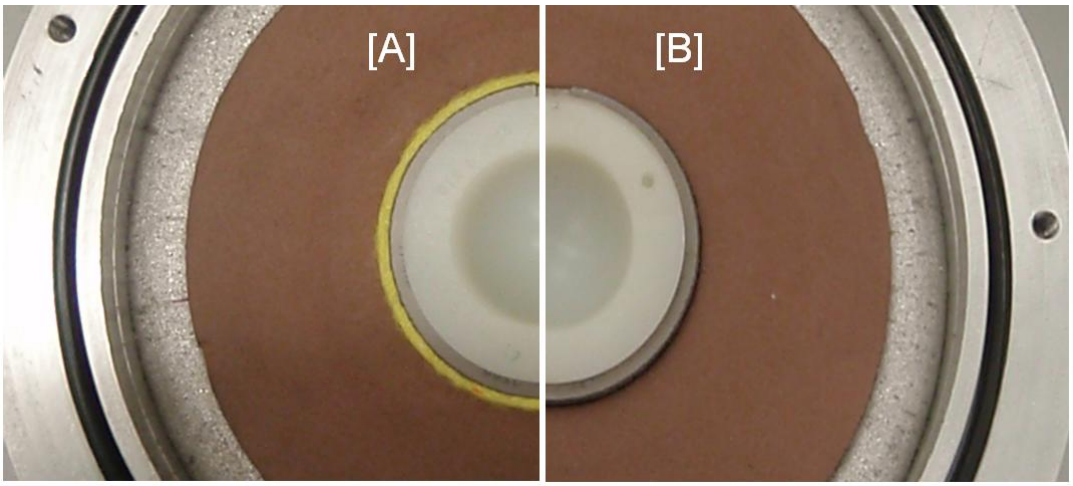

Figure 93: image showing prosthetic cup [A] with membrane and [B] without membrane

To assess the effects of this fibrous rim, pressure amplitudes with and without the membrane were compared. As described in section 3.8, a fibrous membrane was predicted to increase pressures behind the cup, as it would allow greater micromotion between the cup and the test hemisphere, and potentially act as a fluid pump to the periacetabular space. The results of this investigation are shown in Figure 94.

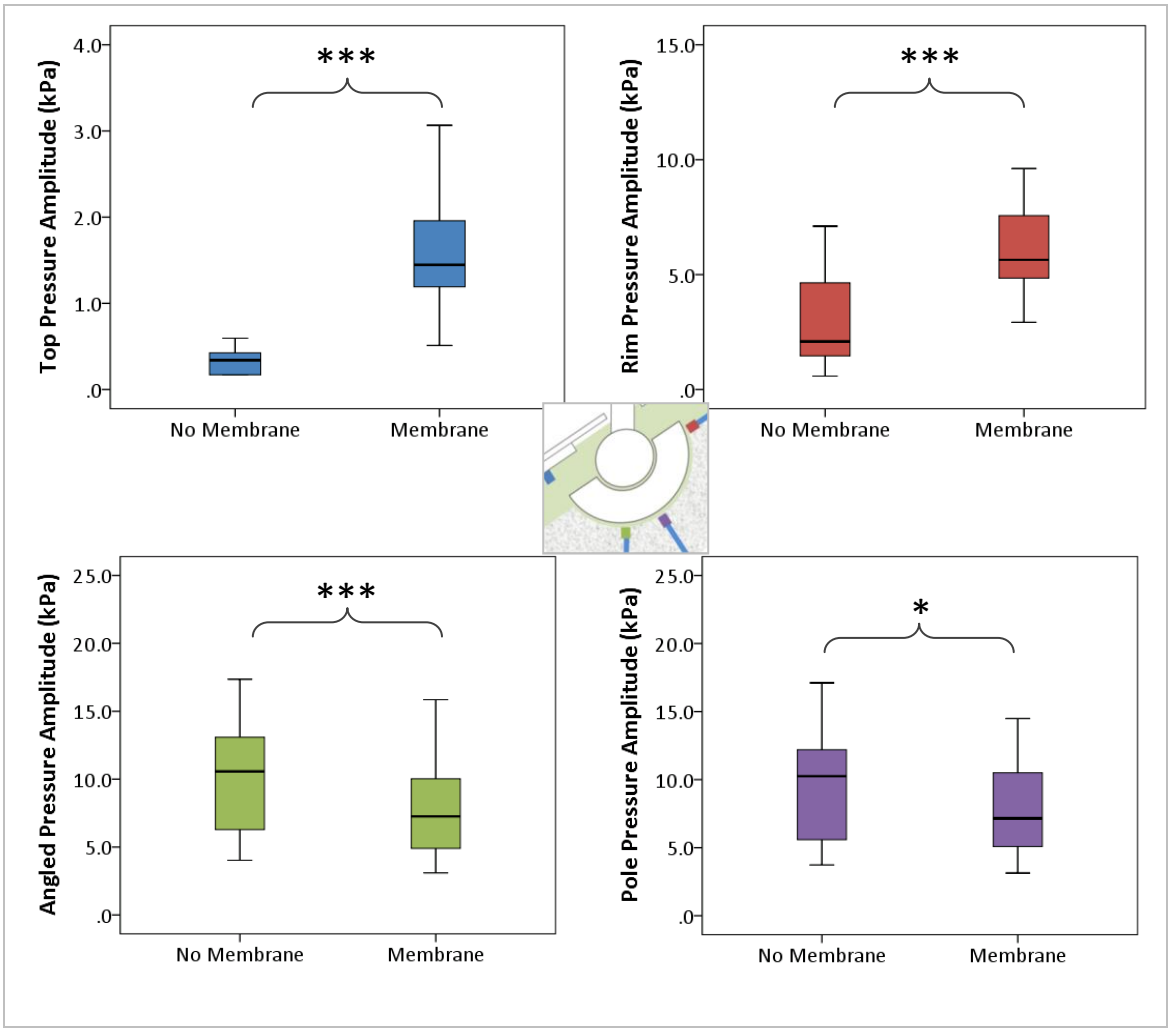

Figure 94: Boxplots showing the effect of a membrane on fluid pressures. Statistically significant difference between tests without a membrane (n=63) and with a membrane (n=72) indicated by stars – [*]= p ≤ 0.05; [**] = p ≤ 0.01; [***] = p ≤ 0.001.

Mann-Whitney analysis showed that the difference in pressure amplitude with a membrane was significantly different at all transducer points. The rim and top transducers measured higher pressure amplitudes in the presence of a membrane ($p < 0.000$, $p < 0.000$); conversely, the pressures measured on the angled and pole transducers were significantly higher in tests *without* a membrane present ($p \leq 0.001$, $p \leq 0.015$). This implies that the membrane is restricting pressure fluctuations behind the cup, while increasing fluctuations at the rim of the cup and in the bulk chamber fluid.

To determine whether this change in pressure was due to an increased displacement (highlighted in the previous section as a potential cause of higher fluid pressure), or due to the membrane material itself, the displacement values were investigated in tests with and without a fibrous rim. The results are shown in Figure 95.

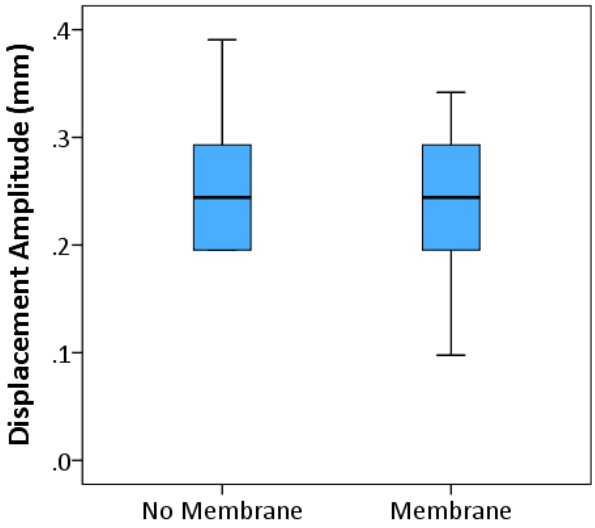

Figure 95: Boxplots showing a comparison of displacement data in tests with and without a fibrous membrane

The analysis showed no difference in displacement between tests with and without a membrane (Mann-Whitney analysis p=0.709), which means it is a property of the membrane material and positioning causing the difference in pressure.

These results indicated that presence of the fibrous layer was causing lower pressures on the angled and pole transducers, and higher pressures at the rim and top transducers. Pressures on the rim transducer were increased in tests with a membrane, as the rim was in direct contact with the membrane, possibly causing a pressure spike due to fluid being forced out of the membrane under load and into the transmission tube. The reduced pressures on the angled and pole transducers, behind the cup, may have been lower in the presence of a membrane, if the membrane was sealing off the periacetabular area from fluid ingress. The sealing effect was observed when setting up the tests in the current series. When oil was introduced into the chamber, the transducers behind the cup were unplugged, to allow the oil to fully drain through all of the transmission tubes before the sensors were attached. In the presence of a membrane this draining took significantly longer, as the rate of flow behind the cup was restricted by the presence of the membrane. This sealing effect has also been observed by other groups - *in vivo* tests with a rabbit model by Frokjær and colleagues showed that the fibrous tissue formed a barrier against debris ingress with a press-fit cup (Frokjær et al., 1999).

Another explanation is that the presence of the membrane causes the cup to sit slightly higher in the cavity, altering the periprosthetic space to allow a larger fluid clearance between the implant and the cup. This higher clearance would reduce the impact of cup movement on the pressures measured on transducers behind the cup. Both of these ideas are illustrated in Figure 96.

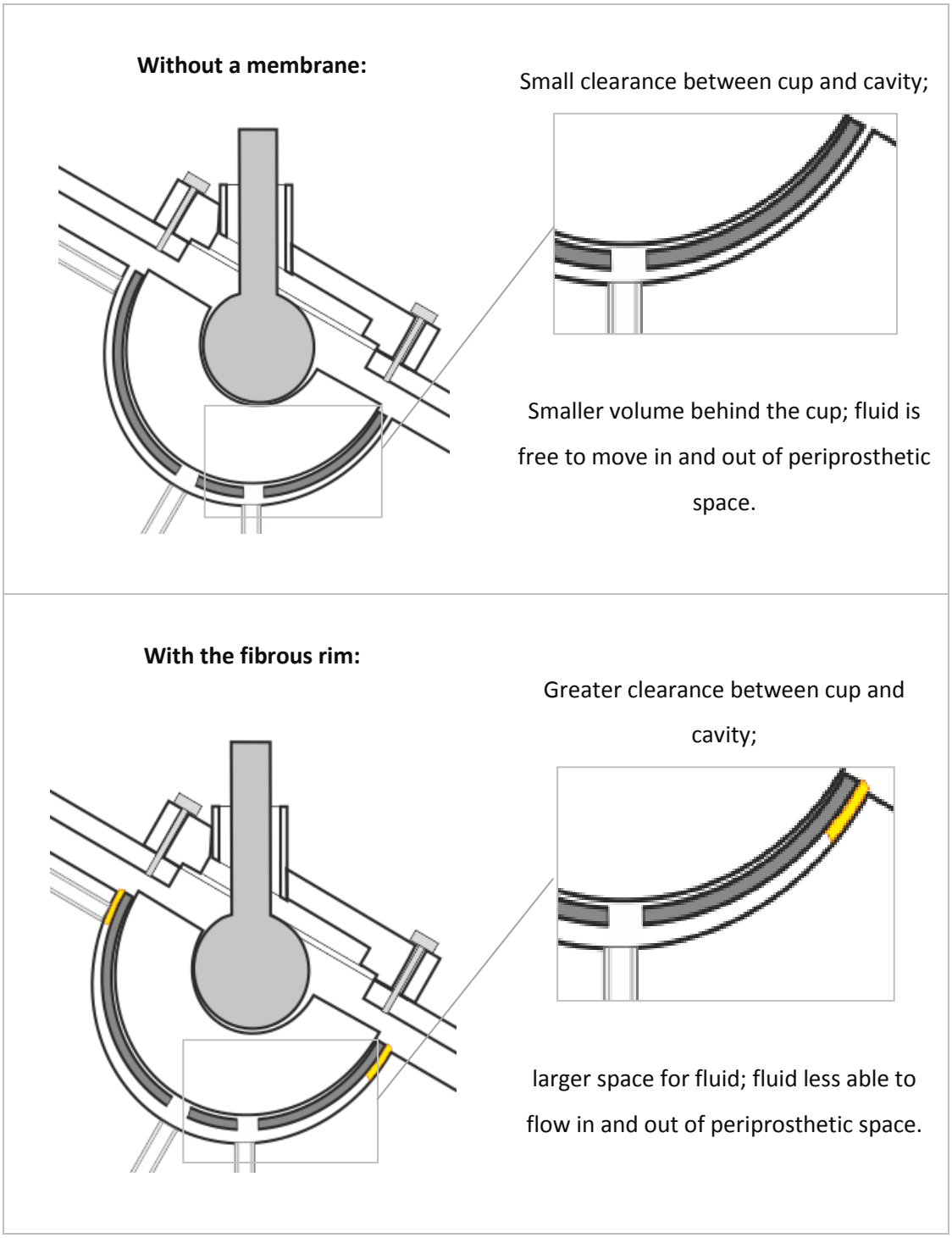

Figure 96: Illustration of cup fixation with and without a fibrous membrane

Analysis of maximum pressures

Under all test conditions, the highest pressures were measured on the angled and pole transducers. To determine whether clinically-damaging pressures (over 35kPa (McEvoy et al., 2002, Evans et al., 2006a)) can be generated with the APTR, the maximum pressures under different loading conditions were investigated. Results of this analysis can be found in Figure 97.

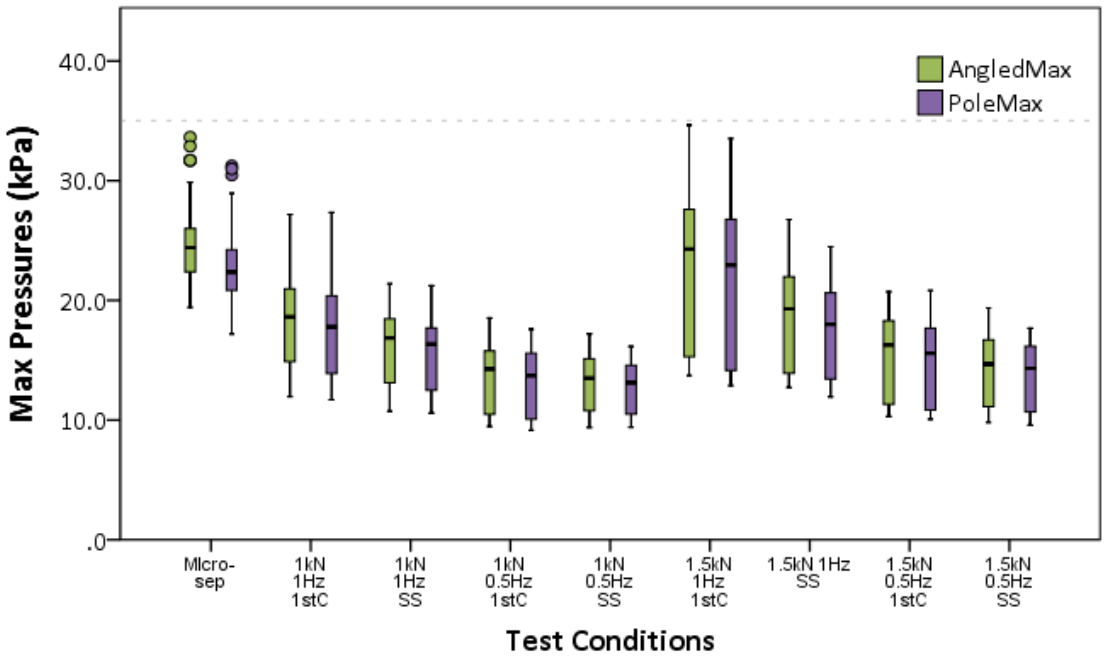

Figure 97: Boxplot showing maximum pressures under different loading and fixation conditions. Green bars represent data from the angled transducer; purple bars indicate the pole transducer. The dotted grey line represents the clinically significant pressure level.

The overall maximum pressure (34.64) was measured on the angled transducer at 1.5kN and 1Hz, without a membrane. None of the loading conditions produced pressures above 35kPa, the level which has been identified as the most clinically damaging (McEvoy et al., 2002, Evans et al., 2006a).

In all tests without a membrane, the angled transducer, in line with the load axis, measured the highest pressures, significantly higher than the pole pressures using the Related samples Wilcoxon signed rank test. These results suggest that the highest fluid pressures tend to be measured along the load axis. In tests with the fibrous rim, the maximum pressures on the pole and angled transducers were not significantly different.

Maximum pressure values were significantly lower than expected, based on the pilot testing (maximum pressure of 204kPa measured in pilot tests loaded at 1kN and 1Hz, compared with a maximum of 27.3kPa under the same load). This may have been due to several factors. First, the APTR is an open system, meaning oil flow out of the rig chamber is possible, unlike the pilot studies where the oil was constrained by a latex sheath. If this flow of oil was prevented, localised pressure peaks would be higher as the volume of fluid would not be able to escape from the chamber. Secondly, leaks in the rig may have reduced peak pressures by providing further avenues for oil to escape (and thus pressure to be released). Finally, the APTR model is more sophisticated than the pilot models, so it is to be expected that results of the two models will differ.

It is possible that the higher pressures in tests without a membrane are due to higher fluid movement being possible, as there is no fibrous barrier to fluid accumulation behind the cup. Further investigation, in combination with an assessment of where in the load cycle these maximum pressures occurred, is required to draw further conclusions about the effects of the membrane on pressures in the APTR.

Interestingly, in the presence of the membrane, there was no statistical difference in maximum pressures on the pole and angled transducers. If, as has been suggested, the fibrous rim forms a barrier to oil ingress, this may have caused the periacetabular space to become a 'closed space', with the hydrostatic pressures increasing the measurements on the pole and angled transducers more equally.

Above-and-below base pressure measurements

To investigate the effect of these pressure amplitudes on conditions inside the APTR, the pressure values above and below the base pressure were investigated (results shown in Figure 98). Pressures above the base pressure were assumed to act as positive pressures, with pressures lower than base pressure acting as negative pressures within the chamber. These negative pressures within the chamber would cause an instantaneous 'suction effect', and the fluid in the APTR chamber would be induced to flow into these areas of negative pressure. Mann-Whitney statistical analysis of the data under different conditions was performed to determine if differences were significant.

This graph shows that both positive and negative pressures, relative to the base pressure, are present in the APTR tests. Pressure amplitudes measured at the rim, in tests with a membrane, were higher than without a membrane. This is reflected in higher maximum pressures, and lower minimum pressures, relative to the base pressure. The higher the magnitude of magnitude of pressures above and below the base pressure, the higher the 'suction effects' forcing fluid to move within the APTR chamber.

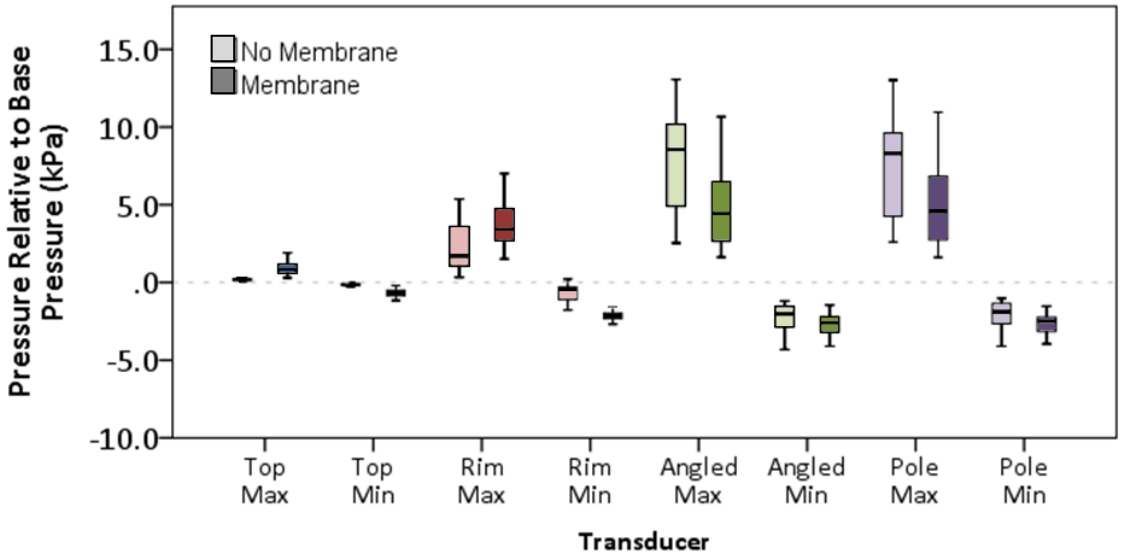

Figure 98: Boxplots showing maximum and minimum pressures, relative to the base pressure, measured with and without membrane, in steady-state period(n = 143). The differences between tests without a membrane (n=63) and with a membrane (n=72) are significant at the p ≤ 0.001 level.

Positive and negative pressure effects were present in the chamber, with and without a fibrous membrane. The presence of a membrane caused the maximum pressures to be significantly lower behind the cup (Figure 98), on the angled and pole transducers. This reduction in positive pressures may have been due to the membrane blocking fluid flow behind the cup.

In order to speculate on the effects of the membrane it would be useful to understand the timing of the peaks of pressure – whether the membrane affects the flow of fluid may be determined by a delay before maximum pressures are achieved, representing the barrier to fluid flow represented by the fibrous rim. This load phase analysis will be examined in the next chapter.

4.11 Discussion and conclusions

This series of tests showed that pressures could be measured behind an acetabular cup under axial load and at a 30° angle. Tests were also intended to assess the effect of changing the load magnitude and frequency, in order to understand the way fluid pressures were generated in the APTR model.

Improvements to rig

Initial improvements to the rig, including widening the transmission holes for better sealing, and modifying the sealing mechanism, improved the ease of rig setup and greatly reduced the degree of leakage. However the introduction of a 30° angle of loading led to higher pressures and a greater degree of difficulty in correctly aligning the rig. These changes led to higher median pressures measured with the APTR – pressures tested at 30° with the improved setup were 7.75kPa higher than the pressures measured in axial tests with the APTR model (x higher than axial tests), but still lower than pressures measured in pilot studies (maximum pressure of 42.9kPa measured without a membrane in pilot testing (see Appendix 1). Tests under different conditions allowed the characteristics of the APTR to be explored; these will now be discussed in more detail.

Effect of change in angle

There was a difference between the pressures measured by transducers behind the cup in 30° angle testing and axial testing. Tests at 30° produced significantly higher pressures than the axial tests. This is assumed to be due to the difference in displacement values between the two tests. As a consequence of the different loading mechanics, for the same displacement value there is a different resulting cup movement. The fact that the liner in this implant was artificially loose meant that a change in loading angle is assumed to deform the liner relative to the metal shell. This deformation is described in Figure 99.

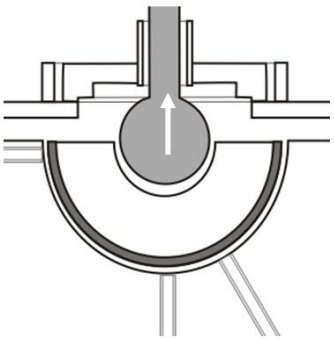

1a. Head moves up inside the chamber

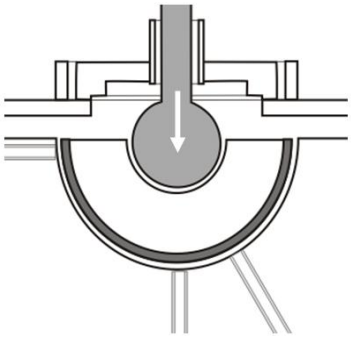

2a. Head moves down inside the chamber, coming into contact with the dome of the cup.

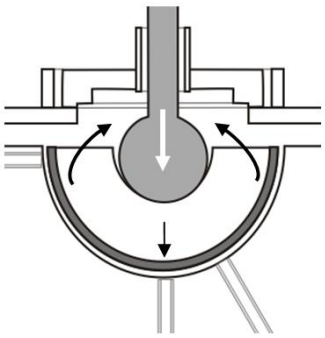

3a. Head presses down on the cup, possibly causing it to move or deform in the manner indicated by black arrows.

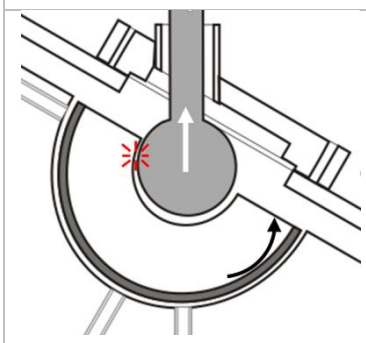

1b. Head moves up in the chamber, possibly initiating rim contact (red lines) and causing movement indicated by black arrow

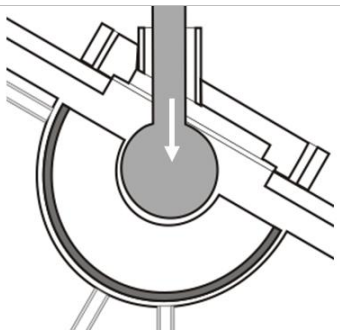

2b. Head moves down inside the chamber, coming into contact with the side of the cup.

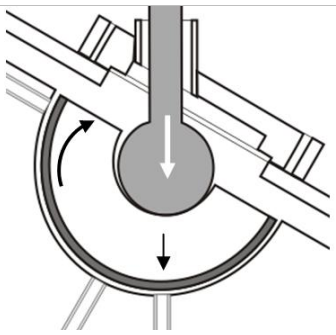

3b. Head presses down on the cup, possibly causing it to move or deform in the manner indicated by black arrows.

Figure 99: Schematic showing probable differences in loading mechanics between testing with the APTR chamber at a) 30° and b) 0°.

The higher pressures measured in this test series may also be due to improvements in rig sealing and not due to the change in loading angle. Highest pressures were almost all measured on the angled transducer (in line with the axis of loading). This increase in pressures in line with the axis of loading was not observed in the previous APTR iteration, possibly due to leaks on the pole transducer (as described in Section 4.5). Higher displacement has previously been linked to higher pressures measured behind the cup (Figure 66); in 30° tests the displacement amplitude was higher than in axial testing, which may also influence the increase in pressure amplitude in 30° testing.

In axial tests, the cup was observed to slip obliquely in the cavity during testing. For this reason a pre-seating routine was introduced for further angled testing. Observations on the cup position after tests at 30° also recorded some changes in the cup orientation. In several tests, it appeared that the cup had slipped under load, possibly in response to the movement illustrated in Figure 99, 3b. This implies that the cup seating protocol did not stop the cup slippage, possibly due to the head-cup suction effect overcoming the rim fixation, as shown schematically in Figure 41.

Effect of liner movement

It is possible that relative movement between the liner and the shell was occurring during loading, similar to the 'piston pumping' liner movement as described by Walter and colleagues (Walter et al., 2005) and shown in Figure 23. The liner in the Osteolock cup was free to move within the shell, approximately 1mm from side to side and 1mm axially.

As the liner is able to move, a channel of fluid access between the liner and the shell is opened by this movement, as described in Figure 100. As the load is removed, the liner lifts up, due to the head-cup adhesion effect. This creates a negative pressure behind the liner, causing oil from the chamber to move into the liner-shell space. When the load is reapplied, this oil is forced through the screw holes and into contact with the transmission channels, causing pressures to be registered.

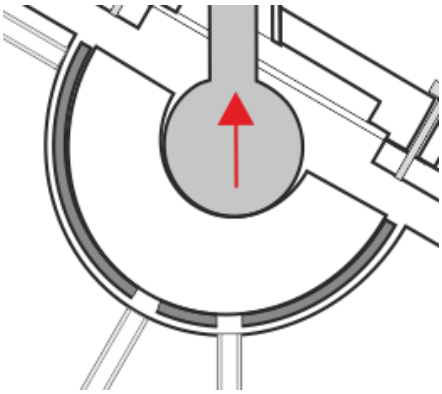

At the bottom of the load cycle, the load is removed.

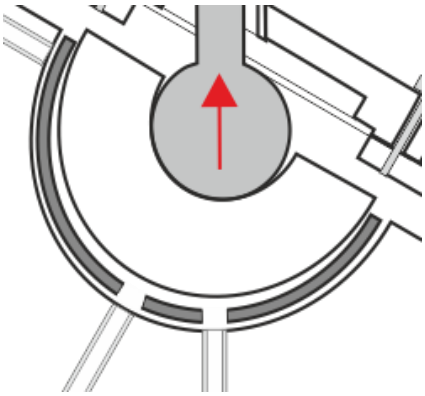

The loading head moves up, moving the liner with it, creating a channel of access behind the cup.

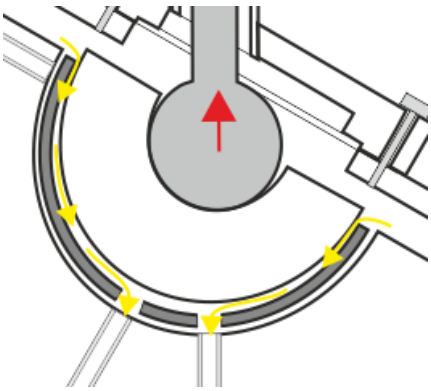

Oil flows behind the liner, filling the space between liner and shell.

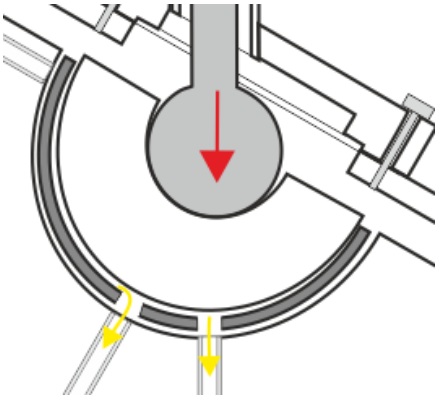

As the loading head moves down, this oil between the shell and the liner is compressed, increasing the pressures measured in the transmission tubes.

Figure 100: Illustration of effects of loose liner

The metal shell behind the Osteolock cup was able to move with respect to the test cavity during loading, simulating loose fixation of the implant. It was not possible to conclude the degree to which each of these movements were occurring, and thus whether the movement of the loose liner, the cup, or a combination of both were influencing pressure fluctuations. For this reason a well-fixed liner was required for further APTR testing.

Base pressure analysis

Base pressures were compared with the expected values calculated from the pressure head equation. Figure 81 shows that the rim, angled and pole base pressures measured during testing closely match the pressures calculated using the geometry in Figure 80. There was a higher variation in the base pressure measurements from the top transducer compared to the other channels. This may have been due to air bubbles trapped in the top of the rig chamber, or due to errors in the offset calculation caused by the initial chamber conditions influencing initial measurements of the top transducer. To avoid air bubbles being trapped, and to attempt to stabilise results from this transducer, a release valve was designed for further testing.

Effects of change in loading regime

The testing described in this chapter showed that the APTR was sensitive to changes in both load magnitude and frequency. Higher loads and load frequencies produced significantly higher pressures behind the cup.

In 30° testing, load was increased from 1kN to 1.5kN during testing. This increase was relatively small, a similar magnitude to a slight increase in gait speed *in vivo*, as described by Bergmann and colleagues (Bergmann et al., 1993). The increase of 1kN to 1.5kN is equivalent to an increase of 150 to 220% BW (see section 3.3), which in the Bergmann study was equivalent to an increase in gait speed of around 2km/h, and this load increase produced an increase in median pressures from 10.6 kPa to 14.2 kPa measured on the angled transducer. The higher loads are accompanied by a higher displacement value (increased from 0.244 to 0.293mm). This increase in load and displacement is assumed to cause more component deformation, and potentially more deformation of the test hemisphere. This increase in deformation would lead to greater pressure fluctuations as there is a greater change in volume of the periacetabular space. Assessment of pressures before and after the application of the higher load suggested that this degree of deformation is recoverable.

The movement of the loading head had a significant effect on pressures. A higher frequency of loading (thus higher speed and acceleration of the loading head) corresponded to greater pressure amplitude measured on all transducers. A higher pressure amplitude was also recorded when the loading head started from a higher position and re-engaged with the cup, a movement which was analogous to *in vivo* re-engagement following microseparation.

It has previously been deduced that a faster head movement causes higher pressures (section 4.5). Increasing the frequency during initial testing led to an increase in pressures measured. In 30° testing, reducing the frequency from 1Hz to 0.5Hz produced a reduction in median pressures from 10.6kPa to 6.4kPa on the angled transducer. This reduction in pressure is assumed to be due to the viscosity of the fluid and its ability to flow behind the cup. In cell culture studies, the frequency of loading was shown to have an effect on the expression of cytokines – the expression of IL-1β was increased by cyclic pressure application at 0.5Hz, but not at the lower frequency of 0.05. (Ferrier et al., 2000). This implies that frequency of loading *in vivo* may have a mechanical effect on fluid flow in the joint, but also influence cellular activity. The results of this study show that the frequency of loading when testing pressure with a viscous fluid will influence results, with higher frequencies causing higher pressures. As the generally accepted gait frequency is 1Hz, all future tests with the APTR will be performed at this frequency. To simulate loading frequency in an *in vivo* gait cycle, a rest period during swing phase should also be incorporated into the loading regime, however the control system of the Dartek did not allow for this complexity of loading.

A higher initial displacement in axial testing caused a pressure spike. This larger initial displacement on the first cycle of loading, simulating a 'relocation after microseparation' condition, also increased the speed of movement of the head as it engaged with the cup. This had a significant effect on pressure results, and was explored further in 30° testing. When the initial displacement gap was higher (median 0.59mm compared to 0.44mm), the pressures were significantly higher (increased from 12.08kPa to 18.53kPa on the angled transducer with higher displacement). With this higher initial displacement, the head travelled further over the same period of time to engage with the cup and apply the load. This greater head movement over time was believed to be the cause of higher pressure amplitudes behind the cup. This is assumed to have a similar effect to increasing the loading frequency, in terms of the velocity of head movement. As vegetable oil is a viscous fluid, it has a resistance to flow, which means that if the volume available is suddenly decreased, there will be an increase in pressure until the fluid can flow out of the space. The faster the volume is changed (ie the faster the loading head moves), the higher this instantaneous pressure will be.

It is possible that rim contact occurred as the loading head was raised during the load cycle (see Figure 99), which may have displaced the loose liner as the head moved up. This may be similar to the effect described by Amirouche and colleagues in their FE study (2008), in which joint subluxation caused micromotion between the liner and the shell.

Since the liner is loose in this cup, and due to the high levels of head-cup adhesion observed, it is possible that the displacement measured in the APTR in this chapter occurred between the liner and the shell, rather than between the head and the cup. The displacement value of 0.6mm between the head and the cup is significantly lower than the 3.3mm average head-cup separation previously measured *in vivo* (Dennis et al., 2001).

Effects of membrane

Initial axial tests with a fibrous rim around the prosthetic cup suggested the membrane increased the pressures measured on the rim transducer, in contact with the fibrous material. The effect of the membrane was further investigated in 30° testing, where the presence of a fibrous rim actually decreased the median amplitude of pressure waves measured behind the cup, from 10.6kPa to 7.25kPa on the angled transducer. The fibrous material acts as a semi-permeable membrane between the joint space and the periacetabular area, restricting the amount of fluid that can move through to the space behind the cup. The presence of the fibrous rim may have simulated a more well-fixed cup situation, with a reduction of access for fluid behind the cup. It is possible that this membrane simulated a rim-fit condition, where cup stability is provided by interference between the rim of the cup and the acetabular rim.

The physical conditions inside the chamber also had an effect on the pressures measured by the APTR unit. Tests showed that the presence of a fibrous membrane significantly increased the pressure measured by the rim transducer, which was in direct contact with this membrane. This result indicates that features close to the transmission tubes in the APTR chamber have a significant effect on the pressures measured at these points.

This was also confirmed by tests on the position of screw holes relative to the angled transmission tube. When the angled transmission tube was covered, the pressures measured on the angled transducer were higher. With the transmission tube uncovered, the local fluid volume at the measurement point was increased, as it was in communication with an open screw hole in the shell of the cup. This assessment of the effect of screw holes in the cup would be better performed with two different component types, with the same basic shell geometry. One component would have cluster screw holes in the shell, whilst the second would be a solid-back shell with a closed apical screw hole.

Pressures on the different transducers

The different pressure amplitudes measured on the three periacetabular transducers implied a pressure gradient behind the cup. Highest pressures were generally measured on the angled transducer, with slightly lower pressure on the pole transducer, and lower still on the rim and top transducers. This is illustrated graphically in Figure 101 (the thickness of fluid has been exaggerated for display purposes). This pressure gradient may allow fluid movement which would cause debris transport *in vivo*.

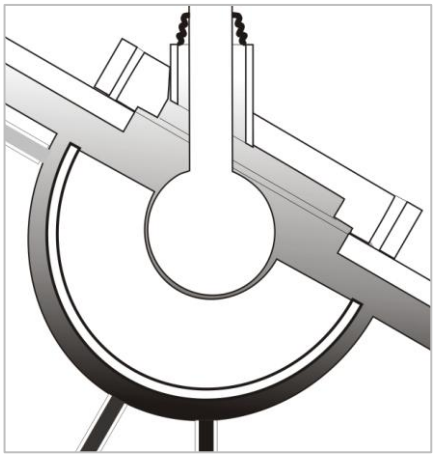

Figure 101: Illustration of APTR chamber representing the assumed pressure gradient (darker areas correspond to higher pressures)

However the top transducer, measuring pressure in the APTR chamber, was affected by some conditions but not others. There was no significant difference in top pressure amplitude with the change in angle, but as the sealing mechanism had been significantly changed it may not be appropriate to compare the top pressures. The change in load frequency also caused no significant difference to the top transducer measurements.

However when a membrane was present, the top transducer measured significantly higher pressures than without a membrane (median pressure 1.45kPa with a membrane; 0.34kPa without membrane). This implies that some increased fluid movement due to loading was occurring to increase the localised pressures at this transducer location. It is possible that fluid absorbed into the fabric of the membrane when the load was at a minimum, and then exuded under the application of load, causing a pressure spike in the fluid contained in the APTR

chamber. This cannot be further investigated without phase analysis, to determine if this assumption is correct.

The base pressure was the pressure measured on each of the transducers in the absence of loading. The pressure results with respect to these base pressure values were investigated as they represented positive and negative pressure effects within the APTR chamber. Both positive and negative pressures relative to the base pressure were measured within the chamber during these tests, adding weight to the theory that fluid movement, and therefore debris movement, is possible behind the acetabular cup.

Maximum pressures

One of the desired outcomes from the APTR testing was to determine whether the pressures measured in the chamber were sufficiently high to cause osteolysis, or to force debris-carrying fluid behind the cup to the periacetabular bone. The maximum pressures (shown in Figure 97) were measured without a membrane, on the angled transducer, under the 'relocation from microseparation' conditions (33.63kPa) and under loading at 1.5kN and 1Hz (34.64kPa). These maximum pressures were not clinically significant – pressures of 35kPa have been shown to lead to osteolysis (Evans et al., 2006a).

As described earlier, the angled transducer generally measured the highest pressures. However in membrane tests there was no statistical difference between maximum pressures on the angled and pole transducers. This may have been another result of the 'sealing' of the periacetabular space by the fibrous rim as described in Figure 96. It was not possible to investigate this further with the data in this testing.

It is assumed that the magnitudes of these maximum pressures were related to the static pressure head applied to the chamber from the elevated oil reservoir. This height of oil was chosen to replicate the base pressure inside a hip with joint effusion (as described in section 3.9). However to determine how a different pressure head would affect pressures measured in the APTR chamber, further tests needed to be performed with the oil reservoir at a different height.

The pressures measured in this chapter were significantly lower than the results of the *in vitro* study by Walter and colleagues, in which a loose liner was loaded and pressures measured behind the liner (2005). The rig used by Walter et al measured pressures of 685kPa with a

loose pistoning liner and 87kPa with a congruent liner. Maximum pressures measured behind the loose cup with loose liner in this chapter were all lower than the 35kPa value associated with osteolysis development.

The greatest amount of head-cup movement in the 'relocation-from-microseparation' tests was 0.9mm (median value 0.6mm). This is significantly lower than the microseparation distance measured during normal gait (a separation distance of 2-3mm (Lombardi et al., 2000, Dennis et al., 2001) can be expected to occur during gait). Therefore the relatively small movement of the loading head in this chapter, even under 're-location from microseparation' conditions, may have caused lower pressures than if the complex multiaxial loading of the *in vivo* hip had been applied.

Improvements or changes to rig/ test procedure

The results presented in this chapter give an indication of the capability of the rig to measure pressures behind an acetabular cup under different conditions. The changes made to the APTR setup for the testing in this chapter have improved this capability. The Matlab program made analysis faster and more consistent and improvements to the sealing mechanism removed most of the leaks in the chamber.

However, more changes were needed to further improve APTR function. To further investigate the sensitivity of the APTR, the test routine needed to be modified to allow testing with the oil reservoir at different levels and to test with different prosthetic components. The sensitivity of the APTR model to these changes could then be assessed.

Variations in the test data needed to be addressed. Some of the variations in the test data were assumed to be due to the angle of loading causing difficulties in repeatably setting up the rig, as well as the possibility of the cup slipping obliquely in the test cavity. The precise geometry of the interaction between the loading components and the rig chamber made it difficult to consistently set up the tests at 30°, and small errors in the test setup caused significant disruption to data (see Figure 75 and Figure 76). Slight differences between the different test setups may have contributed to the inter-test variability of test data. For this reason a change in angle back to axial loading was recommended for further testing. An outlet valve in the top sealing part was required to expel any air bubbles that may collect near the top of the rig, and as a measure to stabilise initial pressure values on the top transducer.

A cup with a loose liner was used in this chapter, however this loosening was artificially induced and may not be representative of liner loosening *in vivo*. It was not possible to tell whether the movement of the cup was coming from liner movement or movement of the metal shell, making it difficult to explain exactly what was influencing pressures. For further testing, a cup with a congruent liner was selected.

Changes in data analysis were also required. To investigate whether the assumptions about fluid movement behind the cup were correct, more information about the fluid behaviour was required. To facilitate this, the phase characteristics of the pressure signals needed to be investigated – the location within the load cycle of maxima and minima in each pressure signal. These changes will be further discussed in Chapter 5.

The displacement values in this series were measured with an insufficient sampling frequency. After investigation of the instrumentation this was found to be due to the way the Dartek produced displacement data while testing in load control. It was not possible to adjust this using the Dartek software, so the displacement data sampling rate would remain low for further testing.

In conclusion, the APTR model was used to assess factors affecting pressures behind the cup, and to determine the conditions under which osteolysis-causing pressures may be generated. Further improvements to the model will allow the definitive APTR setup to be tested, leading to greater understanding of these conditions.

4.12 Chapter summary

- Initial axial tests showed the influence of loading and fixation conditions on pressures, but test results were influenced by leaks and changes to the test setup were required.
- Improvements to the test setup produced higher pressures, and further tests were carried out at a 30° loading angle.
- The pressures measured behind the prosthetic cup were shown to be accurate using expected base pressure calculations.

- Higher loading frequency and magnitude led to higher median pressure amplitudes (higher frequency increased pressures from 6.54kPa at 0.5Hz to 10.57kPa at 1Hz; higher load magnitude increased pressures from 10.57kPa at 1kN to 14.17kPa at 1.5kN).
- Higher initial displacement values significantly increased the pressures measured behind the cup.
- The presence of a membrane decreased median pressure amplitudes at the base of the cup (10.57kPa to 7.25kPa) but increased amplitudes in the chamber (0.34kPa to 1.45kPa).
- Differences in pressures at different points behind the cup, and analysis of pressures relative to the base pressures, implied a pressure gradient and the potential for fluid movement behind the cup.
- Tests with the fibrous membrane appeared to simulate better cup fixation of the prosthetic cup, with reduced fluid access to the periacetabular space.
- Pressures capable of inducing osteolysis (over 35kPa) were not produced in this test series. Maximum pressures were measured under 'relocation-from-microseparation' conditions (33.63kPa), and under the highest load conditions (34.64kPa measured with 1.5kN load and 1Hz frequency) in the absence of a fibrous rim.
- Further improvements to the APTR setup were identified.

5. The Effect of Component Features on Pressure

In order to use the rig to investigate pressures behind different cup designs, the sensitivity of the rig to small changes in the cup design needed to be investigated. This chapter outlines these investigations and their implications for the use of the APTR.

5.1 Chapter aims

In this chapter the definitive APTR setup was described and test results presented. The effect of changes to acetabular cup design, specifically the presence of screw holes, was assessed. The effect of a lower applied pressure head was investigated, and the effect of the presence of a fibrous membrane was investigated. It was also intended to determine which of these factors caused the highest pressures to be generated. To fulfil the chapter aims, these results were discussed and analysed with respect to previous tests as well as their relevance to loose acetabular cups *in vivo*.

5.2 Test Methods

Improvements to test setup

The test rig was set up as previously described. The differences between this test series and the previous series (Chapter 4) are illustrated in Figure 102. The main differences in testing were the axial loading (instead of 30° angled loading) and the new components used (Trident hemispherical cups, one with 6.5mm screw holes in the shell (shown in Figure 103 b) and one with only a threaded apical hole (Figure 103 a). The new components were 54mm cups initially chosen to simulate the under-reaming of the test hemisphere, but due to the inflexibility of the material, the cavities were machined to match the diameter.

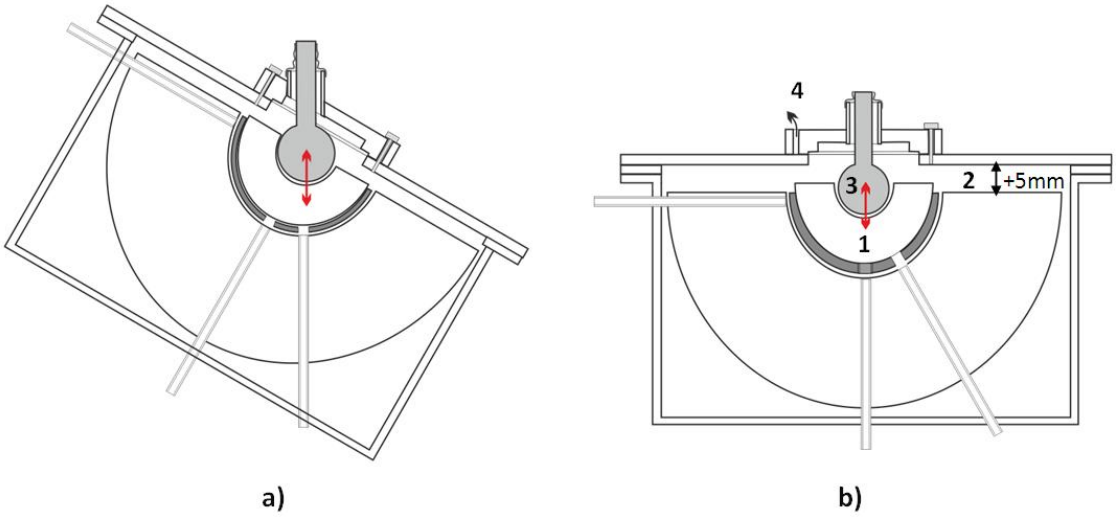

Figure 102: Schematic of changes to rig design, with a) previous rig setup from Chapter 4 testing and b) rig setup for current (Chapter 5) tests. These images show 1) the new 52mm Trident cups, replacing the old Osteolock cup with artificially loose liner; 2) the higher clearance of the rig top to accommodate the higher cup dimensions 3) axial loading direction, 4) screw used as release valve on top seal for oil introduction.

Test method

The fixation conditions used in this chapter are shown in Figure 103. The Trident hemispherical shell with screw holes (Figure 103a) or without screw holes (Figure 103b) in the shell was inserted into the test hemisphere. The threaded hole in the dome of the cup was closed with a dome plug, and then an X3 Poly liner was inserted with both shell types.

The Trident implant was inserted into the test cavity by hand, and aligned using a spirit level so the top of the liner was perpendicular to the axis of loading. The implant was then pre-loaded for 20 cycles at 1kN. When the top sealing plate was in position, oil was introduced into the chamber and allowed to run through the transmission channels before attaching the transducers and closing the top release valve.

To test the effect of a fibrous rim, a 10mm fibrous fabric band was positioned around the rim of the cup and inserted into the test hemisphere (Figure 103c). When oil was introduced into initial tests with this rim, the membrane restricted flow behind to cup, to the extent that no oil was able to flow through the pole and angled transmission tubes. To initiate oil flow, the fibrous material was dipped in oil, and the excess squeezed out, before implantation behind the cup. With the membrane in place the shell sat slightly (less than 1mm) higher in the cavity

than in tests without a membrane, and the membrane itself was compressed to less than 0.5mm thick when compressed between the implant and the test cavity.

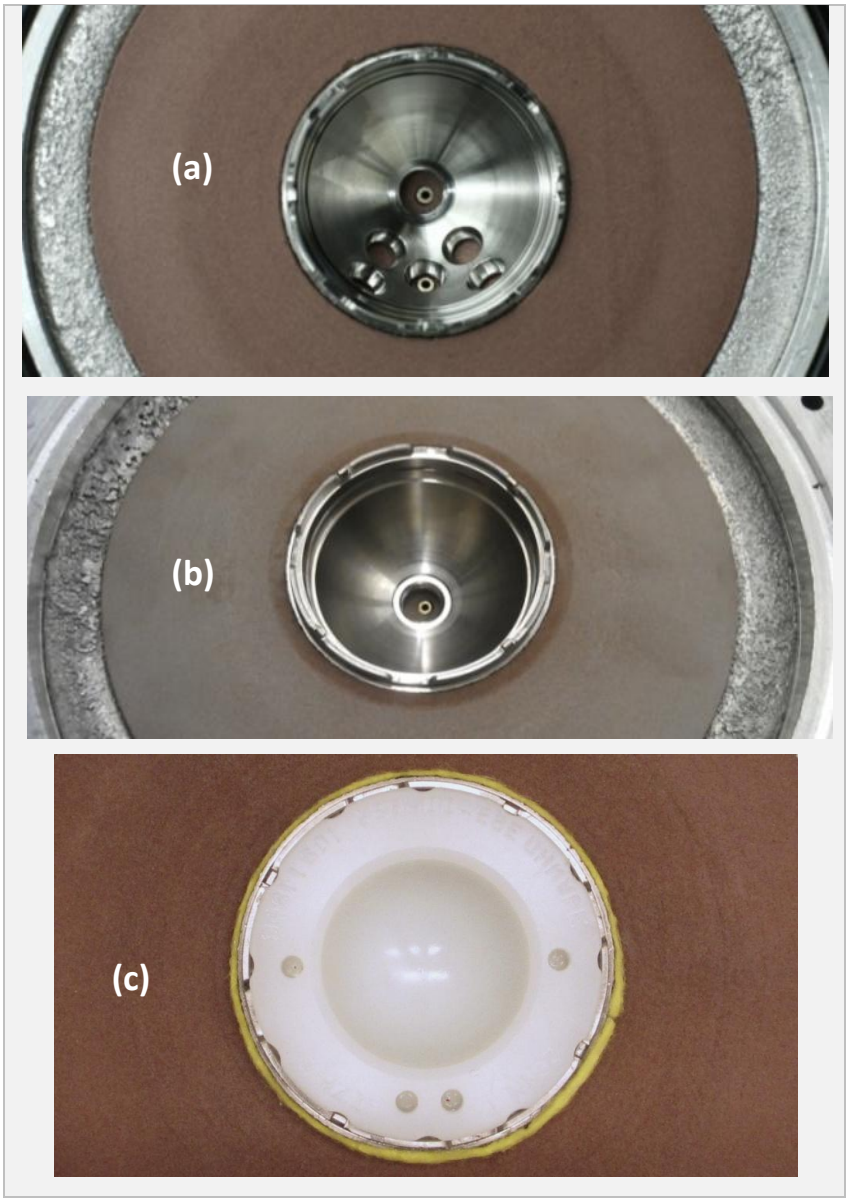

Figure 103: Fixation conditions used in Chapter 5, showing the Trident shell with (a) and without (b) screw holes, and the shell inserted with an X3 Poly liner and fibrous membrane (c).

These conditions were tested according to the test schedule shown in Figure 104. A single test hemisphere was used over the course of this testing, so fixation conditions were alternated to mitigate possible effects of wear in the hemisphere cavity over time, as discussed in the previous chapter. Once the liner was inserted into the metal shell, it was not removed between tests, to maintain the secure lock between the liner and the shell.

In order to determine the effects of the change in metal shell design, the low base pressure applied by a lowered reservoir, and the presence of a membrane, a test routine was developed that varied these conditions. This routine is shown in the schematic in Figure 104 and further described in the following paragraphs.

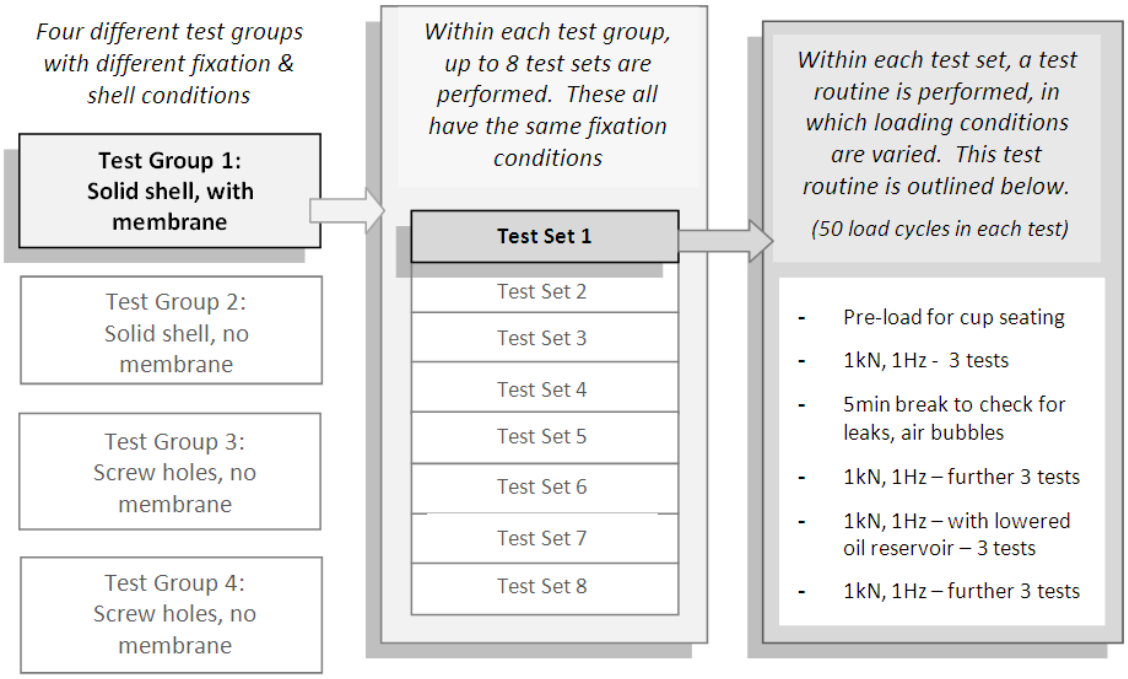

Figure 104: Structure of testing, showing different levels of test organisation.

Checking rig for leaks, air bubbles

After three standard tests, there was a five minute break in the test schedule in which the rig was assessed for leaks and air bubbles. To dislodge any air bubbles, the oil reservoir was moved from its elevated position to a position underneath the APTR chamber, to create a negative pressure within the chamber and cause bubbles to be sucked into the transmission tube. This practice meant the results from the final six tests were more reliable, and the first three tests were therefore discarded for subsequent analysis.

Low-reservoir testing

The sensitivity of the rig to changes in the applied base pressure was not known. To investigate this, low reservoir testing was completed as part of the test schedule. As shown in Figure 105, tests were completed as before, but with the oil reservoir at a level 310mm below the top of the oil chamber (1085mm below usual height).

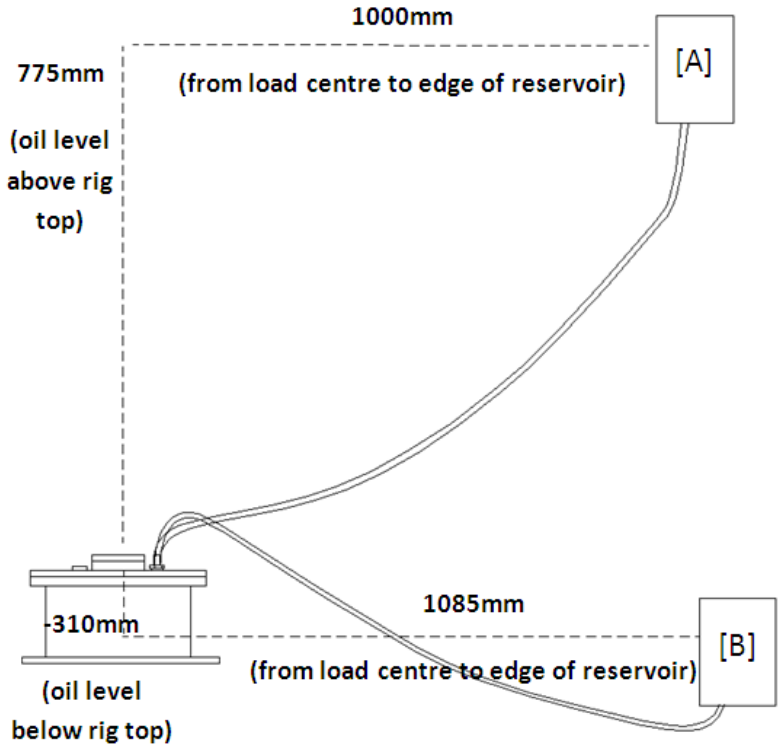

Figure 105: Schematic showing position of oil reservoir during [A] Normal-height testing, and [B] lowered-reservoir testing (not to scale)

Phase testing

The same Matlab routine was used for this chapter, with the addition of a routine identifying cycle 45 and finding the index of the maximum and minimum values in this cycle. Using the data collected from the Matlab analysis, the steady-state maximum and minimum indices (data points at which peaks occur) were plotted against time for a single cycle of each test. The data were normalised with respect to the minimum load value, which was the most negative load measured by the Dartek, representing the maximum compressive load. This point was labelled LoadMaxInv on the graphs. The maximum compressive load was set at 0.2 sec and the positions in time of all other peaks were plotted with respect to this. Boxplots of these data were produced to compare the phase characteristics of each fixation condition.

Statistical analysis

The data obtained in this test series were not normally distributed. Therefore statistical analysis was performed using nonparametric tests. The Mann-Whitney test for two independent samples was used in all cases where direct comparison was made (e.g. investigating the pressure differences in tests with and without a fibrous rim). To simplify the presentation of results, the data come from testing the cup with screw holes at 1kN and 1Hz loading and with the reservoir at normal height, unless otherwise specified.

5.3 Results

Comparison with previous data

The data from this test series was compared with the data from previous tests. Tests performed with the Trident cup with screw holes, with a 1kN axial sinusoidal load and 1Hz frequency, were compared with 1kN1Hz tests from the introductory testing (loaded axially with a Osteolock cup) and the previous test series (loaded at 30° with the Osteolock cup). Mann-Whitney analyses were performed to compare the pressure amplitudes between these groups. The results of these pressure amplitude analyses are shown in Figure 106.

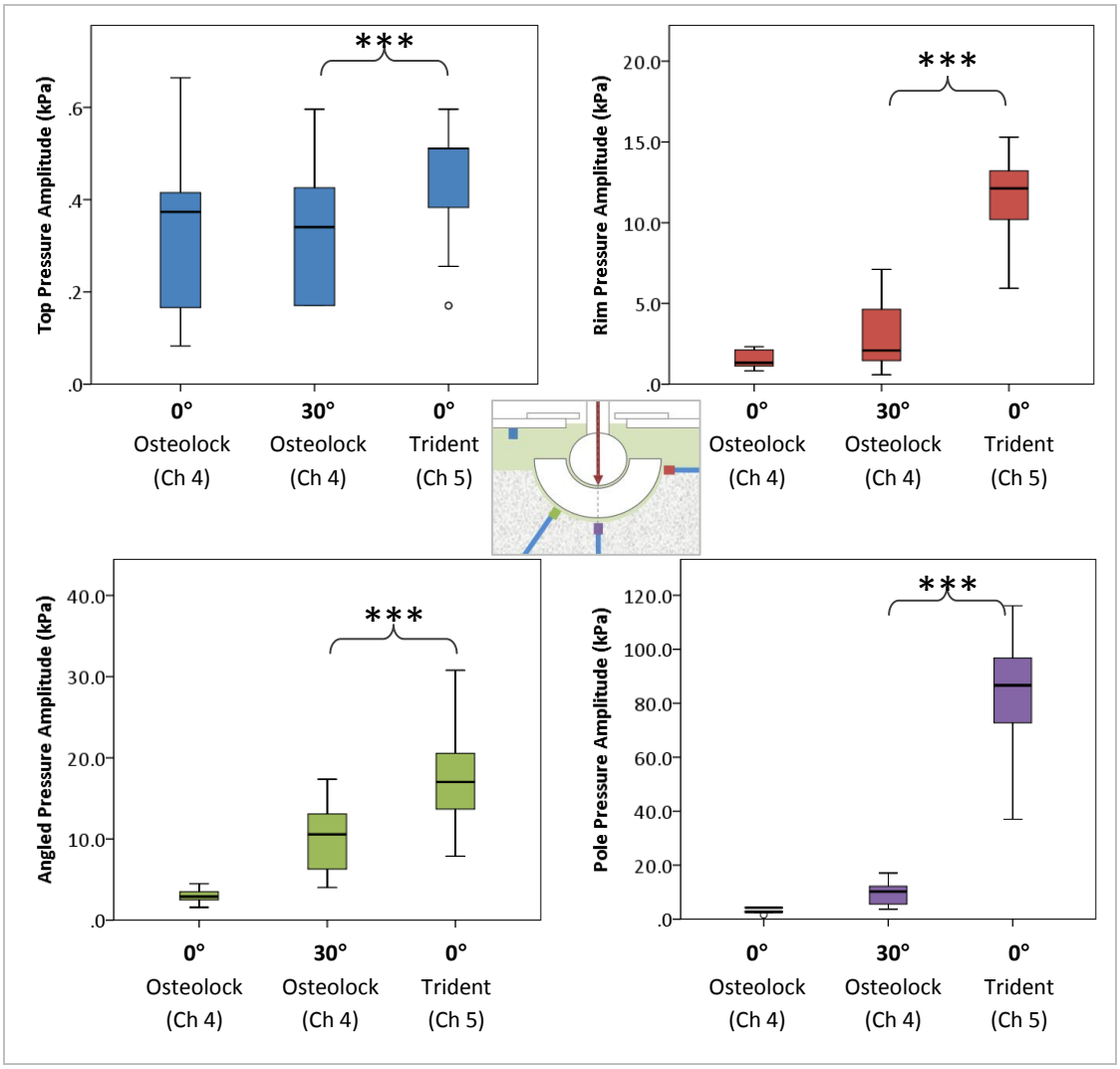

Figure 106: Comparison of pressure amplitudes under previous test conditions with data from Chapter 5. Boxplots show the initial 0° axial tests (n = 16) and 30° testing from Chapter 4 (n = 63), and the axial testing with the new Trident implant (with screw holes, n = 48). The significance of differences in results is indicated with a bracket, and stars indicate the level of significance –[***] = p ≤ 0.001.

Pressures from the current test series were significantly higher than previous test series on all transducer channels. The pole pressure amplitudes showed the most striking difference, with a median pressure of 86.7 kPa, compared with 10.6 kPa in 30° testing and 2.8 kPa in the initial axial tests.

This significant increase in pressures on the pole transducer may be explained by three significant differences between the previous chapter's tests and the current results: the direction of loading, the amount of fluid volume behind the cup and the movement of the liner relative to the shell.

In the current series, the pole transmission hole is in the axis of loading, as shown in Figure 107 (b), while in the previous testing the angled transmission hole was positioned in the axis of loading (Figure 107(a)). As previously discussed in section 4.11, the angle of loading influences the position at which maximum pressures are measured, with highest pressures measured in the axis of loading.

Trident components in this test series were 54mm in diameter, compared to the 52mm diameter Osteolock cup from Chapter 4. This may also have contributed to the higher pressures, as the same magnitude of movement of the cup would have caused a higher volume displacement to occur.

These differences may also be due to design differences between the two components. As shown in Figure 107, the Osteolock cup was tested with an open pole hole, while the Trident cup had an apical screw sealing the hole at the pole of the cup. The pressure differences could be explained by the differences in fluid volume behind the two prosthetic cups, as well as the different loading angle, affecting fluid movement and thus also fluid pressures transmitted to the transducers.

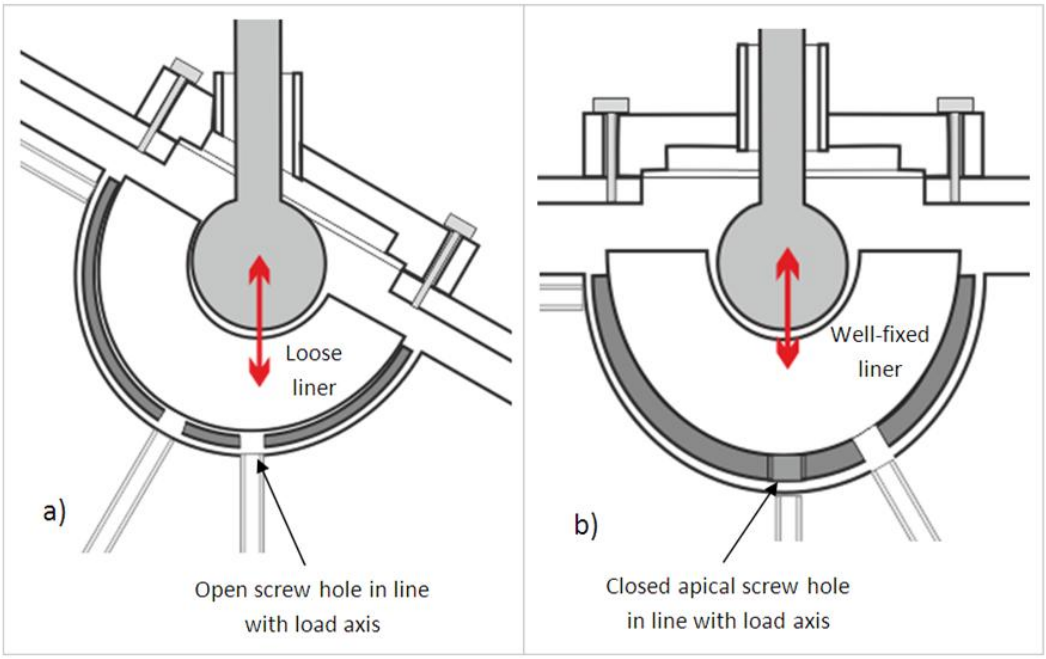

Figure 107: Schematic showing the features of (a) Osteolock cup loaded at 30°, and (b) Trident cup loaded axially

Most significantly, the liner movement relative to the metal shell would have a major impact on periacetabular pressures. In the previous chapter the liner was loose and able to move relative to the shell. In this chapter the liner was securely fixed in the shell. So if head-cup suction would occur, the entire Trident cup could move relative to the fixation cavity, while only the liner would move in tests with the Osteolock cup. This highlights the fact that changes in rig loading and different cup components have a significant effect on measured pressures.

Variability of results

The variability of data collected from each of the eight test repetitions was assessed. This variability can be inter-test variability, caused by the dismantling and reassembly of the test rig between repetitions, or intra-test variability, caused by conditions inside the rig during a test repetition. Boxplots of the pressure amplitude data from each test repetition (without a fibrous rim) are shown in Figure 108.

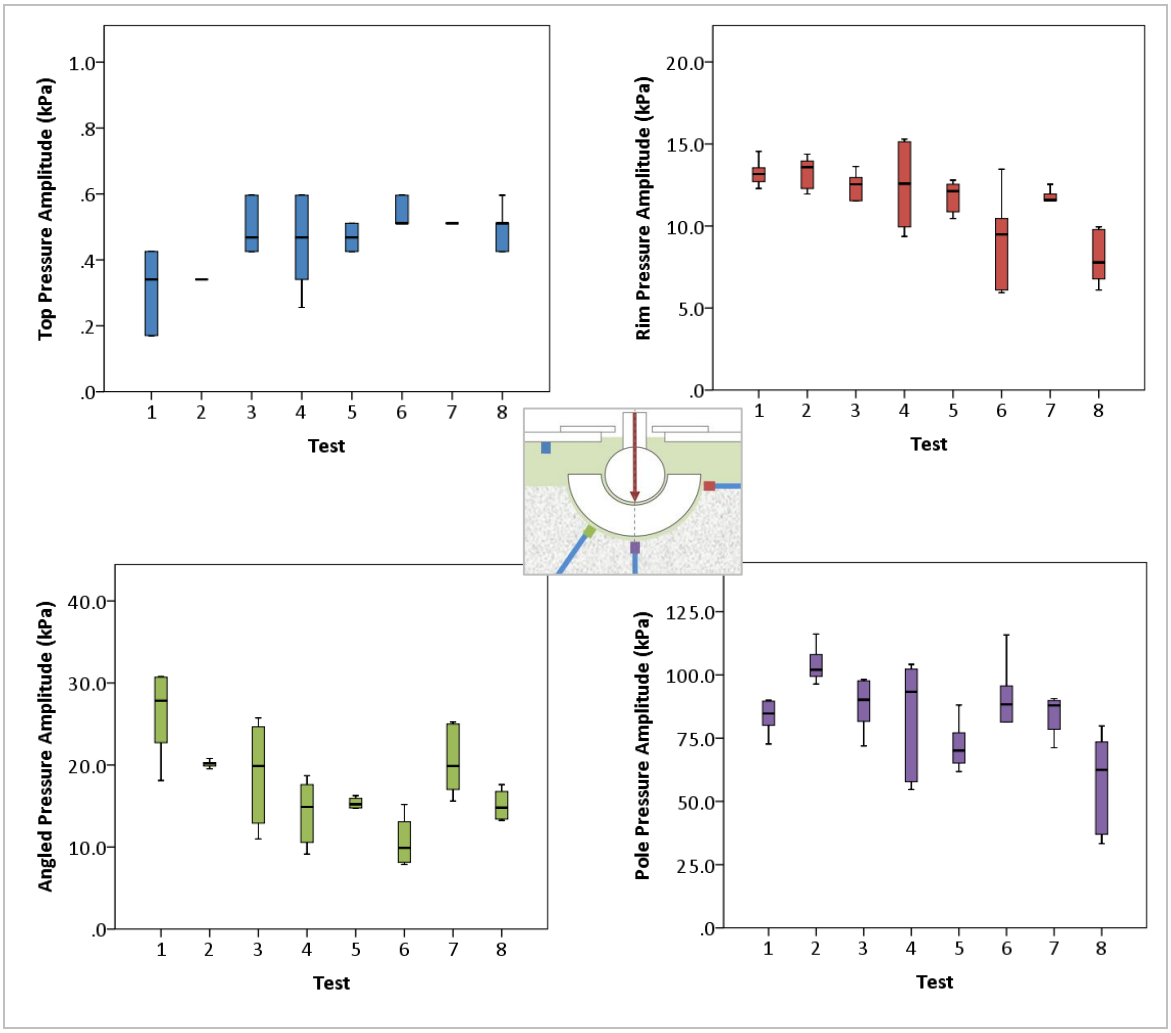

Figure 108: Boxplots showing the spread of pressure amplitude data, within and between test repetitions, from each of the transducers.

This boxplot indicates there is still a degree of variability within the test repetitions, assumed to be caused by the instability of the cup in the test cavity allowing slight changes in alignment under load, even when components are loaded axially.

To assess the variability of results, the median and inter-quartile range (IQR, as described in Figure 59) of the steady-state pressure amplitude results measured with the cluster-back (screw holes) cup were assessed in SPSS. These values were compared with the median and IQR values from the angled transducer (in the axis of loading at 30°) measured from tests in Chapter 4. Values are displayed in Table 11.

Table 11: Comparison of data variability between initial axial tests and angled tests.

Test conditions	Median (kPa)	IQR (kPa)	IQR as % of median
Angled transducer, 30° testing (Ch4)	10.57	6.88	**65.08%**
Pole transducer, axial testing (Ch5)	86.66	24.48	**28.25%**

The IQR, representing the range of values that make up the middle two quarters of the data, can be used as a nonparametric method to assess data variability. Table 11 shows the median pressures from Chapter 4 and 5, and the IQR values associated with the data. The inter-quartile range, representing the variability of data, is higher in the axial tests from Chapter 5. However the relative variability (indicated by the 'IQR as % of median' column) is significantly lower than the relative variability measured in the previous test. This implies that the axial loading configuration with Trident components reduced the variability of test results. This can be attributed to the improvements made after the Chapter 4 testing, including the simplification of the mechanics of loading, the well-fixed liner moving in a more predictable way, and the improvements to the oil introduction process.

First cycle pressure vs steady-state pressure

In the previous chapter, a slightly higher displacement was measured on the first cycle of all tests, simulating a relocation-from-microseparation condition as the head engaged with the cup under load. To determine whether this relocation condition occurred in the current test series, displacement values and first-cycle pressure amplitudes were investigated, at the same points as in the previous chapter (shown in Figure 72 and Figure 73.) A comparison between first-cycle and steady-state pressures is shown in Figure 109.

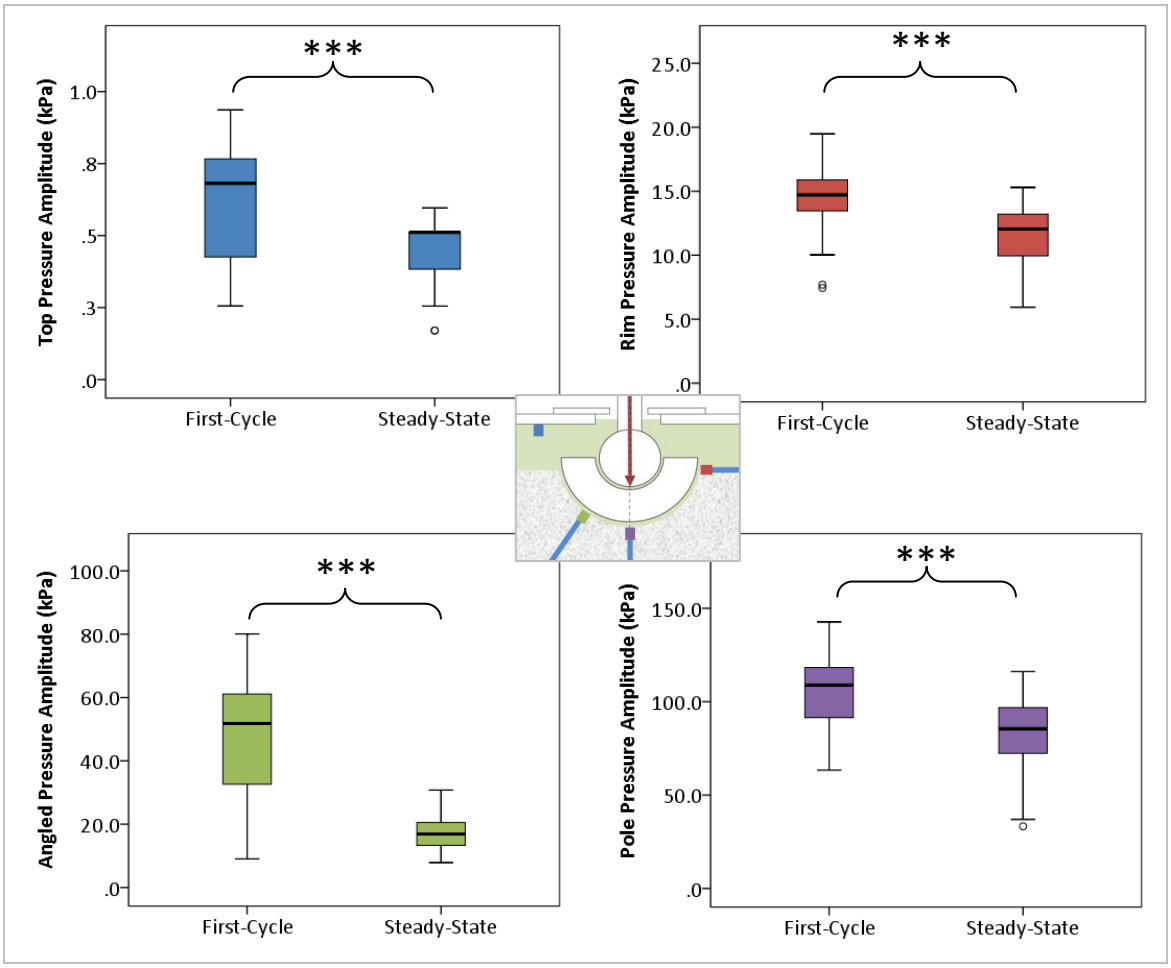

Figure 109: Boxplots showing comparison between first-cycle (n=48) and steady-state (n=48) pressure amplitudes. The significance of differences in results is indicated with a bracket, and stars indicate the level of significance – [***] = p ≤ 0.001.

Mann-Whitney analysis showed that first-cycle pressure amplitudes were significantly higher than steady-state pressures (shown in the boxplots in Figure 109), and the displacement amplitude was also higher (Figure 110).This corresponds with the results from Chapter 4, and implies that the initial relocation condition observed in previous tests was also occurring in this test series.

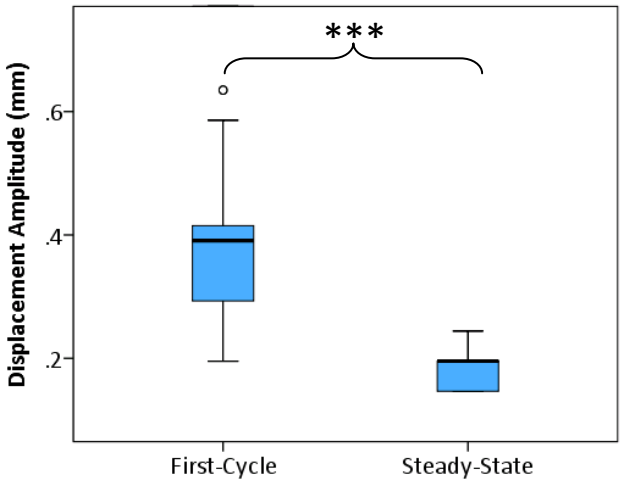

Figure 110: Boxplot showing displacement amplitude data from the first cycle and steady-state periods.

The difference in median displacement between initial and steady-state tests was 0.20mm. This level of initial displacement is lower than the deliberately induced relocation-from-microseparation condition in the previous chapter (0.39mm in Chapter 5 compared to 0.59mm in Chapter 4), but is still capable of producing statistically higher pressures.

Assessment of base pressures

It was expected that the low reservoir tests would have a significant effect on the base pressures, as the position of the reservoir below the APTR chamber would cause a negative pressure head to be applied to the pressure chamber. Predicted base pressures for normal-height and low reservoir tests were calculated in same way as in section 4.10, taking into account the changes in the rig design. Parameters used for base pressure calculation are shown in Figure 111.

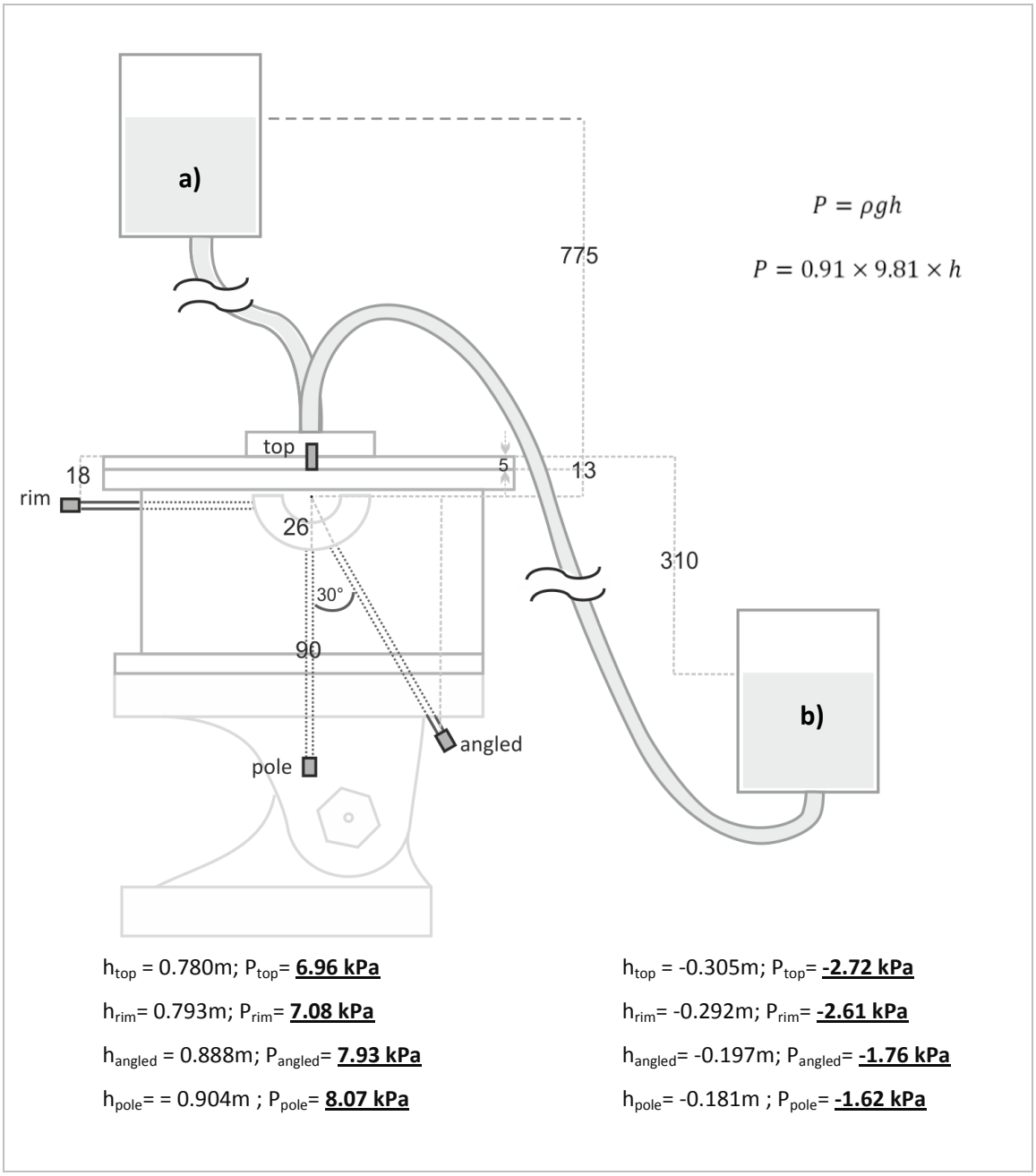

Figure 111: Illustration of base pressure calculation from rig geometry, showing the oil reservoir at (a) normal height, and (b) at low position. The figure also shows normal height values for height and pressure (left column) and low reservoir values (right column).

Shapiro-Wilk tests for normality showed that base pressure data were not normally distributed, so the data were analysed using nonparametric tests. To determine the effect of rig improvements on the variability of base pressure results, the base pressures from the tests with a normal-height reservoir were compared to base pressures from Chapter 4, and their calculated values Figure 112.

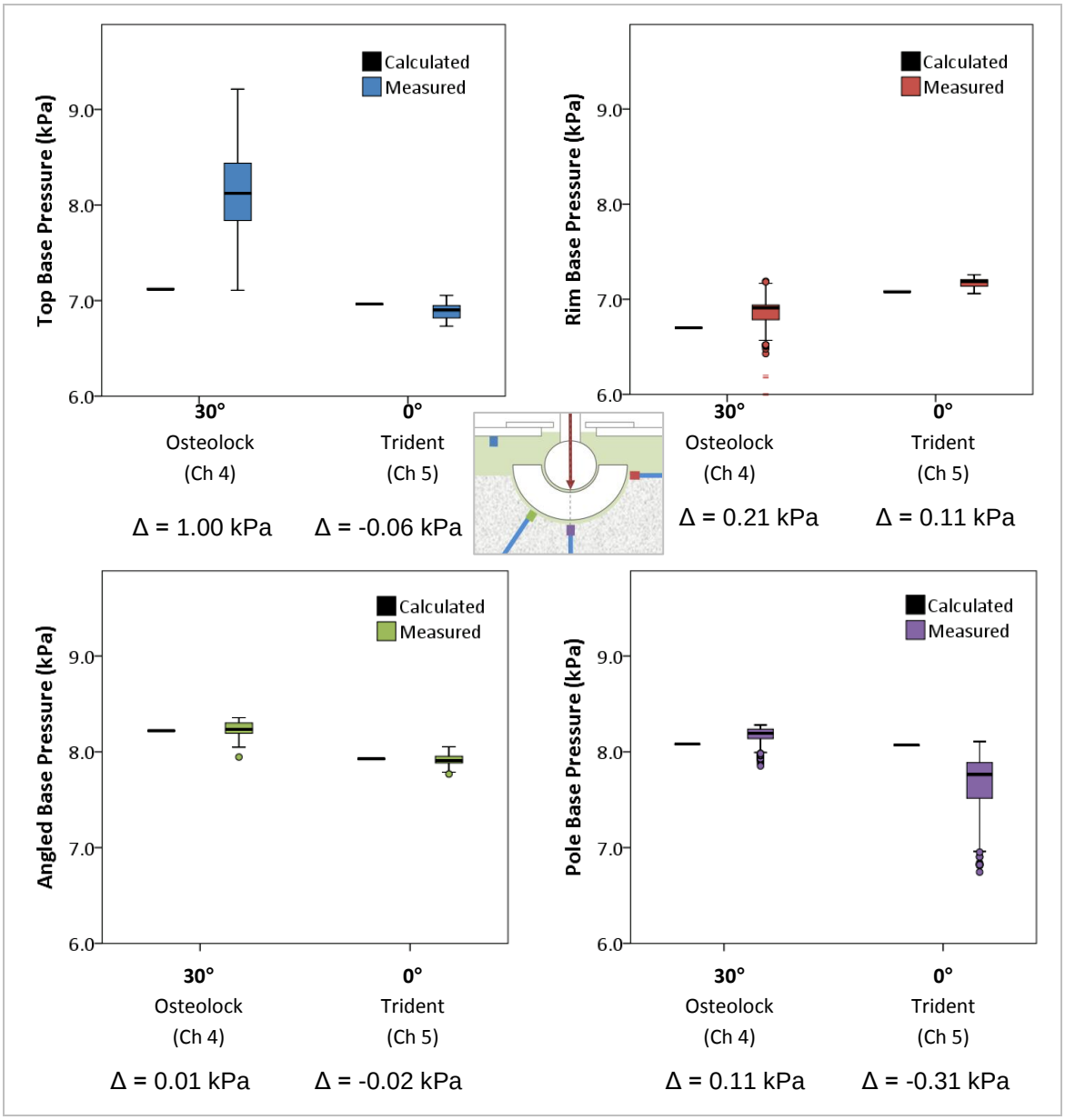

Figure 112: Boxplots showing comparison of calculated and measured base pressure data from Chapter 4 and the current test series.

These results show an improvement in variability of the base pressure on the top transducer, showing that improvements to the top sealing components have improved reliability of results on this transducer. The rim and angled transducers also show an slight decrease in base pressure variability. However, base pressure results from the pole transducer appear to be more variable. This may be due to the ability of the base of the cup, without a fibrous rim, to come into contact with the cavity and 'seal off' the pole transmission channel (explained further in later paragraphs). Slight differences in cup position during insertion would cause differing degrees of sealing, which may have affected the base pressures measured on the pole transducer.

Effect of low reservoir on base pressures

One-sample Wilcoxon signed-rank tests were performed for each transducer channel, using the calculated value as the test value, to compare it with the median measured pressures. Results are shown in Figure 113.

As indicated by pressure head calculations, the base pressure values for each channel were significantly lower with a lowered oil reservoir (using Mann-Whitney test, p = <0.001 on all channels). The difference between measured and calculated pressures on all channels was statistically significant (indicated by stars in Figure 113).

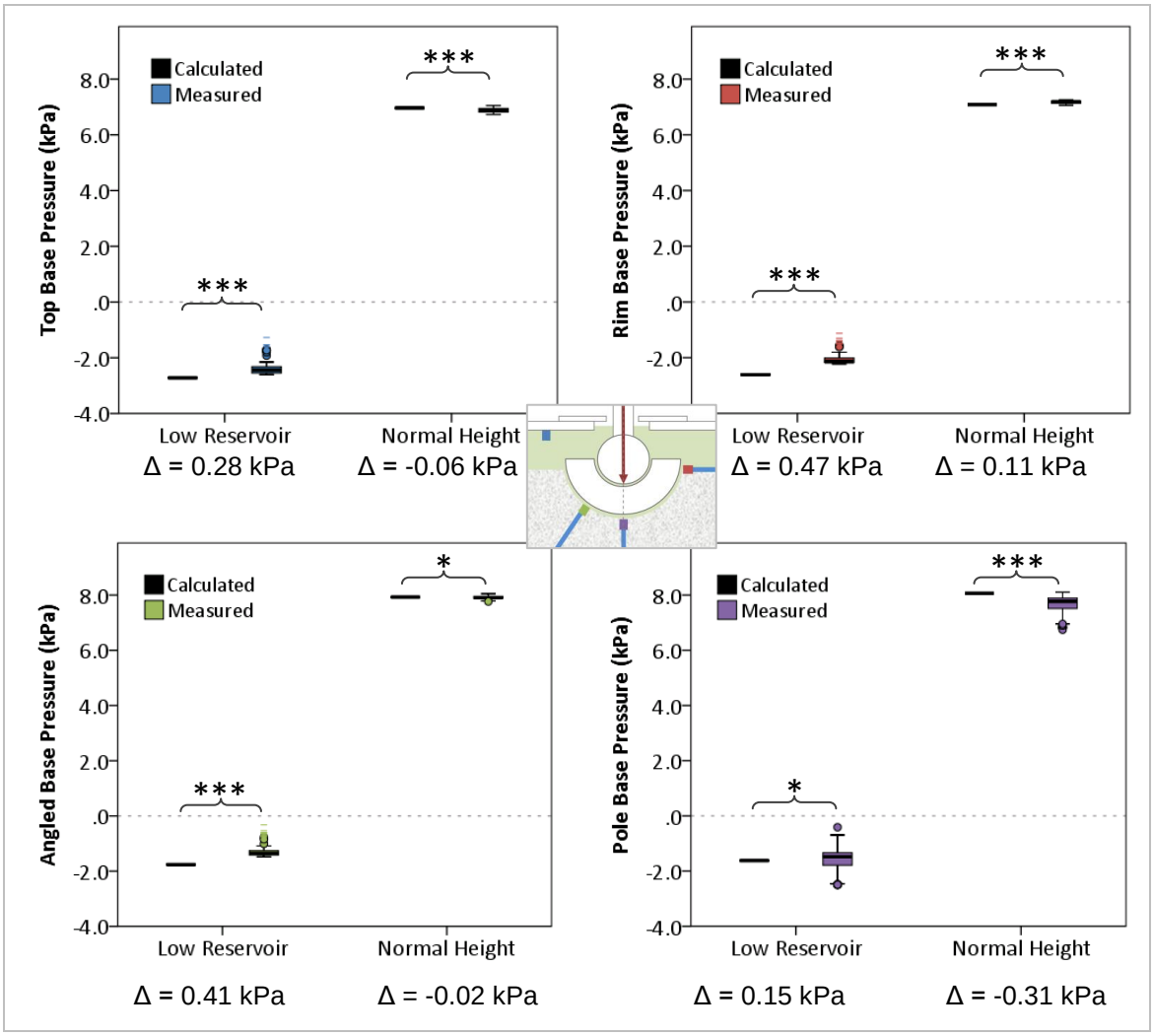

Figure 113: Comparison of calculated and measured data at different reservoir heights – low reservoir (n =64) and normal height (n = 96). The dotted line indicates the point at which pressure = 0 kPa. A statistically significant difference is indicated by stars – [*]= p ≤ 0.05; [**] = p ≤ 0.01; [***] = p ≤ 0.001.

The base pressures were predictably lower with a low oil reservoir, and the differences between measured and calculated values, although statistically significant, were very small (less than 0.5kPa in all cases). This confirms that the pressures measured by the transducers should be representative of the actual pressures in the APTR chamber, with an estimated error of less than 0.5kPa. This testing also confirmed that a lowered oil reservoir produced lower base pressures in the APTR chamber.

Effect of low reservoir on pressure amplitudes

To determine whether this lower reservoir had an effect on pressure generation under load, the pressure amplitude values were investigated, to determine the magnitude of pressure fluctuations within the ATPR. Example data from the two different conditions is shown in Figure 114.

Pressure amplitude data were compared with respect to reservoir height. These data were not normally distributed, so a Mann-Whitney U analysis was performed. No significant difference was observed between the median pressure amplitudes at different reservoir heights ($p = <0.05$ for all transducer channels). A comparison of these results is shown in Figure 115.

Angled transducer data with low- and normal-height reservoir

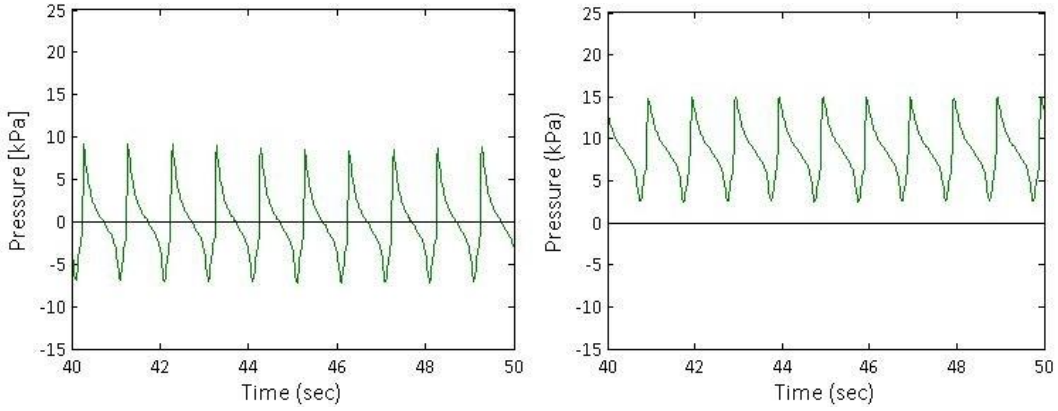

Figure 114: Graph showing sample data outputs from tests with [A] reservoir at normal height, and [B] with a low reservoir

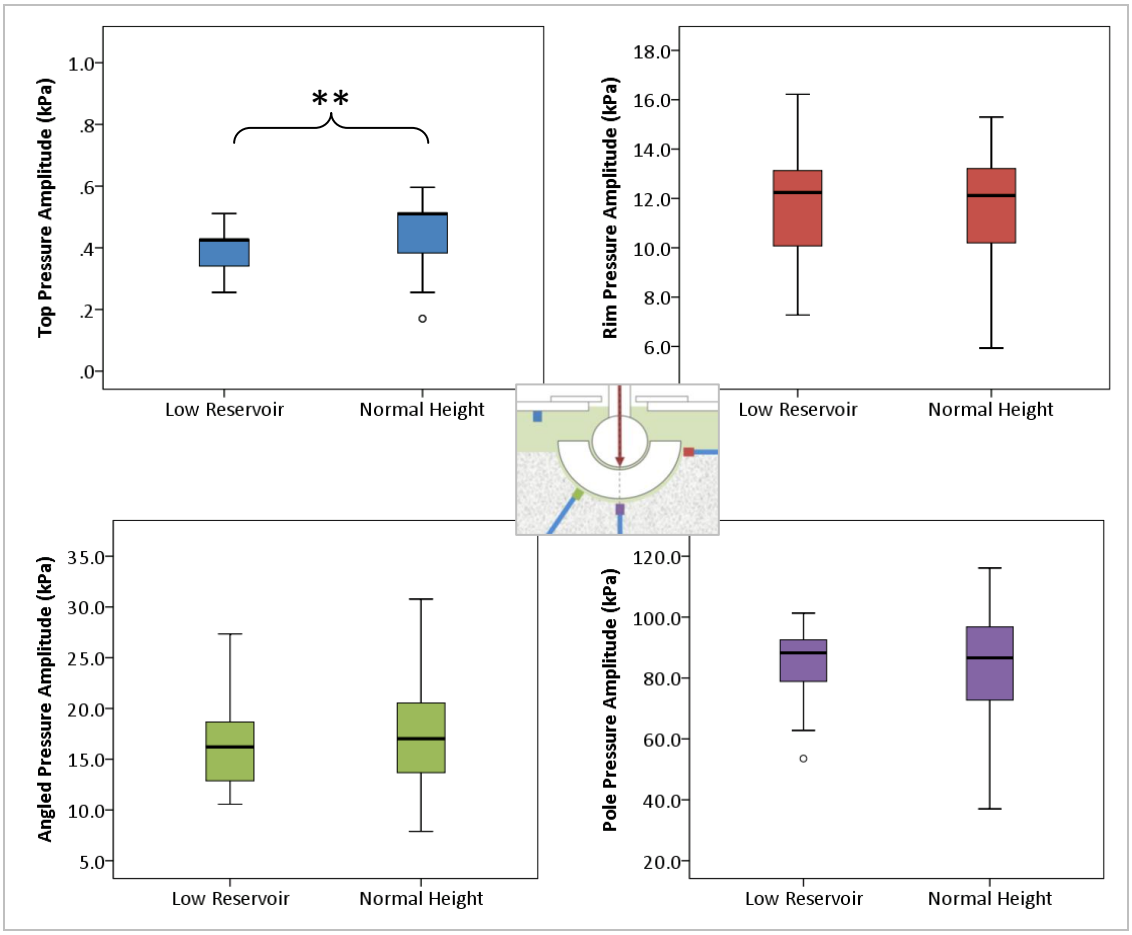

Figure 115: Graphs showing boxplots of the pressure amplitude data from tests with two different reservoir heights, comparing low-reservoir amplitudes (n = 24) with normal-height pressure amplitudes (n = 48).A statistically significant difference is indicated by stars – [**]= p ≤ 0.01.

Although the lower applied pressures caused slightly lower amplitudes on the top transducer, nonparametric tests showed that the height of the reservoir had no effect on the amplitude of the pressure waves behind the cup. This suggests that the movement of components, rather than the external pressure applied to the rig, caused changes in pressure amplitudes on the periprosthetic transducers. This will be discussed further in subsequent sections.

Effect of screw holes (no membrane)

To investigate whether the rig could detect small changes in implant design, two Trident hemispherical acetabular implants were tested, one with screw holes and one with only an apical screw hole. Mann-Whitney U tests were performed in SPSS which showed that there was a significant difference between tests with screw holes and without screw holes ($p < 0.01$ for all pressure channels) (Figure 116). The greatest difference in pressure amplitude was on the angled transducer, which was in communication with a screw hole.

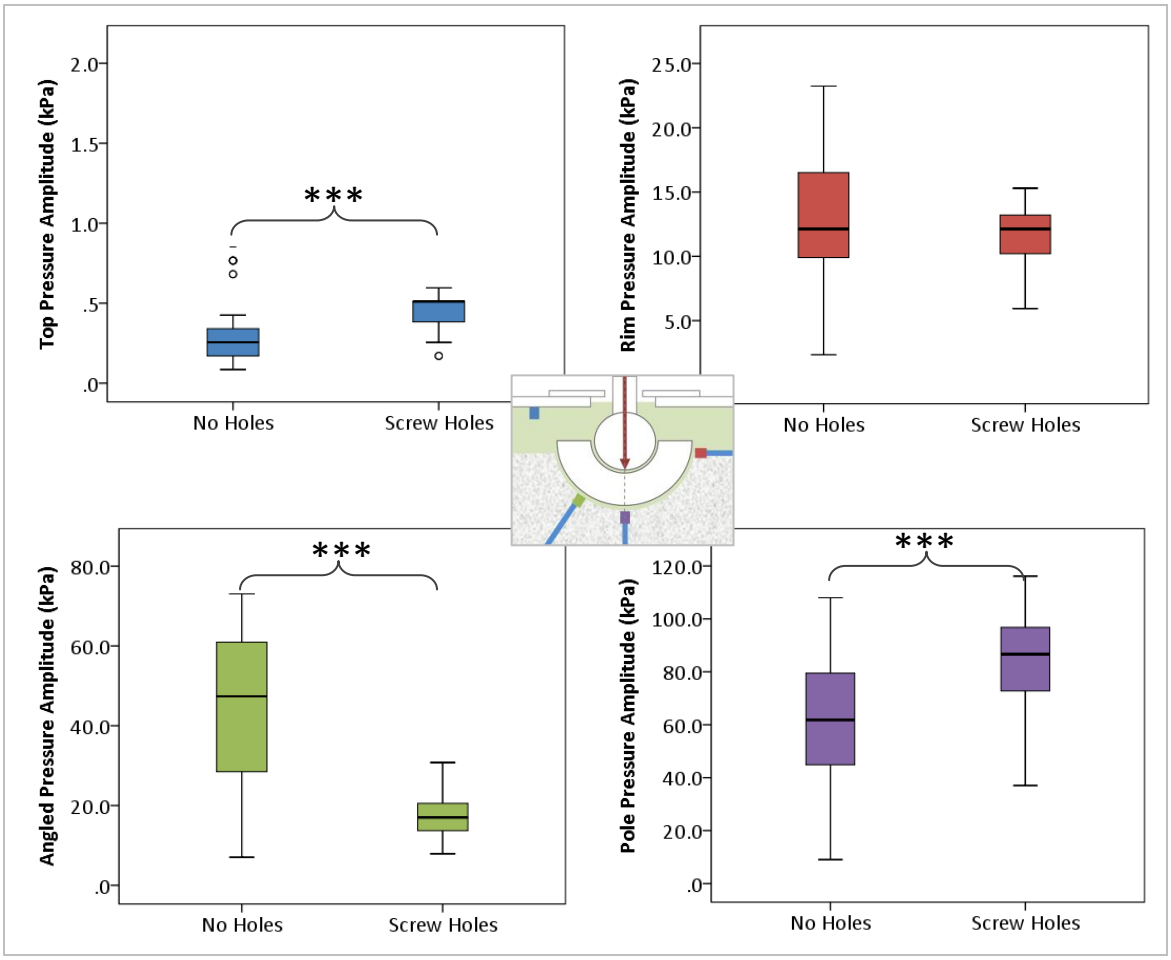

Figure 116: Boxplots showing the effect of the presence of screw holes in the shell on pressures measured. (n = 48) A statistically significant difference is indicated by stars – [***] = p ≤ 0.001.

Top pressures and pole pressures were significantly higher in the presence of screw holes; while angled pressures were significantly lower in the presence of screw holes. This implies that implant surface features have a significant effect on fluid movement between the prosthetic cup and the bone analogue and that the higher periacetabular fluid volume caused by the presence of screw hole cavities can increase pressures measured at the pole, but reduce angled pressures (in direct communication with a screw hole).

Mann-Whitney analysis showed no significant difference in load application or displacement between the two cup designs (p = 0.896 and 0.865 respectively), so the differences in pressure must come from the way fluid interacts with the components. Small differences in component features, as described in Table 12 below, would have affected the fluid-component movement and thus the pressures measured behind the cup.

Table 12: Summary of differences in component features

Feature	No Holes	Screw Holes
Cup surface	Continuous, rough HA-coated surface. 	Rough HA-coated surface, interrupted by a cluster of five screw holes, one of which (indicated with an arrow) was in direct communication with the angled transmission tube. 
Potential for air bubble entrapment	Limited; air bubbles likely to be forced out as oil is introduced into chamber	Potential for air bubbles to be trapped inside the screw hole voids in the shell of the cup during oil introduction.
Periprosthetic fluid volume	Minimal fluid behind cup	Larger periprosthetic space due to presence of screw holes; potential for a greater volume of fluid behind the cup

Behind the cup, fluid flowed between the rough surface of the prosthetic cup and the smoother surface of the test cavity. It can be assumed that fluid interactions between these surfaces would be affected by the presence of screw holes causing gaps in the rough cup surface.

It is likely that a slightly higher fluid volume behind the cup, made possible by the screw hole voids in the cup surface, would affect the fluid behaviour behind this cup compared with a cup without holes. Conversely, it is possible that air bubbles may have been trapped in the screw holes cavities, causing localised pressures to be lower at that point, as the compressible air absorbed the increase in fluid pressure.

Studying Figure 117, it is possible to speculate about which of these effects may be at work when testing in the APTR rig. The lower pressure amplitudes on the angled transducer when the cluster back cup was tested suggests the presence of an air bubble in the communicating screw hole. The higher pressures on the top and pole transducer however, could be due to a higher fluid volume behind the cup causing greater pressure fluctuations within the rig.

The APTR rig was able to measure differences in fluid pressures behind different cup components. However, to draw conclusions about the mechanisms by which these surface features affected the flow of fluid, these should be assessed by other methods such as computational fluid dynamics.

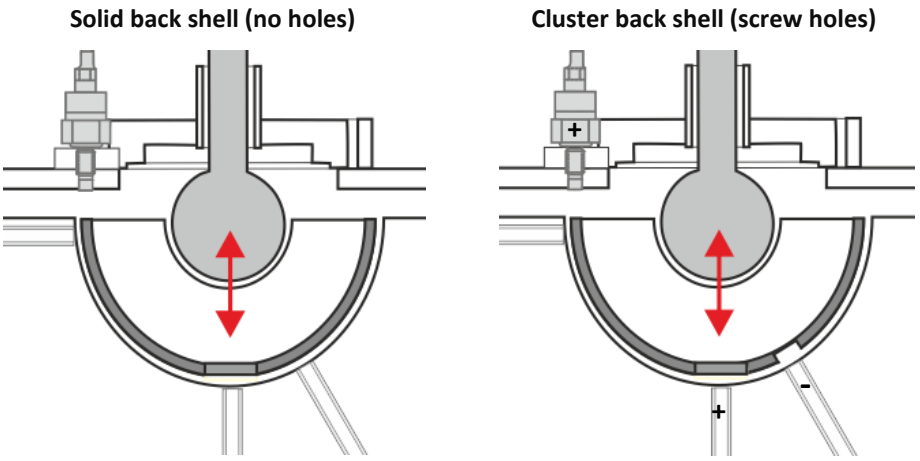

Figure 117: Schematic showing the effect of screw holes on pressures. The top and pole pressures were higher when the cluster back (screw holes) cup was used, while the angled pressures were lower in the presence of a screw hole. No difference was observed on the rim transducer.

Effect of presence of membrane

To investigate the effect of a 10mm fibrous rim on the pressures measured in the APTR, pressures with and without the membrane were compared. Combined results from both cups were analysed in SPSS and displayed in the bar graphs in Figure 118. Mann-Whitney analysis showed that there was a significant difference in pressure results between membrane and non-membrane tests.

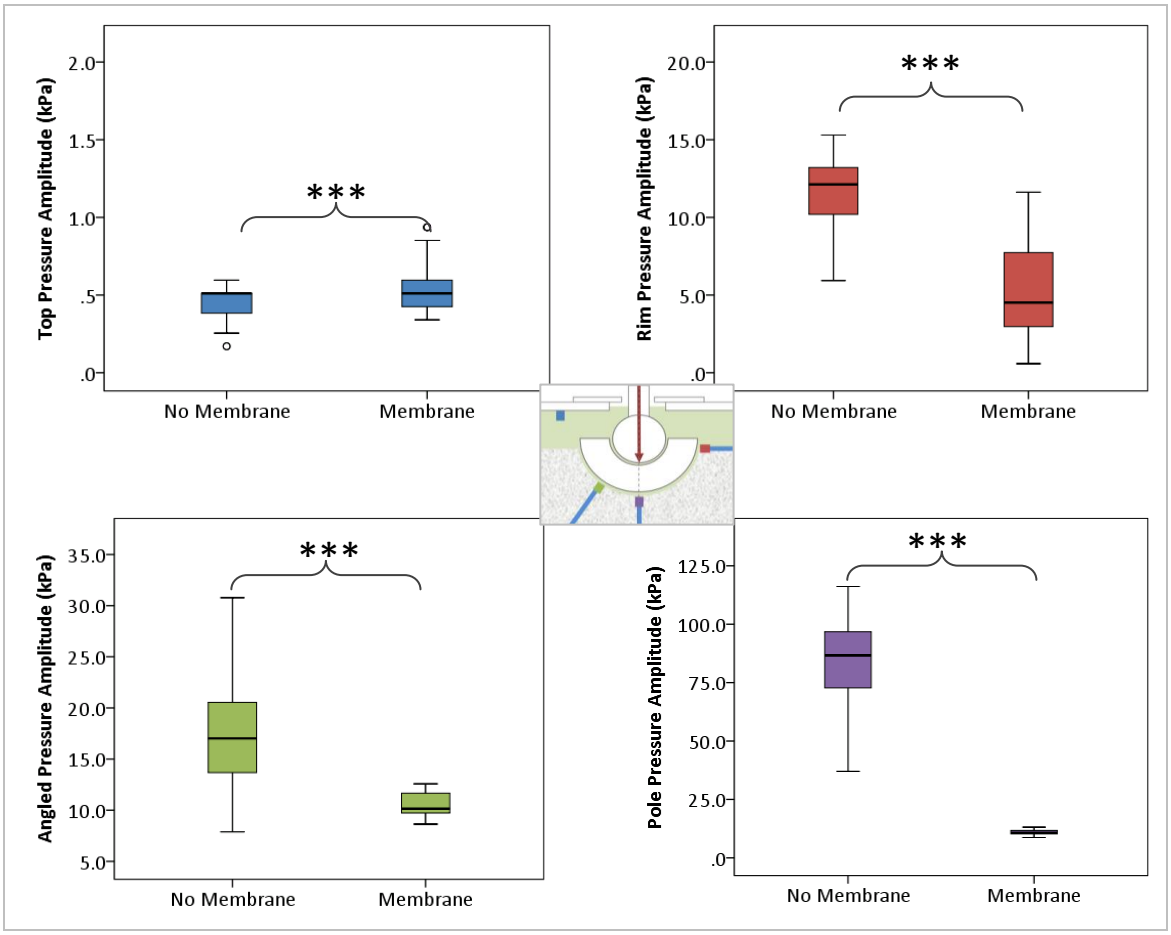

Figure 118: Boxplots showing the effect of a membrane on pressure results (n = 48). A statistically significant difference is indicated by stars - [***] = p ≤ 0.001.

A significant difference in measured pressures was observed on all transducers. As in the previous chapter, the membrane caused significantly higher pressures on the top transducer, and significantly lower pressures on the angled and pole transducers. In tests with a membrane, the median value of the rim transducer was significantly lower than the median without a membrane. This is the opposite trend to that observed on the rim transducer in the previous chapter, a finding that can be explained by the angle of loading. It is likely that with 30° loading, one side of the membrane is being compressed under load (Figure 119, b), while the other side (a, in contact with the rim transmission tube) remains uncompressed. When load is removed the cup may move up, leading to a greater cup movement perpendicular to the rim transducer. This would cause higher pressures than under axial load, where the membrane is believed to restrict fluid movement as well as the movement of the cup.

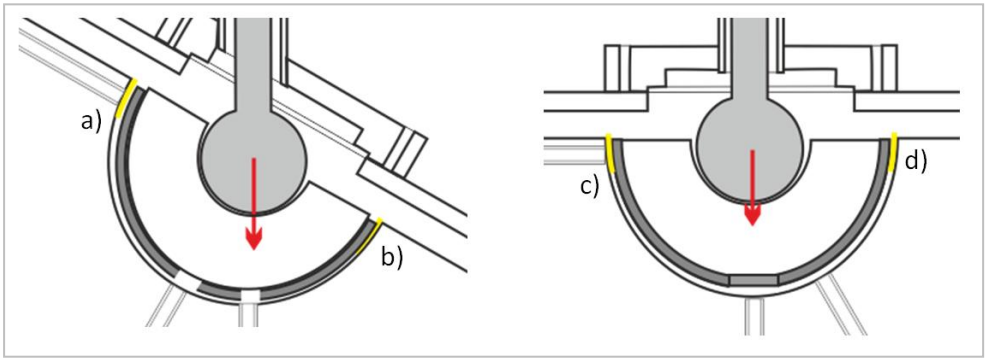

Figure 119: Image showing the hypothesised reason for lower rim pressures in axial testing, with a) uncompressed side of rim (in contact with rim transmission tube) under 30° load; b) compressed rim under 30° load; c) and d) even compression of fibrous rim under axial load.

From the data in Figure 118 it appears that the membrane causes the pressure values to be less variable on the angled and pole transducers, but slightly more variable on the rim. To determine whether variability was affected by the presence of a membrane, the median and IQR values were assessed, as shown in Table 13.

Table 13: Comparison of data variability between tests with and without a membrane

Test conditions	Median (kPa)	IQR (kPa)	IQR as % of median
Rim transducer, no membrane	12.12	3.50	**28.88 %**
Rim transducer, with fibrous rim	4.51	6.18	**137.03 %**
Pole transducer, no membrane	86.66	24.48	**28.25 %**
Pole transducer, with fibrous rim	10.76	1.52	**14.12 %**

The rim transducer is more variable in the presence of the membrane, likely due to slight variations in the placement of the membrane. The variation on the pole transducer was lower in tests with a fibrous rim, possibly indicating improved stability of the implant. This improved stability is also indicated by the fact that median displacement values were lower with a membrane. Without a membrane, higher displacements were measured and higher pressures were recorded (as shown in Figure 120).

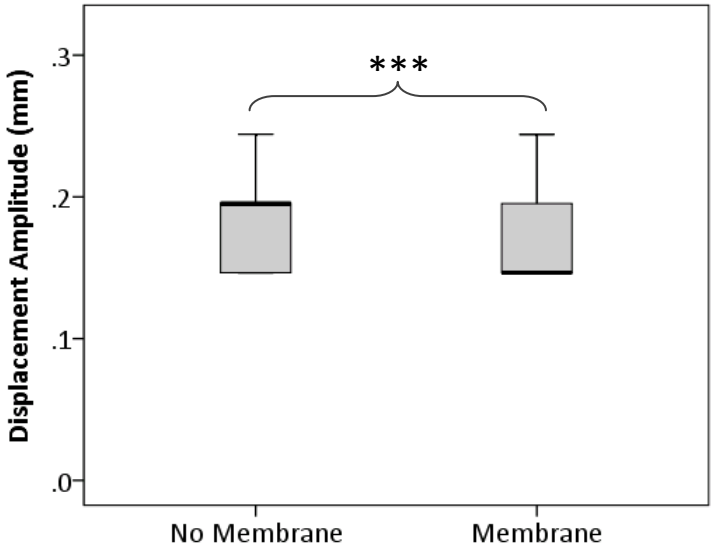

Figure 120: Effect of a membrane on displacement values (values for all normal-height tests, n=141). A statistically significant difference is indicated by stars – [***] = p ≤ 0.001.

Higher displacement has been implicated in higher pressures (Chapter 4). However, to determine whether it was this displacement, or a property of the membrane itself, which was causing this pressure difference, load-displacement-adjusted values were created to negate the effect of slight differences in displacement (Figure 121). These were calculated by dividing pressure values by a Load Factor (LF), where:

$$LF = \frac{Pressure}{100 \times Load \times Displacement}$$

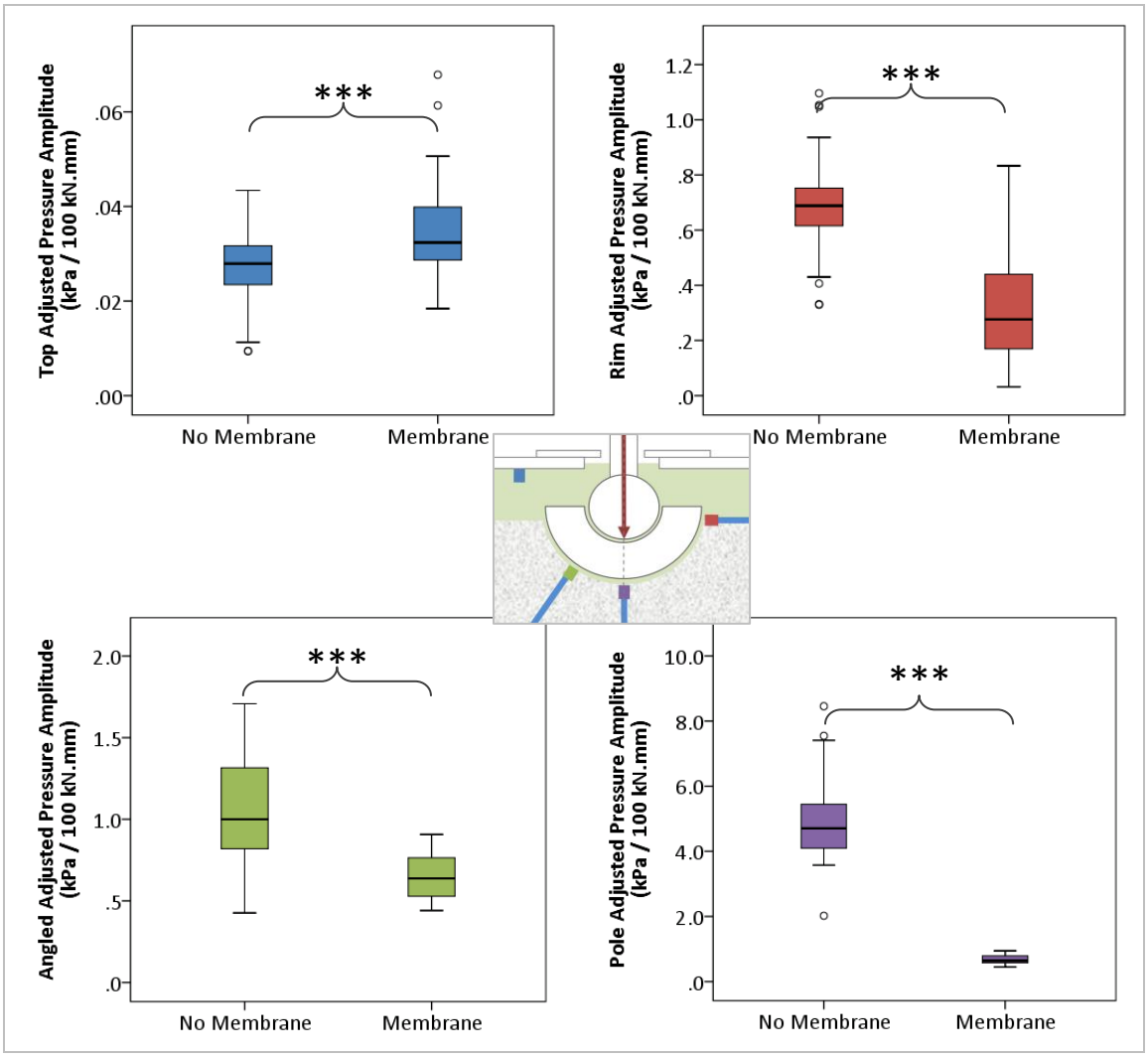

Figure 121: Bar graphs showing the effect of a membrane on load-displacement-adjusted pressures (n = 48). A statistically significant difference is indicated by stars – [***] = p ≤ 0.001.

These LF-adjusted boxplots show that even when displacement values are normalised, the same trends are observed and adjusted pressures are significantly different in the presence of a membrane. This implies that it is not only the displacement having an effect on pressures, but a property of the presence of the fibrous rim itself. The reduction in pressure amplitudes behind the prosthetic cup could be due to the fact that the cavity into which the cup was implanted was not enlarged in the membrane tests, meaning there was a tighter fit between the cup and the cavity in the presence of the fibrous rim. The membrane, wedged between the acetabular cup and the test cavity, may have acted as a barrier to fluid movement behind the prosthetic cup. This wedging-in of the cup also prevented the cup from moving down into the cavity to the same degree as when loaded without a membrane, leaving greater clearance between the component and the transmission tube, thus causing lower pressures to be recorded in the transmission channel.

To determine whether the membrane affected the flow of oil into the periacetabular space of the APTR chamber, the base pressures with and without the membrane were investigated, using Mann-Whitney analysis in SPSS. If the membrane restricted the oil from flowing behind the cup then it is likely that base pressures behind the cup will be lower in the presence of a membrane. The results of this investigation are shown in Figure 122.

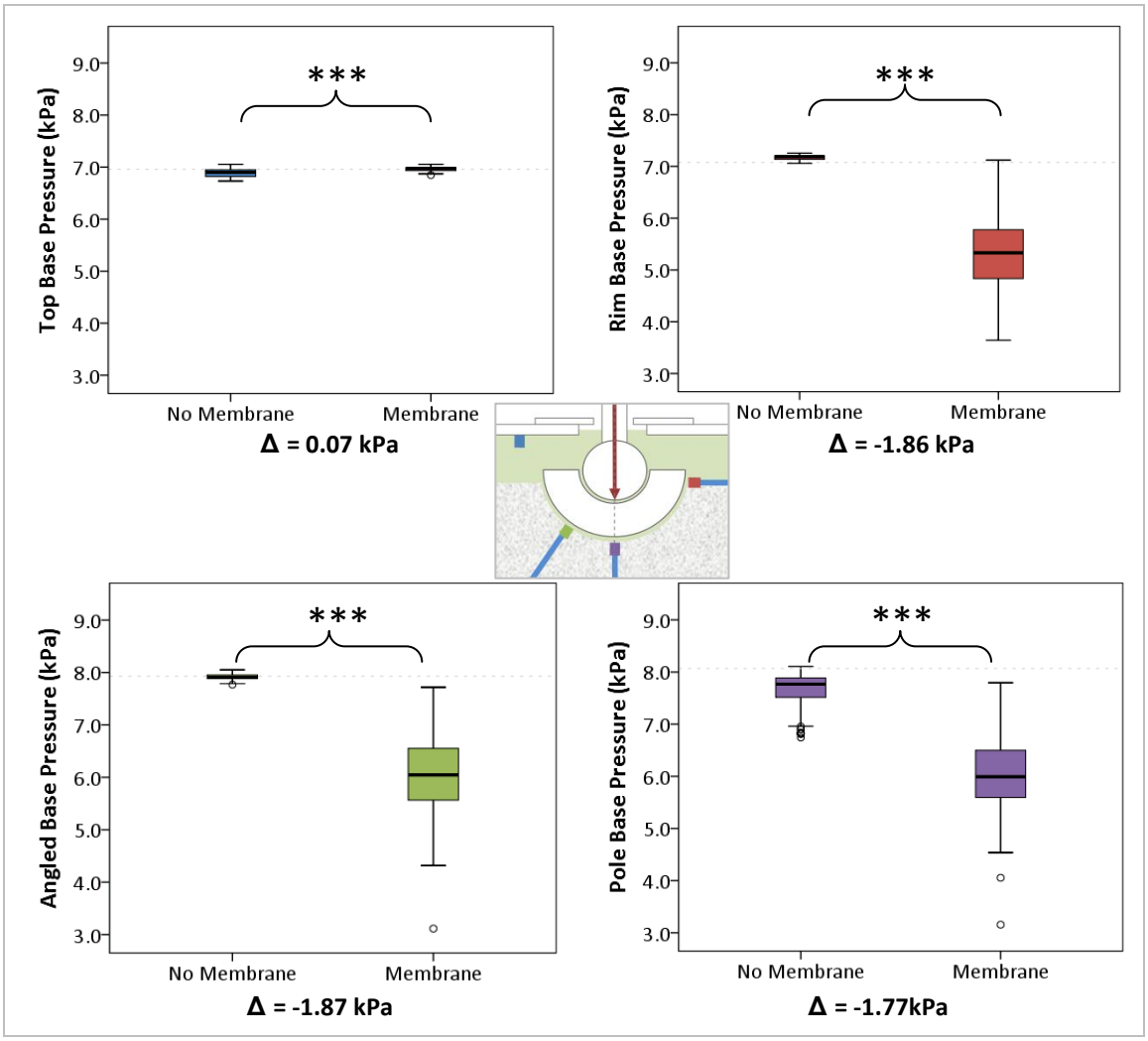

Figure 122: Comparison of base pressures with and without fibrous membrane (n = 280) . Mann-Whitney analysis showed a statistically significant difference, indicated by [***] = p ≤ 0.001, and difference in medians is also displayed (negative value means 'membrane' median was lower than the 'no membrane' value.

In the presence of the membrane, base pressure values were lower on the rim, angled and pole transducers. This indicates that during oil introduction, a lower amount of fluid may have flowed behind the prosthetic cup. This is consistent with observations made during oil introduction (described in section 5.2). These tests were performed to investigate the use of a

fibrous rim in simulating cup fixation, and the effects of the membrane on fluid pressure movement. The hypothesis that the membrane restricted fluid flow behind the cup will be further discussed in the phase testing section.

Observations on wear of the test hemisphere

Bottoming-out (shown in Figure 123) is possibly causing higher pole pressures, as the flat bottom of the cup closes off the area over the pole aperture, preventing fluid release that would reduce pressures.

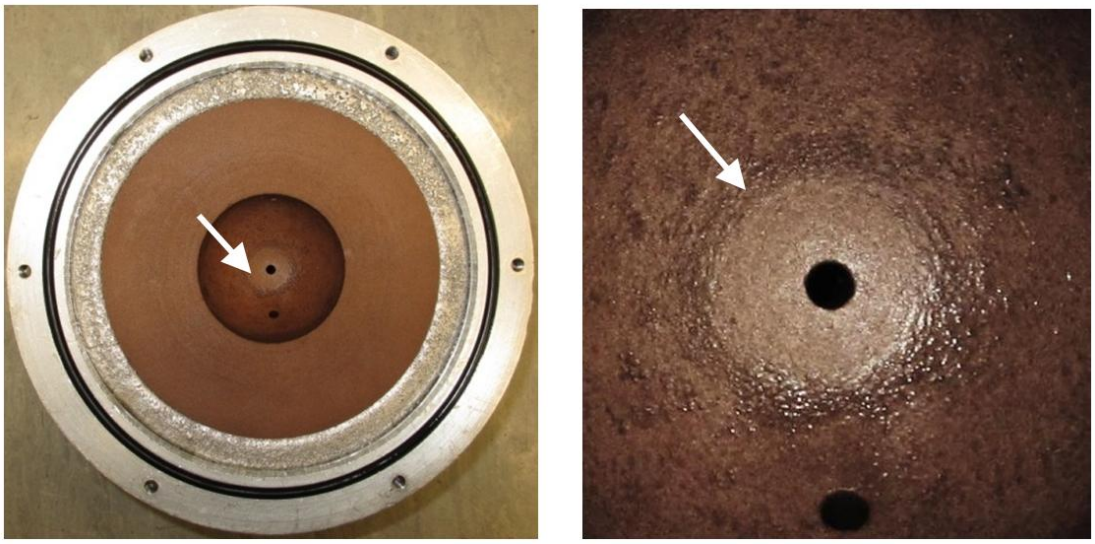

Figure 123: Photographs of test hemisphere after Chapter 5 test series. A clear wear line (indicated by arrows) on the test hemisphere indicates where cups have been bottoming-out.

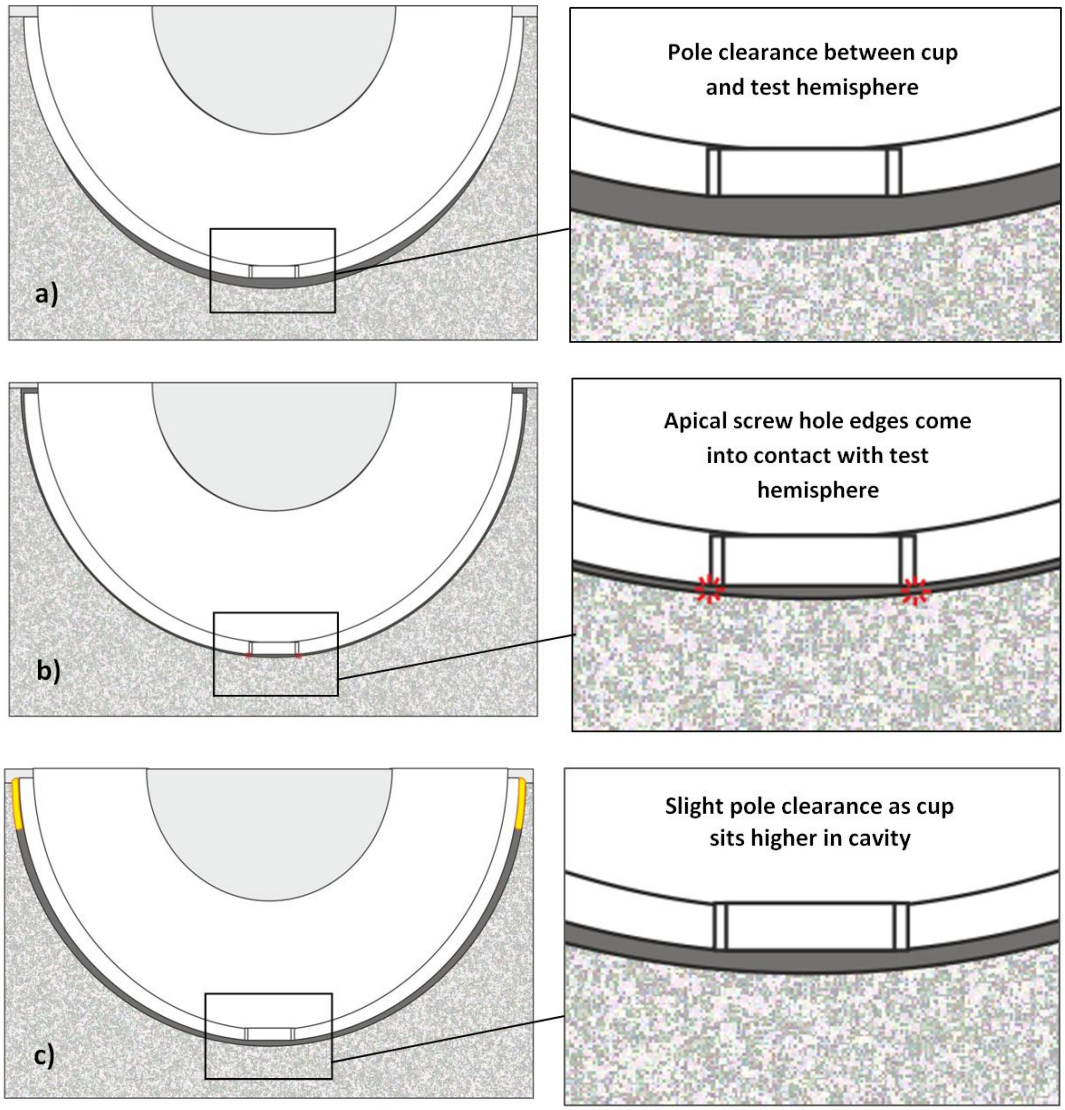

Figure 124: Schematic illustrating the cup clearance under different conditions, with a) good press-fit fixation, b) insufficient press-fit fixation within the APTR chamber, causing bottoming-out of the cup, and c) position of cup with membrane, showing clearance between cup and test hemisphere.

This bottoming-out is likely to be caused by insufficient press-fit fixation of the component. As previously described (Figure 15), cups relying on press-fit fixation require a cavity that is under-sized. As the Trident shell was the same size as the test hemisphere cavity, this press-fit fixation was compromised, leading to this bottoming-out effect as the cup slipped down to make contact with the pole of the cavity (shown in Figure 124). It is likely that in tests with a fibrous rim, the wedging-in of the implant with the membrane is causing a similar effect to that shown with a well-fixed cup – clearance between the cup and the test hemisphere – as the cup sits slightly higher in the cavity.

Maximum pressures

To investigate under which conditions the maximum pressures were generated, and which transducer these are measured on, the maximum and minimum pressures of the first cycle and the steady-state period were collected for different test conditions, and these were displayed in boxplots using SPSS.

To determine which pressure values were significant in terms of osteolysis, a horizontal line was placed at 35 kPa on each plot, to allow observation of which condition(s) produced potentially damaging pressures. In the previous chapter, results showed that first-cycle tests produced the highest pressures, and maximum pressures were measured under a relocation-from-microseparation condition. Analysis of the results from the current test series show a similar slight pressure spike in the first-cycle tests (Figure 109), so first-cycle pressures, as well as steady-state pressures, were included in maximum pressure analysis. These results are shown in Figure 125, with pressures capable of inducing osteolysis marked with a star symbol (*) to indicate that the median was greater than 35kPa.

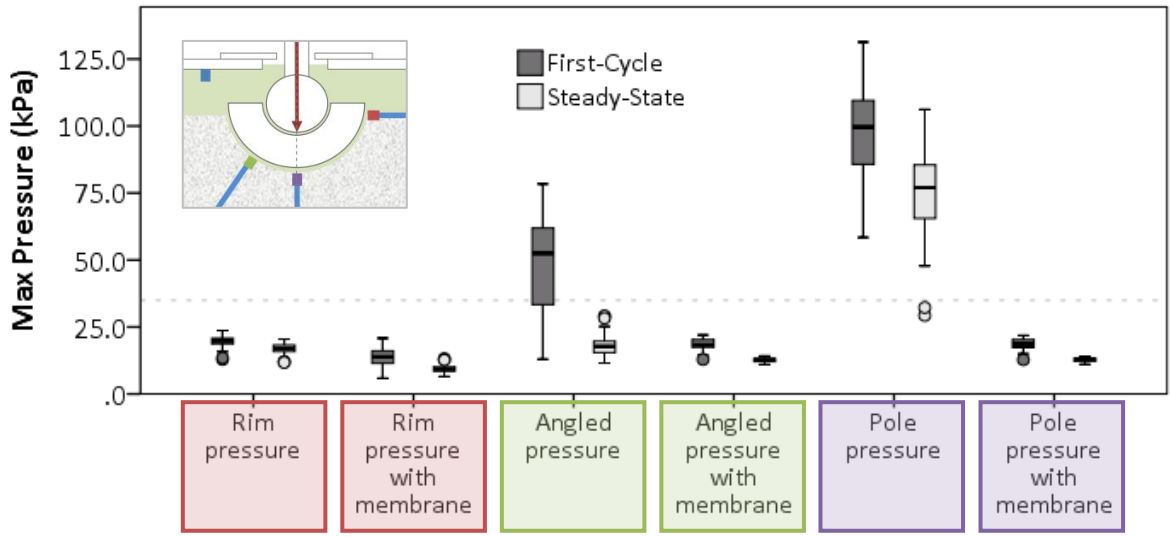

Figure 125: Boxplot showing maximum pressure data from rim, angled and pole transducers. Darker shading indicates first-cycle pressure; lighter shading indicates steady-state pressure. A dotted line indicates the 35kPa pressure level.

No maximum pressures reached 35kPa in the bulk fluid in the chamber, measured by the top transducer, or at the rim of the cup. However, clinically significant maximum pressures were consistently measured on the pole transducer. The highest pressure value measured during testing was 131.3kPa, on the pole transducer on the first cycle of loading. The median values in tests without a membrane was higher than 35kPa (Figure 125), in the first cycle (99.65kPa)

and the steady-state period (77.00kPa). The median of first-cycle pressures on the angled transducer (52.53kPa) was also higher than 35kPa, in the absence of a fibrous rim.

This section shows that pressures capable of inducing osteolysis were measured behind the cup and that the presence of a fibrous rim generally reduced pressures to below this threshold. However it is difficult to draw conclusions about the effects of these test conditions as the component movements and fluid flow inside the chamber cannot be visualised. In order to obtain more information about these movements, phase analysis was conducted.

Phase analysis

To further investigate the pressure distribution inside the rig, the phase characteristics of the pressure signals were explored, as described in the methods paragraph in Section 5.2. It was hoped that this would provide a clearer picture of what was happening inside the rig, with respect to head-cup movement and its effect on pressure. The time points at which the maximum and minimum pressures were measured in the steady-state load cycle were recorded and assessed. The positions of these time points in the load cycle, relative to the point at which the maximum load was applied, were assessed, and the results of this analysis are shown in Figure 126. The compressive load and the corresponding displacements were recorded as negative values, so for the purposes of visual comparison these values were inverted in the graphs, so the minimum load (the point at which the load was most negative, the highest amount of compressive load) was displayed as LoadInvMax.

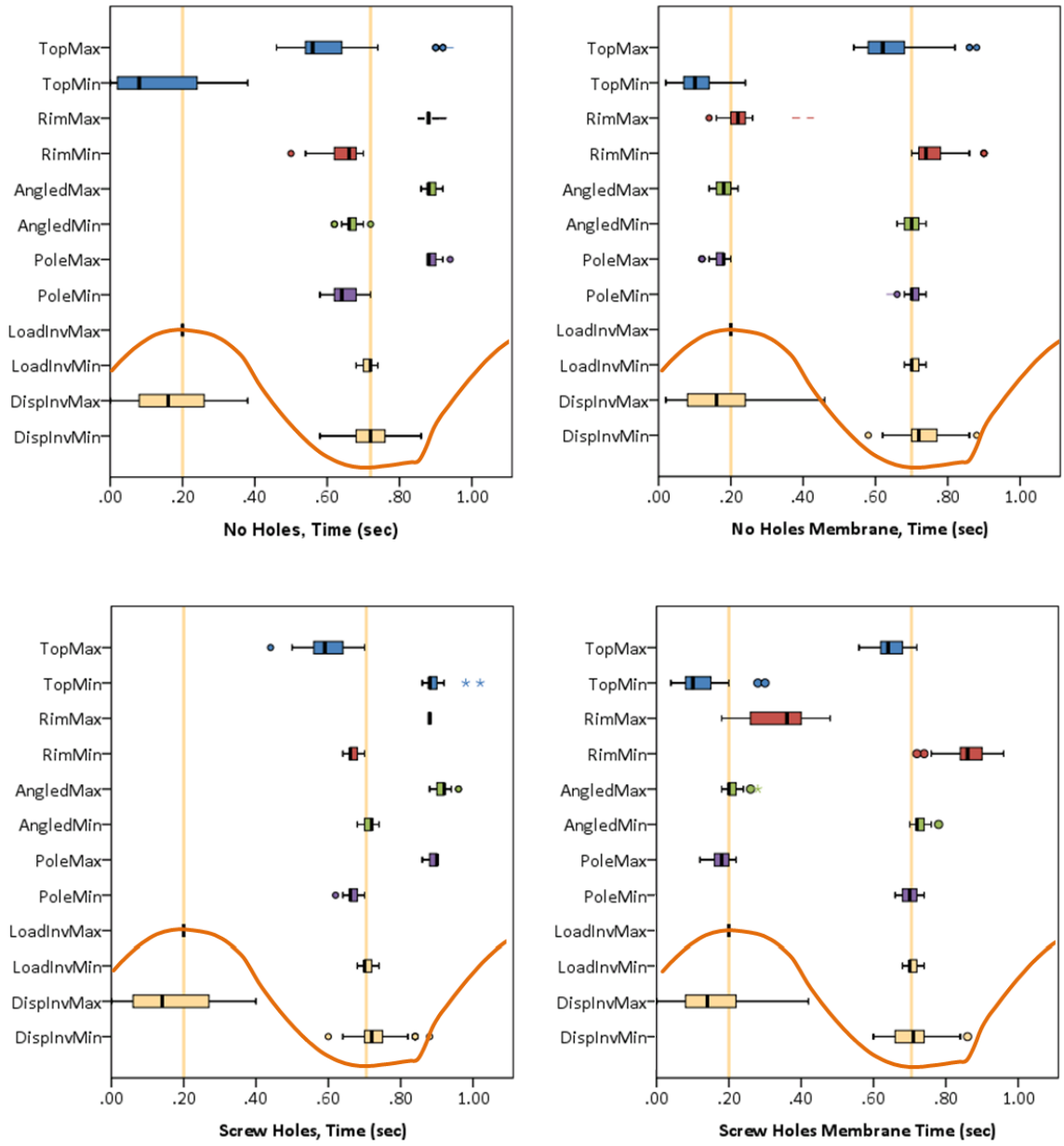

Figure 126: Boxplots showing phase characteristics of the APTR model under different conditions, showing data with and without the fibrous membrane. N=48 for each boxplot

The vertical orange lines represent the points in the load cycle at which the load magnitude is at a maximum (0.2 seconds) and minimum (0.7 seconds). A sample load cycle is superimposed over the graph to illustrate this more clearly.

Several observations can be made from this figure. Under all test conditions, the top transducer signal is out of phase with the channels behind the cup, as was also observed in the Chapter 4 testing. Slightly before the maximum pressures are being recorded behind the cup (on the rim, angled and pole transducers), the pressures in the load chamber (measured by the

top transducer) are at a minimum. This can be attributed to the movement of components during loading – as the loading head (and cup) move up, the volume in the chamber decreases, leading to a peak in chamber pressure and an decrease in pressure behind the cup. Minimum pressures on the top transducer occur when the head is at its lowest point, at the point of maximum load, when the free fluid volume within the chamber was highest.

In the boxplots from tests without a membrane (boxplots on the left), the minimum pressures measured behind the cup (on the rim, angled and pole transducers) occur just before the minimum load and displacement values occur. The maximum pressures behind the cup occur well before the maximum load is applied, at the point at which the compressive load is increasing rapidly (shown on these plots towards the end of the time axis - the beginning of the next load cycle). This implies that the maximum pressures are occurring due to the movement of the loading head, rather than the degree of the load being applied.

The trends observed from the cup without screw holes (boxplots in the top row) were also observed in the test with screw holes (boxplots on the bottom). It was believed that this phase analysis would allow the differences in fluid interactions between the two cup designs to be assessed, however the angled transducer, in communication with the screw hole in the cluster-back cup, shows peaks in the same place as in tests with the cup without screw holes. The presence of screw holes has been shown to affect the amplitude of the pressure signal but not the phase characteristics.

The most significant finding from these boxplots is the effect of the membrane on the timing of pressure peaks behind the cup. While the maximum pressures without a membrane appear to occur at the start of the application of compressive load, in tests with a fibrous rim these maxima occur at the point at which load is a maximum. As the load is applied, and the volume of fluid is compressed, the pressure keeps rising to the point at which load begins to decrease again. The synchronisation of the peaks of pressure with the peaks of loading imply that fluid is not flowing in and out of the periprosthetic space, as in the tests without a fibrous rim. The pressures appear to be directly influenced by the volume changes due to loading and not by the movement of fluid.

These boxplots show a clear difference in the way peak pressures occur under conditions with and without a membrane. To obtain more information than just the maxima and minima, and get a greater understanding of the nature of the pressure signal over a whole load cycle, a new

phase analysis technique was developed. Steady-state pressure signals from two 1kN1Hz tests from each test set were adjusted in time so the application of maximum load occurred at the same time point (total number of signals used = 16 for each of the four different conditions tested). The pressure signals from the transducers at each time point were then averaged to create an average pressure wave shape for each of the four different conditions tested. The results for each of the transducer channels are shown in Figure 127 to Figure 130, showing the four different conditions as well as the load and displacement signals. Again, load and displacement values were inverted in the graphs. Maximum pressures were marked with vertical blue lines, and maximum load points were marked with vertical orange lines.

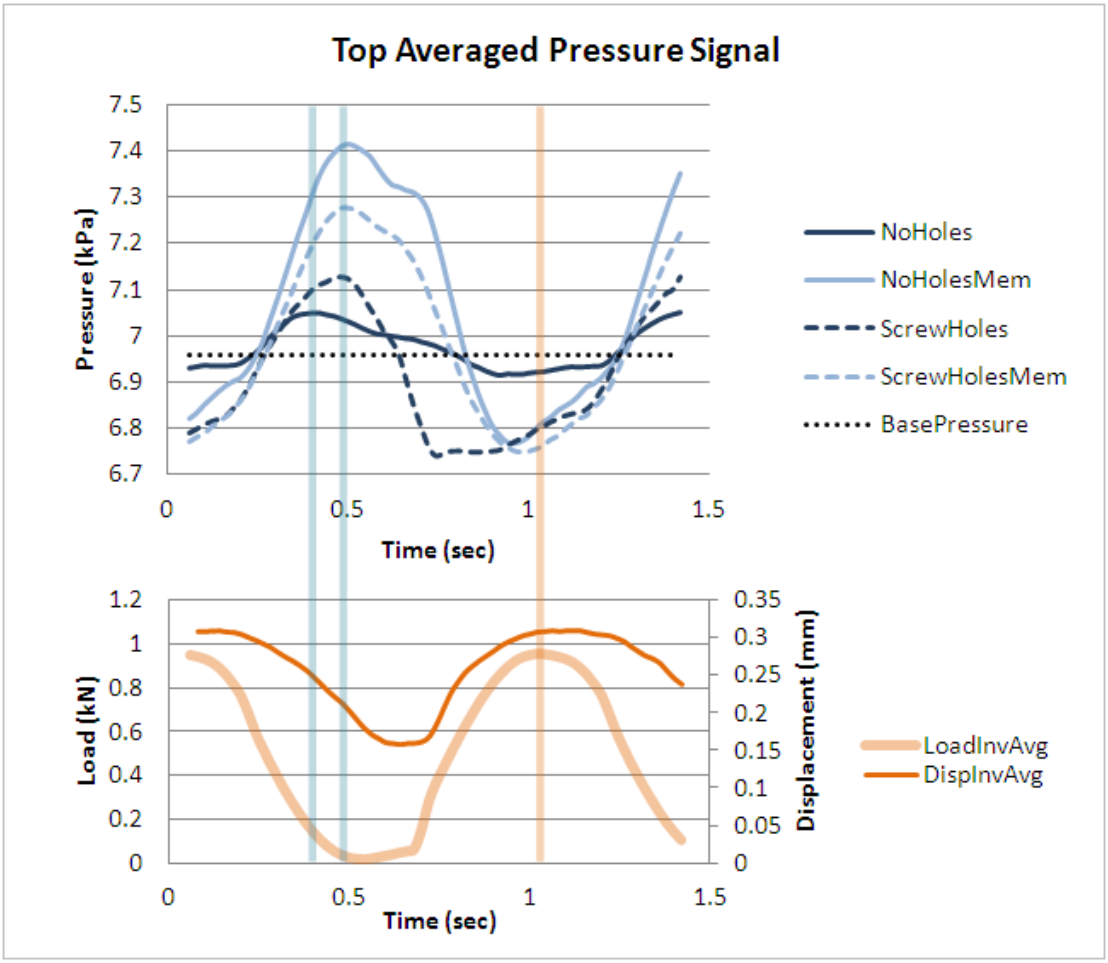

Figure 127 Analysis of pressure signal from top transducer. The top graph shows the pressure signals under different conditions. Maximum pressures without a membrane are marked with the vertical blue line; maximum load are marked with the vertical orange line. The median base pressure for this transducer is shown by the black dotted line. Load and displacement signals are shown below the pressure graph.

One of the findings from Chapter 4 was that the top pressures with a membrane were significantly higher than without a membrane. This is also observed in the current chapter (see Figure 118). The theory for why this occurred was that fluid absorbed into the fabric of the membrane when the load was at a minimum, was forced out of the material under the application of load, causing a pressure spike in chamber fluid that was measured on the top transducer. Studying the phase characteristics on the top transducer (Figure 127), pressure signals under all conditions appeared to be out of phase with the load signal by half a cycle (π radians) – pressures reached their maximum as the load and displacement values reached their minimum. It is possible that the fluctuations in top pressure signal are caused primarily by these fluctuations in chamber volume. The phase data does *not* support the theory that high pressure fluid is exuded from the membrane under load, as this would cause the higher top pressures to occur in phase with the application of load.

An alternative theory for why top pressures are higher with a membrane than without relies on the assumption that the head-cup suction effect (as described in Chapter 3) in these tests is greater than the fixation between the cup and the hemisphere. In other words, the acetabular cup moves *with* the loading head, with the two components moving together, instead of the head moving up and down relative to the cup. As the load decreases and the loading head moves up within the chamber, the cup also moves up, reducing the available free fluid space in the chamber. Without the membrane, the fluid in this space would be free to flow behind the cup to equalise the chamber pressure. In the presence of a membrane this movement would be constricted and a higher pressure would be recorded on the top transducers.

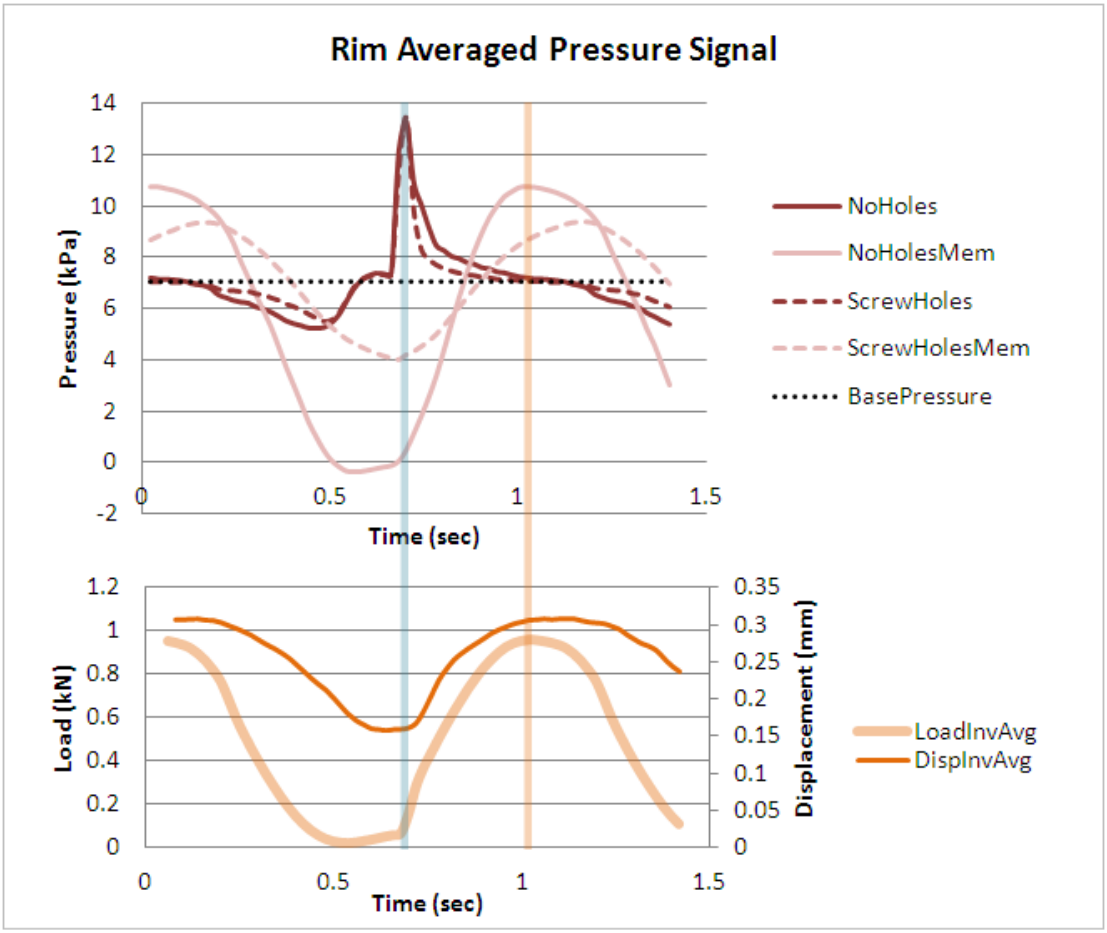

Figure 128: Analysis of pressure signal from rim transducer. The top graph shows the pressure signals under different conditions. Maximum pressures without a membrane are marked with the vertical blue line; maximum load are marked with the vertical orange line. The median base pressure for this transducer is shown by the black dotted line. Load and displacement signals are shown below the pressure graph.

On the rim transducer, in tests with a membrane (shown with lighter red lines in Figure 128), the peak pressures occurred at the same point as the peak load, slightly later in the implant with screw holes. In tests without a membrane (darker red lines) the peak pressures occurred *before* the maximum load was applied, at the point at which the gradients of the load and displacement signals were highest.

The same trend was also observed on the pole transducer (Figure 130). The signals on the Angled transducer (Figure 129) followed a slightly different pattern – the peak pressure measured in the Trident cup with screw holes (shown by the darker dotted line) occurred slightly later than the peak pressure with no holes, and the peak pressure is much lower (13.95 kPa compared with 27.17 kPa without screw holes).

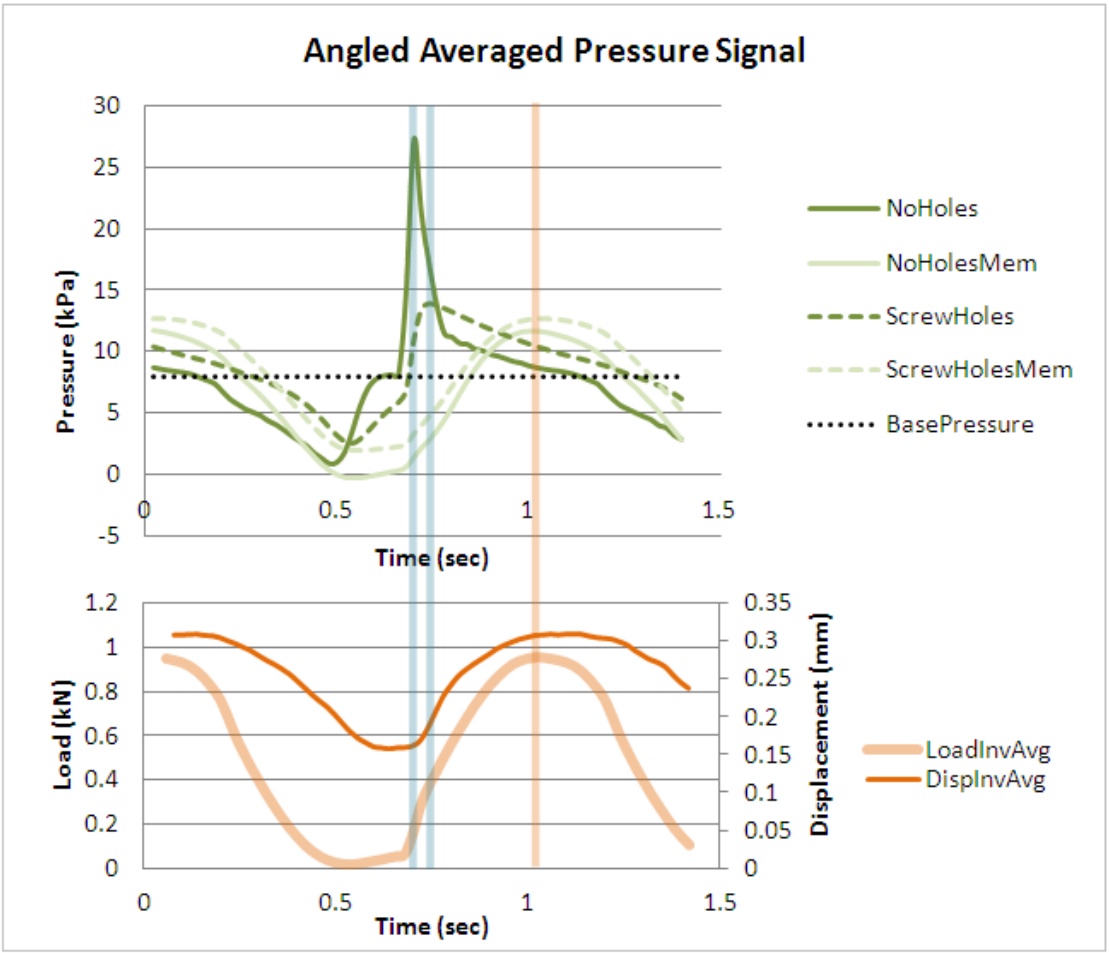

Figure 129: Analysis of pressure signal from angled transducer. The top graph shows the pressure signals under different conditions. Maximum pressures without a membrane are marked with the vertical blue line; maximum load are marked with the vertical orange line. The median base pressure for this transducer is shown by the black dotted line. Load and displacement signals are shown below the pressure graph.

The peak of the pressure signal corresponds to the point at which fluid flow can be assumed to be the highest – the load is still being applied, causing the free volume in communication with the transmission tube to continue to fall, but the pressure is reducing as the fluid is forced out of that space. The gradient of the pressure drop can be related to the fluid movement – a higher gradient means a faster drop in pressure, which can be attributed to faster fluid movement out of the periprosthetic space.

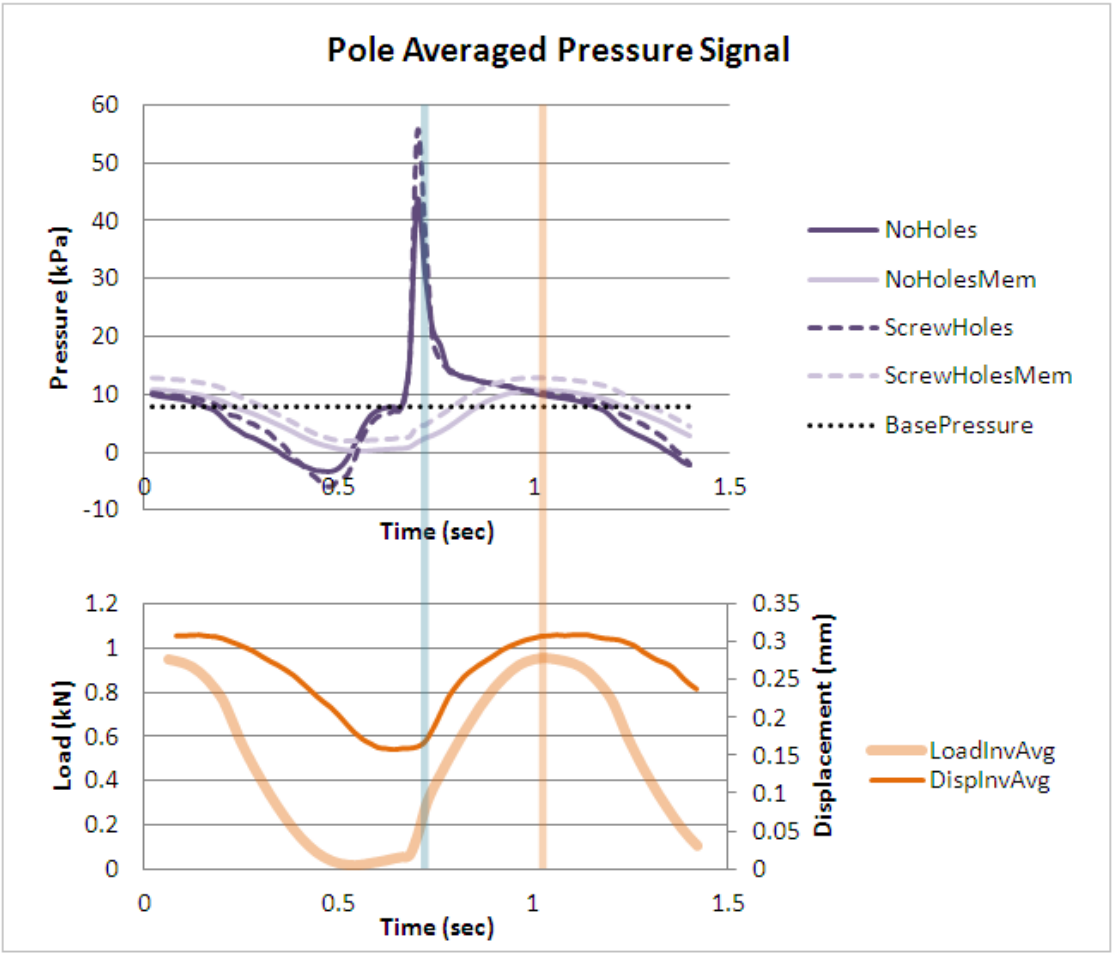

Figure 130: Analysis of pressure signal from pole transducer. The top graph shows the pressure signals under different conditions. Maximum pressures without a membrane are marked with the vertical blue line; maximum load are marked with the vertical orange line. The median base pressure for this transducer is shown by the black dotted line. Load and displacement signals are shown below the pressure graph.

The phase results from the pole transducer add weight to the theory that the fibrous rim causes restriction of fluid movement behind the acetabular cup. Without a membrane, the minimum pole pressure occurs just before the minimum load, which suggests that there is an initial drop in fluid pressure when the volume behind the cup increases as the loading head is lifted. This minimum is followed by a recovery of pressure, which was inferred to be fluid from the chamber moving behind the cup to equalise the pressure. As pressure reaches the base pressure level, the applied load reaches the point in the cycle where load begins to rapidly increase.

Without a membrane, this is where a sharp pressure spike occurs – at the point at which the gradients of the load and displacement lines are highest – when there is the most rapid head

movement and the steepest load increase. It can be inferred that this sharp increase in pressure is followed by a rapid movement of fluid from behind the cup into the APTR chamber, causing the pressure to rapidly drop again. When the loading head begins to descend sharply, the instantaneous pressure increases rapidly, causing a pressure spike as the extra fluid behind the cup is compressed by the loading movement. This spike rapidly reduces as the fluid behind the cup flows back into the chamber.

This effect is seen on the angled transducer but not to the same extent – angled pressure amplitudes are significantly lower in the presence of screw holes (Figure 116) and so the pressure spike was not as high. Without a membrane, the tests with and without screw holes followed a similar trend but there appeared to be a lag in the test with screw holes. A screw hole in the shell of the cup was in communication with the angled transmission tube. It is possible that an air bubble was trapped in this screw hole, which would act as a 'pressure damper'. Air is compressible and a small pocket of deformable air would reduce the pressure fluctuation measured at the transducers, by 'absorbing' the extremes of pressure at that point. This may also explain why there is a lag in the data - the air bubble would have compressed first, before any changes to the fluid due to movement would have occurred. As the transmission tube. The presence of the screw hole caused there to be larger volume of fluid in contact with the angled transmission tube. Under cyclic loading, this larger fluid volume caused the relative fluid volume change due to loading to be lower, and so the same degree of cup movement or deformation may have caused lower pressure amplitudes.

In the presence of a membrane, the highest pressures behind the cup occur at the same point in time as the highest loads, with the opposite trend observed in the top transducer (measuring chamber pressure). This suggests a straightforward relationship between loading head movement and pressure – when the loading head moved down to apply load, chamber volume increased and pressure decreased, while periprosthetic volume decreased and so the pressure increased. The two modes of fluid movement and pressure are illustrated in Figure 131 and Figure 132.

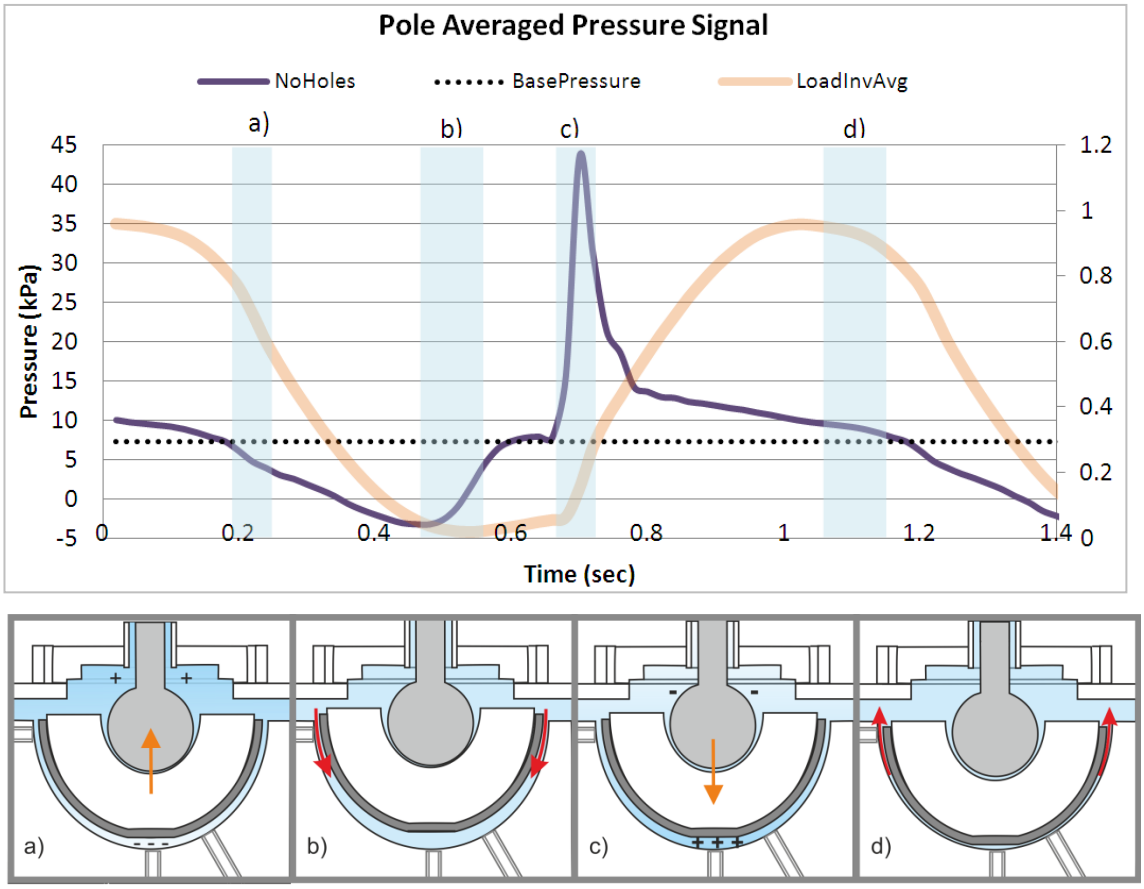

Figure 131: Schematic showing the pole pressure data, and the hypothesised corresponding fluid movement characteristics in tests without the fibrous rim. Orange arrows show the movement of the head and cup; red arrows show the fluid movement.

Without a membrane, the head and cup move up as load is lifted off (Figure 131a), and there is a drop in pressure behind the cup, and an instantaneous increase in chamber fluid pressure, as the upward movement of the cup decreases the volume in the chamber and increases periacetabular volume. Before the head begins moving down again to apply compressive load (b), fluid is able to flow behind the cup to equalise the pressures in the chamber (this can be seen by the pressure value increasing rapidly towards the base pressure). At point c) the pressure on the pole transducer has equalised with the base pressure, which means the space behind the cup is filled with fluid. When the head and cup move down into cavity, this increased periacetabular fluid causes a pressures spike, as the volume decreases before the fluid has time to escape from the space behind the cup.

The fluid then flows out as the loading head continues moving down, causing the pressure to rapidly diminish. At the bottom of the loading stroke (d), fluid is able to flow out from the periacetabular space, to bring pressures back to the base pressure level.

The bottoming-out effect, previously described in this chapter, was thought to be the cause of higher pressures on the pole transducer, as the flattened dome of the cup came into contact with the test cavity, restricting fluid outflow from the pole transmission tube and causing higher pressures. The results of phase testing contradict this theory, as the peak of pressure occurs at the start of the application of load, before the cup reaches its maximum displacement (the point at which the cup would 'bottom-out'). It is likely that the flat apical surface affects the fluid movement behind the cup, however it is not possible to further analyse its effect with the current APTR model.

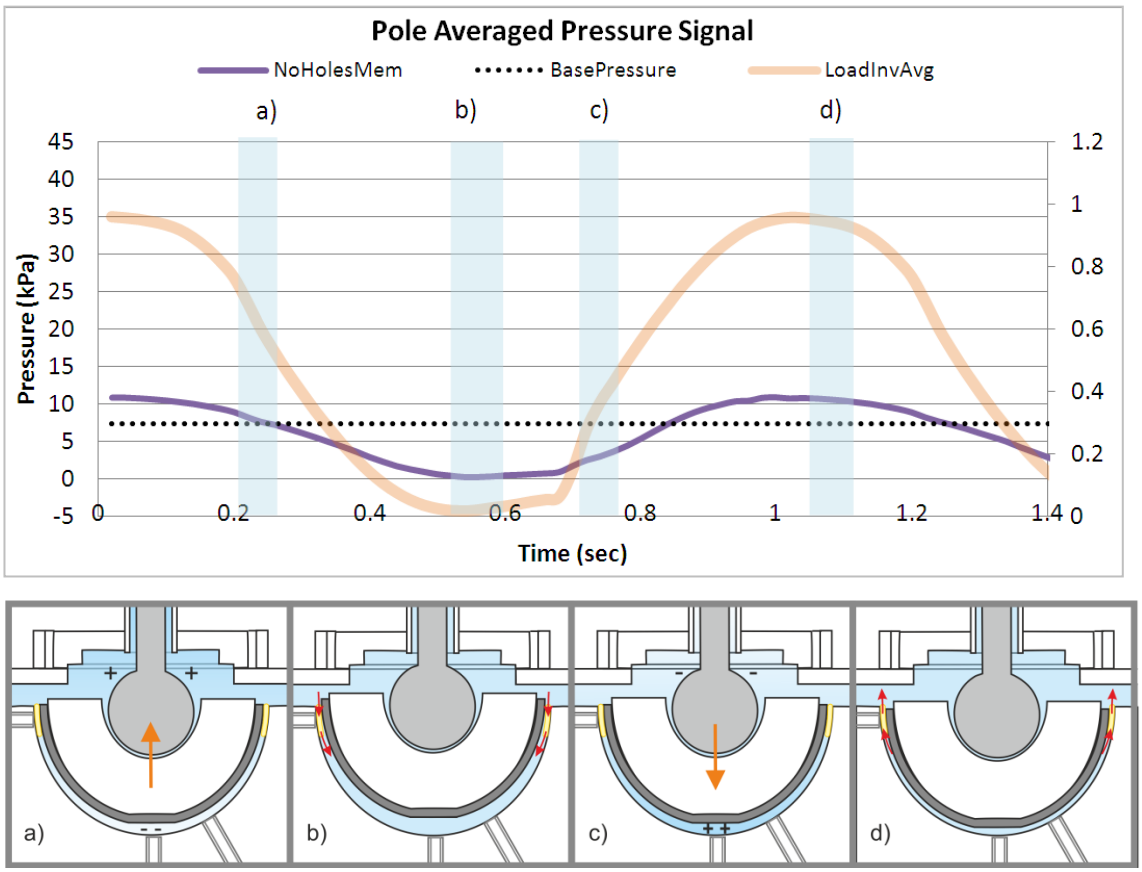

Figure 132: Schematic showing the pole pressure data, and the hypothesised corresponding fluid movement characteristics in tests with the fibrous rim (shown as a yellow area in the image).

With a membrane, the head and cup move up as load is lifted off (Figure 132 a), causing pressures behind the cup to decrease slightly below base pressures, as the volume increases with the lifting of the components. The top of the loading head displacement cycle is shown in b). Unlike the tests without a membrane, only a small amount of fluid can get through the membrane to equalise the pressure. There is not a large increase in pressure back to the base pressure; this occurs gradually and in proportion to the movement of the head and cup. The

head and cup then move down into cavity (c), causing an increase in pressures to above the base pressure level. Because the amount of periacetabular fluid did not increase significantly, and due to the higher clearance between cup and cavity, the pressure peak is not as extreme as in tests without a membrane. The bottom of the loading head displacement cycle is shown in d). Again, only a little fluid can escape through the membrane, but the amount of fluid required to bring the pressures down to the base pressure level is much lower, as there was not as much periacetabular fluid to begin with. The smoothness of the pressure data in Figure 131, compared to Figure 132, indicates the lack of fluid movement behind the cup.

This testing produced more information about what is occurring within the rig chamber during testing under different conditions. The cup movements described in this phase analysis rely on the assumption that the cup fixation force was lower than the head-cup adhesion force, an assumption derived from observations of the head-cup suction effect when dismantling the APTR after testing. The data showed again that the presence of screw holes affects the localised pressure at these points, and also provided a potential explanation for the mechanism by which the fibrous rim affects rig pressures.

5.4 Discussion and conclusions

The aims of this chapter were to measure and analyse how changes to cup design and fixation affected the pressures measured by the APTR. These aims were achieved, with the presence of a fibrous membrane causing reduced fluid flow and fluid pressure amplitudes to be measured behind the prosthetic cup, and the presence of screw holes also affecting pressures. The improvements made to the test procedure allowed these effects to be measured by the APTR model.

In the healthy hip there is a neutral pressure within the joint capsule, becoming negative in the swing phase of gait. Osteoarthritis and THA are commonly accompanied by joint effusion, in which increased intra-articular fluid increases the resting pressure in the hip joint. The mean resting intra-articular pressure measured in 20 osteoarthritic hips *in vivo* was 5.8kPa (Goddard and Gosling, 1988) with pressures reaching 10.8kPa in painful effusive hips. The mean base pressure within the APTR chamber was 7.0kPa (± 1.0kPa) which shows that the base pressures applied to the rig were representative of capsular effusion in osteoarthritic hips *in vivo*, further validating the pressure measurements produced by loading the APTR.

In the APTR model, positive and negative pressures with respect to base pressure may create fluid flow behind the cup, which has itself been shown to be an important factor causing osteolysis (Fahlgren et al., 2010). The rig is not a closed system, and fluid flow can occur between the cup and the test hemisphere. This test series demonstrated the effects of changing reservoir height – the lower reservoir caused more negative rig pressures, but the amplitude of pressures measured was not significantly different. This showed that while changing the chamber pressure affected maximum and minimum pressure values, the amplitude of pressures remained the same. From this observation it can be concluded that the amplitude of pressures measured in the APTR model is related to the flow of fluid, which is caused by the movement of components and the ability of the fluid to access periacetabular spaces.

This fluid flow can be affected by component features, as shown by the tests comparing pressures with the Trident acetabular cup with and without five screw holes in the shell. Nonparametric statistical analysis of the data showed that there was a significant difference in pressure on all transducers with the different cup designs. Pressures on the top and pole transducers were higher with screw holes, while the rim and angled pressures were lower in the presence of screw holes. The largest difference between tests with and without screw holes is observed on the Angled pressure transducer (median pressure of 42.3kPa compared to 14.17kPa with screw holes). The lower pressures on the angled transducer in the presence of screw holes may indicate the larger volume provided by the screw hole reduced the peak pressures, or it may mean that air bubbles were present behind the screw holes that caused a damping effect on pressures measured.

Fluid flow is also affected by the first-cycle relocation-from-microseparation effect, where the head and cup become fully engaged in the first cycle of loading, and subsequent load cycles have slightly lower displacements. As was shown in Chapter 4, this relocation leads to higher pressures due to faster initial head movement, and the gradient of the reduction of these pressure spikes represents the speed of fluid flow out of the pressurised area. The phase analysis section of this chapter detailed how the movement of the loading head, rather than the magnitude of the applied load, was responsible for these observed pressure 'spikes'.

However, the most significant factor affecting fluid flow in these tests was the presence of a fibrous membrane around the rim of the cup. Significantly lower pressures were measured

when a fibrous rim was introduced between the cup and the test hemisphere. This is due to the rim "wedging in" around the implant. In this way the membrane is likely to have simulated conditions as described by Frokjær and colleagues (1999), in which a press-fit cup with fibrous rim forms a barrier against the ingress of polyethylene particles, and presumably also the flow of fluid to periacetabular bone. Cups inserted with a membrane also sat slightly higher in the cavity, leading to a greater amount of periprosthetic volume between the cup and the test hemisphere. This greater clearance may have reduced the effect of the cup movement on maximum pressures by reducing the magnitude and velocity of fluid flow, as well as red.

The Trident cups are designed to have press-fit fixation, with the cup being oversized for the cavity. However, the cup could not be implanted into an undersized test cavity as the bone material was too stiff. The 54mm Trident cup was therefore implanted into a 54mm diameter test cavity and the rim contact, usually achieved by press-fit fixation, was less stable. When the fibrous rim was introduced it added to the interference between the acetabular cup and the bone analogue, effectively creating a better rim fit fixation. If the fibrous membrane around an implant *in vivo* is thinner than 0.5mm, the component can be classified as stable (Schmalzried et al., 1992b). In the APTR, the membrane is compressed to less than 0.5mm when load is applied to the prosthetic cup, possibly representing this stable condition. This improvement in fixation led to lower pressures being measured behind the cup - the presence of the membrane caused most maximum pressures to fall below the 35KPa level previously identified to cause osteolysis.

In vivo the fibrous tissue would occupy spaces where bone had been resorbed, or where there was a gap between implant and bone. In the APTR test cavity, to simulate membrane formation without increasing the stability of the implant, the bone analogue should have been modified to allow extra space for the introduction of the membrane.

The movement of the cup relative to the bone analogue is significantly affected by the head-cup suction effect. This causes the head and cup to move together as a single unit, as the adhesive force from the thin film of fluid in the articulation causes the cup to adhere strongly to the head. This effect has been observed in other studies (Clarke et al., 2003) as well as in previous APTR tests. In cases of poor fixation, such as the tests performed in this chapter with the Trident cup without a fibrous rim, the adhesive force clearly overcomes fixation force and causes head and cup to move as a single unit.

It is unlikely that this exact cup movement will occur *in vivo*, as the completely loose (inadequate press-fit fixation) situation is unlikely to be present unless surgeon error causes the acetabular cavity to be over-reamed. The loosening at the rim would not commonly occur in uncemented cups over time, as uncemented cups tend to present localised expansile osteolysis. The fixation situation modelled in these tests is more similar to the linearly-progressing osteolysis progressing from the rim to the pole, commonly seen in cemented cups.

It is likely that the fibrous rim improved fixation strength, to the extent that the head-cup adhesion effect was minimised and the loading head was able to move independently of the acetabular cup. This would also explain the lower pressures measured in the presence of the fibrous membrane, as the displacement of fluid would decrease as cup movement decreased. This effect was previously described in Chapter 4, however the phase analysis presented in this chapter provides further proof of the effect of the fibrous rim on fluid flow within the APTR chamber.

The presence of a membrane also appeared to decrease the variability of results on the angled and pole transducers. It is possible that the membrane, wedging in between the implant and the cavity, is stabilising the movement of the implant, in the manner of a more well-fixed cup, and that this stabilised movement is causing more repeatable pressures to be measured.

From varying these test parameters, the conditions under which maximum pressures were measured were determined to be Trident cups without screw holes, inserted without a fibrous rim, in the first cycle of loading. The maximum pressure measured under these conditions was 147kPa (median max pressures from all tests 71.7kPa), while the median pressure amplitude at the pole of the cup was 61.8kPa (±20.4kPa). This pressure was lower than the pressures measured by Walter (685kPa, measured behind a loose pistoning liner) but higher than pressures measured by Bartlett (17kPa, measured behind a half-sized femoral stem). Although these two studies, as in the APTR study, dealt with implants with loose components, there were some significant differences that accounted for the difference in pressures between the three APTR models. The similarities and differences between these test rigs are summarised in Table 14.

Table 14: Summary of rig designs from different studies. Design features in common with the APTR are shown in bold.

	APTR study Ch5	**Walter (2005)**	**Bartlett (2008)**
PRESSURE	Maximum 147kPa in axis of loading (median 71.7kPa)	Mean 680kPa in axis of loading	5 - 17kPa
Prosthetic Components	Trident hemispherical metal shells with X3 Poly liner 28mm metal femoral head	UHMWPE custom-machined liners **28mm metal femoral head**	Custom-machined half-sized Exeter size 1 stem
Component fixation modelling	Uncemented cup fixation with insufficient press-fit	Simulated good cup fixation but with loose pistoning liner	Loose stem within cement mantle
Loading	Axial loading to 1kN 1Hz frequency 50 cycles	23° and 46° angled loading to 2kN **1Hz frequency** 100 cycles	Axial load to 1.3kN, plus torque loading **1Hz frequency** 30 cycles
Bone analogue	Polyurethane hemisphere similar to Sawbones 30pcf	None – loose liner was fitted into an aluminium block	None – components were loaded within a thick cement mantle, without bone analogue.
Synovial analogue	Vegetable oil at room temperature (20°C)	Bovine serum at **room temperature (20°C)**	**Vegetable oil** at body temperature (37°C)
Pressure measure-ment	Pressures measured by miniature ruggedised pressure transducers, at positions behind the prosthetic cup, through rigid transmission tubes.	Pressures measured by subminiature flush diaphragm transducer, through a hole behind the apex of the loose liner.	Pressures measured by external pressure transducers, through **transmission channels** moulded into the cement mantle.

As described in Table 14, there are significant differences between these studies. All three investigate the effects of the movement of a loose component on fluid pressures, with relatively similar loading and pressure measurement setups. However components and fixation situations are significantly different, with the results of the two previous studies within two orders of magnitude from each other (17kPa – 680kPa), and the APTR results at an intermediate level (147kPa).

The pumping of fluid caused by a loose pistoning liner was investigated by Walter et al. (2005), with fluid flow behind the loose liner causing extremely high axial pressures. The loading in this test was twice as high as in the APTR study and an increase in load magnitude has been previously shown to cause higher pressures (Chapter 4). The simplicity of this model may contribute to the high pressures, as the only outlet for fluid flow under load was behind the loose liner, where pressures were measured. In the APTR there are more interfaces for fluid to penetrate and thus the effects of volume changes on pressure were diffused through the chamber.

A 'femoral stem pump' was simulated by Bartlett et al. (2008) with a loose femur within a cement mantle. This femoral pumping motion caused periprosthetic pressures to be generated in the synovial analogue (vegetable oil). The component geometry and fixation conditions between the APTR and Bartlett studies were significantly different so it is logical that results differ, however the fact that this difference is within one order of magnitude suggests component movements in the two studies produced a similar degree of pressures.

Maximum pressures in this test series were significantly higher than those measured in the previous chapter (131.3kPa compared to 34.6kPa). The Osteolock cup used in Chapter 4 had a loose locking liner, which was able to move up and down within the shell in a manner similar to the pistoning effect described by Walter and colleagues in their study of fluid pumping mechanisms (2005), although resulting in much lower pressures. Polyethylene liners used with the Trident cups were securely fixed in the shells and so any relative movement occurred with the entire cup and not just the liner. This may have led to a much higher displacement of fluid under axial loading, causing the higher pressures measured in tests with the Trident cups.

These pressure results were validated by the comparison of measured base pressures with the expected base pressures calculated using the pressure head equation. Although base pressures were statistically different from the calculated values, this difference was less than 0.5kPa in all cases, which indicates the fidelity of pressure measurements from the APTR.

From these tests with the APTR, phase data combined with statistical analysis provided a good basis for speculation about fluid movement behind the cup and within the chamber. However it would be desirable to check these results against a computational fluid dynamics model to determine if the same trends can be observed, thereby strengthening the conclusions from the APTR testing.

5.5 Chapter summary

- Changes to cup design and fixation affected the pressures measured by the APTR.
- The presence of a fibrous membrane caused lower median pressure amplitudes to be measured behind the cup (10.76kPa compared to 86.66 without a membrane on the pole transducer).
- Greater interference between the rim of the cup and the bone analogue and greater clearance at the pole, caused by interposition of a fibrous rim between the two surfaces, led to a reduction in maximum pressures to below 35kPa.
- The presence of a fibrous rim simulated better fixation of the implant, as shown by the lower measured pressures, and the evidence of lower fluid flow and improved cup stability.
- The presence of screw holes affected pressures, especially on the angled transducer, which recorded median pressure amplitudes of 47.38kPa with a solid-back cup, compared to 17.49kPa for a cup with screw holes.
- Decreasing the applied pressure on the chamber (by lowering the oil reservoir) decreased the maximum and minimum pressure magnitudes, but not the amplitudes of the pressure waves. The magnitude of pressure fluctuations is caused by the movement of components and not the externally applied pressure.
- Maximum pressures were measured using Trident cups without screw holes, inserted without a fibrous rim, in the first cycle of loading (highest recorded pressure 131.3kPa).
- The phase analysis process described in this chapter provides a large amount of information about fluid movement within the rig chamber.

6. Assessment of APTR model

The aim of this thesis was to investigate periacetabular pressure generation through the construction and testing of a physical model of the replaced hip joint, the Acetabular Pressure Transmission Rig (APTR). Critical design decisions for the rig were made using information from pilot studies and from the wider literature. Due to the complexity of the human hip joint, these design decisions were based on the elements most likely to affect fluid pressure measurement – the bone analogue, synovial fluid, the joint capsule chamber, joint loading and component fixation. This chapter will discuss the different rig components simulating *in vivo* hip features and then assess the performance of these components during the tests described in this thesis.

6.1 Assessment of rig design elements

Axial loading approximating loads in the gait cycle

Joint loading *in vivo* is very different from the loading regime proposed for the APTR model. The multidirectional loading of the natural hip was deemed too complex for the development of this rig, so only a single load magnitude and direction was made possible for each test. The inverse loading configuration allowed the application of axial load at different load angles. This axial loading, although simplified, has been used in other studies, such as the tests of pressures due to liner pistoning performed by Walter and colleagues (2005). In the APTR model this axial setup provided consistent loads and the simplified comparison of different conditions within the chamber.

It would be useful to attach the rig chamber to a loading apparatus capable of applying more complex loads, to better simulate *in vivo* loading directions. However this would require significant modification of the rig cover plate to allow multi-axial load application. Also, the use of phase analysis to draw conclusions about component and fluid movements in the chamber would no longer be appropriate, as the movements would be too complex and analysis using CFD would be required.

It would also be useful to include a rest period in the testing. The average walking frequency is generally accepted to be 1Hz, or one gait cycle per second. However *in vivo* this 1Hz loading does not correspond to a simple sinusoidal load on the hip, as used in the APTR testing, as the

hip joint is loaded in stance phase, and unloaded during swing phase. Therefore a more representative load cycle would include a rest period to simulate a simple swing phase, as shown in Figure 133. The tests in this thesis were loaded using (a) the full sine load pattern, and a more physiological load pattern (b) is shown with a rest period.

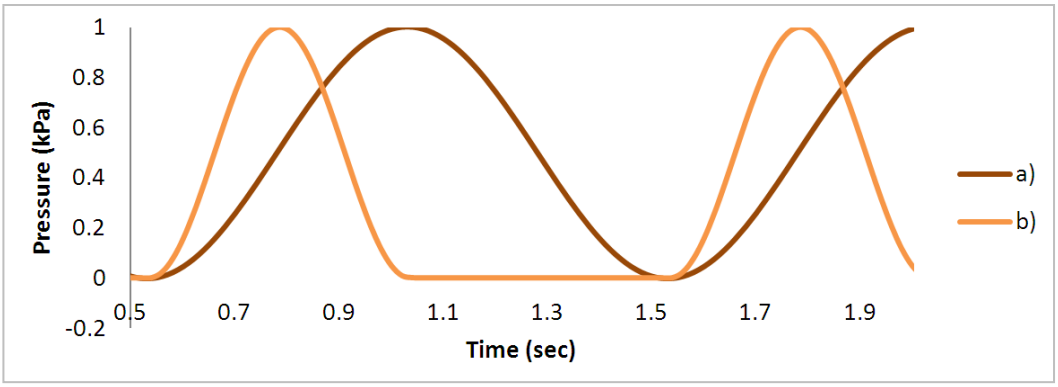

Figure 133: Graph showing a) loading using a full sine wave, and b) loading with a rest period.

Including a rest period in the load cycle increases the speed at which load is applied, which would increase pressures measured by the APTR (as shown in Chapter 4). However using the Dartek control system this load-rest pattern was not able to be applied.

The loading regime also allowed relocation-from-microseparation conditions to be introduced at the start of tests, with a separation distance of up to 1.2mm. However this should be higher in future tests to better represent an *in vivo* separation of up to 5mm (Dennis et al., 2001). Microseparation *in vivo* involves the disengagement of the head and the cup, followed by relocation. In these tests only the relocation phase was simulated, and further testing should include a disengagement condition as well. It is believed this disengagement will cause high negative pressures, leading to clinically-significant fluid movement and pressure amplitudes. Due to the head-cup suction effect, it is unknown how much of the head motion observed in APTR tests is a separation between head and cup and how much is between the cup and the bone analogue. Future CFD analysis should take potential head-cup suction forces into account, as this effect has a significant impact on the movement of components *in vitro*.

Vegetable oil approximating synovial fluid

Vegetable oil does not reproduce the composition and thixotropy of synovial fluid. Thixotropic fluids would flow differently within the chamber, and respond differently to changes in the frequency of loading, as the viscosity reduces when the fluid is subjected to increased shear

stress. However, the viscosity of vegetable oil at room temperature is similar to that of synovial fluid in osteoarthritis and was chosen due to its ease of use in the development of the APTR unit.

As previously described by Bartlett (2008), transmission tubes can transmit pressure waves at an interface to transducers at a distance from this interface. In the APTR, if these transmission tubes were not completely full of fluid there was the potential for pressure measurement errors. Air is a compressible fluid and would distort pressure measurements by damping the interface pressures as they are transmitted to the transducers. Modifications made during preliminary testing ensured that the transmission tubes were completely full of oil, and that the rig was completely sealed against leaks.

The synovial analogue selection can influence how the fluid flows in the joint and how it reacts to pressure and shear forces under anatomical load. The adhesive and cohesive forces within the chosen fluid determine how easily it can flow between two close surfaces – for example, between the cup and the bone analogue *in vitro,* or through the narrow transmission tubes. In the APTR, the pressure transmission tubes were designed to be very small to disrupt the test interface as little as possible. It is possible that the effect of friction on the walls of the narrow transmission tubes affected the magnitudes of pressures measured. However, the comparisons made between different test conditions are still valid, as this friction effect would be the same across all tests.

Rig chamber approximating hip capsule

The APTR chamber enclosed the test components and bone analogue, and sealed the synovial fluid inside the test area, effectively simulating an inelastic arthritic joint capsule. The ability of fluid to flow out of the rigid APTR chamber through the oil introduction tube is assumed to approximate the ability of a hip joint with elastic components to reduce the pressure in the joint (capsular distension). The fact that this oil outflow is limited by the narrow aperture of the oil tube effectively approximates the lower elasticity of an osteoarthritic joint capsule.

The elevated pressure reservoir of the APTR allowed a constant pressure to be applied to the test chamber, an effect previously used in tests by Bartlett and colleagues with the use of an elevated filler tank (Bartlett et al., 2008). In the APTR tests described in Chapter 5, this applied

pressure was positive when the reservoir was higher than the chamber and negative when held below the chamber.

As the oil reservoir was clamped to a retort stand, the APTR is capable of representing resting joint pressures, measured on the top transducer, of between 6.96kPa (at the maximum height of stand) and -2.72kPa (on the lowest point of the test bench). The capability for testing at different chamber heights, representing different resting joint pressures and thus different levels of joint effusion, is a novel element to the APTR model.

Although the pressure results could not be validated against *in vivo* measurements, the base pressures were very close to expected values calculated using the pressure head equation, indicating the fidelity of pressures measured on the transducers.

Machined model board hemisphere approximating pelvic bone

The bone analogue, a hemisphere of M650 polyurethane model board, could not exactly replicate the behaviour of the pelvis under load. However the material has extremely consistent material properties and a precise machining process that can be used to make more complex shapes for future studies, to better replicate the periacetabular bone.

Although the rig was designed to accommodate different-sized test hemispheres, only a 120mm hemisphere was used in the tests described in this thesis. Likewise, the design of the test hemispheres allowed the precise, repeatable machining of bone defects, an improvement over previous models (Adler et al., 1992, Jamieson et al., 2010), however this capability was not exploited in the studies described in this thesis.

In the replaced hip *in vivo*, the remaining acetabular bone has a trabecular structure, which is porous, with the space between the trabeculae filled with soft tissue - bone marrow and blood vessels. The deformability and porosity of this structure would affect the way fluid interacts with the bone under load. However when developing a test rig such as the APTR, it is important to develop a stable measurement system before testing a more complex bone analogue. In the tests described in this thesis, the movement of the loading head was more influential on the fluid pressures than the magnitude of the applied load. It is likely that with a more deformable bone analogue material, the magnitude of loading will become more significant to results.

While the bulk structure was not as complex as in other studies with bone analogue materials (Jamieson et al., 2010), the M650 model board provided a consistent, precisely formed bone analogue with appropriate mechanical properties, the use of which is novel to the APTR.

Cup fixation into test hemisphere approximating *in vivo* prosthetic fixation

In the APTR model, uncemented fixation with insufficient press-fit was modelled with a Stryker Trident acetabular cup. The press-fit components chosen for testing were inserted into the rig under a 'completely-loose condition, with and without a fibrous rim to represent linear membrane growth *in vivo*. This is not an accurate representation of *in vivo* conditions, as linear resorption beginning at the rim usually occurs in cemented cups, with uncemented press-fit cups (such as the ones used in the APTR) presenting with localised ballooning lesions. However this fixation condition allowed the sensitivity of the measurement system to be determined with regards to changes in the rig chamber.

It was apparent through the APTR testing that the adhesive forces between the head and cup were able to overcome the fixation forces holding the cup within the test hemisphere, causing the head and cup to move together as a single unit. Assuming the head-cup suction effect was present, the displacement of the head as measured by the Dartek could be assumed to be the movement of the cup relative to the bone analogue.

The adhesive forces are caused by viscous tension from the thin film of fluid between head and cup, and the stiffness of the two surfaces (Clarke et al., 2003, Carr, 1996). This means that different bearing surfaces will have different levels of adhesive force and thus will behave differently *in vivo*. While the APTR studies have implicated head-cup adhesion in increased pressures, as it causes the cup to move out of the cavity with the loading head, *in vivo* this adhesion has been linked to a positive effect - a lower dislocation rate, due to the difficulty in separating the head from the cup. An investigation into different bearing surfaces and their effects on pressure is required to analyse the effects of this head-cup adhesion on fluid flow in the hip capsule.

This fibrous membrane was capable of absorbing and exuding fluid under compressive load, described by Hori and Lewis (1982) as a property of the fibrous periacetabular tissue *in vivo*. This interaction between the interface membrane material and the synovial fluid analogue is unique to the APTR model, as previous studies have concentrated on mechanical properties

rather than the fluid interactions (Waide et al., 2004a, Waide et al., 2004b, Cherukuri et al., 2010).

Approximately 1mm thick unloaded, this membrane is compressed with the insertion of the prosthetic cup into the cavity to less than 0.5mm. This compression causes an improvement of fixation and no increase in micromotion, the opposite effect to that observed *in vivo* (Schmalzried et al., 1992b) and with other *in vitro* models (Cherukuri et al., 2010).

This prevention of fluid ingress is only observed because the test hemisphere did not contain an area of osteolysis (bone loss) into which the fibrous material was inserted; instead, the fibrous rim was interposed between cup and bone without any bone material removal, causing greater interference between cup and bone than without the membrane. Future studies using the fibrous material should incorporate an 'osteolytic cavity' in which the membrane material can be seated, to represent areas of bone loss into which the fibrous membrane grows *in vivo*.

In the tests described in Chapter 4, pressures behind a cup with a loose liner were measured when the APTR was loaded at an angle of 30°. The movement of the liner within the shell can be described as a pistoning effect, and has previously been shown to produce high periacetabular pressures *in vitro* (Walter et al., 2005). The pressures measured in the Walter study (2005) were significantly higher than those measured with the APTR. These higher pressures are likely to be caused by the differences in cup fixation – while the Walter rig had an aluminium block representing a completely well-fixed metal shell, the shell in APTR tests was completely loose, allowing fluid to escape through the gap between the hemisphere and the shell, instead of being forced through the screw holes to the measurement point.

Although the pressure measurement system worked extremely well, this was only under extremely poor fixation conditions. The current APTR design relies on the slight clearance between the 52mm cup and the test cavity of the same diameter to allow oil to drain through the cavity and cause transmission tubes behind the cup to fill with fluid. If the APTR was to simulate good fixation, another method for filling these transmission tubes would be required - if the transmission tubes are not completely full of oil, correct fluid pressures will not be recorded (as described in Appendix 2).

To the author's knowledge this is the first time a rig has been used to measure pressures behind commonly-available full-sized prosthetic components. It is also the first time a

permeable material has been used as a fibrous membrane analogue for *in vitro* mechanical tests.

6.2 Discussion

The most significant limitation of the current APTR design is the inability for a multiaxial loading regime to be applied to the model. The other elements of the design provide a good approximation of the features likely to influence periacetabular pressures.

The APTR model contains several novel elements. These include the use of M650 model board as a bone substitute material (with the potential for repeatable bone defect simulation), the use of a permeable fibrous material to simulate the interfacial membrane, the ability to replicate different levels of joint effusion (by changing oil reservoir height) and the ability to test pressures behind currently-available full-sized implant components. To the best of the author's knowledge these elements have not been used in conjunction with the measurement of periacetabular pressures *in vitro*.

Although the full potential of the APTR model has not yet been exploited, the creation of this rig has allowed the measurement of pressures behind an uncemented cup with insufficient press-fit fixation. The features of the APTR allow comparison of new implant designs with existing components, to determine the effect of design changes on periacetabular pressures. This information will be useful in a clinical context, to ensure future prosthesis designs are less likely to contribute to damaging fluid pressures in the hip joint. Further work can be performed to exploit the full potential of the APTR, as well as to improve its design; this will be discussed in Chapter 8.

7. Conclusions

Osteolysis is still the dominant postoperative problem in total hip arthroplasty. A comprehensive literature review indicated that osteolysis can be caused by wear debris, fluid pressure, or a combination of the two. Although this review found that wear debris and its effect on osteolysis has been extensively explored, fewer studies were found that investigated fluid pressures and the mechanisms by which high pressures can be generated. This highlighted the need for a rig that would allow researchers to determine experimentally the conditions under which clinically significant fluid movement can occur behind an acetabular cup.

The aim of this thesis was to create a model capable of reproducing significant features of the hip following THA, and to use this model to test fluid pressures measured around currently-available acetabular cup components. The process of designing and testing this physical model, called the Acetabular Pressure Transmission Rig (APTR), has been presented in detail (Chapter 3 and Chapter 4). Preliminary testing confirmed the successful measurement of periprosthetic pressures by the APTR.

Further testing showed that the APTR was capable of measuring pressure changes caused by changes to cup design, component fixation and loading. Pressures over 35kPa, previously shown by other groups to cause osteolysis, were routinely measured within the APTR. Although tests were initially performed at 30° (as described in Chapter 4), axial testing produced higher pressures and more consistent results (Chapter 5). Maximum pressures were measured during axial testing (131.3kPa), using Trident cups without screw holes, in the first cycle of loading. These pressures are lower than those measured by other groups - pressures of over 600kPa have been measured in other *in vivo* mechanical tests with loose implants.

In contrast with clinical observations, where the presence of fibrous tissue between implant and bone is likely to lead to increased periprosthetic pressures and poor implant fixation, tests of the APTR with a fibrous membrane appeared to simulate better cup fixation of the prosthetic cup. In this model interposition of a fibrous rim between the two surfaces caused greater rim interference and greater pole clearance between the cup and the bone analogue. This led to reduced fluid access to periacetabular space, and a reduction in maximum periacetabular pressures to below 35kPa. At the base of the cup, median pressure amplitudes

were reduced from 86.7kPa without a membrane to 10.8kPa in the presence of a fibrous rim, an 88% reduction.

Relocation from microseparation between the loading head and the acetabular cup caused a significant increase in measured pressure amplitudes, with a 0.15mm increase in head-cup separation (from 0.44mm to 0.59mm) leading to an increase in pressure from 12.1kPa to 18.5kPa, a 53% increase, as measured in Chapter 4. This higher displacement and subsequent higher pressure occurred in the first cycle of testing, as the head and cup first came into contact.

Higher loading frequency and magnitude led to higher median pressure amplitudes (an increase in frequency from 0.5Hz to 1Hz caused a 62% increase in pressure, while an increase in loading magnitude from 1kN to 1.5kN caused a 34% increase in pressure. The presence of different component features, such as screw holes in the metal shell, also affected pressures. The transducer in direct communication with the screw hole recorded median pressures of 47.4kPa with a solid-back cup, compared to 17.5kPa with screw holes, a reduction of 63%.

Decreasing the applied pressure on the chamber by lowering the oil reservoir decreased the maximum and minimum pressure magnitudes but did not change the amplitudes of the pressure waves, leading to the hypothesis that pressure amplitudes were caused by component movement due to loading, and were not an effect of higher chamber pressures.

A pressure differential was observed within the chamber, as the instantaneous pressure peaks within the rig occurred at different times on different transducers (as demonstrated by the phase analysis section in Chapter 5). This pressure differential implied the ability for fluid flow behind the cup, which is responsible *in vivo* for the transportation of particulate debris to periacetabular bone.

The tests described in this thesis have shown that the developed rig, the APTR, is capable of measuring clinically-significant pressures behind an uncemented cup with insufficient press-fit fixation. The APTR will be useful in a clinical context, as it is capable of testing a broad range of component types under a wide range of conditions. Results of these tests can be used to ensure future prosthesis designs are less likely to produce damaging fluid pressures in the hip joint.

8. Future Work

Several items of future work have been identified to fully exploit the potential of the APTR model. Required design improvements have been identified during the testing process, including modifications to the loading regime, bone analogue and fixation modelling.

Different prosthetic components should be tested with the APTR model. For example, ceramic-on-polyethylene bearings have lower adhesion forces and thus a lower degree of head-cup suction compared to metal-on-metal bearing surfaces (Clarke et al., 2003). The effects of different bearing surfaces should be investigated in further tests, using cups with the same metal shell but different liner materials. The Trident acetabular cup system is appropriate for further testing as several bearing options are available – metal-on-polyethylene, ceramic-on-polyethylene, and ceramic-on-ceramic (to test metal-on-metal bearings a different component system is required).

Different head sizes have been associated with different levels of wear and osteolysis (Callaghan et al., 2003). To determine whether head size also has an effect on pressure generation within the joint capsule, different loading head sizes can be used with appropriately-sized liners. No modification to the APTR design is required to perform these tests.

The sealing effect of the membrane, described in Chapter 5, can be further investigated by the introduction of particles into the APTR. Particles can be introduced into the bulk chamber fluid before the components are loaded, and the extent to which particles are able to migrate behind the cup under cyclic load may be assessed. Oil can be collected from behind the cup, and filtered to assess the number of particles, and thus the degree of particle migration, as previously performed by Khalily and colleagues (Khalily et al., 1998).

Modifications to the loading regime of the APTR are required to better replicate loading angles and magnitudes on the replaced hip *in vivo*. To simulate the flexion-extension, adduction-abduction and internal-external rotation movements the current inverted loading setup can be used but the rig chamber must be dynamically angled around the axis of loading to represent the different load positions during gait. Another recommended modification to the loading regime is an increase in the magnitude of head-cup separation when performing relocation-from-microseparation tests. The tests described in Chapter 4 and 5 used displacement values

up to 1.2mm, while *in vivo* measurements of this movement have indicated magnitudes of 3-5mm during gait. This must be programmed into the multiaxial loading regime. It is predicted that the 'disengagement' phase of microseparation, where the head is separated from the cup, would cause significant negative pressures to be recorded due to the head-cup suction effect. This phase should also be modelled in microseparation tests.

A different method of filling the pressure transmission tubes must be found, to allow more stable fixation to be modelled within the APTR. The current method relies on the poor fixation between the 52mm cup and the test cavity to allow oil to move between them and fill the periacetabular transmission tubes. To remove the need for clearance around the cup component, the transmission tubes could be modified to include an oil introduction valve and an air outlet valve. In this way, oil can be introduced when the transducer is already attached.

With this solution, different fixation modes can also be introduced to the APTR model. Improved press-fit fixation can be simulated by slightly reducing the diameter of the test cavity, to provide an interference fit when components are implanted. After testing with improved fixation, the fixation strength of the implant should be tested by using a lever-out test to assess the final fixation strength of the component. It is also possible for the surface of the test cavity to be roughened during the machining process to allow the implantation of cemented components with varying degrees of interdigitation.

Future studies using the fibrous material should incorporate an 'osteolytic cavity' in which the membrane material can be seated, to represent areas of bone loss into which the fibrous membrane grows *in vivo*. These osteolytic cavities or bone defects can be precisely machined into the bone analogue during the machining process (Appendix 4).

Tests using different hemisphere sizes should be performed to determine whether a thinner test hemisphere can still be used with this pressure measurement system and what effect a more flexible bone analogue structure has on the pressure results. This information paves the way for the use of more complex shapes for future studies, which can be machined to better replicate the periacetabular bone, with the eventual use of a composite hemipelvis model as the bone analogue.

With the more complex loading regime described earlier, the phase analysis procedures described in Chapter 5 would no longer be sufficient to draw conclusions about fluid

movement in the rig. A computational fluid dynamics (CFD) model would be required to assess the effects of different rig parameters on fluid movement. This CFD model could provide validation of the conclusions drawn using the phase analysis method detailed in Chapter 5, as well as detecting the precise effects of different component features and surface finishes on the movement of periprosthetic fluid.

References

1990. BS 7251-7:1990 Orthopaedic joint prostheses. Guide to hip joint simulators.

ADLER, E., STUCHIN, S. A. & KUMMER, F. J. 1992. Stability of press-fit acetabular cups. *Journal of Arthroplasty,* 7**,** 295-301.

ALLEN, M., BRETT, F., MILLETT, P. & RUSHTON, N. 1996. The effects of particulate polyethyelene at a weight-bearing bone-implant interface: a study in rats. *Journal of Bone & Joint Surgery, British Volume,* 78-B**,** 32-37.

AMIROUCHE, F., ROMERO, F., GONZALEZ, M. & ARAM, L. 2008. Study of micromotion in modular acetabular components during gait and subluxation: a finite element investigation. *Journal of Biomechanical Engineering,* 130**,** 021002.

AMSTUTZ, H. C., CAMPBELL, P., KOSSOVSKY, N. & CLARKE, I. C. 1992. Mechanism and clinical significance of wear debris-induced osteolysis. *Clinical Orthopaedics and Related Research***,** 7-18.

ANDERSON, G. I., MACQUARRIE, R., OSINGA, C., CHEN, Y. F., LANGMAN, M. & GILBERT, R. 2001. Inhibition of leukotriene function can modulate particulate-induced changes in bone cell differentiation and activity. *Journal of Biomedical Materials Research,* 58**,** 406-414.

AOA 2012. Australian Orthopaedic Association (AOA) National Joint Replacement Registry. Annual Report. *Joint Replacement Registry Australia.* Adelaide: Australian Orthopaedic Association.

ASPENBERG, P. & HERBERTSSON, P. 1996. Periprosthetic bone resorption. Particles versus movement. *Journal of Bone & Joint Surgery, British Volume,* 78**,** 641-6.

ASPENBERG, P. & VAN DER VIS, H. 1998. Fluid pressure may cause periprosthetic osteolysis. Particles are not the only thing. *Acta Orthopaedica Scandinavica,* 69**,** 1-4.

BAKER, P. N., MCMURTRY, I. A., CHUTER, G., PORT, A. & ANDERSON, J. 2009. THA with the ABG I Prosthesis at 15 Years: Excellent Survival with Minimal Osteolysis. *Clinical Orthopaedics and Related Research*.

BALEANI, M., FOGNANI, R. & TONI, A. 2001. Initial stability of a cementless acetabular cup design: experimental investigation on the effect of adding fins to the rim of the cup. *Artificial Organs,* 25**,** 664-9.

BARTLETT, G. E., BEARD, D. J., MURRAY, D. W. & GILL, H. S. 2008. The femoral stem pump in cemented hip arthroplasty: An *in vitro* model. *Medical Engineering & Physics,* 30**,** 1042-1048.

BARTLETT, G. E., BEARD, D. J., MURRAY, D. W. & GILL, H. S. 2009a. *In vitro* comparison of the effects of rough and polished stem surface finish on pressure generation in cemented hip arthroplasty. *Acta Orthopaedica,* 80**,** 144-9.

BARTLETT, G. E., GILL, H. S., MURRAY, D. W. & BEARD, D. J. 2009b. *In vitro* influence of stem surface finish and mantle conformity on pressure generation in cemented hip arthroplasty. *Acta Orthopaedica,* 80**,** 139-43.

BERGMANN, G., DEURETZBACHER, G., HELLER, M., GRAICHEN, F., ROHLMANN, A., STRAUSS, J. & DUDA, G. N. 2001. Hip contact forces and gait patterns from routine activities. *Journal of Biomechanics,* 34**,** 859-71.

BERGMANN, G., GRAICHEN, F. & ROHLMANN, A. 1993. Hip joint loading during walking and running, measured in two patients. *Journal of Biomechanics,* 26**,** 969-990.

BISCHOFF, U. W., FREEMAN, M. A., SMITH, D., TUKE, M. A. & GREGSON, P. J. 1994. Wear induced by motion between bone and titanium or cobalt-chrome alloys. *Journal of Bone & Joint Surgery, British Volume,* 76**,** 713-6.

BITSCH, R. G., LOIDOLT, T., HEISEL, C. & SCHMALZRIED, T. P. 2008. Cementing techniques for hip resurfacing arthroplasty: development of a laboratory model. *Journal of Bone and Joint Surgery, American Volume,* 90 Suppl 3**,** 102-10.

BRONZINO, J. D. 2000. The Biomedical Engineering Handbook. 2 ed. Boca Raton: CRC Press LLC.

CALLAGHAN, J. J., PEDERSEN, D. R., JOHNSTON, R. C. & BROWN, T. D. 2003. Clinical biomechanics of wear in total hip arthroplasty. *Iowa Orthopaedic Journal,* 23**,** 1-12.

CARMONA, R. H. 2004. Bone Health and Osteoporosis: A Report of the Surgeon General. . Rockville, MD: Office of the Surgeon General, U.S. Department of Health and Human Services.

CARR, A. J. 1996. (i) Biomechanics of shoulder stability. *Current Orthopaedics,* 10**,** 146-150.

CHARLES, M. N., BOURNE, R. B., DAVEY, J. R., GREENWALD, A. S., MORREY, B. F. & RORABECK, C. H. 2004. Soft-Tissue Balancing of the Hip. The Role of Femoral Offset Restoration. *J Bone Joint Surg Am,* 86**,** 1078-1088.

CHERUKURI, A. R., MILLER, M. A., RACE, A., IZANT, T. H. & MANN, K. A. 2010. A wax barrier to simulate bone resorption for pre-clinical laboratory models of cemented total hip replacements. *Journal of Biomechanics,* 43**,** 2855-7.

CJRR 2012. Hip & Knee Replacements In Canada - Canadian Joint Replacement Registry (CJRR) 2011 Clinical Data. Ottawa, Ontario: CIHI.

CLARKE, M. T., LEE, P. T. & VILLAR, R. N. 2003. Dislocation after total hip replacement in relation to metal-on-metal bearing surfaces. *Journal of Bone & Joint Surgery, British Volume,* 85**,** 650-4.

CLOHISY, J. C. & HARRIS, W. H. 1999. Primary hybrid total hip replacement, performed with insertion of the acetabular component without cement and a precoat femoral component with cement. An average ten-year follow-up study. *Journal of Bone & Joint Surgery, American Volume,* 81**,** 247-55.

CRAWFORD, R. W., EVANS, M., LING, R. S. & MURRAY, D. W. 1999. Fluid flow around model femoral components of differing surface finishes: *in vitro* investigations. *Acta Orthopaedica Scandinavica,* 70**,** 589-95.

DELEE, J. G. & CHARNLEY, J. 1976. Radiological demarcation of cemented sockets in total hip replacement. *Clinical Orthopaedics and Related Research***,** 20-32.

DENNIS, D. A., KOMISTEK, R. D., NORTHCUT, E. J., OCHOA, J. A. & RITCHIE, A. 2001. *In vivo* determination of hip joint separation and the forces generated due to impact loading conditions. *Journal of Biomechanics,* 34**,** 623-9.

DUMBLETON, J. H., MANLEY, M. T. & EDIDIN, A. A. 2002. A literature review of the association between wear rate and osteolysis in total hip arthroplasty. *Journal of Arthroplasty,* 17**,** 649-661.

EGAWA, H., HO, H., HOPPER JR, R. H., ENGH JR, C. A. & ENGH, C. A. 2009a. Computed Tomography Assessment of Pelvic Osteolysis and Cup-Lesion Interface Involvement with a Press-Fit Porous-Coated Acetabular Cup. *Journal of Arthroplasty,* 24**,** 233-239.

EGAWA, H., POWERS, C. C., BEYKIRCH, S. E., HOPPER, R. H., JR., ENGH, C. A., JR. & ENGH, C. A. 2009b. Can the volume of pelvic osteolysis be calculated without using computed tomography? *Clinical Orthopaedics and Related Research,* 467**,** 181-7.

EMANS, P. J., BROEKE, R. H., VAN MULKEN, J. M., KUIJER, R., VAN RHIJN, L. W. & GEESINK, R. G. 2009. Results of total hip arthroplasties in the young patient; further evidence for a barrier against articular wear debris by hydroxyapatite coatings. *Hip International,* 19**,** 343-51.

ENGH, C. A., BOBYN, J. D. & GLASSMAN, A. H. 1987. Porous-coated hip replacement. The factors governing bone ingrowth, stress shielding, and clinical results. *Journal of Bone & Joint Surgery, British Volume,* 69**,** 45-55.

ENGH, C. A., SYCHTERZ, C. J., YOUNG, A. M., POLLOCK, D. C. & TOOMEY, S. D. 2002. Interobserver and intraobserver variability in radiographic assessment of osteolysis. *Journal of Arthroplasty,* 17**,** 752-759.

ENGH, C. A., ZETTL-SCHAFFER, K. F., KUKITA, Y., SWEET, D., JASTY, M. & BRAGDON, C. 1993. Histological and radiographic assessment of well functioning porous-coated acetabular components. A human postmortem retrieval study. *Journal of Bone & Joint Surgery, American Volume,* 75**,** 814-24.

EVANS, C. E., MYLCHREEST, S. & ANDREW, J. G. 2006a. Age of donor alters the effect of cyclic hydrostatic pressure on production by human macrophages and osteoblasts of sRANKL, OPG and RANK. *BMC Musculoskeletal Disorders,* 7**,** 21.

EVANS, C. E., MYLCHREEST, S., MEE, A. P., BERRY, J. L. & ANDREW, J. G. 2006b. Cyclic hydrostatic pressure and particles increase synthesis of 1,25-dihydroxyvitamin D3 by human macrophages *in vitro*. *International Journal of Biochemistry & Cell Biology,* 38**,** 1540-6.

FAHLGREN, A., BOSTROM, M. P., YANG, X., JOHANSSON, L., EDLUND, U., AGHOLME, F. & ASPENBERG, P. 2010. Fluid pressure and flow as a cause of bone resorption. *Acta Orthopaedica,* 81**,** 508-16.

FAHLGREN, A., NAM, D., DVORZHINSKIY, A. & BOSTROM, M. Fluid pressure induced osteoclast activation and bone loss is not dependent on fibrous tissue in the peri-implant zone. ORS 2012 Annual Meeting, 2012 San Francisco, California.

FAM, H., BRYANT, J. T. & KONTOPOULOU, M. 2007. Rheological properties of synovial fluids. *Biorheology,* 44**,** 59-74.

FERGUSON, S. J., BRYANT, J. T., GANZ, R. & ITO, K. 2000. The influence of the acetabular labrum on hip joint cartilage consolidation: a poroelastic finite element model. *Journal of Biomechanics,* 33**,** 953-960.

FERGUSON, S. J., BRYANT, J. T., GANZ, R. & ITO, K. 2003. An *in vitro* investigation of the acetabular labral seal in hip joint mechanics. *Journal of Biomechanics,* 36**,** 171-8.

FERRIER, G. M., MCEVOY, A., EVANS, C. E. & ANDREW, J. G. 2000. The effect of cyclic pressure on human monocyte-derived macrophages *in vitro*. *Journal of Bone & Joint Surgery, British Volume,* 82**,** 755-9.

FLIVIK, G. 2005. Fixation of the cemented acetabular component in hip arthroplasty. *Acta Orthopaedica. Supplementum,* 76**,** 3-30.

FROKJÆR, K., OVERGAARD, S., LIND, M., BUNGER, C. & SOBALLE, K. 1999. Failure of migration by injected polyethylene particles around press fit implants: an experimental study in rabbits. *Hip International,* 9**,** 173-177.

GARCIA-CIMBRELO, E. & MUNUERA, L. 1992. Early and late loosening of the acetabular cup after low-friction arthroplasty. *Journal of Bone & Joint Surgery, American Volume,* 74**,** 1119-29.

GARELLICK, G., KÄRRHOLM, J., ROGMARK, C. & HERBERTS, P. 2010. Swedish Hip Arthroplasty Register - Annual Report 2009. Göteborg, Sweden: Sahlgrenska University Hospital.

GODDARD, N. J. & GOSLING, P. T. 1988. Intra-articular fluid pressure and pain in osteoarthritis of the hip. *Journal of Bone & Joint Surgery, British Volume,* 70**,** 52-5.

GOLDRING, S. R., SCHILLER, A. L., ROELKE, M., ROURKE, C. M., O'NEIL, D. A. & HARRIS, W. H. 1983. The synovial-like membrane at the bone-cement interface in loose total hip replacements and its proposed role in bone lysis. *Journal of Bone & Joint Surgery, American Volume,* 65**,** 575-84.

GOODMAN, S. B. 1994. The effects of micromotion and particulate materials on tissue differentiation: Bone chamber studies in rabbits. *Acta Orthopaedica,* 65**,** 1-43.

GRAY, H. 1918. Anatomy of the human body. *In:* LEWIS, W. H. (ed.) 20 ed. Philadelphia: Lea & Febiger.

HAILER, N. P., GARELLICK, G. & KÄRRHOLM, J. 2010. Uncemented and cemented primary total hip arthroplasty in the Swedish Hip Arthroplasty Register. *Acta Orthopaedica,* 81**,** 34-41.

HALLAN, G., LIE, S. A. & HAVELIN, L. I. 2006. High wear rates and extensive osteolysis in 3 types of uncemented total hip arthroplasty: a review of the PCA, the Harris Galante and the Profile/Tri-Lock Plus arthroplasties with a minimum of 12 years median follow-up in 96 hips. *Acta Orthopaedica,* 77**,** 575-84.

HAMADOUCHE, M., BOUTIN, P., DAUSSANGE, J., BOLANDER, M. E. & SEDEL, L. 2002. Alumina-on-alumina total hip arthroplasty: a minimum 18.5-year follow-up study. *Journal of Bone & Joint Surgery, American Volume,* 84-A**,** 69-77.

HARRIS, W. H. 1995. The problem is osteolysis. *Clinical Orthopaedics and Related Research*, 46-53.

HARRIS, W. H. 2001. Wear and periprosthetic osteolysis: the problem. *Clinical Orthopaedics and Related Research*, 66-70.

HARRIS, W. H. & PENENBERG, B. L. 1987. Further follow-up on socket fixation using a metal-backed acetabular component for total hip replacement. A minimum ten-year follow-up study. *Journal of Bone & Joint Surgery, American Volume,* 69, 1140-3.

HARRIS, W. H., SCHILLER, A. L., SCHOLLER, J. M., FREIBERG, R. A. & SCOTT, R. 1976. Extensive localized bone resorption in the femur following total hip replacement. *Journal of Bone & Joint Surgery, American Volume,* 58, 612-8.

HENDRIX, R. W., WIXSON, R. L., RANA, N. A. & ROGERS, L. F. 1983. Arthrography after total hip arthroplasty: a modified technique used in the diagnosis of pain. *Radiology,* 148, 647-52.

HERNIGOU, P., ZILBER, S., FILIPPINI, P. & POIGNARD, A. 2009. Ceramic-ceramic bearing decreases osteolysis: a 20-year study versus ceramic-polyethylene on the contralateral hip. *Clinical Orthopaedics and Related Research,* 467, 2274-80.

HLAVACEK, M. 2001. The thixotropic effect of the synovial fluid in squeeze-film lubrication of the human hip joint. *Biorheology,* 38, 319-34.

HOLZER, A., SCHRODER, C., WOICZINSKI, M., SADOGHI, P., MULLER, P. E. & JANSSON, V. 2012. The transport of wear particles in the prosthetic hip joint: A computational fluid dynamics investigation. *Journal of Biomechanics*.

HORI, R. Y. & LEWIS, J. L. 1982. Mechanical properties of the fibrous tissue found at the bone-cement interface following total joint replacement. *Journal of Biomedical Materials Research,* 16, 911-27.

HOROWITZ, S. M., DOTY, S. B., LANE, J. M. & BURSTEIN, A. H. 1993. Studies of the mechanism by which the mechanical failure of polymethylmethacrylate leads to bone resorption. *Journal of Bone & Joint Surgery, American Volume,* 75, 802-13.

HOWIE, D. W., VERNON-ROBERTS, B., OAKESHOTT, R. & MANTHEY, B. 1988. A rat model of resorption of bone at the cement-bone interface in the presence of polyethylene wear particles. *Journal of Bone & Joint Surgery, American Volume,* 70, 257-63.

INGHAM, E. & FISHER, J. 2000. Biological reactions to wear debris in total joint replacement. *Proceedings of the Institution of Mechanical Engineers, Part H: Journal of Engineering in Medicine,* 214, 21-37.

JACOB, H. A., HUGGLER, A. H., DIETSCHI, C. & SCHREIBER, A. 1976. Mechanical function of subchondral bone as experimentally determined on the acetabulum of the human pelvis. *Journal of Biomechanics,* 9, 625-7.

JAMIESON, M. L., RUSSELL, R. D., INCAVO, S. J. & NOBLE, P. C. 2010. Does an enhanced surface finish improve acetabular fixation in revision total hip arthroplasty? *Journal of Arthroplasty*.

JAYSON, M. D. A. J. 1970. Intra-articular pressure in rheumatoid arthritis of the knee. II. Effect of intra-articular pressure on blood circulation to the synovium. *Annals of the Rheumatic Diseases,* 29, 266-8.

JOHANSSON, L., EDLUND, U., FAHLGREN, A. & ASPENBERG, P. 2009. Bone resorption induced by fluid flow. *Journal of Biomechanical Engineering,* 131, 094505.

JOHNSTON, J. D., NOBLE, P. C., HURWITZ, D. E. & ANDRIACCHI, T. P. 2000. Biomechanics of the Hip. *In:* BRONZINO, J. D. (ed.) *The Biomedical Engineering Handbook.* 2 ed. Boca Raton: CRC Press LLC.

JONES, L. C., FRONDOZA, C. & HUNGERFORD, D. S. 2001. Effect of PMMA particles and movement on an implant interface in a canine model. *Journal of Bone & Joint Surgery, British Volume,* 83, 448-58.

KANEKO, I., MOGAMI, IWASE 2000. The initial fixation of press-fit acetabular socket. Its clinical observation and fundamental study. *European Journal of Orthopaedic Surgery & Traumatology,* 10.

KESTIN, J., KHALIFA, H. E. & CORREIA, R. J. 1981. Tables of the Dynamic and Kinematic Viscosity of Aqueous NaCl Solutions in the Temperature Range 20-150° C and the Pressure Range 0.1-35 MPa. *Journal of Physical and Chemical Reference Data,* 10**,** 71-87.

KHALILY, C., TANNER, M. G., WILLIAMS, V. G. & WHITESIDE, L. A. 1998. Effect of locking mechanism on fluid and particle flow through modular acetabular components. *Journal of Arthroplasty,* 13**,** 254-8.

KIAER, T. 1994. Bone perfusion and oxygenation. Animal experiments and clinical observations. *Acta Orthopaedica Scandinavica. Supplementum,* 257**,** 1-41.

KIENAPFEL, H., SPREY, C., WILKE, A. & GRISS, P. 1999. Implant fixation by bone ingrowth. *Journal of Arthroplasty,* 14**,** 355-368.

KITAMURA, N., NAUDIE, D. D. R., LEUNG, S. B., HOPPER, R. H., JR. & ENGH, C. A., SR. 2005. Diagnostic features of pelvic osteolysis on computed tomography: the importance of communication pathways. *Journal of Bone & Joint Surgery, American Volume,* 87**,** 1542-1550.

KOBAYASHI, A., FREEMAN, M. A., BONFIELD, W., KADOYA, Y., YAMAC, T., AL-SAFFAR, N., SCOTT, G. & REVELL, P. A. 1997. Number of polyethylene particles and osteolysis in total joint replacements. A quantitative study using a tissue-digestion method. *Journal of Bone & Joint Surgery, British Volume,* 79**,** 844-8.

KOMISTEK, R. D., DENNIS, D. A. & MAHFOUZ, M. R. 2000. Kinematics of the hip. *In:* BRONZINO, J. D. (ed.) *The Biomedical Engineering Handbook.* 2 ed. Boca Raton: CRC Press LLC.

KOSEKI, H., MATSUMOTO, T., ITO, S., DOUKAWA, H., ENOMOTO, H. & SHINDO, H. 2005. Analysis of polyethylene particles isolated from periprosthetic tissue of loosened hip arthroplasty and comparison with radiographic appearance. *Journal of Orthopaedic Science,* 10**,** 284-90.

KUBO, T., SAWADA, K., HIRAKAWA, K., SHIMIZU, C., TAKAMATSU, T. & HIRASAWA, Y. 1999. Histiocyte reaction in rabbit femurs to UHMWPE, metal, and ceramic particles in different sizes. *Journal of Biomedical Materials Research,* 45**,** 363-369.

KURTZ, S., ONG, K., LAU, E., MOWAT, F. & HALPERN, M. 2007. Projections of primary and revision hip and knee arthroplasty in the United States from 2005 to 2030. *Journal of Bone & Joint Surgery, American Volume,* 89**,** 780-5.

KURTZ, S. M., HARRIGAN, T. P., HERR, M. & MANLEY, M. T. 2005. An *in vitro* model for fluid pressurization of screw holes in metal-backed total joint components. *Journal of Arthroplasty,* 20**,** 932-938.

LANDGRAEBER, S., VON KNOCH, M., LÖER, F., WEGNER, A., TSOKOS, M., HUßMANN, B. & TOTSCH, M. 2008. Extrinsic and intrinsic pathways of apoptosis in aseptic loosening after total hip replacement. *Biomaterials,* 29**,** 3444-3450.

LEUNG, S., NAUDIE, D., KITAMURA, N., WALDE, T. & ENGH, C. A. 2005. Computed tomography in the assessment of periacetabular osteolysis. *Journal of Bone & Joint Surgery, American Volume,* 87**,** 592-7.

LEUNG, S. B., EGAWA, H., STEPNIEWSKI, A., BEYKIRCH, S., ENGH JR, C. A. & ENGH SR, C. A. 2007. Incidence and volume of pelvic osteolysis at early follow-up with highly cross-linked and noncross-linked polyethylene. *Journal of Arthroplasty,* 22**,** 134-139.

LEVICK, J. R. 1983. Joint pressure-volume studies: their importance, design and interpretation. *Journal of Rheumatology,* 10**,** 353-7.

LIBOUBAN, H., MASSIN, P., GAUDIN, C., MERCIER, P., BASLE, M. F. & CHAPPARD, D. 2009. Migration of wear debris of polyethylene depends on bone microarchitecture. *Journal of Biomedical Materials Research Part B-Applied Biomaterials,* 90**,** 730-7.

LIDE, D. R. 1991. *Handbook of Chemistry and Physics*, CRC Press, Inc.

LING, R. S. 1986. Observations on the fixation of implants to the bony skeleton. *Clinical Orthopaedics and Related Research***,** 80-96.

LING, R. S., LEE, A. J. C., GIE, G. A., TIMPERLEY, A. J., HUBBLE, M. J. W., HOWELL, J. R. & WHITEHOUSE, S. L. 2010. *The Exeter Hip: 40 Years of Innovation in Total Hip Arthroplasty*, Exeter Hip Publishing.

LLOYD-ROBERTS, G. C. 1953. The role of capsular changes in osteoarthritis of the hip joint. *Journal of Bone & Joint Surgery, British Volume,* 35-B**,** 627-42.

LOMBARDI, A. V., JR., MALLORY, T. H., DENNIS, D. A., KOMISTEK, R. D., FADA, R. A. & NORTHCUT, E. J. 2000. An *in vivo* determination of total hip arthroplasty pistoning during activity. *Journal of Arthroplasty,* 15**,** 702-9.

LUNDBERG, H. J., PEDERSEN, D. R., BAER, T. E., MUSTE, M., CALLAGHAN, J. J. & BROWN, T. D. 2007. Effects of implant design parameters on fluid convection, potentiating third-body debris ingress into the bearing surface during THA impingement/subluxation. *Journal of Biomechanics,* 40**,** 1676-85.

MACDONALD, W., CARLSSON, L. V., CHARNLEY, G. J. & JACOBSSON, C. M. 1999. Press-fit acetabular cup fixation: principles and testing. *Proceedings of the Institution of Mechanical Engineers, Part H: Journal of Engineering in Medicine,* 213**,** 33-9.

MACQUARRIE, R. A., FANG CHEN, Y., COLES, C. & ANDERSON, G. I. 2004. Wear-particle-induced osteoclast osteolysis: the role of particulates and mechanical strain. *Journal of Biomedical Materials Research Part B-Applied Biomaterials,* 69**,** 104-12.

MALONEY, W., GALANTE, J., ANDERSON, M., GOLDBERG, V., HARRIS, W., JACOBS, J., KRAAY, M., LACHIEWICZ, P., RUBASH, H., SCHUTZER, S. & WOOLSON, S. 1999. Acetabular fixation in primary total hip arthroplasty. *Clinical Orthopaedics and Related Research,* 369**,** 157-164.

MANLEY, M. T., D'ANTONIO, J. A., CAPELLO, W. N. & EDIDIN, A. A. 2002. Osteolysis: a disease of access to fixation interfaces. *Clinical Orthopaedics and Related Research***,** 129-37.

MANN, K. A., WERNER, F. W. & AYERS, D. C. 1999. Mechanical strength of the cement-bone interface is greater in shear than in tension. *Journal of Biomechanics,* 32**,** 1251-4.

MASSIN, P., VANDENBUSSCHE, E., LANDJERIT, B. & AUGEREAU, B. 1996. Experimental study of periacetabular deformations before and after implantation of hip prostheses. *Journal of Biomechanics,* 29**,** 53-61.

MCEVOY, A., JEYAM, M., FERRIER, G., EVANS, C. E. & ANDREW, J. G. 2002. Synergistic effect of particles and cyclic pressure on cytokine production in human monocyte/macrophages: proposed role in periprosthetic osteolysis. *Bone,* 30**,** 171-7.

MERKEL, K. D., ERDMANN, J. M., MCHUGH, K. P., ABU-AMER, Y., ROSS, F. P. & TEITELBAUM, S. L. 1999. Tumor Necrosis Factor-α Mediates Orthopedic Implant Osteolysis. *American Journal of Pathology,* 154**,** 203-210.

MJOBERG, B. 1994. Theories of wear and loosening in hip prostheses. Wear-induced loosening vs loosening-induced wear--a review. *Acta Orthopaedica Scandinavica,* 65**,** 361-71.

MORSCHER, E. W. 1992. Current status of acetabular fixation in primary total hip arthroplasty. *Clinical Orthopaedics and Related Research***,** 172-93.

MORSHED, S., BOZIC, K. J., RIES, M. D., MALCHAU, H. & COLFORD, J. M. 2007. Comparison of cemented and uncemented fixation in total hip replacement. *Acta Orthopaedica,* 78**,** 315-326.

MOSKOWITZ, R. W. 2007. Osteoarthritis: diagnosis and medical/surgical management. *In:* MOSKOWITZ, R. W. (ed.) 4 ed. Philadelphia: Wolters Kluwer / Lippincott Williams & Wilkins.

MULLINS, M. M., NORBURY, W., DOWELL, J. K. & HEYWOOD-WADDINGTON, M. 2007. Thirty-year results of a prospective study of Charnley total hip arthroplasty by the posterior approach. *Journal of Arthroplasty,* 22**,** 833-9.

MULROY, R. D., JR. & HARRIS, W. H. 1990. The effect of improved cementing techniques on component loosening in total hip replacement. An 11-year radiographic review. *Journal of Bone & Joint Surgery, British Volume,* 72**,** 757-60.

MULROY, W. F. & HARRIS, W. H. 1996. Revision total hip arthroplasty with use of so-called second-generation cementing techniques for aseptic loosening of the femoral component. A fifteen-year-average follow-up study. *Journal of Bone & Joint Surgery, American Volume,* 78**,** 325-30.

MURPHY, L. B., HELMICK, C. G., SCHWARTZ, T. A., RENNER, J. B., TUDOR, G., KOCH, G. G., DRAGOMIR, A. D., KALSBEEK, W. D., LUTA, G. & JORDAN, J. M. 2010. One in four people may develop symptomatic hip osteoarthritis in his or her lifetime. *Osteoarthritis and Cartilage,* 18**,** 1372-1379.

MURRAY, D. W. & RUSHTON, N. 1990. Macrophages stimulate bone resorption when they phagocytose particles. *Journal of Bone & Joint Surgery, British Volume,* 72**,** 988-92.

NASHED, R. S., BECKER, D. A. & GUSTILO, R. B. 1995. Are cementless acetabular components the cause of excess wear and osteolysis in total hip arthroplasty? *Clinical Orthopaedics and Related Research***,** 19-28.

NJR 2012. National Joint Registry for England and Wales, 9th Annual Report 2012. NJR.

NORDIN, M. & FRANKEL, V. H. 2001. *Basic biomechanics of the musculoskeletal system,* Philadelphia, PA, Lippincott, Williams and Wilkins.

NOUREDDINI, H., TEOH, B. & DAVIS CLEMENTS, L. 1992. Viscosities of vegetable oils and fatty acids. *Journal of the American Oil Chemists' Society,* 69**,** 1189-1191.

NZOA 2012. New Zealand Joint Registry Thirteen Year Report: January 1999 to December 2011. New Zealand Orthopaedic Association.

OLORY, B., HAVET, E., GABRION, A., VERNOIS, J. & MERTL, P. 2004. Comparative *in vitro* assessment of the primary stability of cementless press-fit acetabular cups. *Acta Orthopaedica Belgica,* 70**,** 31-7.

PAPAGELOPOLOUS, P. J. & MORREY, B. F. 2003. Cemented Acetabular Components. *In:* MORREY, B. F. (ed.) *Joint Replacement Arthroplasty.* 3rd ed.: Churchill-Livingstone.

PEDERSEN, D. R., CROWNINSHIELD, R. D., BRAND, R. A. & JOHNSTON, R. C. 1982. An axisymmetric model of acetabular components in total hip arthroplasty. *Journal of Biomechanics,* 15**,** 305-15.

PERREN, S. M. 2002. Evolution of the internal fixation of long bone fractures. The scientific basis of biological internal fixation: choosing a new balance between stability and biology. *Journal of Bone & Joint Surgery, British Volume,* 84**,** 1093-110.

PLUOT, E., DAVIS, E. T., REVELL, M., DAVIES, A. M. & JAMES, S. L. J. 2009. Hip arthroplasty. Part 1: prosthesis terminology and classification. *Clinical Radiology,* 64**,** 954-960.

RITTER, M. A., CARR, K., HERBST, S. A., EIZEMBER, L. E., KEATING, E. M., FARIS, P. M. & MEDING, J. B. 1996. Outcome of the contralateral hip following total hip arthroplasty for osteoarthritis. *Journal of Arthroplasty,* 11**,** 242-246.

RITTER, M. A., KEATING, E. M., FARIS, P. M. & BRUGO, G. 1990. Metal-backed acetabular cups in total hip arthroplasty. *Journal of Bone & Joint Surgery, American Volume,* 72**,** 672-7.

ROBERTSON, D. D., SUTHERLAND, C. J., LOPES, T. & YUAN, J. 1998. Preoperative description of severe acetabular defects caused by failed total hip replacement (vol 22, pg 444, 1998). *Journal of Computer Assisted Tomography,* 22**,** CP4-CP4.

ROBERTSSON, O., WINGSTRAND, H., KESTERIS, U., JONSSON, K. & ONNERFALT, R. 1997. Intracapsular pressure and loosening of hip prostheses. Preoperative measurements in 18 hips. *Acta Orthopaedica Scandinavica,* 68**,** 231-4.

ROBERTSSON, O., WINGSTRAND, H. & ONNERFALT, R. 1995. Intracapsular pressure and pain in coxarthrosis. *Journal of Arthroplasty,* 10**,** 632-5.

ROPES, M. W., BENNETT, G. A. & BAUER, W. 1939. The origin and nature of normal synovial fluid. *The Journal of Clinical Investigation,* 18**,** 351-372.

ROPES, M. W., ROSSMEISL, E. C. & BAUER, W. 1940. The origin and nature of normal human synovial fluid. *The Journal of Clinical Investigation,* 19**,** 795-799.

SAMPATHKUMAR, K., JEYAM, M., EVANS, C. E. & ANDREW, J. G. 2003. Role of cyclical pressure and particles in the release of M-CSF, chemokines, and PGE2 and their role in loosening of implants. *Journal of Bone & Joint Surgery, British Volume,* 85**,** 288-91.

SARA, B., JOAO, F., PAULO, R. F. & JACINTO, M. The Influence of the Pelvic Bone on the Computational Results of the Acetabular Component of a Total Hip Prosthesis. *Journal of Biomechanical Engineering,* 132**,** 054503.

SCHMALZRIED, T. P. 2007. Why Total Hip Resurfacing. *Journal of Arthroplasty,* 22**,** 57-60.

SCHMALZRIED, T. P., BROWN, I. C., AMSTUTZ, H. C., ENGH, C. A. & HARRIS, W. H. 1999. The role of acetabular component screw holes and/or screws in the development of pelvic osteolysis. *Proceedings of the Institution of Mechanical Engineers, Part H: Journal of Engineering in Medicine,* 213**,** 147-53.

SCHMALZRIED, T. P., FOWBLE, V. A. & AMSTUTZ, H. C. 1998. The fate of pelvic osteolysis after reoperation. No recurrence with lesional treatment. *Clinical Orthopaedics and Related Research***,** 128-37.

SCHMALZRIED, T. P., JASTY, M. & HARRIS, W. H. 1992a. Periprosthetic bone loss in total hip arthroplasty. Polyethylene wear debris and the concept of the effective joint space. *Journal of Bone & Joint Surgery, American Volume,* 74**,** 849-63.

SCHMALZRIED, T. P., KWONG, L. M., JASTY, M., SEDLACEK, R. C., HAIRE, T. C., O'CONNOR, D. O., BRAGDON, C. R., KABO, J. M., MALCOLM, A. J. & HARRIS, W. H. 1992b. The mechanism of loosening of cemented acetabular components in total hip arthroplasty. Analysis of specimens retrieved at autopsy. *Clinical Orthopaedics and Related Research***,** 60-78.

SCHULTE, K. R., CALLAGHAN, J. J., KELLEY, S. S. & JOHNSTON, R. C. 1993. The outcome of Charnley total hip arthroplasty with cement after a minimum twenty-year follow-up. The results of one surgeon. *Journal of Bone & Joint Surgery, American Volume,* 75**,** 961-75.

SINGH, M., CHAND, H. & GUPTA, K. C. 2005. The Studies of Density, Apparent Molar Volume, and Viscosity of Bovine Serum Albumin, Egg Albumin, and Lysozyme in Aqueous and RbI, CsI, and DTAB Aqueous Solutions at 303.15 K. *Chemistry & Biodiversity,* 2**,** 809-824.

SKOGLUND, B. & ASPENBERG, P. 2003a. PMMA particles and pressure--a study of the osteolytic properties of two agents proposed to cause prosthetic loosening. *Journal of Orthopaedic Research,* 21**,** 196-201.

SKOGLUND, B. & ASPENBERG, P. 2003b. PMMA particles and pressure—a study of the osteolytic properties of two agents proposed to cause prosthetic loosening. *Journal of Orthopaedic Research,* 21**,** 196-201.

SKRIPITZ, R. & ASPENBERG, P. 2000. Pressure-induced periprosthetic osteolysis: a rat model. *Journal of Orthopaedic Research,* 18**,** 481-4.

SOTO-HALL, R., JOHNSON, L. H. & JOHNSON, R. A. 1964. Variations in the intra-articular pressure of the hip joint in injury and disease. A probable factor in avascular necrosis. *Journal of Bone & Joint Surgery, American Volume,* 46**,** 509-16.

SPECTOR, M., SHORTKROFF, S., HSU, H. P., LANE, N., SLEDGE, C. B. & THORNHILL, T. S. 1990. Tissue changes around loose prostheses. A canine model to investigate the effects of an antiinflammatory agent. *Clinical Orthopaedics and Related Research***,** 140-52.

STAMENKOV, R. B., HOWIE, D. W., NEALE, S. D., MCGEE, M. A., TAYLOR, D. J. & FINDLAY, D. M. 2010. Distribution of periacetabulorosteolytic lesions varies according to component design. *Journal of Arthroplasty,* 25**,** 913-919.

STANSFIELD, B. W., NICOL, A. C., PAUL, J. P., KELLY, I. G., GRAICHEN, F. & BERGMANN, G. 2003. Direct comparison of calculated hip joint contact forces with those measured using instrumented implants. An evaluation of a three-dimensional mathematical model of the lower limb. *Journal of Biomechanics,* 36**,** 929-36.

STAUFFER, R. N. 1982. Ten-year follow-up study of total hip replacement. *Journal of Bone & Joint Surgery, American Volume,* 64**,** 983-90.

SZIVEK, J. A., THOMPSON, J. D. & BENJAMIN, J. B. 1995. Characterization of three formulations of a synthetic foam as models for a range of human cancellous bone types. *Journal of Applied Biomaterials,* 6**,** 125-8.

SZUSZCZEWICZ, E. S., SCHMALZRIED, T. P. & PETERSEN, T. D. 1997. Progressive bilateral pelvic osteolysis in a patient with McKee--Farrar metal--metal total hip prostheses. *Journal of Arthroplasty,* 12**,** 819-824.

TACHDJIAN, M. O. & GRANA, L. 1968. Response of the hip joint to increased intra-articular hydrostatic pressure. *Clinical Orthopaedics and Related Research,* 61**,** 199-212.

TARASEVICIUS, S., KESTERIS, U., GELMANAS, A., SMAILYS, A. & WINGSTRAND, H. 2007. Intracapsular pressure and elasticity of the hip joint capsule in osteoarthritis. *Journal of Arthroplasty,* 22**,** 596-600.

THIRIET, M. 2008. Rheology. *Biology and Mechanics of Blood Flows.* Springer New York.

TOMPKINS, G. S., JACOBS, J. J., KULL, L. R., ROSENBERG, A. G. & GALANTE, J. O. 1997. Primary total hip arthroplasty with a porous-coated acetabular component. Seven-to-ten-year results. *Journal of Bone & Joint Surgery, American Volume,* 79**,** 169-76.

TONG, J., ZANT, N. P., WANG, J. Y., HEATON-ADEGBILE, P. & HUSSELL, J. G. 2008. Fatigue in cemented acetabular replacements. *International Journal of Fatigue,* 30**,** 1366-1375.

UDOFIA, I. J., YEW, A. & JIN, Z. M. 2004. Contact mechanics analysis of metal-on-metal hip resurfacing prostheses. *Proceedings of the Institution of Mechanical Engineers, Part H: Journal of Engineering in Medicine,* 218**,** 293-305.

VAN DER VIS, H., ASPENBERG, P., DE KLEINE, R., TIGCHELAAR, W. & VAN NOORDEN, C. J. 1998a. Short periods of oscillating fluid pressure directed at a titanium-bone interface in rabbits lead to bone lysis. *Acta Orthopaedica Scandinavica,* 69**,** 5-10.

VAN DER VIS, H. M., ASPENBERG, P., MARTI, R. K., TIGCHELAAR, W. & VAN NOORDEN, C. J. 1998b. Fluid pressure causes bone resorption in a rabbit model of prosthetic loosening. *Clinical Orthopaedics and Related Research***,** 201-8.

VAN DER VIS, H. M., ASPENBERG, P., TIGCHELAAR, W. & VAN NOORDEN, C. J. 1999. Mechanical compression of a fibrous membrane surrounding bone causes bone resorption. *Acta Histochemica,* 101**,** 203-12.

WAIDE, V., CRISTOFOLINI, L., STOLK, J., VERDONSCHOT, N., BOOGAARD, G. J. & TONI, A. 2004a. Modelling the fibrous tissue layer in cemented hip replacements: experimental and finite element methods. *Journal of Biomechanics,* 37**,** 13-26.

WAIDE, V., CRISTOFOLINI, L. & TONI, A. 2004b. An experimental analogue to model the fibrous tissue layer in cemented hip replacements. *Journal of Biomedical Materials Research Part B-Applied Biomaterials,* 69**,** 232-40.

WALDE, T. A., WEILAND, D. E., LEUNG, S. B., KITAMURA, N., SYCHTERZ, C. J., ENGH, C. A., CLAUS, A. M. & POTTER, H. G. 2005. Comparison of CT, MRI, and radiographs in assessing pelvic osteolysis - A cadaveric study. *Clinical Orthopaedics and Related Research***,** 138-144.

WALTER, W. L., CLABEAUX, J., WRIGHT, T. M., WALSH, W., WALTER, W. K. & SCULCO, T. P. 2005. Mechanisms for pumping fluid through cementless acetabular components with holes. *Journal of Arthroplasty,* 20**,** 1042-1048.

WALTER, W. L., WALTER, W. K. & O'SULLIVAN, M. 2004. The pumping of fluid in cementless cups with holes. *Journal of Arthroplasty,* 19**,** 230-4.

WANG, J. Y., HEATON-ADEGBILE, P., NEW, A., HUSSELL, J. G. & TONG, J. 2009. Damage evolution in acetabular replacements under long-term physiological loading conditions. *Journal of Biomechanics,* 42**,** 1061-1068.

WEINANS, H., HUISKES, R. & GROOTENBOER, H. J. 1990. Trends of mechanical consequences and modeling of a fibrous membrane around femoral hip prostheses. *Journal of Biomechanics,* 23**,** 991-1000.

WIKIPEDIA. 2006. *Muscles of the hip* [Online]. Available: http://en.wikipedia.org/wiki/Muscles_of_the_hip [Accessed 23.11.2012 2012].

WILLERT, H. G., BERTRAM, H. & BUCHHORN, G. H. 1990. Osteolysis in alloarthroplasty of the hip. The role of bone cement fragmentation. *Clinical Orthopaedics and Related Research***,** 108-21.

WILLIAMS, H. D., BROWNE, G., GIE, G. A., LING, R. S., TIMPERLEY, A. J. & WENDOVER, N. A. 2002. The Exeter universal cemented femoral component at 8 to 12 years. A study of the first 325 hips. *Journal of Bone & Joint Surgery, British Volume,* 84**,** 324-34.

WINGSTRAND, H., WINGSTRAND, A. & KRANTZ, P. 1990. Intracapsular and atmospheric pressure in the dynamics and stability of the hip. A biomechanical study. *Acta Orthopaedica Scandinavica,* 61**,** 231-5.

WON, C. H., HEARN, T. C. & TILE, M. 1995. Micromotion of cementless hemispherical acetabular components. Does press-fit need adjunctive screw fixation? *Journal of Bone & Joint Surgery, British Volume,* 77**,** 484-9.

WRIGHT, S., SYDNEY, S. E. & MILES, A. W. Synthetic material to replicate fibrous tissue occurring in joint replacement. European Orthopaedic Research Society, 2012 Amsterdam.

YAMAGUCHI, M., BAUER, T. W. & HASHIMOTO, Y. 1999. Deformation of the acetabular polyethylene liner and the backside gap. *Journal of Arthroplasty,* 14**,** 464-469.

ZIMLICH, R. H. & FEHRING, T. K. 2000. Underestimation of pelvic osteolysis - The value of the iliac oblique radiograph. *Journal of Arthroplasty,* 15**,** 796-801.

Appendices

Appendix 1: Validation of pressure measurement technique

A preliminary pilot study was completed, to determine whether pressure could be measured through 'worst-case' conditions – ie in a completely loose cup. *In vivo* elements were modelled using the methods outlined in the figure below:

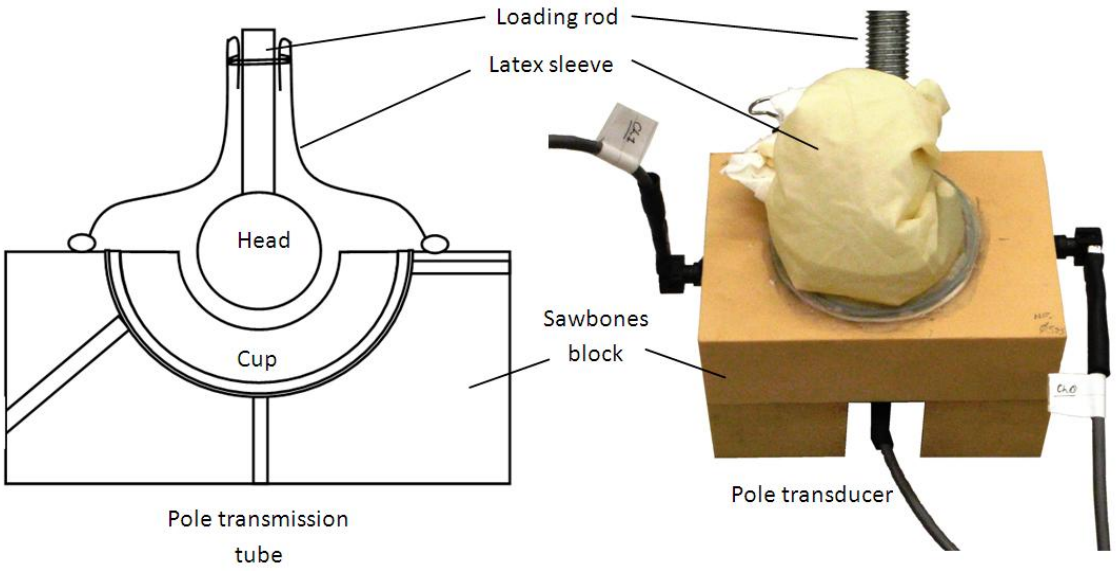

Joint capsule (latex sleeve sealed with Silicone sealant)
Implant (Stryker Opera PE cup, with flange, ID 28mm, ED 43mm, and 28mm SS femoral head).
Joint fluid (60mL water-soluble coolant fluid)
Fixation (Simplex P bone cement used to make a fully loose cement mantle. Thin latex film was used as a fibrous membrane analogue for some tests.)
Bone analogue (30 pcf Sawbones, reamed to 54mm)
Loading (1Hz cyclic axial load (0 – 1000N) applied to loading rod by Instron hydraulic test machine for 50 cycles).

Instrumentation

The output of the experiment (i.e. degree of fluid pressure) must be able to be measured. Before assembly in the model, screw holes were tapped into the sawbones block at the dome, periphery and midpoint of the cavity. Pressure transducers (RS 100psi gauge transducers', RS Electronics, UK) were screwed into holes which were then filled with silicone grease to allow

pressure transmission from the interface. Transducers were calibrated and then connected via cables to a PC with data acquisition card. Data collection was performed using a program with the HP VEE software, with the output from the transducers in Volts. Data were analysed in Microsoft Excel. Pressure results were calculated in Microsoft Excel using calibration factors.

Results:

Test 1: without latex membrane

Model was loaded using the Instron and pressure results were recorded (Figure 134). Pressure at the dome was highest and pressure at the periphery was lowest. The pressure peaks for the periphery were slightly out of phase, occurring 1/6 of a cycle earlier than the dome or midpoint peaks.

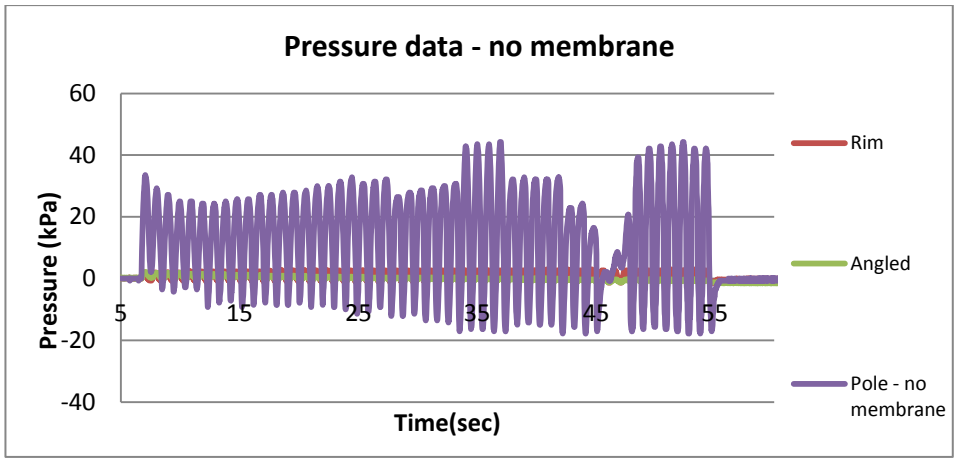

Figure 134: Pressure data recorded in tests without a membrane

The loading head adhered to the cup component during tests and it was difficult to separate the two after testing was completed.

Test 2: 2-3mm latex membrane

Again, pressure at the dome was highest and pressure at the rim was lowest (Figure 135).

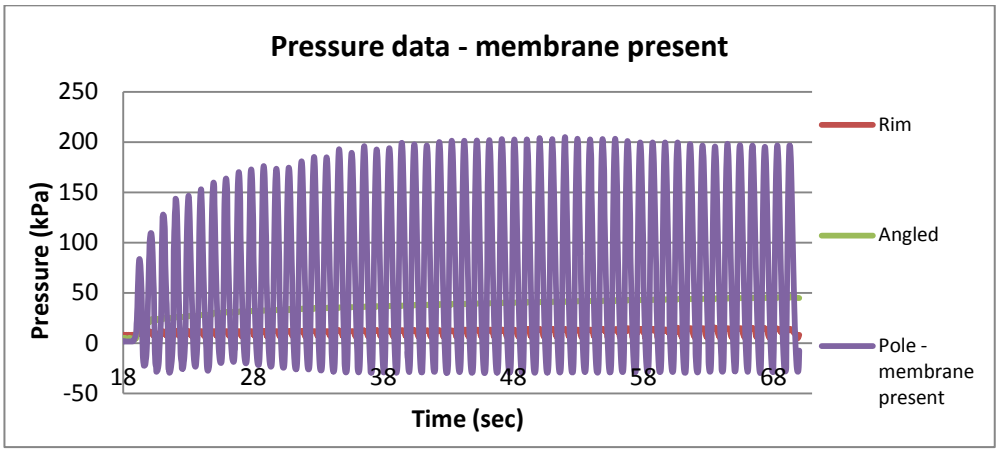

Figure 135: Pressure data recorded in tests with a latex membrane

Again, the head-cup adhesion after this test was very strong and significant force was required to separate the two components after loading. Much greater pole pressures were measured in the presence of a latex membrane (204.3kPa) compared to tests without a membrane (42.9kPa). This is shown in the graph in Figure 136.

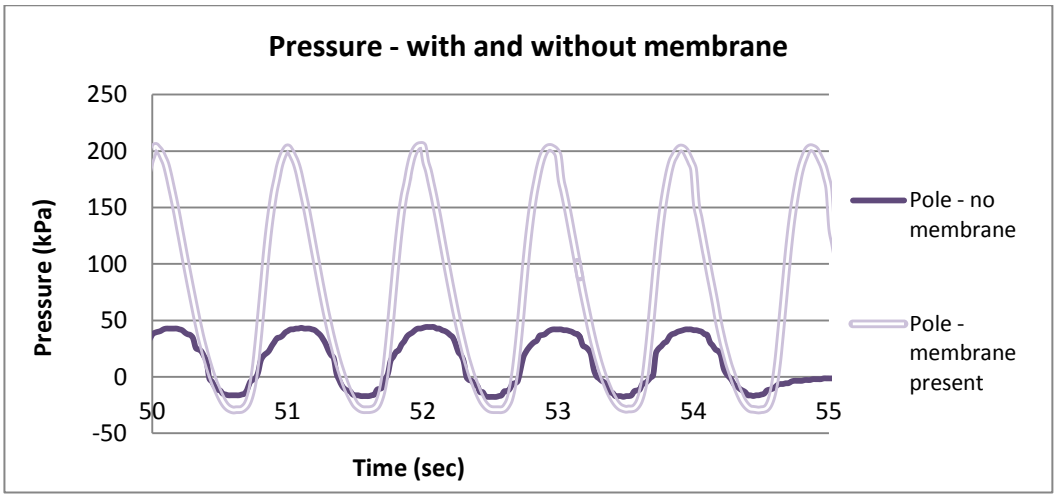

Figure 136: Comparison of pole pressure signal measured with and without latex membrane

Repeatability

To test repeatability of the system, the rig was disassembled, reassembled and re-tested, twice, with an improved capsule system. In both tests, the seals failed, preventing comparison with previous results.

Discussion

The model showed that, in a simple model of a completely loose cemented cup, positive and negative fluid pressures can be measured behind the acetabular component. Clear effects of the presence of a membrane on pressure behind a loose cup can also be observed. It appears

that the membrane is acting as a 'diaphragm', amplifying pressure waves behind the cup component. Adhesion of the head onto the cup after loading has been observed in this pilot study and should be taken into account in future tests. The sealing issues demonstrate the need for a mechanical seal rather than a chemical (silicone) seal on the rig.

The appropriateness of a flexible capsule was questionable, as it was possible that the deformation of the capsule was causing pressure waves in the silicone grease. The Sawbones block material was only available in expensive preformed blocks, and questions of its appropriateness for use also arose. Under load, even in the absence of components or vegetable oil, pressure waves could be recorded in the silicone grease as the block deformed.

Conclusions:

The current physical model proved it was possible to measure pressure behind a loose cup when load is applied. The rig performs these functions adequately but the model does have several issues, notably the inadequate simulation of *in vivo* conditions and in the lack of repeatability between tests. To address these problems, a new rig design was developed for further testing (Appendix 2).

Appendix 2 – Testing Epoxy hemisphere, flexible tubing

Pilot rig 2: Validation of use of pressure transmission tube

The following questions were posed, following the initial pilot study:

1) Can fluid pressure be measured through flexible tubes?
2) Can an alternative material be used as a bone analogue?
3) What effect does a latex membrane have on pressure signal?
4) What effect does the fit of the implant have on pressure signal?

To find answers to these questions, another test rig was developed, and its features are described in the figure below.

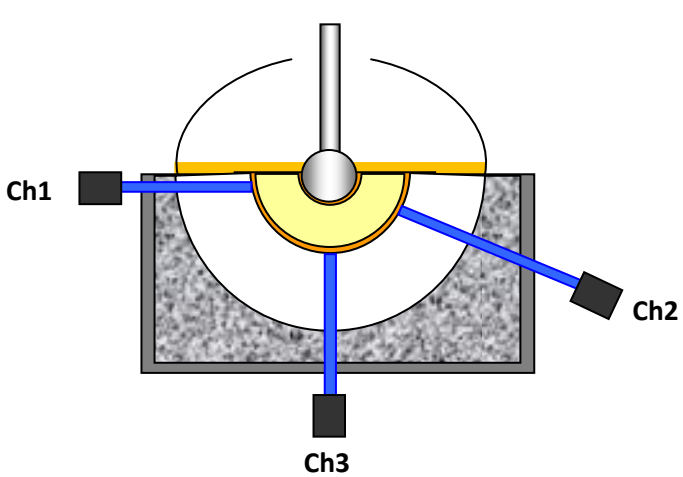

Joint capsule - plastic hemisphere to constrain oil, with hole for loading
Implant -Stryker Contemporary PE cup(ID 28mm, ED 48mm); Smith & Nephew Opera cup with flange, (ID 28mm, ED 43mm, with thin cement mantle attached); and 28mm SS femoral head).
Joint fluid - vegetable oil
Fixation –loose cement mantle, Simplex P bone cement. Some tests with latex film as membrane analogue.
Bone analogue (epoxy foam, moulded into a 140mm diameter hemisphere)
Loading -1Hz cyclic axial load (0–1000N) applied to loading rod by Dartek hydraulic test machine, 50 cycles

Flexible hydraulic tubing was used to transmit pressures from the measurement interface to the transducers. The measurement system was the same as that described in Appendix 1. Two different implants were used – a Stryker Contemporary cup and a Smith & Nephew flanged Opera cup. The Opera cup had a thin cement mantle attached to it, however the fit between the Contemporary cup and the test cavity was better due to the larger external diameter.

Results

Sample pressure results are shown in the figure below.

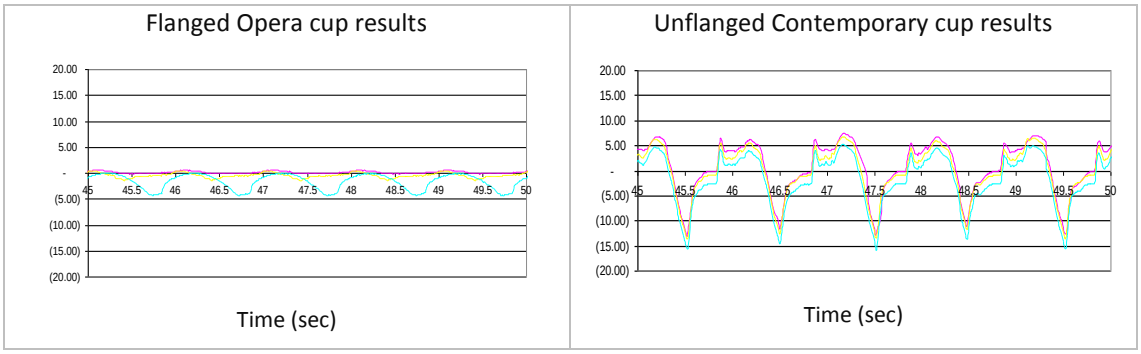

The 'fit' between cup and cavity had a large impact on results. The unflanged cup had a much smaller gap between cup and foam, and it always produced higher pressures than the flanged cup. Thus, a tighter-fit cup produced higher pressure waves, as the volume through which fluid can move was reduced. The improved fit between cup and hemisphere also led to all the channels being equally affected by pressure. When the cup only loosely fit into the cavities, all pressures were decreased and the rim and angled transducers registered smaller pressure changes. Again, head-cup adhesion was observed during this test series.

Discussion of rig performance

Flexible transmission tubes were able to transmit pressures, but results were variable. The transducers exhibited significant variations in resting pressures, suggesting a more reliable measurement system was required. The amount of oil in the rig was highly influential – if the amount of fluid was insufficient, transmission tubes were not completely full of oil and pressures could not be measured on the transducers.

The movement of the foam hemisphere relative to the rig was thought to affect pressures measured through transmission tubes. As shown in Figure 137, slight movement of the test hemisphere caused deformation of the tubes, leading to errors in pressure measurement . Furthermore, pressures at the end of all the tests were lower than at the start of the tests,

implying fluid losses due to leaks in the pressure transmission system. Therefore an alternative to these flexible transmission tubes was sought.

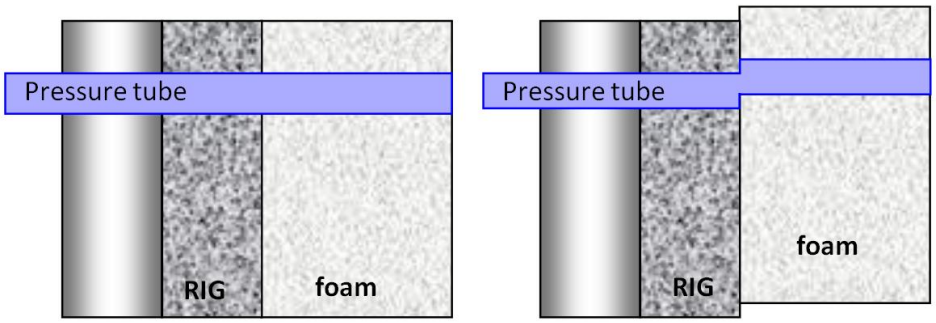

Figure 137: Effect of foam hemisphere movement relative to rig

The foam hemispheres, although able to withstand the applied loads, had variable properties due to the difficulties with moulding the material. A better bone analogue was required; the search for this new analogue is described in Appendix 3.

Conclusions

Tubing between the measurement interface and the transducer can transmit pressures, but flexible tubing is not appropriate for these tests. Moulded epoxy hemispheres have variable structural properties, making them inappropriate for further pressure testing.

Despite the problems with this rig design, a clear difference between pressures measured behind different cup designs was measured. Improvements to the bone analogue material, the pressure transmission/measurement system and rig sealing were required for further testing.

Appendix 3 – Testing bone analogue materials

Introduction

This section details the testing of several readily-available materials for suitability as a bone analogue for use in the APTR model.

Bone analogue materials used in pilot studies

Pilot studies described in Appendix 1 and Appendix 2 used sawbones closed-cell foam and moulded epoxy hemispheres respectively. Sawbones is a widely-used orthopaedic test material, and it was used due to its consistent material properties and its ubiquity as a bone substitute in orthopaedic mechanical testing.

However when it was decided that a hemispherical block would be used for testing, it was not possible to obtain the right sized materials from Sawbones. The decision to use a moulded epoxy hemisphere was made as it would be able to simulate bone porosity, as well as have appropriate mechanical properties. Tests with the epoxy hemispheres showed that while the material was able to withstand the applied loads, the hemispheres were difficult to mould; it was hard to get consistent moulding density and the internal structure was not repeatable. From these pilot studies, the need for a machinable material with controllable shape properties and a homogeneous intra- and inter-specimen internal structure was identified. Four new potential materials were obtained for testing.

Testing bone analogue materials

The following materials were obtained for testing:

1. Sawbones 30pcf closed-cell PU foam
2. JBB678 epoxy tooling board (John Burn, UK)
3. Sikablock M450 model board (John Burn, UK)
4. Sikablock M650 model board (John Burn, UK)

The material properties provided by the manufacturer of each of these materials are shown in Table 15, compared to the material properties of cortical and trabecular bone. (Nordin and Frankel, 2001, Udofia et al., 2004, Bronzino, 2000)

Table 15: Material properties of bone and analogue materials

	Density (g/cm^3)	Elastic modulus (GPa)	Compressive modulus (GPa)	Ultimate compressive strength (MPa)
Cortical	2	10-17		130-180
Trabecular	1	0.1 – 2.2		5-50
Sawbones 30 pcf	0.48	0.640	0.553	20
JBB678 tooling board	0.7	-	-	52
M450 model board	0.45	0.43	-	10*
M650 model board	0.58	0.7	-	17*

* at 10% compressive strain

To assess the suitability of these materials, test methods based on BS ISO standards for testing of plastics was developed. Due to the size of samples sent from the manufacturers, only a 50 x 37 x 13mm piece of material was available to complete the tests.

Hypothesis: one of these materials will have:

a) Elastic modulus in the acceptable range for bone (Test: compression)
b) Recoverable properties under cyclic loading (Test: cyclic compression)
c) Acceptable behaviour in 3-point bending (Test: 3-point bend test)
d) Good machinability (Test: qualitative assessment)

Test methods and results:

a) Properties in Compression

According to EN ISO 604:2003, the test specimens (50 x 10 x 5mm) were compressed along their major axis at 1mm/min until the specimens fractured. The load sustained by the specimen was measured during this procedure. Results are shown in Table 16.

Table 16: Results of compressive tests, compared with stated compressive values and bone modulus values

Material	Stated compressive strength (MPa)	Measured Compressive Strength (MPa)	Compressive Modulus (GPa)
Cortical bone	130-180	-	10-15
Trabecular bone	5-50	-	0.1-2.2
Sawbones 30pcf	20	**13.1**	0.250
JBB678 tooling board	52	**44.5**	0.929
M450 model board	10*	**7.8**	0.218
M650 model board	17*	**14.3**	0.356

*at 10% compressive strain

All the test materials had compressive strength and compressive modulus values within the range of trabecular bone. The Sawbones and M650 model board results from compression testing were very similar.

b) Recovery from compressive loading

Further compression tests were performed, to compare the degree of material recovery from deformation. The results of this analysis are shown in Figure 138.

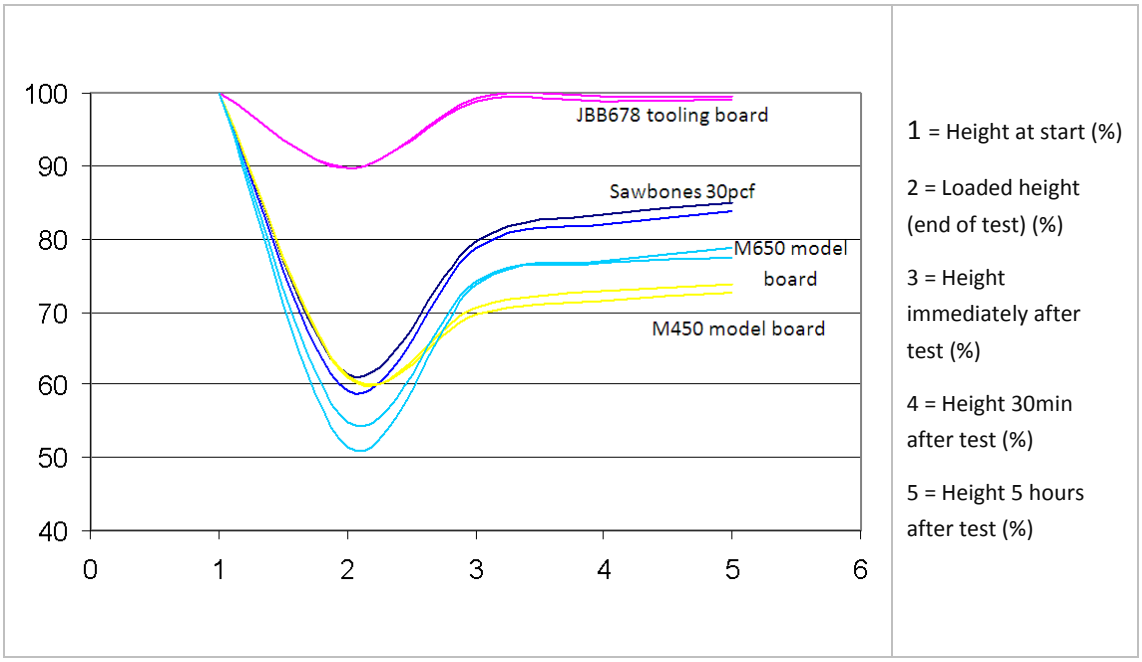

Figure 138: Recovery from compression

Although the JBB678 tooling board had the most complete recovery from loading, it was shown to be only slightly deformable – one of the desirable qualities of a bone substitute material. The material with the least recovery following loading was the M450, while Sawbones and M650 both produced intermediate levels of recovery, with the M650 undergoing the greatest deformation of the materials.

c) Flexion properties

According to EN ISO 178:2003, a three-point bending test was performed, with a test specimen size of 50 x 25 x 2.5mm. These specimens, supported as a beam, were deflected at 1mm/min at the mid-span until the specimen fractures and force applied to the test specimen was measured. Results of this testing are shown in Figure 139.

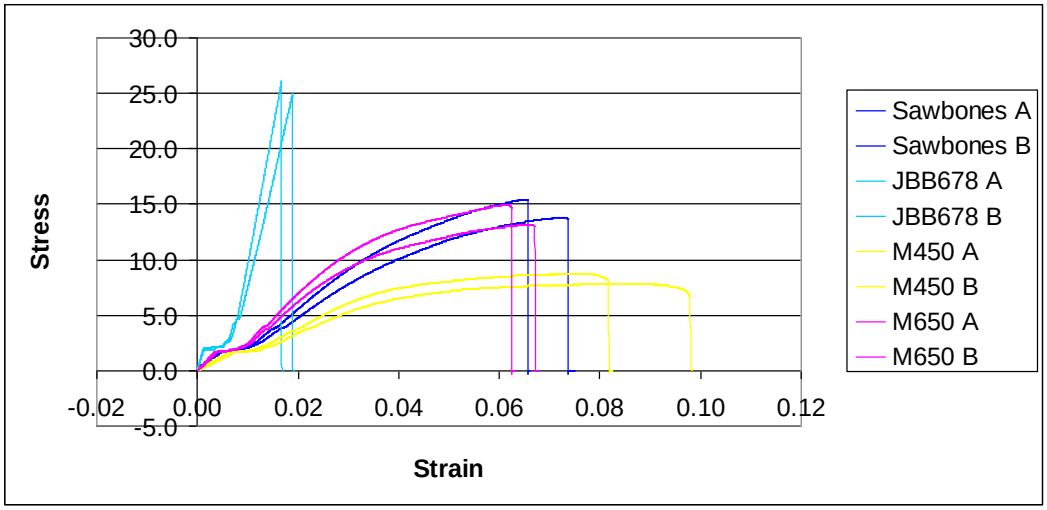

Figure 139: Results of flexion tests

As expected from previous results, the JBB678 tooling board was the stiffest material. M450 was the most flexible, with Sawbones and M650 recording similar flexion profiles.

d) Machinability

Tested subjectively for ease of machining, cleanliness of cuts. All materials were classified as 'easily machinable'.

Conclusions about materials

All the materials were deemed suitable from a machinability perspective. However the JBB678 material was extremely stiff and therefore unsuitable for use as a bone analogue. The M450 did not recover as well as other materials, and as the bone analogue will be subjected to repeated loading this made it less suitable. The M650 model board was shown to be very similar to Sawbones 30pcf foam. Its lower cost and flexibility of shape options meant it was the material chosen to be machined into the bone analogue for testing.

Appendix 4 – Machining test hemispheres

Test hemispheres were machined by the following process. First, blocks of 135 x 135 x 85mm M650 polyurethane foam were attached via screws to a machining guide (Figure 140). These blocks were then machined with a test cavity (Figure 141), using a CNC machine. The centre of the top surface of the block was defined as the origin of the machining movements. In this phase of machining any acetabular defects in the cavity can also be machined.

The guide and block were removed from the machining unit and inverted, so that the test cavity fitted over the cylindrical protrusion on the machining guide. The back of the test hemisphere was then machined, leaving a hemisphere with a block of waste material on the top surface (Figure 142). This waste block was precisely parted-off using a lathe, leaving the completed test hemisphere.

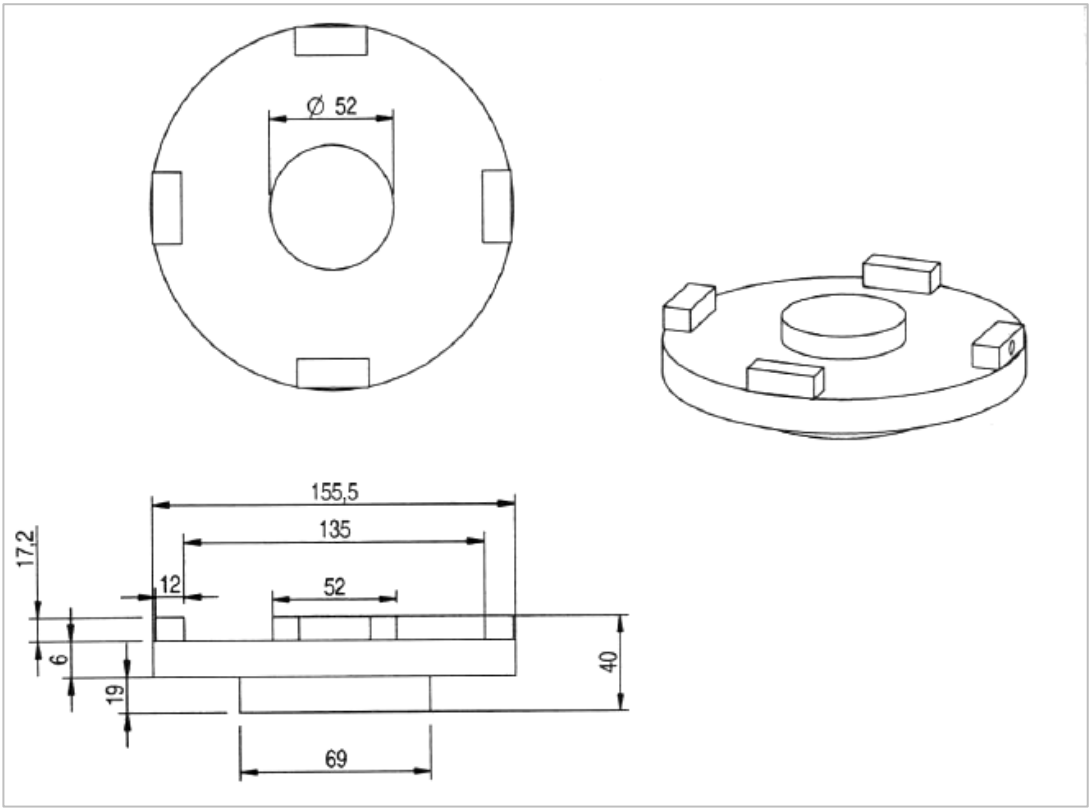

Figure 140: Machining guide for PU blocks

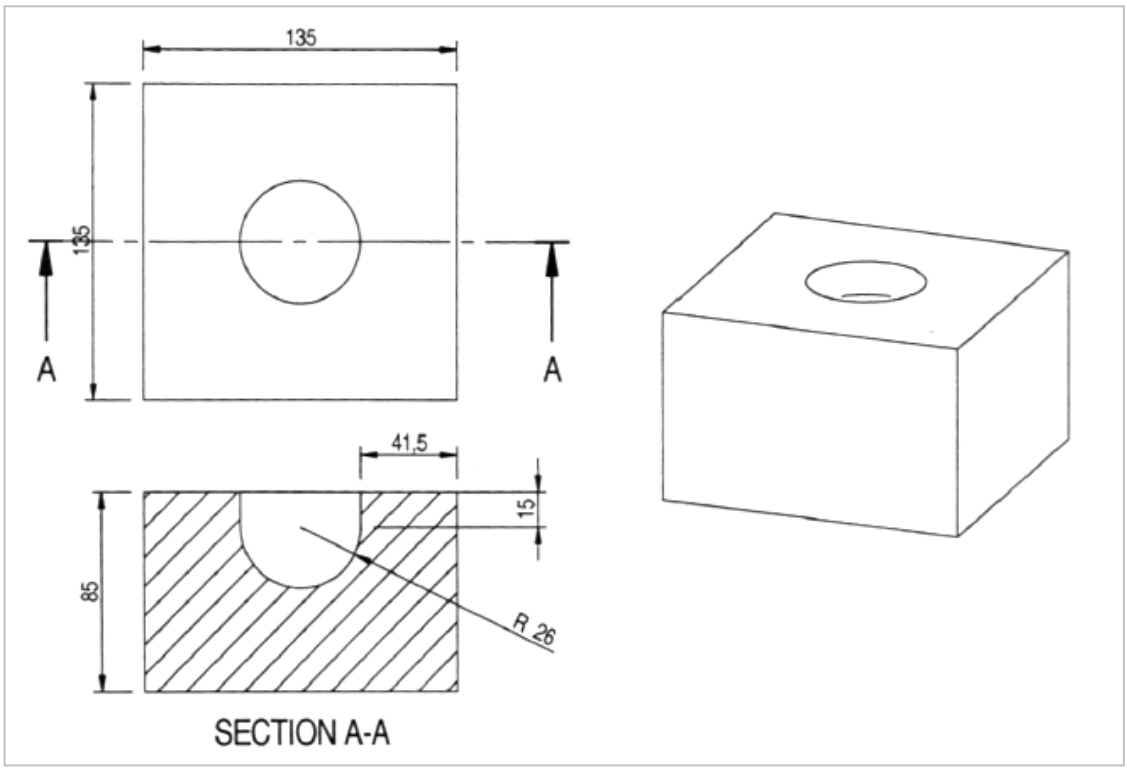

Figure 141: PU Block with machined test cavity

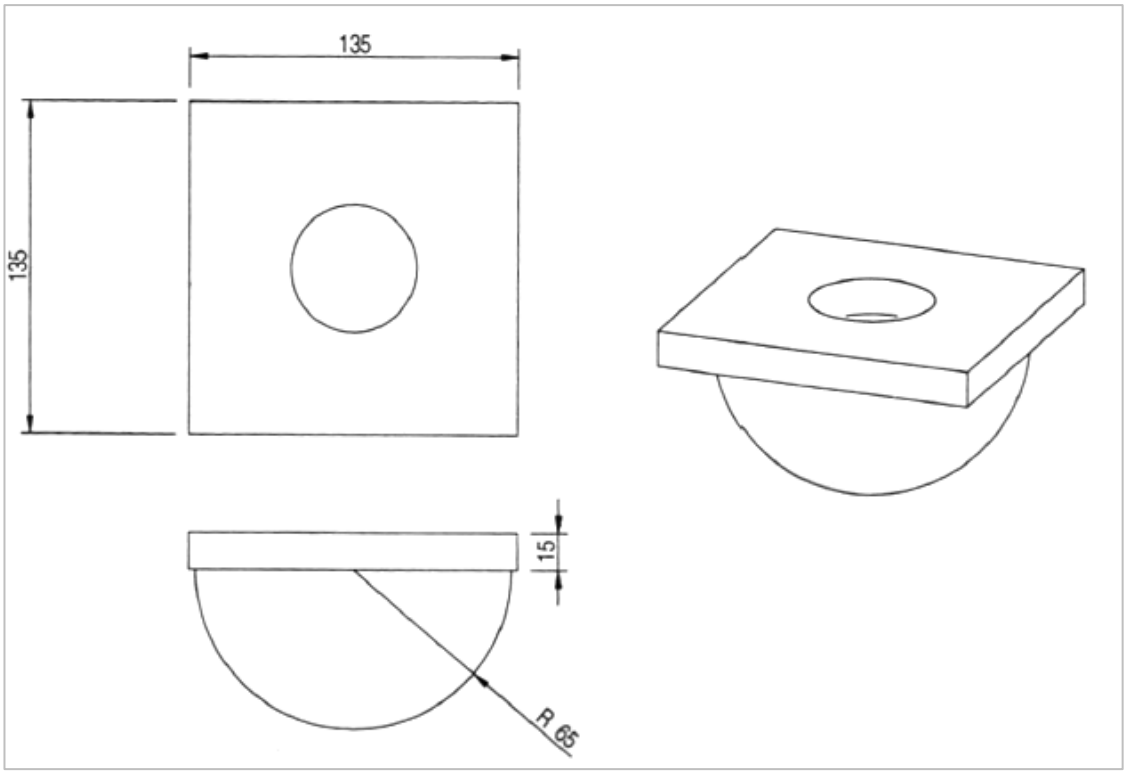

Figure 142: PU block, including waste material from machining process

Appendix 5 – Membrane test procedures

Characterisation of membrane materials was carried out by a colleague (Wright et al., 2012) to provide the values shown in Table 8. The test procedures that were followed to obtain these values are described below.

Permeability

Circular samples of the test material were placed in a chamber, on a wire mesh suspended above a petri dish, as shown in Figure 143. Vegetable oil was poured into the top of the chamber and loaded through a piston at 10mm/min, for a maximum stroke of 20mm. The presence of oil in the petri dish determined the permeability of the material.

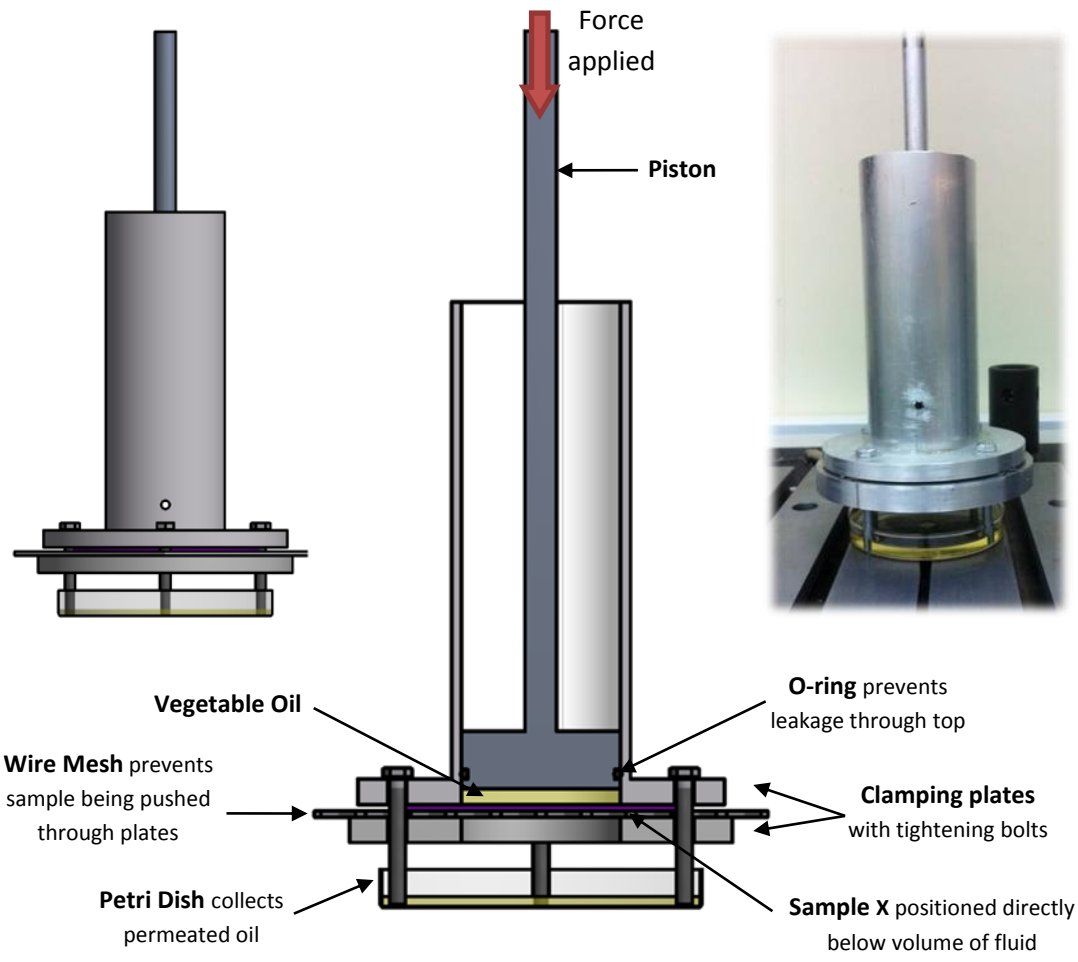

Figure 143: Image showing permeability test apparatus. From Wright et al. (2012), reproduced with permission.

Reabsorption

Reabsorption testing was performed on the samples according to the flow diagram shown in Figure 144. Percentage reabsorption values were obtained by comparing the weight of fluid after the second absorption with the initial weight of fluid absorbed by the unloaded sample. This represented the degree to which fluid lost by the samples under compression could be reimbibed by the material.

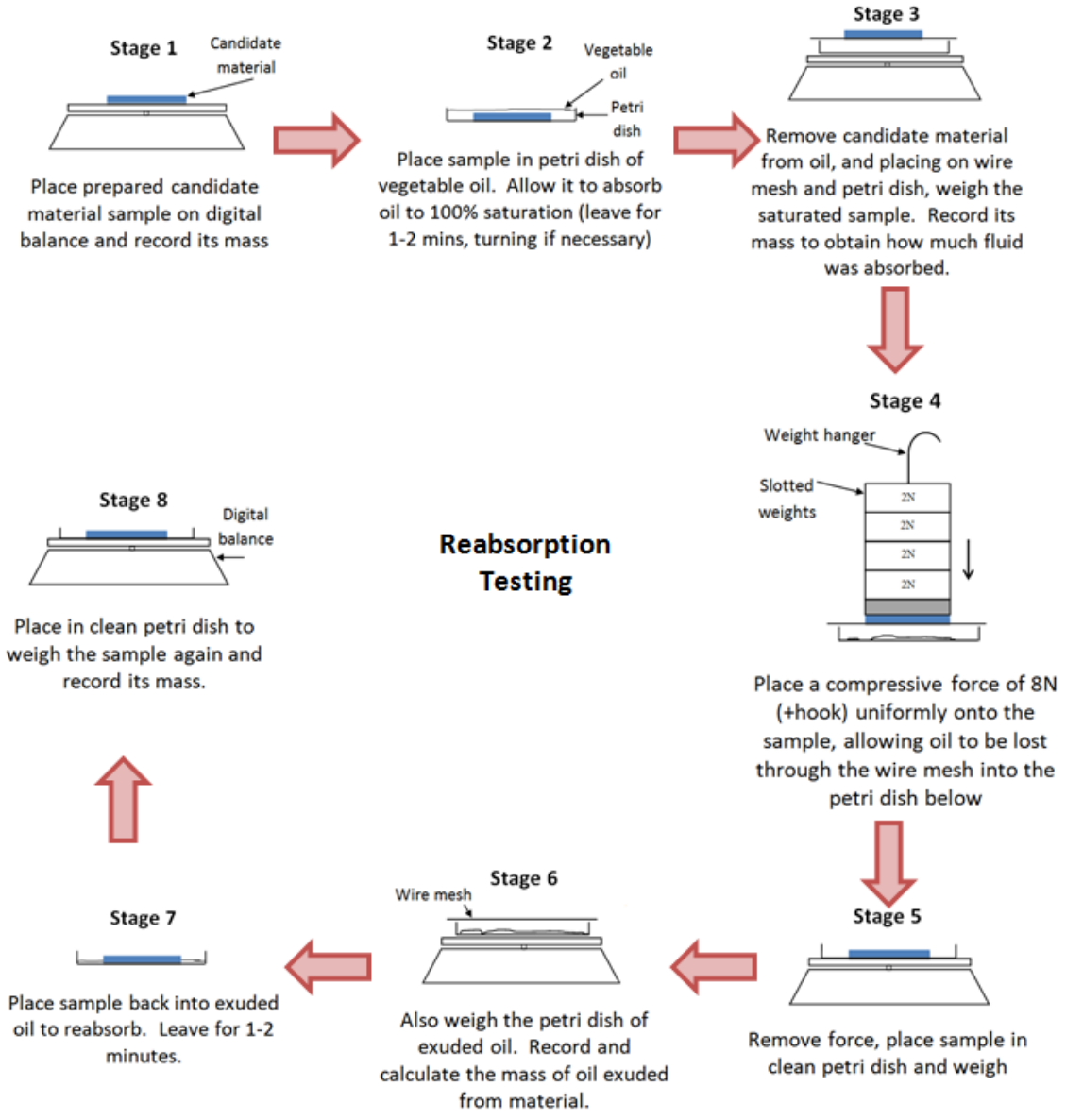

Figure 144: Diagram of reabsorption testing protocol. Image adapted from Wright et al. (2012), with permission.

Elastic modulus

Each sample was placed in vegetable oil and allowed to absorb to maximum saturation. The sample was then placed in an Instron 3366 test machine as shown in Figure 145, and loaded in compression at 2mm/min to a maximum of 1kN. Compression curves were plotted, and using the cross-sectional area and original length values, values for elastic modulus were obtained.

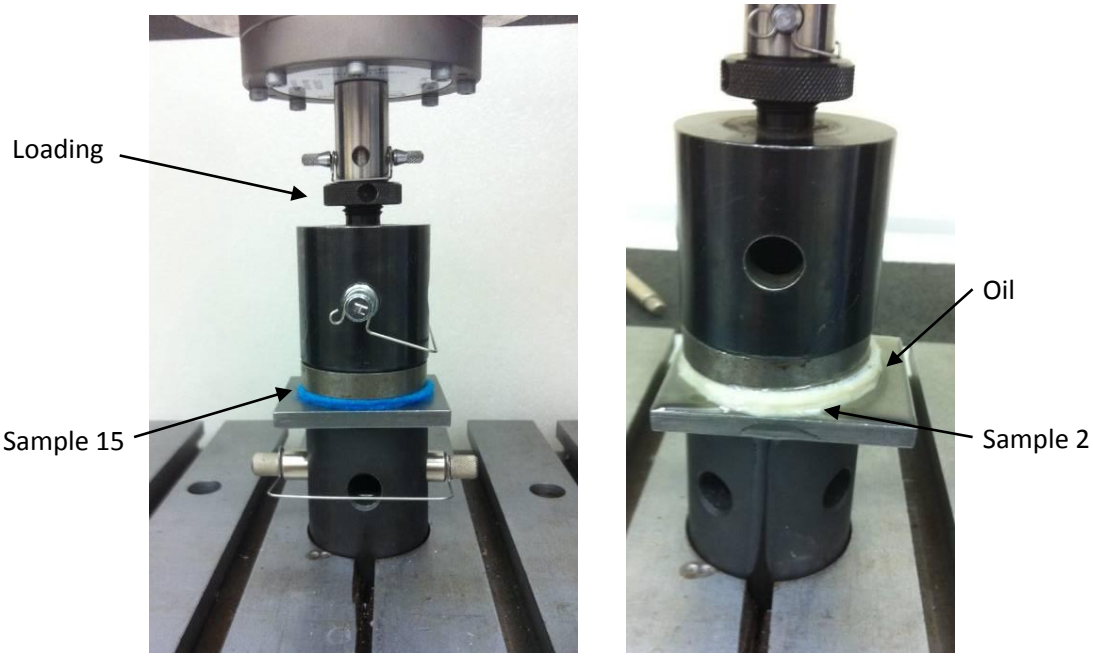

Figure 145: Images showing the configuration of compressive testing with fibrous materials

Appendix 6 – Dismantling and cleaning rig

Cleaning procedure

Based on the guidelines in British Standard (BS 7251-7:1990, Annexe A), a thorough cleaning procedure was established. When testing was complete, oil was allowed to drain completely from rig. The oil reservoir was emptied, and the transducers were unscrewed to allow oil to flow from chamber. After 20 minutes of draining, excess oil was wiped from all surfaces with paper towelling.

The entire rig was disassembled, by unscrewing the loading head from the Dartec, removing the top seal and rig top chamber from the angle plate and removing the rig chamber from the angle plate. Transmission tubes and prosthetic components were removed from the rig. All equipment was washed in warm water, with a fragrance- and additive-free detergent (Surcare liquid detergent). The rig components were rinsed thoroughly to remove all traces of detergent. Components were allowed to air dry and then the drying process was completed with clean paper towel. A small pipe brush was used to clean any traces of silicone from transmission tubes.

When rig base was clean and dry, the hemisphere was removed by covering the interior pole hole with a finger and blowing pressurised air through the other end, forcing the hemisphere out of the cavity. The hemisphere and rig base were re-washed to remove residual oil. The British Standard recommends cleaning in an ultrasonic bath but as very little particulate debris was expected with such a low number of cycles, this was deemed unnecessary.

Re-setting between tests

For tests within a Test Group (with a re-use of the hemisphere) the test hemisphere remained in the Woods metal cradle after washing and the clean transmission tubes were re-sealed into the transmission channels with silicone sealant.

When a new hemisphere was inserted, the used test hemisphere was removed and the transmission holes in the rig were sealed with 4mm custom tube plugs. Then the whole rig chamber was immersed in boiling water to melt the Woods metal. A new hemisphere could then be inserted into the melted Woods metal and a new test set up. When re-setting the rig, oil was changed to ensure the cleanliness and consistency of the synovial analogue.

Appendix 7 – Matlab routine

```
function [M1,N1, M2, N2, Av1, Av2,peaksX, IX,peaksN, IN]= Analyse_Data(Calib_Data,start1, end1, start2, end2)
%This function will take filename and offset and give back max and min
%values

%find the average of the first second
Av1 = mean(Calib_Data(1:50,:));

%Average of the last second
Av2 = mean(Calib_Data(end-50:end,:));
[peaksX, IX]=max(Calib_Data(start2-49:start2,:));
[peaksN, IN]=min(Calib_Data(start2-49:start2,:));

%middle bit of data data we're interested in:
M1 = max(Calib_Data(start1:end1,:));
N1 = min(Calib_Data(start1:end1,:));
M2 = max(Calib_Data(start2:end2,:));
N2 = min(Calib_Data(start2:end2,:));
```

```
function Offset= OffsetFinder(FileName)

%*******************Open the file and get the data**************************
FileID = fopen(FileName);
line = fgetl(FileID); % Get first line

while strncmp('Channel 00:',line,11)==0
   line = fgetl(FileID); % Get next line
end

Data = fscanf(FileID,'%f, %f, %f, %f, %f, %f',[6 inf]);
% Close file
fclose(FileID);

%*****************Manipulate the data*************
Data = Data';
FirstData=Data(1:20,:);
Offset = mean(FirstData,1);
end
```

```
function [Results, Peaks, Calib_Data, Time] = Open_File(FileName, Offset, F1)
```

```
%*************Open the file and get the data************************
FileID = fopen(FileName);
line = fgetl(FileID); % Get first line

while strncmp('Channel 00:',line,11)==0
   line = fgetl(FileID); % Get next line
end

Data = fscanf(FileID,'%f, %f, %f, %f, %f, %f',[6 inf]);
% Close file
fclose(FileID);
Data = Data';

%Calibration factors
Gains=[17.438,17.123,17.176,17.349,10,1];

%Step 1: multiply off sets by gains
Calib_Offset = Offset.*Gains;
Calib_Offset(5)=0;
Calib_Offset(6)=0;

%Step 2: multiply data by gains and subtract offsets
for a=1:size(Data,1)
   Calib_Data(a,:) = (Data(a,:).*Gains)-Calib_Offset;
end

% for all files except MSmin0#plus0#
%find the start and end values
dT = 1/50; %[s]
Time=0:dT:(size(Calib_Data,1)-1)*dT;

ind = find(Calib_Data(:,6)<=-0.7, 1);
start1=ind-(1/F1)*50; %First row number when below -0.7 - one cycles worth of row numbers
end1=start1+(2/F1)*50;
start2 = find(Time>(48/F1));
start2=start2(1);
end2 = start2+(2/F1)*50;

[M1,N1, M2, N2, Av1, Av2,peaksX, IX,peaksN, IN]= Analyse_Data(Calib_Data,start1, end1, start2, end2);

    Amp1 = M1-N1;
    Amp2= M2-N2;
```

```
    Results = [Av1;M1;N1;Amp1;M2;N2;Amp2; Av2];
    Peaks = [IX;peaksX; IN;peaksN ];
```

```
function [Results, Peaks, Calib_Data, Time] = Open_File2(FileName, Offset, F1)
% This is for the MS files

%*************Open the file and get the data*************************
FileID = fopen(FileName);
line = fgetl(FileID); % Get first line

while strncmp('Channel 00:',line,11)==0
   line = fgetl(FileID); % Get next line
end

Data = fscanf(FileID,'%f, %f, %f, %f, %f, %f',[6 inf]);
% Close file
fclose(FileID);
Data = Data';

%*****************Manipulate the data according Sarah's wishes*************
Gains=[17.438,17.123,17.176,17.349,10,1]; %Calibration factors

Calib_Offset = Offset.*Gains; %Step 1: multiply off sets by gains
Calib_Offset(5)=0;
Calib_Offset(6)=0;

for a=1:size(Data,1)  %Step 2: multiply data by gains and subtract offsets
   Calib_Data(a,:) = (Data(a,:).*Gains)-Calib_Offset;
end

dT = 1/50; %[s] %find the start and end values
Time=0:dT:(size(Calib_Data,1)-1)*dT;

CutOff = mean(Calib_Data(:,5)); %average of channel 5 for our cutoff point

P1 = Calib_Data(1,5); %then we find the first position (channel5):

if P1 >=CutOff%Stroke/2
   %our first point is found by
   ind=find(Calib_Data(:,5)<=CutOff);%Stroke/2);
else
   ind = find(Calib_Data(:,5)>=CutOff);%Stroke/2);
```

```
end

indMinus=ind-(1/F1)*50;  %this is sometimes a negative number so...
if indMinus(1)<=0
   start1=ind(1);
else
   start1=indMinus(1);
end
end1=start1+(2/F1)*50;
start2 = find(Time>(48/F1));
start2=start2(1);
end2 = start2+(2/F1)*50;

[M1,N1, M2, N2, Av1, Av2,peaksX, IX,peaksN, IN]= Analyse_Data(Calib_Data,start1, end1, start2, end2);

      Amp1 = M1-N1;
      Amp2= M2-N2;
      Results = [Av1;M1;N1;Amp1;M2;N2;Amp2; Av2];
      Peaks = [IX;peaksX; IN;peaksN ];
```

```
% for the other files
clc
clear
DateName='120209_ScrewHoles1';  %CHANGE THIS BIT:
%TestNameShort=DateName(8:end-2); %for longerTestNumber(10+)
TestNameShort=DateName(8:end-1); %for ScrewHoles/NoHoles(1-9)!
DataPath='X:\MechEng\Research\General\AWM\AWM-0003\SS_PhD\PhD_Testing\R05\';

a=1;
Frequency=1;
F1=1; %Hz unless otherwise specified
First_Value = -0.7; %unless otherwise specified

FileName1 =  %Filename for offset
strcat(DataPath,TestNameShort,'\',DateName,'\',DateName,'_OilIntroduction')
Offset= OffsetFinder(FileName1); %Work out offsets

%so for filename2 we need to know which files are in the folder
%and there are 4 different types of file
Folder_contents1 = dir(strcat(DataPath,TestNameShort,'\',DateName,'\',DateName,'_MS*'));
C1 = size(Folder_contents1,1);
```

```
Folder_contents2 = dir(strcat(DataPath,TestNameShort,'\',DateName,'\',DateName,'_1*'));
C2 = size(Folder_contents2,1);

Folder_contents3 = dir(strcat(DataPath,TestNameShort,'\',DateName,'\',DateName,'_Mi*'));
C3 = size(Folder_contents3,1);
Folder_contents4 = dir(strcat(DataPath,TestNameShort,'\',DateName,'\',DateName,'_Low*'));
C4 = size(Folder_contents4,1);

C=[C1,C2,C3,C4];

FC=cat(1,Folder_contents1, Folder_contents2, Folder_contents3,Folder_contents4);

% All_Results=zeros(8,6,numel(FC));

for v=1:numel(FC) %ie for all tests
 disp(v)
    FileName2 = strcat(DataPath,TestNameShort,'\',DateName,'\',FC(v,1).name)

    if v>C(1) && v<=(C(1)+C(2)); %i.e when we have the 1kn etc files
       Frequency = FC(v,1).name;

       Frequency = str2double(Frequency(end-5));
       if Frequency >1
          Frequency = Frequency/10;
       end
     end

    if v>=1 && v<=(C(1)) %i.e. when the MS ones are being done
[Results, Peaks, Calib_Data, Time] = Open_File2(FileName2, Offset,Frequency); %Results = (8x6)
    else %for Mi and Low
[Results, Peaks, Calib_Data, Time] = Open_File(FileName2, Offset,Frequency); %Results = (8x6)
       if v==(C1+6)
          subplot(2,1,1)
          Calib_Data=Calib_Data';
          plot(Time,Calib_Data(3,:),'-','Color',[0 0.5 0])
          hold on

          xlabel('Time [s]')
          ylabel('Pressure [kPa]')
          ylim([-10 50])

          x2=60;
          xlim([0 x2])
```

```
            plot([Time(1,1),x2],[0,0],'k-')
            hold off
        elseif v == (C1+C2+C3+4)
            Calib_Data=Calib_Data';
            subplot(2,1,2)
            plot(Time,Calib_Data(3,:),'-','Color',[0 0.5 0])
            hold on
            xlabel('Time [s]')
            ylabel('Pressure [kPa]')
            ylim([-10 50])

            x2=60;
            xlim([0 x2])
            plot([Time(1,1),x2],[0,0],'k-')
            hold off
        end
    end
All_Results(v).name =FC(v,1).name;
All_Results(v).Results = Results;
All_Results(v).Peaks = Peaks; %Peaks = [IX;peaksX; IN;peaksN ];
% (:,:,v) = Results;

end

  clearvars -except All_Results DateName FC

  filename=strcat(DateName,'.mat');
  save(filename, 'All_Results', 'DateName', 'FC')
```

Appendix 8 - Publications

Sydney S E, Wright S, Turner I G, Miles A W M. (2012). Measurement of fluid pressures behind an acetabular cup *in vitro*. European Orthopaedic Research Society Transactions Vol 20, Amsterdam.

Wright, S, Sydney S E, Miles A W M. (2012). Synthetic material to replicate fibrous tissue occurring in joint replacement. European Orthopaedic Research Society Transactions Vol 20, Amsterdam.